Marzena Ciszak

ANTICIPATED SYNCHRONIZATION: NUMERICAL AND THEORETICAL STUDY

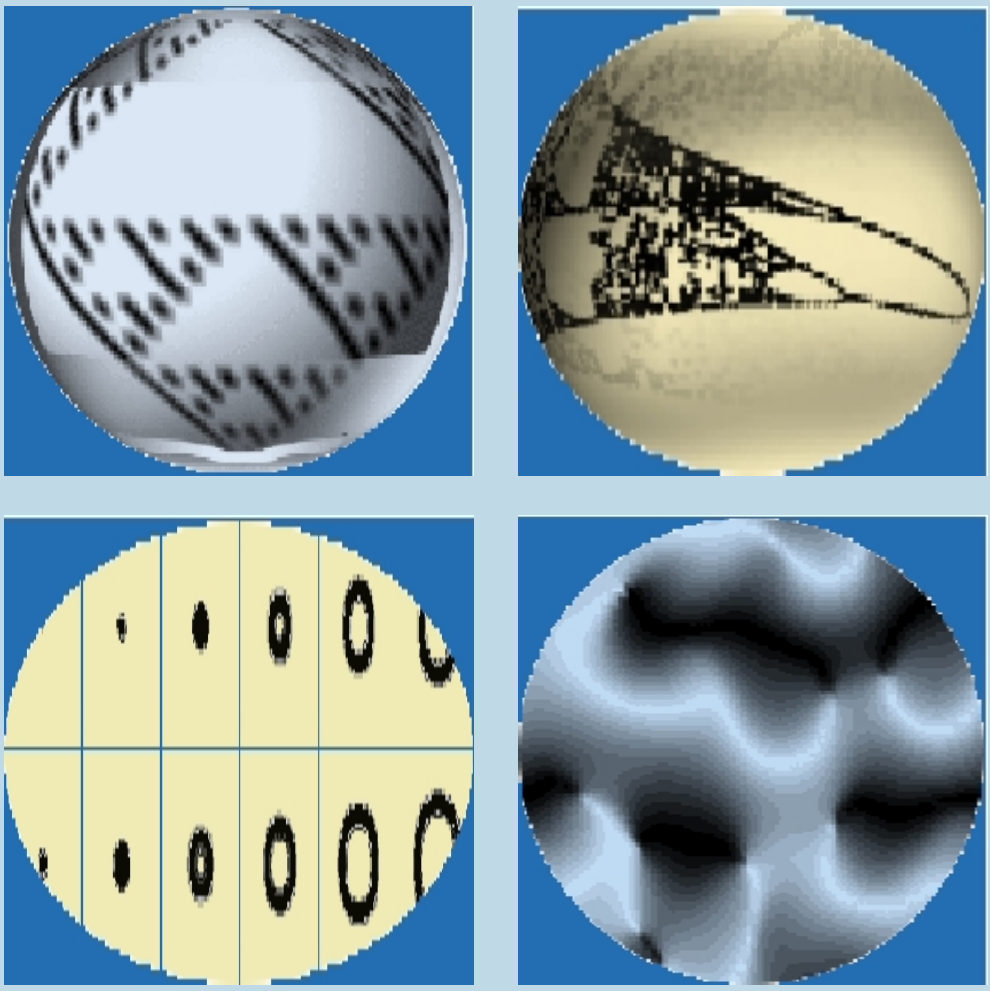

Ph.D. Thesis

ANTICIPATED SYNCHRONIZATION: NUMERICAL AND THEORETICAL STUDY

PhD Thesis of Marzena Ciszak
Supervisors: Claudio Mirasso and Raúl Toral
University of Balearic Islands

To Janina Jaworska

Contents

Acknowledgements

I wish to express my gratitude to everyone who contributed to making this thesis a reality. At first I must single out my supervisors, Claudio Mirasso and Raúl Toral, who proposed me the realization of this project. I owe special thanks to them for their scientific support during the last years of my doctorate studies. I am also grateful for their patience and time dedicated during the corrective stage of the thesis preparation.

The part of this thesis related to the study of anticipated synchronization in neural networks is the result of the collaboration with José Manuel Gutiérrez to who I am deeply indebted. I especially appreciate his hospitality during my stage at the University of Cantabria in Santander. In addition, the results on the dynamical mechanism of anticipated synchronization in excitable systems were the fruit of the interaction with Francesco Marino and Salvador Balle. I owe special thanks to them for the interest they put in the subject of my studies and for very stimulating discussions we had. I also want to thank Emilio Hernández-Garcia for his insightful comments and helpful advice related to delayed and spatiotemporal systems.

Durante los últimos cinco años de mi estancia en la Universidad de las Islas Baleares he tenido la oportunidad de conocer a muchas personas, quienes pasaron por la EFE, GE e IMEDEA. Siempre recordaré los buenos momentos que he tenido aquí con ellos/as, que hicieron los días largos de trabajo agradables y felices.

Dziekuję moim Rodzicom, siostrze Beatce i siostrzeńcowi Dominikowi (który otworzył swoje oczka po raz pierwszy niedawno), za ich bliskość, pomimo odległości która nas dzieliła, za ich miłość i wsparcie.

Pracę tę dedykuję kochanej Babuni, Janinie Jaworskiej, która czekała z niecierpliwością na moment ukończenia mojej pracy doktorskiej, i która nie doczekała się tego, opuszczając nas zbyt wcześnie.

Resumen

En esta tesis estudiamos el fenómeno de sincronización entre dos o más sistemas acoplados unidireccionalmente. El acoplamiento esta diseñado de tal manera que permite que ocurra sincronización ácrona, más específicamente la sincronización anticipada. La sincronización anticipada se refiere a la situación en que un sistema sincroniza con la dinámica futura de otro sistema.

El marco de esta tesis toca muchos problemas relacionados con la sincronización anticipada, poniendo particular interés en los sistemas excitables y espaciotemporales. En este estudio se proporciona una descripción teórica del fenómeno, en su mayor parte a través de simulaciones numéricas, pero también, en un caso particular de sistemas exitables, a través de resultados experimentales. Además, modelamos la sincronización anticipada en reacciones químicas consistentes en la oxidación de CO sobre una superficie de platino. El estudio se realiza desde el punto de vista de los requisitos experimentales y sus limitaciones.

Mostramos además que células excitables separadase spacialmente y acopladas, con el esquema de la sincronización anticipada y bajo las condiciones particulares, pueden contribuir a la sincronización a tiempo cero. Relacionamos este resultado con las observaciones experimentales de la sincronización a tiempo cero entre áreas cerebrales separadas espacialmente.

Considerando la dinámica espaciotemporal, a través de un ejemplo de los autómatas celulares acoplados, demostramos la equivalencia entre el acoplamiento basado en las variables retrasadas en el tiempo y aquellas retrasadas en el espacio. Relacionamos este resultado con los estudios anteriores sobre las propiedades espaciales de los sistemas con retraso.

Revelamos el mecanismo dinámico de la sincronización anticipada en los sistemas excitables mostrando que la anticipación aparece debido a una reducción del umbral de excitabilidad en el esclavo inducido por el término de acoplamiento con retraso.

También intentamos responder al problema del mecanismo dinámico de la sincronización anticipada en los sistemas caóticos, utilizando el enfoque de los sistemas modificados.

Finalmente estimamos el uso práctico de la sincronización anticipada. Presentamos un nuevo método de control, al que llamamos *método de control de predecir-prevenir* para sistemas excitables. Además comparamos la capacidad de predicción del esquema de la sincronización anticipada implementado en redes neuronales con los métodos estándar de predicción a través de las redes neuronales.

Abstract

In this thesis we study the phenomena of synchronization between two or more constituents coupled in an unidirectional way. The coupling is designed in a way which permits the occurrence of achronal synchronization, more specifically anticipated synchronization. Anticipated synchronization refers to the situation in which one system synchronizes to the future dynamics of other system.

The framework of this thesis touches many problems related to dynamical systems, for which we characterize the occurrence of anticipated synchronization with a special interest in excitable and spatiotemporal ones. We provide a theoretical description of the phenomenon, mostly through numerical simulations, but also in the particular case of excitable systems, through experimental results. Moreover we model the anticipation of the chemical reaction consisting on the oxidation of the CO on the platinum surface and provide the study from a point of view of the experimental requisites and limitations.

We show that spatially separated and coupled excitable cells with the anticipated synchronization scheme under particular conditions may contribute to zero-lag synchronization. We relate this result to the experimental observation of zero-lag synchronization between spatially separated brain areas. Considering further spatiotemporal dynamics we demonstrate on the example of coupled cellular automata the equivalence between the coupling based on time-delayed and on space-delayed variables. We relate this finding to the previous study on the spatial properties of time-delayed systems.

We uncover the dynamical mechanism of anticipated synchronization in excitable systems showing that the anticipation is due to the lowering of the excitability threshold of the slave by the delayed coupling term. Also we try to answer the question about the dynamical mechanism of anticipated synchronization in chaotic systems in terms of a modified system approach.

Finally we estimate the practical usage of anticipated synchronization. We present a new control method which we call *predict-prevent control method* for excitable systems.

We also compare the prediction capacity of the anticipated synchronization scheme implemented in neural networks modules with the standard prediction methods given by neural networks.

Chapter 1

Introduction

Synchronization processes were intensively studied by Wiener [1]. He was the first one to argue that frequency adjustment was a universal mechanism for self - organization operating everywhere in Nature. Later studies, including some of the human body, revealed that many processes, specially the self-organized ones, work thanks to the mutual cooperation of many constituents. In biology, at the biochemical level, such cooperation is a wonderful fruit of evolution, which encountered a way to accomplish the sophisticated tasks of maintaining life. It was also noticed by Blekhman in Ref. [2] that many phenomena in nature tend to oscillate. The coherent behaviour between interacting, oscillating systems is called synchronization.

There is a hope that a profound study of synchronization phenomena will lead to understand the occurrence of many biological self-organized processes, and could contribute to reveal the mystery of life, how it appeared and how it can continue in such a perpetual way. When people became conscious of the existence of cooperative processes in nature based on mutual interactions, they started to analyze them intensively, building step by step the theory of synchronization with the study of its physical and mathematical basis, its effects in biology and even its use in practical applications.

In this thesis we study the phenomena of synchronization between two or more constituents coupled in an unidirectional way. The coupling is designed in a way which permits the occurrence of achronal synchronization, more specifically anticipated synchronization. We pretend to contribute to the synchronization theory through an extensive study of this phenomenon from different points of view. After providing exhaustive characterization of the phenomenon, an important goal is to understand the dynamical mechanism underlying the anticipated synchronization. When understood, a wide branch of potential applications, in nature as well as in technology, come out in a natural way.

In the next Chapter we present numerical and theoretical results on the anticipated synchronization, which refers to the situation in which one system (the *slave*) synchronizes to the future dynamics of other (the *master*). The framework of this thesis touches many problems related to dynamical systems, for which we provide a short review in Chapter 2. In Section 2.1 we briefly describe mathematical models for excitable systems. In Section 2.2 we discuss the predictability of chaotic systems dynamics and the

roots of the limitations imposed, not by the methods' inefficiencies, but by the dynamical properties of chaotic systems themselves. Moreover we describe two approaches to control chaotic systems, namely the Ott-Grebogi-York and Delayed Feedback Control methods. Further in Sections 2.3 and 2.4 spatiotemporal systems and delayed differential equations are described. In Section 2.5 we provide a short overview on neural networks. Finally, in Section 2.6 we review the problems related to synchronization and anticipated synchronization phenomena.

Our work is divided in three main parts which are consequently described in the following three Chapters of the thesis, Chapters 3, 4 and 5. Chapter 3 is related to the characterization of anticipated synchronization in different dynamical systems with a special interest in excitable (Section 3.1) and spatiotemporal (Section 3.2) ones. We provide a qualitative description of the phenomenon, mostly through numerical simulations, but also in the particular case of excitable systems, through experimental results (Section 3.1.4). The stage of the studies described in Chapter 3 is the journey through many physical systems, which are very different from the dynamical point of view. This allows us to make a more deep insight into the physical realities which they model, mostly through numerical simulations which occurred to be an indispensable tool during this work.

In this thesis we put special attention in excitable systems subject to an external singular or random perturbation. Why excitable systems? Excitable systems often model real neurons which involve a large number of variables. Nevertheless, the essential features of their excitable behavior can be captured with a suitably reduced description. In particular we deal with the Adler and the FitzHugh-Nagumo equations which provide arguably the simplest representation of excitable dynamics, although in both systems different types of bifurcation lead to the excitability (in Adler system a saddle-node bifurcation on an invariant circle and in FitzHugh-Nagumo system a Hopf bifurcation). Since the central nervous system environment, in which the neurons process electrical signals, is noisy we direct our study to coupled excitable units driven by noise.

In Section 3.2 we study anticipated synchronization in spatiotemporal systems, starting with the complex Ginzburg-Landau equations in Section 3.2.1, since these equations have general properties which are representative of many physical systems. In Section 3.2.2 we model the anticipation of the chemical reaction consisting on the oxidation of CO on a platinum surface. We provide the study from a point of view of the experimental requisites and limitations.

Further in Section 3.2.3 we study spatially isolated and coupled excitable cells showing that under particular conditions anticipated synchronization may contribute to zero-lag or no delay synchronization. We relate this result to the experimental observation that distinct brain areas can synchronize without time lag despite of the spatial separation between them. Such a synchronization gives rise to the phenomenon known as

feature binding, which is a recently posed brain theory for the mechanism of perception.

The last part of the Chapter 3, Section 3.2.4, deals with coupled cellular automata demonstrating the equivalence between the coupling based on time-delayed and on space-delayed variables. We relate this finding to the previous study on the spatial properties of time-delayed systems.

After the characterization of the anticipated synchronization in the different dynamical systems mentioned above we concentrate in Chapter 4 on the mechanism underlying this synchronization. We uncover the dynamical mechanism of anticipated synchronization in excitable systems showing that the anticipation is due to the lowering of the excitability threshold of the slave by the delayed coupling term (Section 4.1). It is clear that an excitable dynamics is different from that of chaotic systems. We tried to answer the question about the dynamical mechanism of anticipated synchronization in chaotic systems. The results of these considerations are presented in terms of a modified system approach in Section 4.2 as well as in Section 4.3 where the similarity between anticipated synchronization and delayed feedback control is revealed. Such a resemblance allows us to make a more deep insight into the phenomenon of anticipated synchronization and to consider it from a general point of view of control theory.

Finally in Chapter 5 we estimate the practical usage of anticipated synchronization. In Section 5.1 we present a new control method which we call predict-prevent control method for excitable systems. This method allows us to control the perturbed excitable systems by first predicting the response of this perturbed system and then by suppressing its response before it happens. In the last Section 5.2 we compare the prediction capacity of the anticipated synchronization scheme implemented in neural networks modules with the standard prediction methods given by neural networks. The main results of this thesis, as well as some open problems, are summarized in Chapter 6.

Chapter 2

Background

2.1 Modelling excitability

The human brain consists of about 10^{11} neurons with an average of more than 10^4 synaptic connections each. Neurons are slow and unreliable when considered separately, but together they form a highly sophisticated computational system. Three types of neurons exist: multipolar, motor and sensory neurons. Multipolar interneurons (Fig. 2.1a) posses profusely branched dendrites, which receive synaptic signals from several hundreds of other neurons, and a single long axon that branches laterally at its terminus. They are found only in the central nervous system where they connect neurons to neurons. Motor neurons (Fig. 2.1b) innervate muscle cells and typically have a single long axon extending from the cell body to the effector cell and short dendrites which transmit messages from the central nervous system to the muscles (or to glands). Finally, sensory neurons (Fig. 2.1c) typically have a long dendrite and a short axon, and carry messages from sensory receptors to the central nervous system.

The changes in the electrical potential across a cell's membrane (the action potential) play a crucial role in neuron communications. The creation of the action potential requires the contribution of sodium Na^+, calcium Ca^{2+} and potassium K^+ ions. An increase of the potential in a membrane opens Na^+ and Ca^{2+} channels, inducing a rapid inflow of ions, causing a further increase of the membrane potential. This activates a slower process of closing Na^+ and Ca^{2+} channels, but at the same time opening K^+ channels, which reduces the membrane potential. A neuron is *quiescent* if the membrane potential is in a rest state or exhibits small amplitude subthreshold oscillations.

From the dynamical point of view, neurons are classical prototypes of excitable systems: their response to an external electrical stimulus is highly non-linear and depends on its magnitude and timing. If the stimulus is small the action potential evolves back to the steady state; but if the stimulus exceeds a certain threshold, the neuron fires a pulse-like spike and after that returns to the equilibrium. From this dynamical point of view, neurons are excitable because they are near a bifurcation (transition) from quiescence to repetitive firing [3]. Following the onset of the excitation, there is an interval, called refractory period, during which another perturbation does not induce a new pulse.

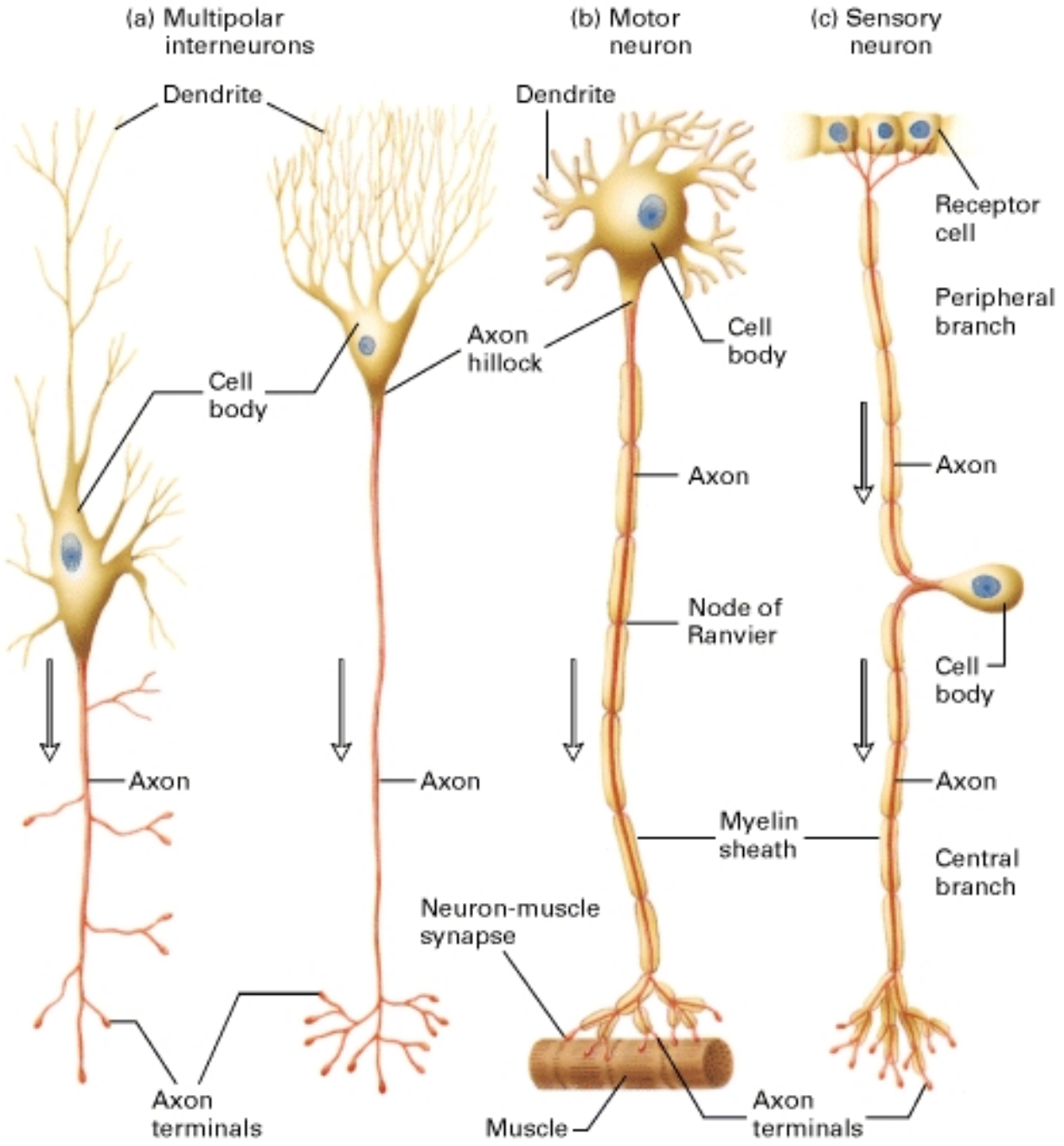

Figure 2.1: *Structure of typical mammalian neurons. Arrows indicate the direction of conduction of action potentials in axons. (a) Multipolar interneurons, (b) a motor neuron that innervates a muscle cell, (c) a sensory neuron. Picture by W. H. Freeman taken from URL http://www.ncbi.nlm.nih.gov/.*

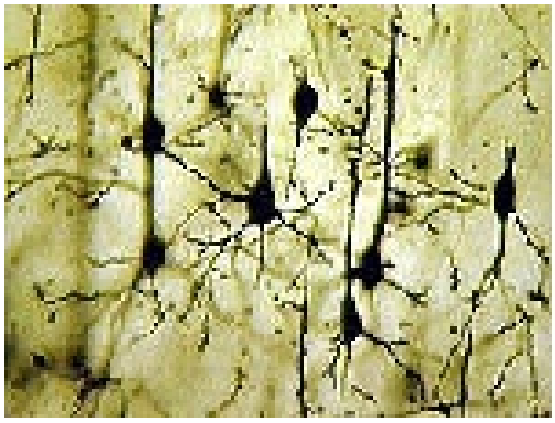

Figure 2.2: *Photo of neurons in the Hippocampus taken from URL http://faculty.washington.edu/chudler/ca1pyr.html.*

Although real neurons (see photo in Fig. 2.2) are complicated non-linear systems involving a large number of variables, the essential features of their excitable behaviour can be captured with a much reduced description. A simple model of the nerve membranes was introduced by the English physiologists Hodgkin and Huxley in 1952 [4], for which they were awarded the Nobel prize. The model concerned originally the axon of the giant squid. The axon is a long cylindrical tube, which extends from each neuron, where electrical signals propagate along its outer membrane about $50 - 70\mathring{A}$ thick. The electrical pulses arise because the membrane is preferentially permeable to various chemical ions with the permeabilities altered by the present currents and potentials. The key elements in the system are potassium (K^+) ions and sodium (Na^+) ions. In the rest state there is a transmembrane potential difference V of about -70 mV due to the higher concentration of K^+ ions within the axon as compared with the surrounding medium. A basic model for a cell membrane takes the form:

$$C\dot{V} = -\frac{V - V_{eq}}{R} + I_a \tag{2.1}$$

where C is the membrane capacitance, R the resistance, V_{eq} the rest potential, V the potential across the inner and outer surfaces of the membrane, and I_a represents the applied current. The membrane permeability properties change when subjected to a stimulating electrical current I_a. Based on experiments, Hodgkin and Huxley developed the model equation:

$$C\dot{V} = -g_K n^4 (V - V_K) - g_{Na} m^3 h (V - V_{Na}) - g_L (V - V_L) + I_a \tag{2.2}$$

where the contribution from the sodium, potassium and 'leakage' currents have been taken into account. The g_K, g_{Na} and g_L are constant conductances and V_{Na}, V_K and V_L are constant equilibrium potentials. The m, n and h are called gating variables. They

evolve according to the differential equations:

$$\dot{\omega} = \alpha_\omega(V)(1-\omega) - \beta_\omega(V)\omega, \qquad \omega = n, m, h \tag{2.3}$$

where $\alpha_\omega(V)$ and $\beta_\omega(V)$ are functions of V describing the activation of sodium, potassium and leakage channels, determined from experimental data. Equations 2.2 and 2.3 constitute the 4-variable model of Hudgkin-Huxley. If $I_a = 0$, the system is linearly stable, but excitable. That is, if the perturbation from the steady state (at $V \approx -70mV$ for the original set of parameter values used by Hodgkin and Huxley) is sufficiently large there is a large excursion of the variables in their phase space before returning to the steady state. If $I_a \neq 0$ there is a range of values where regular repetitive firing occurs, which is the mechanism of limit cycle characteristics. A set of modified Hodgkin-Huxley equations were used by Braun et. al [109] to model the electro-receptor neurons. The equations are the following:

$$C_M\dot{V} = -I_{Na} - I_K - I_{sd} - I_{sr} - I_L + I_a \tag{2.4}$$

where C_M is the capacitance of the membrane. I_{Na} and I_K are fast sodium and potassium currents that generate the action potential, I_{sd} and I_{sr} are slow depolarization and repolarization currents and finally I_L is the leakage current:

$$I_{Na} = \rho g_{Na} a_{Na}(V - V_{Na}) \tag{2.5}$$
$$I_K = \rho g_K a_K(V - V_K) \tag{2.6}$$
$$I_{sd} = \rho g_{sd} a_{sd}(V - V_{sd}) \tag{2.7}$$
$$I_{sr} = \rho g_{sr} a_{sr}(V - V_{sr}) \tag{2.8}$$
$$I_L = g_L(V - V_L) \tag{2.9}$$

where the g's are the conductances and the a's contain the switching characteristics of the channels.

Due to the complexity of the Hodgkin-Huxley system, various simpler mathematical models, which still capture the key features of the full system, have been proposed. One of the best known is the FitzHugh-Nagumo model [5, 6]. The time scales for m, n and h in Eq. 2.3 are not all of the same order. The time scale for m is much faster than that of n and h, so it is reasonable to assume that it relaxes immediately to its value m_∞ determined by setting $\frac{dm}{dt} = 0$. Moreover, for the parameter values specified by Hodgkin and Huxley, $n + h$ remains constant and is approximately equal to 0.8. These approximations lead to a two variable model, called the fast-slow phase plane model:

$$\begin{aligned} C\dot{V} &= -g_K n^4(V - V_K) - g_{Na} m_\infty^3(0.8 - n)(V - V_{Na}) - g_L(V - V_L) + I_a \\ \dot{n} &= \alpha_n(V)(1-n) - \beta_n(V)n \end{aligned} \tag{2.10}$$

where $\alpha_n(V) = A\frac{V}{1-e^{-V}}$ and $\beta_n(V) = Be^{-V}$ with A, B constant. FitzHugh observed that the V-null cline had the shape of a cubic function and the n-null cline could be approximated by a straight line. Thus the resulting two variables model in V and n in Eq. 2.10 can be qualitatively approximated by the dimensionless system:

$$\begin{aligned} \dot{x}_1 &= f(x_1) - x_2 + I_a \\ \dot{x}_2 &= bx_1 - \epsilon x_2 \end{aligned} \tag{2.11}$$

where $f(x_1) = x_1(a-x_1)(x_1-1)$, $0 < a < 1$ (for excitable regime) and ϵ and b are positive constants. Here x_1, proportional to the membrane potential V, is the fast variable, and x_2 represents the slow variable. For $I_a = 0$ there can be no periodic solutions. If $I_a \neq 0$ then the steady state can become unstable and limit cycle oscillations are possible. The null clines for Eq. 2.11 are plotted in Fig. 2.3.

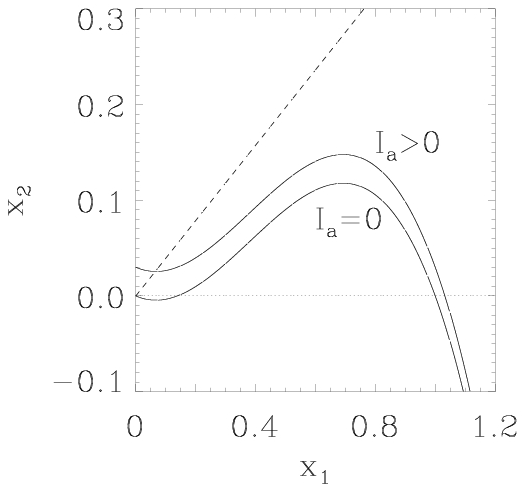

Figure 2.3: *Null clines for the FitzHugh-Nagumo system for the parameters:* $b = 2.54$, $\epsilon = 0.008$ *and* $a = 0.139$.

After scaling the time variable to $t' = \sqrt{b}t$, Eqs. 2.11 take the form:

$$\begin{aligned} \ddot{x}_1 &= -k(x_1 - q_-)(x_1 - q_+)\dot{x}_1 + I - x_1 + \frac{\epsilon}{b}f(x_1) \\ \text{with} \quad q_\pm &\equiv \frac{1}{3}[(a+1) \pm \sqrt{(a+1)^2 - 3(a+\epsilon)}], \end{aligned} \tag{2.12}$$

$k \equiv \frac{3}{\sqrt{b}}$ and $I = \frac{\epsilon I_a}{b}$. The dynamics of the FitzHugh-Nagumo system is preserved qualitatively and quantitatively to a very close approximation, when the cubic function $f(x_1)$ in the left hand side of Eq. 2.12 is neglected. The reason for this is that in the range $q_- < x_1 < q_+$ this function is very small compared to unity. Thus we obtain the following reduced model [7]:

$$\ddot{x}_1 = -k(x_1 - q_-)(x_1 - q_+)\dot{x}_1 + I - x_1 \tag{2.13}$$

This is the equation of a van der Pol - like oscillator parameterized by positive dynamical boundaries $q_- < x_1 < q_+$ (without these boundaries, the system would not show a refractory behaviour).

A further simplification of the reduced model in Eq. 2.13 is the *weighted step model* [7]. The smooth parabolic function $k(x_1 - q_-)(x_1 - q_+)$ is approximated by a step function $k'\sigma$ where $k' = \frac{k}{4}(q_- - q_+)^2$:

$$\begin{aligned} \ddot{x}_1 &= -\sigma k' \dot{x}_1 - x_1 + I \\ \sigma &= \begin{cases} -1 & \text{for } q_- < x_1 < q_+, \\ +1 & \text{otherwise} \end{cases} \end{aligned} \tag{2.14}$$

The above model represents the so-called *all-or-nothing* mechanism featuring either monotonic decay to a steady state below the barrier q_- or relaxation oscillation of asymptotically long period just above the threshold barrier.

As mentioned before, excitable behaviour appears near a bifurcation from a stable fixed point to a stable limit cycle. Two examples are the saddle-node bifurcation on an invariant circle (or Andronov bifurcation) [8, 9] and the Hopf bifurcation (or Andronov-Hopf bifurcation) [10].

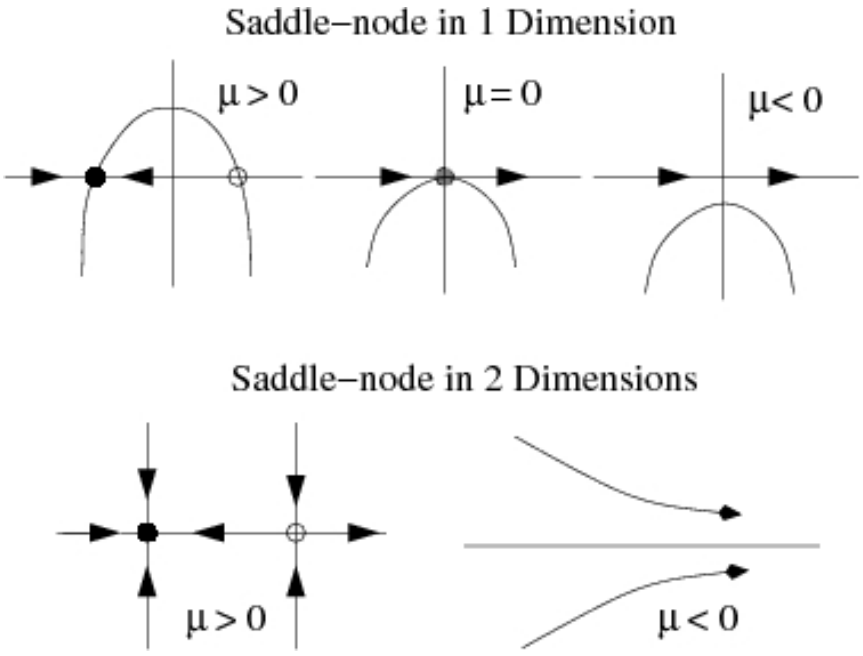

Figure 2.4: *Schematic presentation of the dynamics during the saddle-node bifurcation in one and two dimensional system.*

A saddle-node bifurcation can appear in any dimension and its mechanism consists in the creation and destruction of fixed points. As a parameter of the system is varied two fixed points, one stable and one unstable, move toward each other, collide and

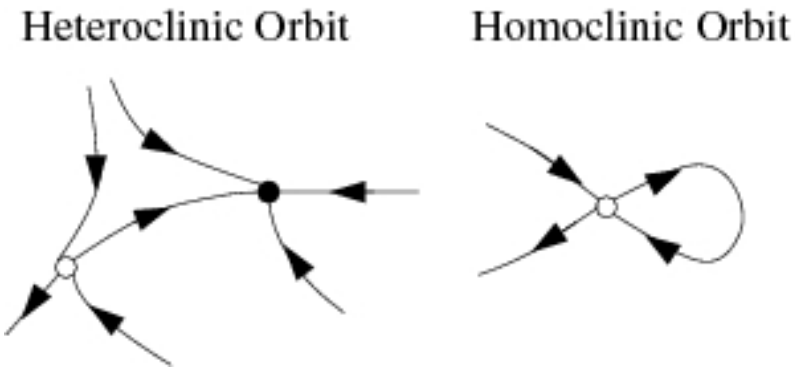

Figure 2.5: *Schematic presentation of the heteroclinic and homoclinic orbits.*

mutually annihilate. An example of a one dimensional system in which a saddle-node bifurcation occurs is $\dot{x} = \mu - x^2$ (see Fig. 2.4). If $\mu > 0$ there are two fixed points, when $\mu = 0$ the two fixed points coalesce and a half-stable fixed point appears. Finally for $\mu < 0$ the fixed points disappear. In two dimensions the mechanism is the same and also consists in the creation and annihilation of fixed points. In this case the behaviour of the trajectories near the fixed points are modelled with the so-called *normal form equations*[1]: $(\dot{x}, \dot{y}) = (\mu - x^2, -y)$, where the additional y direction in the state space is added. If $\mu > 0$ there are two fixed points, a stable node and an unstable saddle which are connected by a so-called heteroclinic connection (see Fig. 2.5) (there exist also other types of connections, e.g. the homoclinic connection which connects a saddle point to itself). At $\mu = 0$ a bifurcation occurs with two fixed points annihilating each other and finally for $\mu < 0$ there are no fixed points. .

A saddle-node bifurcation on an invariant circle appears for example in a model of an overdamped pendulum. The equation for a damped pendulum with a torque is the following:

$$mL^2\ddot{\theta} + b\dot{\theta} + mgL\sin\theta = \Gamma \tag{2.15}$$

where m is the mass of the pendulum, L its length, b is a viscous damping constant, Γ is a constant applied torque and θ is an angular variable. In the overdamped limit $b\dot{\theta}$ is assumed to be much larger than $mL^2\ddot{\theta}$ and we get the following equation which we write in a dimensionless form:

$$\dot{\theta} = \mu - \sin\theta \tag{2.16}$$

where $t \to t\frac{mgL}{b}$ and $\mu = \frac{\Gamma}{mgL}$. The parameter μ is the ratio of the applied torque to the maximum gravitational torque. Since viscosity is assumed to be very large, the oscillations are only possible because of the applied torque. If $\mu > 1$ then the applied torque

[1]The term normal form is used for a representative element, which is in the simplest and most manageable form.

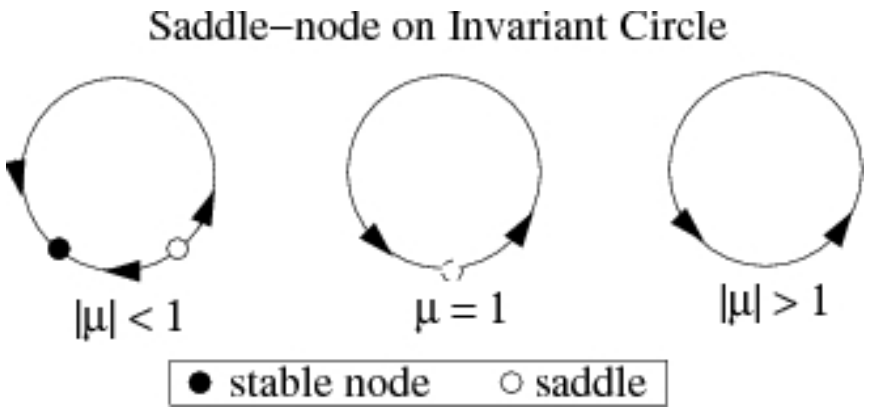

Figure 2.6: *Schematic presentation of the dynamics during the saddle-node bifurcation in Adler system.*

can never be balanced by the gravitational torque and the pendulum always makes an excursion over the unstable fixed point. If $\mu < 1$ the pendulum is not able to reach an unstable fixed point and it always returns to the stable fixed point. Note also that the rotation is nonuniform since gravity helps the applied torque on one side and opposes it on the other. Equation 2.16 appears not only in mechanics in the form of overdamped pendulum with a constant torque, but it also appears in condensed-matter physics to model the dynamics of the Josephson junction, as well as in biology to model oscillating neurons, firefly flashing rhythm and human sleep-wake cycle. Usually this prototype equation wears the name of *Adler's equation*. This equation preserves all features if the *sine* function is replaced by a *cosine* function:

$$\dot{\theta} = \mu - \cos\theta \tag{2.17}$$

where θ is an angular dimensionless variable (modulus 2π) and μ is the so-called control parameter. For $|\mu| < 1$, there are two fixed points at $x_{\pm} = \pm \arccos \mu$, one being a stable focus (x_{-}) and the other an unstable saddle point (x_{+}). If $|\mu| > 1$, there are no fixed points, and the flow consists of an oscillation of the variable x. This limit cycle develops through a saddle node on an invariant circle (Andronov) bifurcation at $\mu = \pm 1$ (see Fig. 2.6), where the two fixed points collide and annihilate. For $|\mu| < 1$, the system displays excitable behaviour: if we kick the system out of its stable state with a large enough perturbation, the trajectory returns to the initial state (modulo 2π) through a deterministic orbit that closely follows the heteroclinic connection of the saddle and the node. During this orbit (refractory period), the system is barely sensitive to external perturbations of moderate amplitude. It is worth noting that in a system with a saddle-node bifurcation the key element to obtain excitability is a heteroclinic connection between the manifolds of the fixed points.

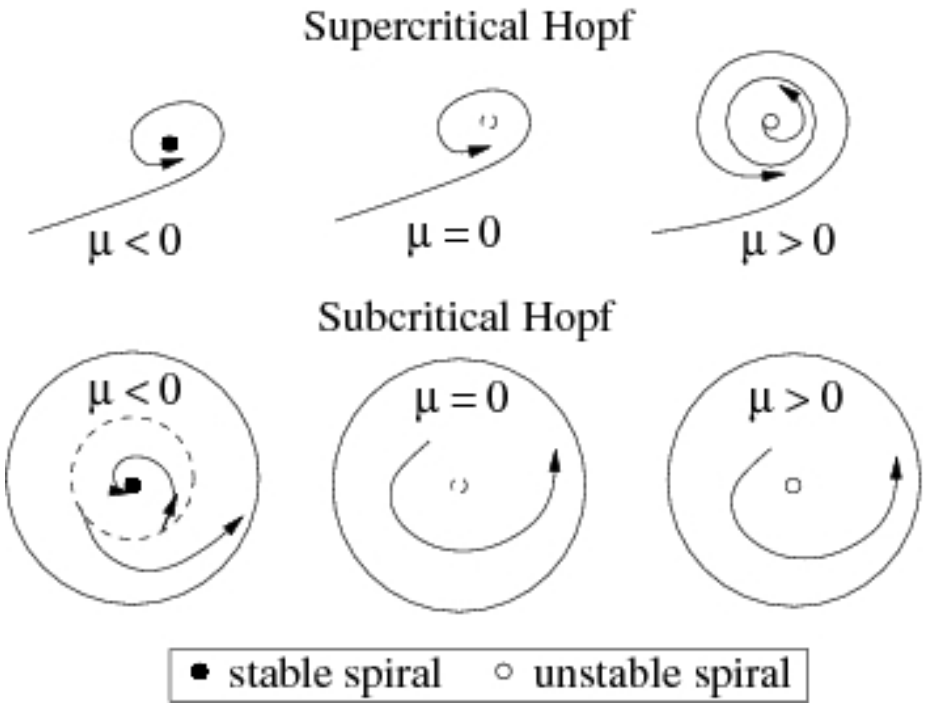

Figure 2.7: *Schematic presentation of the possible dynamics during the Hopf bifurcations.*

At variance with a saddle-node bifurcation, the Hopf bifurcation can occur only in two or more dimensions. The Hopf bifurcation can be either supercritical or subcritical. In terms of the flow in phase space, a supercritical Hopf bifurcation appears when a stable spiral changes into an unstable spiral surrounded by a limit cycle. The simplest example in which this type of bifurcation occurs is: $(\dot{r}, \dot{\theta}) = (\mu r - r^3, \omega)$ (see Fig. 2.7), where the parameter μ controls the stability of the fixed point $r = 0$ and ω gives the frequency of oscillations. For $\mu < 0$, there exists a stable spiral, meanwhile for $\mu > 0$ there exists a stable limit cycle.

One possible scenario for a subcritical Hopf bifurcation appears in a system: $(\dot{r}, \dot{\theta}) = (\mu r + r^3 - r^5, \omega)$ (see Fig. 2.7). For $\mu < 0$ the system has two attractors: a stable limit cycle and a stable fixed point at the origin. Between these two attractors lies an unstable limit cycle. At $\mu = 0$ the unstable limit cycle shrinks to the origin, which becomes unstable, and the stable limit cycle remains but with larger amplitude of oscillations. Subcritical Hopf bifurcations occur when modelling the dynamics of nerve cells, but also in aeroelastic flutter and other vibrations of airplane wings and in instabilities of fluid flows.

A definition of the Hopf bifurcation is formulated in the Hopf bifurcation theorem [11], which states that, in a given system, the Hopf bifurcation appears if when

changing some parameter of the system we observe that the real part of both eigenvalues (in two-dimensional case) changes from negative to positive. The parameter value for which the eigenvalues are purely imaginary (the real part vanishes meanwhile imaginary ones are non-zero) corresponds to the bifurcation point.

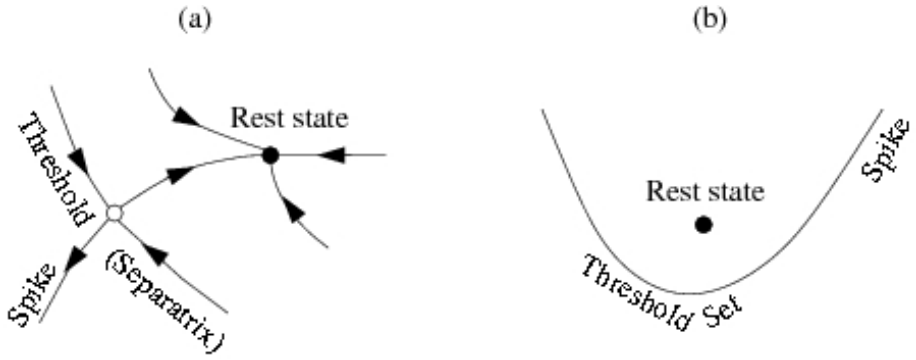

Figure 2.8: *Schematic presentation of the thresholds in Class 1 (a) and Class 2 (b) excitable neurons.*

Neurons were categorized by Hodgkin in 1948 [12] into two classes according to the bifurcation type: class 1 excitable systems are the ones with a saddle-node bifurcation on invariant circle (for example Adler system, Morris-Lecar, Connor [13] and Wilson-Cowan [14] models). Class 2 excitable systems are characterized by the appearance of the Hopf bifurcation, as in the Hodgkin-Huxley and FitzHugh-Nagumo models. The type of bifurcation determines the neuro-computational properties of the cells, which are briefly described below.

When the rest state is near a saddle-node bifurcation (Class 1 excitability) the cell has a well-defined threshold determined by the stable manifold of the saddle (see Fig. 2.8a), often referred to as separatrix since it separates two regions of the phase space having different qualitative behaviour (attracting and repelling). Thus, only the perturbation which is larger than the distance between the saddle and the node can induce a spike in the system and for that reason the response of such a system is often called all-or none. It can fire spikes with an arbitrary low frequency which increases with increasing of the applied current (see Fig. 2.9a). Moreover, the system under consideration acts as an integrator, i.e. the higher the frequency of the incoming pulses, the sooner it fires. It was shown numerically in [15] and analytically in [13] that Class 1 excitable neurons with saddle-node bifurcation are difficult to synchronize.

In contrast, when the rest state is near a Hopf bifurcation (Class 2 excitability), the cell does not have a well-defined threshold manifold and one can talk about threshold set rather than one threshold value (see Fig. 2.8b). Such a system fires in a certain frequency range which is relatively insensitive to the changes of the applied current (see Fig. 2.9b). Moreover it acts as a resonator, i.e. it responds preferentially to a certain

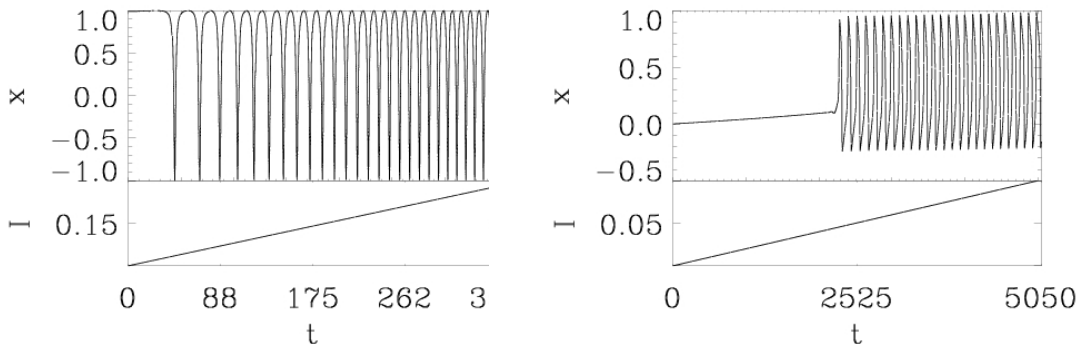

Figure 2.9: *Response to the external stimulus of (a) Adler system (Class 1 excitable system) and (b) FitzHugh-Nagumo system (Class 2 excitable system).*

(resonant) frequency of the input. An increase of the input frequency can delay or terminate its firing. In particular the resonator responds to a pair of stimuli whose timing corresponds to the period of the small amplitude damped oscillations existing at the equilibrium. Thus such a system acts as a bandpass filter extracting the component of the external input that corresponds to the resonant frequency and neglects the rest of the spectrum. This characteristics is an important information processing capability, since it can enable the selective communication between neurons.

Since real excitable cells in the brain or heart occupy a finite volume, then more realistic models for these cells should contain spatial variables. The spatiotemporal model for FitzHugh-Nagumo system can be obtained by simply adding diffusive terms:

$$\begin{aligned} \dot{x}_1 &= x_1(a - x_1)(x_1 - 1) - x_2 + I_a + D_1\nabla^2 x_1 \\ \dot{x}_2 &= \epsilon(x_1 - bx_2) + D_2\nabla^2 x_2 \end{aligned} \tag{2.18}$$

where $D_{1,2}$ are diffusion constants. The inclusion of spatial dimensions in the system allows one to observe travelling waves (in all dimensions), spiral waves (in two dimensions) and scroll waves (in three dimensions). The study of spatiotemporal excitable systems attracted a lot of attention because they can be used to model arrhythmias as atrial flutter and fibrillation in the heart tissue [16] or reverberating cortical depression waves in the brain cortex [17]. An excitable behaviour of spatiotemporal dynamics was also observed in chemical reactions, for instance in Belousov-Zhabotinskii reaction [18, 19] and in the reaction of catalytic oxidation of carbon monoxide on a platinum (110) surface [20].

2.2 Chaotic systems

Chaotic behaviour can appear not just in complex systems, but also in simple ones with only few active degrees of freedom. Its main characteristic is an aperiodic behaviour which looks random, despite of the fact that we know the deterministic equations describing the time-evolution of the system. The long-time prediction in a chaotic system is impossible. This is because of the sensitive dependence to the initial conditions: nearby trajectories of a given variable separate exponentially fast; in other words, the system has a positive Lyapunov exponent (see Section 2.2.1). Nevertheless, a chaotic system is deterministic: if we knew "exactly" (with arbitrary accuracy) the values of the initial conditions, we could predict the time evolution of the trajectory. However, knowing the initial conditions with the highest precision is in principle impossible. Dripping water from a faucet is a well-known example of chaotic dynamical systems easily seen in daily life. In 1984 Shaw [21] investigated this problem and showed that when increasing the velocity of the water flow from the faucet, the time intervals between the drops change from regular to chaotic ones.

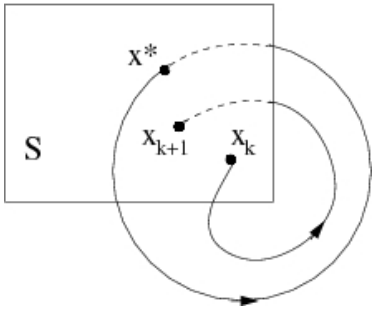

Figure 2.10: *The Poincaré map: a carefully chosen (curved) plane in the phase space that is crossed by almost all orbits of the system.*

Deterministic chaos was discovered by Henri Poincaré at the end of the 19th century. He studied extensively the problem of the motion of three objects with mutual gravitational attraction, the so-called three-body problem. Poincaré found that there can exist non-periodic orbits which never approach a fixed point, nevertheless stay bounded in the phase space. He developed a very useful tool for the visualization of periodic, quasi-periodic and chaotic flows in a phase space of more than two dimensions, the so-called Poincaré map. The Poincaré map **P** is a curved plane in the phase space that is crossed by almost all orbits. The map relates two consecutive intersection points that come from the same side of the plane. If $x_k \in S$ (see Fig. 2.10) denotes the kth intersection with the surface S, then the discrete representation of a continuous dynamical system, the Poincaré map, is defined by:

$$\mathbf{x}_{k+1} = \mathbf{P}(\mathbf{x}_k) \tag{2.19}$$

The trajectory starting at $\mathbf{x}^*$ returns to $\mathbf{x}^*$ after some time T, and is therefore a closed orbit for the original system $\dot{\mathbf{x}} = \mathbf{f}(\mathbf{x})$. On the other hand the point $\mathbf{x}^*$ is a fixed point of the Poincaré map $\mathbf{P}$ if $\mathbf{P}(\mathbf{x}^*) = \mathbf{x}^*$. Thus the map $\mathbf{P}$ has one dimension less than the phase space.

Chaos appears only in nonlinear systems. A nonlinear system can be defined as one in which the response is not proportional to the stimulus. Significant qualitative and quantitative changes, when some parameters of the system are varied, can happen only in the presence of nonlinearity, which is the crucial component that induces irregularity. Such sudden changes in the behaviour of the system are called bifurcations and a cascade of bifurcations lead to the so-called route to chaos. It is important to mention that the nonlinearity is crucial for a system to be chaotic, but not the opposite: not all nonlinear systems are necessarily chaotic. It is because an essential characteristic of a system to be chaotic is also its dimensionality: it was shown that chaos in a system described by a differential equation can appear only when the dimension of the system is larger than two. It is a result of the Poincaré-Bendixson theorem [22], which shows that in two-dimensional systems, only fixed points, stable periodic orbits and heteroclinic cycles can exist (see section 2.1).

There exist two famous chaotic systems which are cited whenever the chaotic dynamics is discussed, namely, the Rössler and the Lorenz systems. In 1976 Otto Rössler found the inspiration from a taffy-pulling machine for the derivation of his dynamical system [23]. The taffy-pulling machine is a machine to make taffy candies. With each successive cycle of the machine, the taffy is stretched and kneaded, and the points move progressively farther away from each other. Thus, after only a few number of cycles, the points can be separated by large distances, and it would be impossible to predict where they are. Rössler system has one nonlinearity xz and it is three-dimensional:

$$\begin{aligned} \dot{x} &= -y - z \\ \dot{y} &= x + a\,y \\ \dot{z} &= b + z\,(x - c) \end{aligned} \tag{2.20}$$

where a, b and c are constant parameters. To observe the route to chaos in this system usually $a = b = 0.2$ are fixed meanwhile the parameter c is varied. When c is approximately 5 the chaotic attractor can be observed. In the Rössler system the stretching and folding processes take place, being the reason for the long-term unpredictability of this chaotic system. The working mechanism of the taffy-pulling machine is also described by other mathematical models, such as the so-called horseshoe map developed by Stephen Smale [24].

The Lorenz system was derived in the early 1960's by Edward Lorenz. He described the phenomenon of "sensitivity to initial conditions" using a simple system [25] being

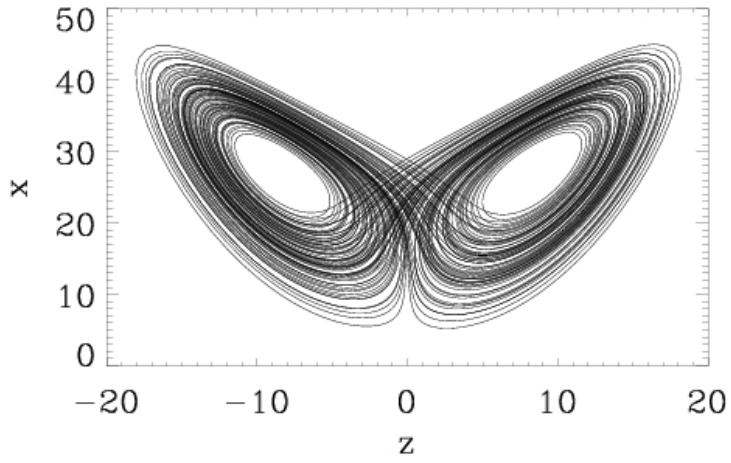

Figure 2.11: *A projection of the three-dimensional Lorenz attractor into $x - z$ phase space. The typical parameters has been used in Eq. 2.21: $\sigma = 10$, $b = 8/3$ and $r = 28$.*

a simplified version of a mathematical model of the convection in the atmosphere:

$$\begin{aligned} \dot{x} &= \sigma(y - x) \\ \dot{y} &= -x\,z + r\,x - y \\ \dot{z} &= x\,y - b\,z \end{aligned} \tag{2.21}$$

where σ, r and b are constant parameters. Equations 2.21 describe the motion of an incompressible fluid contained in a cell which has a higher temperature at the bottom and lower temperature at the top. He sketched the outlines of one of the first recognized chaotic attractors (see Fig. 2.11). In Lorenz's meteorological computer modelling, he found the underlying mechanism of deterministic chaos: simply-formulated systems with only a few variables can display a highly complicated behavior that is unpredictable. He plotted the time series for slightly different input numbers and saw that tiny differences in one variable had strong effects on the outcome of the whole system. He discovered that a simple-looking deterministic system could have extremely erratic dynamics over a wide range of parameters where the solutions oscillate irregularly never exactly repeating but always remaining in a bounded region of phase space. This was one of the first clear demonstrations of sensitive dependence to the initial conditions and of its occurrence in a simple, but physically relevant model. In a 1972 meeting [26], Lorenz gave a talk entitled "Predictability: Does the Flap of a Butterfly's Wings in Brazil set off a Tornado in Texas?". This sensitivity is now known as the *butterfly effect*.

While two-dimensional motions give rise to very simple attractors, such as fixed points and limit cycles, three-dimensional motion can be chaotic and give rise to what are known as strange attractors, i.e. attractors that can have very complex structure.

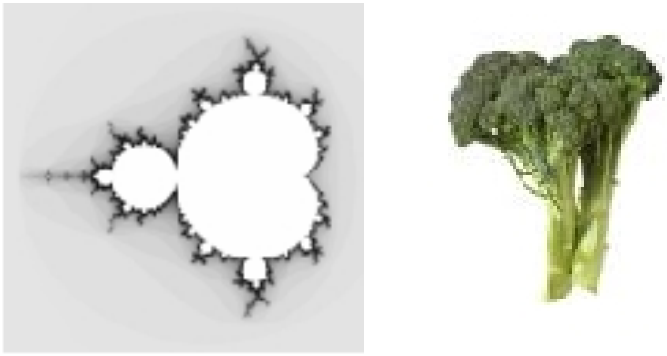

Figure 2.12: *From left to right: Mandelbrot set and broccoli.*

The attractor is called strange if it has a fractal dimension. A fractal is a geometrical object that is irregular on all length scales. As an example, the coastlines have fractal structure since its length depends on the scale at which the measurement is done. Apart of the coastlines, fractal structures are very common in nature in micro and macro scales and can be found for instance in the snowflakes, blood vessels and nervous systems of animals, in the broccoli and trees, and even in the stellar constellations. In 1975 Benoit Mandelbrot highlighted the common properties of these objects such as self-similarity, scale invariance and non-integer dimension [27]. He generated on his computer for the first time the fractal structure, called the Mandelbrot set (see Fig. 2.12). Other famous mathematical fractals are the Koch curve, Sierpiński triangle and Cantor set.

However, most real systems are composed of a huge number of particles and influenced by uncontrolled external effects exhibiting a random behaviour instead of chaotic. Such non-chaotic systems with irregular dynamics are called stochastic systems. Stochastic models include additive or multiplicative (parametric) noise [28] which is an explicit function of time. Thus stochastic systems are non-autonomous; in autonomous systems the (independent) time variable does not appear explicitly [29]. Contrary to the chaotic systems, the stochastic ones exhibit unpredictable dynamics even for short times. Many biological systems display stochastic behaviours, for example neurons in the brain [30], cardiorespiratory systems [31] or population systems [32]. For this reason a great deal of interest has been given to the synchronization properties of stochastic systems [33].

2.2.1 Lyapunov exponents

The Lyapunov exponents of a dynamical system $\dot{\mathbf{x}} = \mathbf{F}(\mathbf{x}, t)$ is a set of numbers that characterize the rate of separation of infinitesimally close trajectories evaluated from slightly different initial conditions. To obtain the Lyapunov spectra, an infinitesimal small ball with radius dr set at the initial state of a trajectory is used (see Fig. 2.13). After a finite time t all orbits which have started in that ball will be deformed into an ellipsoid. Following this description, the ith Lyapunov exponent is defined as follows:

$$\lambda_i = \lim_{t\to\infty} \frac{1}{t} \ln \left| \frac{dl_i(t)}{dr} \right| \tag{2.22}$$

where N is the dimension of the system $\dot{\mathbf{x}} = \mathbf{F}(\mathbf{x}, t)$, $i = 1, \ldots, N$ and $dl_i(t)$ is the radius of the ellipsoid along the ith direction. For N-dimensional dissipative system there are N Lyapunov exponents since the divergence of the trajectories can occur for any variable of the given system. The largest Lyapunov exponent represents the largest rate of exponential divergence.

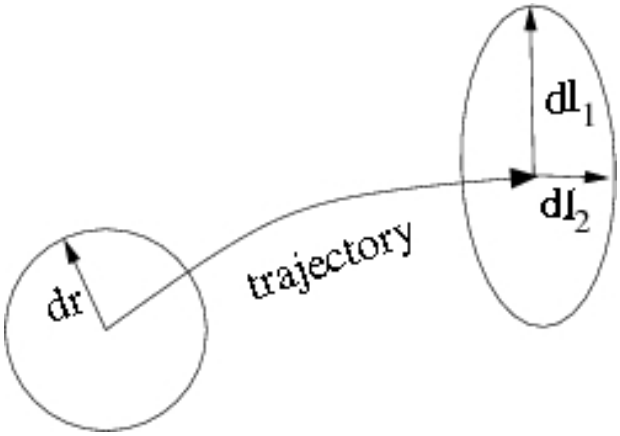

Figure 2.13: *Schematic illustration of the trajectory divergence.*

The initial N-dimensional volume in the phase space can be described by the formula:

$$V(t) = V_0 e^{(\lambda_1+\lambda_2+\ldots+\lambda_N)t} \tag{2.23}$$

For Hamiltonian systems which are conservative, the Lyapunov exponents exist in opposite signed pairs $\pm\lambda_i$, such that they add up to 0 ($\sum_i \lambda_i = 0$) and thus conserve the volume $V(t)$. For a one-dimensional harmonic oscillator (with a two-dimensional phase space), the two Lyapunov exponents are $\lambda_1 = \lambda_2 = 0$ and the motion in this case is not chaotic. For autonomous and continuous systems, one Lyapunov exponent must

always be equal to 0, since a perturbation along the path does not give divergence. Reversely to the conservative systems, in dissipative ones the existing Lyapunov exponents satisfy the following condition $\sum_i \lambda_i < 0$. It is because the phase space of dissipative systems does not conserve its volume during the time evolution (the volume collapses). Therefore, for a two-dimensional phase space of a dissipative system, $\lambda_1 = 0$ and $\lambda_2 < 0$. For a three-dimensional phase space, there are three possibilities:

1. $\lambda_1 = 0$, $\lambda_2 = 0$ and $\lambda_3 < 0$
2. $\lambda_1 = 0$, $\lambda_2 <$ and $\lambda_3 < 0$
3. $\lambda_1 = 0$, $\lambda_2 > 0$ and $\lambda_3 < -\lambda_2 < 0$

Condition 3 is valid for three-dimensional chaotic system, in which at least one Lyapunov exponent is positive and its absolute value has to be larger than the absolute value of the negative Lyapunov exponent. For N-dimensional system it is common to just refer to the largest Lyapunov exponent, because it determines the predictability of a dynamical system.

One of the interests of physics, as well as of other sciences, is to predict the future states of the systems under interest. The simplest method for prediction of chaotic systems was introduced by Lorenz [25]. It is based on the idea that short sequences of points in the chaotic series repeat in all series. In particular the short sequence from the end of some measured time series has a similar appearance at the beginning of that series. Thus taking into account the past, we can predict the future. This method can be useful when the dimension of an attractor is not too high, and the time series contain many points. Let us assume that the system is characterized by a positive Lyapunov exponent λ and the initial state is known with an accuracy ϵ. Then, after time T, the uncertainty of that coordinate grows as:

$$L \sim \epsilon e^{\lambda T} \tag{2.24}$$

where T is the prediction time for the system. Thus the limit for the predictability of a chaotic systems is related to the largest positive Lyapunov exponent. The prediction time is proportional to the inverse of the Lyapunov exponent: $T \sim \lambda^{-1}$. For large λ's the prediction time decreases, meanwhile for smaller λ's it increases. Also the quality of prediction depends significantly on the initial conditions.

2.2.2 Reconstruction of an attractor

Chaotic states exist in the world around us although it is very difficult to construct proper mathematical models for them. The problem lays in the judgement of whether the observed phenomena, which are the sources of our experimental data, are chaotic or not. Sometimes the periodic oscillations seem to be chaotic due to fluctuations of some parameter of the system and the use of filters to eliminate these fluctuations is dangerous because it can destroy information about the dynamics. The first step to overcome this problem is to reconstruct the chaotic attractor, if it exists. Usually we have no information about all the degrees of freedom of the observed system, but we very often have only the time series of one observable to extract useful information. The method to extract information from the time series of a single variable was developed by Packard [34] with mathematical background given by Takens [35] and Mané [36]. Reconstruction of the chaotic attractor from a single time series requires the creation of additional variables. These variables, displayed in the low-dimensional phase space, will reveal the geometrical structure of the dynamical system. Such a geometrical structure is called *reconstructed attractor* and it is treated as a topological equivalence of an attractor which would be obtained by solving numerically the differential equations describing the given system, if they could be known. In particular, the dimension and the Lyapunov exponents are ideally the same for the real and reconstructed attractor. The method for the reconstruction of the attractor is called *embedding method*. Having a time series $x(t)$ (the stroboscopic points) measured with the sampling time Δt, we construct the following embedding vectors:

$$\begin{aligned} y_1(t) &= x(t), \\ y_2(t) &= x(t+T), \\ y_3(t) &= x(t+2T), \\ &\vdots \\ y_d(t) &= x(t+(d-1)T) \end{aligned} \tag{2.25}$$

where d is the dimension of the embedding vector and T is the delay time defined as an integer multiplication of Δt. For example, to reconstruct the chaotic attractor of the three dimensional Lorenz system $\{x(t), y(t), z(t)\}$ defined in Eq. 2.21, we take $x(t)$ as the measured variable and construct from it the embedding vector with $d = 3$. We obtain the new set of variables $\{x(t), x(t+T), x(t+2T)\}$. In Fig. 2.14b it is seen that indeed the reconstructed Lorenz attractor is similar to the original one for $\{x(t), y(t), z(t)\}$ plotted in Fig. 2.11, but only if the appropriate delay time T is chosen. The choice of the proper delay time T is far from trivial. If it is too small the coordinates $x(t), x(t+T), x(t+2T), \ldots$ are almost equal to each other (Fig. 2.14a). On the other hand we know that the

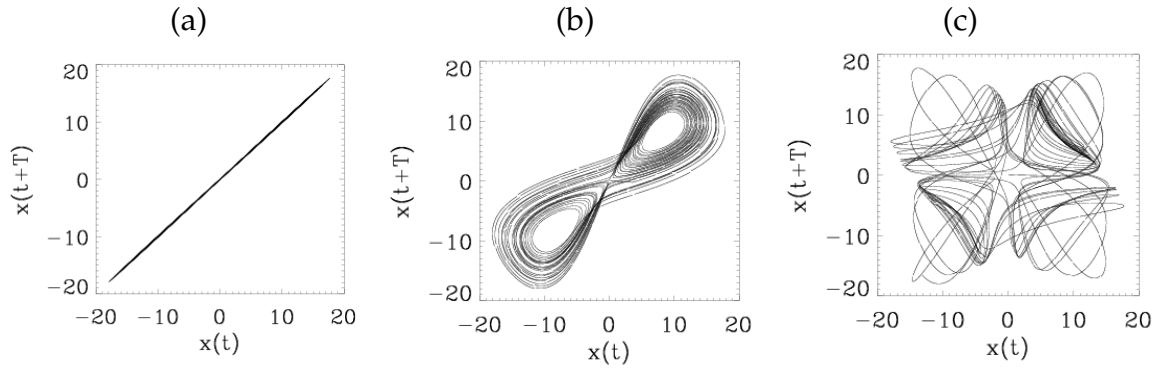

Figure 2.14: *The projection of the Lorenz attractor obtained from the embedding of $x(t)$ variable into the new system $\{x(t), x(t+T), x(t+2T)\}$ with the delay time: (a) $T = 10\Delta t$, (b) $T = 1000\Delta t$ and (c) $T = 10000\Delta t$, where $\Delta t = 10^{-4}$.*

correlations between dynamical states of a chaotic system last during quite a short time, which depends on the values of the positive Lyapunov exponents (see Section 2.2.1). Thus if T is too long, the coordinates become uncorrelated (Fig. 2.14c). The magnitude of T depends also on the magnitude of the sampling time Δt which is determined during the experiment.

There are some methods to properly estimate the delay time T. If some approximate periodicity exists in the system, then we choose the value slightly smaller than the period. If there is no dominant period in the system then we calculate the correlation between a pair of points as a function of their separation in time:

$$C(s) = \frac{\frac{1}{N}\sum_t x(t)x(t+s) - \frac{1}{N}\sum_t x(t)\frac{1}{N}\sum_t x(t+s)}{\frac{1}{N}\sum_t x(t)^2 - [\frac{1}{N}\sum_t x(t)]^2} \tag{2.26}$$

where the sums are taken over all points in the time series. Next we define s_0 as the time at which $C(s)$ crosses zero for the first time and we take $T = s_0$.

Another method [37] to estimate the delay time T is based on the calculation of the mutual information. Mutual information is a measure of the probability that the neighboring points $x(t)$ and $x(t+s)$ are not statistically independent. If $P(x(t))$ and $P(x(t+s))$ are the probability distributions of neighboring points and $P(x(t), x(t+s))$ is the joint probability distribution, the mutual information is defined as:

$$I(s) = \sum_t P(x(t), x(t+s)) \ln \frac{P(x(t), x(t+s))}{P(x(t)) \cdot P(x(t+s))} \tag{2.27}$$

Then, the delay time is defined as $T = s_{min}$, where s_{min} is the first value of s for which the mutual information is minimum.

There are some cases where the criterion for the delay time estimation does not work. Then the best method used by scientists is to adjust the delay time by trail and error.

2.2.3 Control of chaos

The control of dynamical systems is a classical problem of engineering science. One method for stabilizing unstable periodic orbits is the Ott-Grebogi-Yorke control method [39]. This method uses small perturbations in a certain parameter to control the trajectory of the system. First the unstable low-periodic orbits that are embedded in the chaotic attractor are determined. After examination of these orbits, the one which guarantees the improved system performance is chosen. Then, small time-dependent parameter perturbations are applied to stabilize the already existing, but unstable, periodic orbit. Let us consider the system:

$$\dot{\mathbf{x}} = \mathbf{f}(\mathbf{x}, p, t) \tag{2.28}$$

where $\mathbf{x}$ is the vector variable and p is a scalar parameter available for an external adjustment. Let us assume that the parameter p can be modified within a small interval around its nominal value p_0 such that $p \in [p_0 - \delta p, p_0 + \delta p]$, where δp is the maximum admissible change in the parameter p. Then a two-dimensional Poincaré surface S is chosen defining a Poincaré map $\mathbf{P}$. The trajectory of the system 2.28 is represented by the point x on the surface S through which it crosses for the first time. If we want to stabilize a period-1 orbit (an unstable fixed point x_F of the map $\mathbf{P}$) existing at the parameter $p = p_0$, we make the first-order approximation of $\mathbf{P}$ in the neighbourhood of (x_F, p_0):

$$\mathbf{P}(x, p) \approx \mathbf{P}(x_F, p_0) + \mathbf{A} \cdot (x - x_F) + \mathbf{w} \cdot (p - p_0) \tag{2.29}$$

where $\mathbf{A}$ is a Jacobian matrix of $\mathbf{P}$ at x_F and $\mathbf{w} = \frac{\partial \mathbf{P}}{\partial p}(x_F, p_0)$ is the derivative of $\mathbf{P}$ with respect to the parameter p. Stabilization of the fixed point is achieved by realizing feedback of the form:

$$p(x) = \mathbf{c}^T (x - x_F) \tag{2.30}$$

where $\mathbf{c}$ is computed using the expression:

$$\mathbf{c} = -\frac{\lambda_A}{\mathbf{f}_A^T \cdot \mathbf{w}} \mathbf{f}_A^T \tag{2.31}$$

where λ_A is the unstable eigenvalue and $\mathbf{f}_A$ is the unstable eigenvector of $\mathbf{A}$.

The Ott-Grebogi-Yorke control method relies on the fact that chaotic systems are extremely sensitive to initial conditions and that there are typically an infinite number of unstable periodic orbits that co-exist with chaotic motion. For instance, in the case of the so-called transient chaos [40], this method fails, because the time evolution of the system temporarily stops being chaotic. From the point of view of this method, the

existence of chaos in a real system can be beneficiary since the system would have the possibility to choose the best periodic orbit for which the performance is optimal.

The authors of the Ott-Grebogi-Yorke method suggested that such a flexibility of chaotic system control can be essential for higher life forms, in particular that chaos can be a necessary ingredient in the brain functioning. However, in real applications, a continuous analysis of the state of the system is required. The changes in parameters can only be discrete since the Ott-Grebogi-Yorke method uses the Poincaré map of the system. Thus the method can be used only to stabilize those orbits whose largest Lyapunov exponent is small compared to the reciprocal of the time interval between parameter changes [41]. The Ott-Grebogi-Yorke control method was for the first time successfully applied to control a parametrically driven magnetoelastic ribbon [42]. Other successful experimental realizations of this method concerned many other different systems, e.g. in a chaotic Duffing's oscillator [43] and a neural tissue [44].

Another control method was introduced by Pyragas, the Delayed Feedback Control method [45]. This method uses a delayed feedback to stabilize the system. The Delayed Feedback Control method consists in applying to the system a term which is the difference between the current state of the system and its state one period in the past so that the control signal vanishes when the stabilization of the desired orbit is attained. We consider the system of the form given by Eq. 2.28. The control is achieved via the modification of the parameter p in the following way:

$$p(t) = K(y(t-\tau) - y(t)) \tag{2.32}$$

being τ the period of the oscillations we want to stabilize from the chaotic ones. The Delayed Feedback Control method has been experimentally implemented in many systems, e.g. in chaotic flows, cardiac systems and others. This method is efficient for stabilizing unstable periodic orbits of chaotic systems. The Delayed Feedback Control method applies a feedback proportional to the deviation of the current state of the system with respect to its state one period in the past. For this reason the method is also called time-delay auto-synchronization, since the stabilization of the desired orbit occurs due to the synchronization between the current state of the system with its delayed one.

Chaotic signals are composed of many unstable orbits with different periods. Periodic dynamics, with a period T, in the chaotic system can be stabilized by using the Delayed Feedback Control method: for this purpose it is necessary to apply the delayed signal with a delay time τ which corresponds to the desired period T, i.e. $\tau = T$. The fundamental property of a chaotic attractor is that it contains a countable but infinite number of unstable periodic orbits. The trajectories of the chaotic attractor are dense because if we choose in an arbitrary way a point within the attractor and a small sphere of radius ϵ around it, the trajectory will eventually pass through this sphere after a finite

time (which can be very long). The fact that the chaotic system is sensitive to small perturbations helps in controlling it. Thus by applying a perturbative, small control terms one can obtain the desired effect. The advantage of this method is that it only requires a priori the knowledge of the period of the system, and does not require any previous computation.

Since the control method requires the use of delayed variable, the modified system becomes hard to treat analytically even through linear stability analysis. Nevertheless there are some general analytical result on stability of this method [46, 47, 48, 49]. It was shown that Delayed Feedback Control method works only for low dimensional systems whose unstable periodic orbits are originated from a period doubling bifurcation (T-periodic orbits). It was also proven that the steady state can never be stabilized if the system has an odd number of real positive eigenvalues [50]. This limitation was overcome by introducing into a feedback loop an additional unstable degree of freedom [51]. Such a feedback loop with an additional unstable degree of freedom serves to construct an adaptive controller for stabilizing unknown states of the dynamical system [52]. As an example for two dimensional systems, the limitation states that only an unstable focus and node can be stabilized, meanwhile a saddle-type steady states require an additional unstable degree of freedom [50].

2.3 Reaction-diffusion systems

As the name reveals, the reaction-diffusion models require two ingredients : reaction and diffusion. Fick's law of diffusion establishes that the flux J of some matter is proportional to the gradient of concentration of the matter:

$$J = -D\frac{\partial c}{\partial x} \tag{2.33}$$

where $c(x,t)$ is the concentration of the matter and D its diffusivity. The minus sign indicates that diffusion transports matter from high to low concentration. The conservation law establishes that the rate of change in the amount of matter in a given region is equal to the rate of flow across the boundary plus any matter that is created within the boundary. The general conservation equation establishes that the rate of change of the amount of matter in the volume V is equal to the rate of flow of matter across the surface S enclosing V plus the matter created in V:

$$\frac{\partial}{\partial t}\int_V c(\mathbf{x},t)dv = -\int_S \mathbf{J}\cdot\mathbf{ds} + \int_V f dv \tag{2.34}$$

where $\mathbf{J}$ is the flux of matter and f represents the source of matter and may depend on c, $\mathbf{x}$ and t. We apply the divergence theorem to the surface integral assuming that $c(\mathbf{x},t)$ is continuous:

$$\int_V \left[\frac{\partial c}{\partial t} + \nabla\cdot\mathbf{J} - f(c,\mathbf{x},t)\right] dv = 0 \tag{2.35}$$

Thus we get:

$$\frac{\partial c}{\partial t} + \nabla\cdot\mathbf{J} = f(c,\mathbf{x},t) \tag{2.36}$$

Introducing $\mathbf{J} = -D\nabla c$ into Eq. 2.36 we get:

$$\frac{\partial c}{\partial t} = f + \nabla\cdot(D\nabla c) \tag{2.37}$$

where D can be function of $\mathbf{x}$ and c. When considering many interacting species or chemical components Eq. 2.37 becomes:

$$\frac{\partial \mathbf{u}}{\partial t} = \mathbf{f} + \nabla\cdot(D\nabla\mathbf{u}) \tag{2.38}$$

where D is now a matrix (diagonal if there is no cross diffusion among the species or chemicals) and $\mathbf{u}$ is a complex vector. Equation 2.38 is called reaction-diffusion or interacting population diffusion system. This equation was proposed as a model for the

chemical basis of morphogenesis by Turing [53]. If $f = 0$ then the diffusion process will lead to the homogenous solution in which all particles will be distributed uniformly in space as $t \to \infty$. To observe an unstable solutions and spatiotemporal chaos is necessary to choose the function f to be nonlinear, and for simplicity, of the lowest possible order. The simplest example of a bifurcation leading to an oscillatory behavior in two-dimensional system is a supercritical Hopf bifurcation during which a stable focus becomes unstable upon change of an appropriate control parameter, and a stable limit cycle appears. Close to the bifurcation point the oscillations are harmonic and their amplitudes show a square dependence with the distance to the bifurcation point. The dynamics of the system undergoing the Hopf bifurcation, in a small neighborhood of the rest state is described by the normal form [3]:

$$\dot{z} = (a + ib)z \pm z|z|^2 \tag{2.39}$$

where z is a complex variable and a and b are constant parameters. The functional form of the right hand side in Eq. 2.39 was used by Landau to describe phase transitions, like the transition between liquids and solids, or the transition between a magnetic and a normal matter. To describe a phase transition, he introduced a function or order parameter that is zero in one phase (liquid) and different from zero in the other phase (solid). In this case it is assumed that the parameter that drives the transition is the temperature.

Adding the spatial dimension and assuming the assymetric coupling we get:

$$\frac{\partial z}{\partial t} = (a + ib)z \pm z|z|^2 + D\frac{\partial^2 z}{\partial x^2} \tag{2.40}$$

Equation 2.40 displays a rich variety of spatiotemporal dynamics. It has monostable, bistable, excitable, oscillatory stable or unstable (chaotic) solutions, depending on the values of the constant parameters a, b and D. Rescaling z and redefining the parameters we arrive to the complex Ginzburg-Landau (CGL) equation:

$$\dot{A} = \epsilon A - (1 + ic_2)|A|^2 A + (1 + ic_1)\frac{\partial^2 A}{\partial x^2} \tag{2.41}$$

where $A(x,t) \equiv \rho(x,t)e^{i\phi(x,t)}$ is a complex field of amplitude ρ and phase ϕ. The space variable x is defined over $0 \leq x \leq L$ where L is the system length. ϵ is a control parameter inducing instability if it is positive, c_2 is a measure of the nonlinear dispersion and finally c_1 is the linear dispersion parameter. This model was initially phenomenological but it appeared later that a rigorous microscopic derivation is possible in some cases. Eq. 2.41 is also used in particle physics to describe the appearance of massive particles like Higgs bosons. For $c_1 = c_2 = 0$ Eq. 2.41 reduces to the so-called real Ginzburg-Landau equation which is used to describe superconductivity in the absence of a magnetic field. In the limit $c_1, c_2 \to \infty$ the equation reduces to the nonlinear Schrödinger equation with the well-known soliton solutions.

Equation 2.41 admits a plane wave solutions of the form:

$$A_q = \sqrt{\epsilon - q^2} e^{i(qx+\omega' t)} \tag{2.42}$$

where q is the wave number in a Fourier space bounded by $-\sqrt{\epsilon} \leq q \leq \sqrt{\epsilon}$ and $\omega' = -c_2 - (c_1 - c_2)q^2$ is the dispersion relation. All plane waves become unstable when crossing the so-called Benjamin-Feir or Newell line (valid for $\epsilon = 1$) $c_1 c_2 = -1$ [54]. Above this line different regimes are identified: defect turbulence, phase turbulence, bichaos and spatio-temporal intermittency (see Fig. 2.15). Defect turbulence is a strongly disordered region, in which defects as well as other localized structures appear, displaying a rich dynamics. Phase turbulence is a state which is weakly disordered in amplitude and strongly disordered in phase. Bichaos is an alternating mixture of phase and defect turbulence states. In the spatio-temporal intermittency region stable travelling waves interrupted by turbulent bursts exist. The Ginzburg-Landau equation is a universal model describing the evolution of an order parameter (as is often called model A in analogy with phase transitions) during which the homogeneous state loses stability through an oscillatory Hopf bifurcation. As an example, it can be derived from the

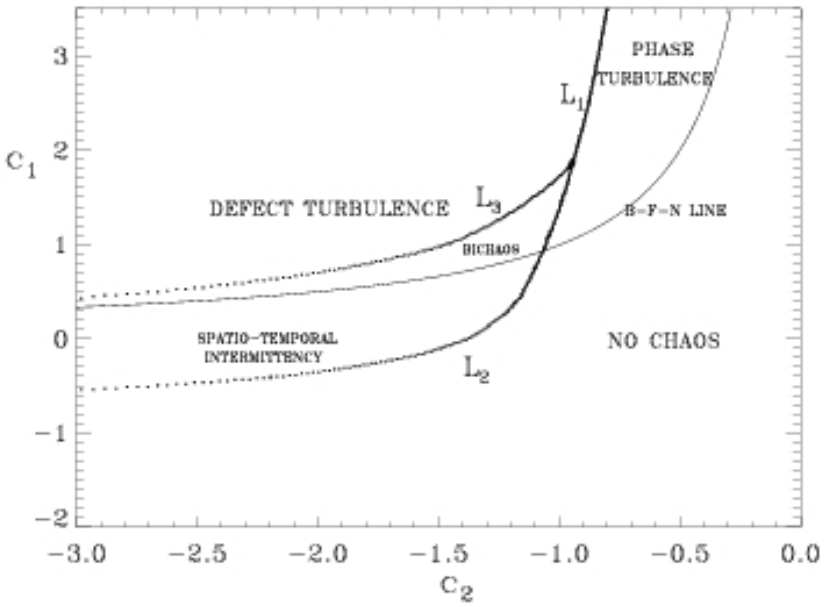

Figure 2.15: *Regions of the parameter space for the one dimensional complex Ginzburg-Landau equations in different dynamical regimes, regular and chaotic. The figure was taken from Ref. [148].*

model of symmetrically coupled FitzHugh-Nagumo cells, where the membrane potential $v(t)$ is taken to be $v(t) = A(t) \exp(i\omega |A|^2 t)$ [55]. In this case the chaotic behavior is possible because of the additional degrees of freedom introduced by the spatially extended excitable cells. Such an analogy to coupled FitzHugh-Nagumo cells can be done

because the diffusion term in the reaction-diffusion equation of the general form:

$$\dot{\mathbf{u}} = \mathbf{f}(\mathbf{u}, x) + D\nabla^2\mathbf{u} \tag{2.43}$$

describes nearest-neighbours bidirectionally coupled cells, where each cell undergoes the internal dynamics ruled by $\dot{\mathbf{u}} = \mathbf{f}(\mathbf{u})$. In one spatial dimension the diffusion term in Eq. 2.43 is defined in the following discrete form:

$$D\nabla^2\mathbf{u}_i = \frac{D}{\delta x^2}(u_{i-1} + u_{i+1} - 2u_i) \rightarrow \frac{D}{\delta x^2}(u_{i-1} - u_i) - \frac{D}{\delta x^2}(u_i - u_{i+1}) \tag{2.44}$$

where δx is the spatial integration step. The term $\frac{D}{\delta x^2}$ plays the role of the coupling constant which is closely related to the size of the spatial integration step. Thus the spontaneous emergence of patterns in extended systems far from thermodynamic equilibrium can be interpreted as an effect of an interplay between local dynamics and coupling of individual system elements. From the above considerations the stable oscillatory solutions are related to the synchronized state of coupled elements. When the synchronization is lost under the change of the system parameters and the diffusion constant, then the turbulent behavior develops. Thus, chaos in reaction-diffusion systems corresponds to desynchronization processes.

In Section 3.2.2 we will consider the model of the catalytic oxidation of the CO on the platinum Pt(110) surface. This chemical reaction appears for example in the catalyst in cars which is the most common heterogeneous catalyst and its function is to decrease the concentration of carbon monoxide, CO, and nitrogen oxides. The role of the heterogeneous surface catalyst functions is to decrease the activation energy for the chemical reaction. The chemical reaction of the CO oxidation on the platinum surface can be exemplified by:

$$2CO + O_2 \rightarrow 2CO_2$$

which is in fact much more complex and involves desorption[2] of the reacting gases on specific surface sites, dissociation[3] of the desorbed molecules, surface diffusion and reaction and desorption of the reaction products. Figure 2.16(1-4) shows the reaction between CO and O_2 as they reach the platinum surface. An adsorbed[4] O_2 on the platinum

[2]Desorption occurs in a system being in the state of adsorption equilibrium between fluid (e.g. gas or liquid solution) and adsorbing surface (solid, or boundary separating 2 fluids) and when the concentration of adsorbed substance in the fluid is lowered. The result is the decrease of the amount of adsorbed substance.

[3]Dissociation is a process in which complexes of molecules split into smaller molecules, usually in a reversible manner.

[4]Adsorption (a process opposite of desorption) is a process that takes place when a liquid or a gas accumulates on the surface of a solid, forming a molecular or atomic film.

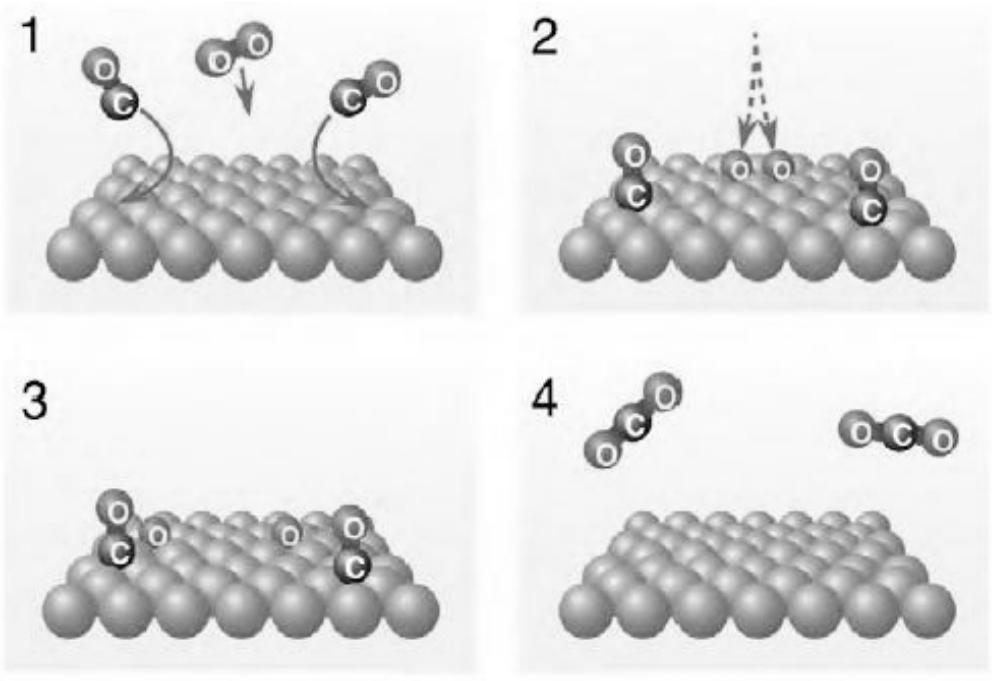

Figure 2.16: *Schematic view on the chemical reaction of the CO oxidation on the platinum surface. See description in the text. Figure taken from the lecture presented by Gerhard Ertl.*

surface dissociates in a pair of oxygen atoms which then occupy two sites at the surface (Fig. 2.16-2). An adsorbed CO molecule can react with an adsorbed oxygen atom from a neighboring lattice site to form a carbon dioxide (Fig. 2.16-3) which is immediately released into the gas phase (Fig. 2.16-4), leaving two vacant cells for adsorption of new molecules. If both reactants are present in the gas phase they compete for empty adsorption sites on the catalyst surface. CO is in a more favorable situation since the dissociative adsorption of oxygen requires two adjacent free adsorption sites, meanwhile single free adsorption site is sufficient for the CO molecule.

The equations describing the reaction of CO oxidation on platinum surface were developed by Krisher, Eiswirth and Ertl [56]. The model was further modified by different authors. The final form we will consider here is that of reference [57]. The model in one spatial dimension is the following:

$$\begin{aligned} \dot{u} &= k_1 s_{CO} p_{CO}(1-u^3) - k_2 u - k_3 uv + D\nabla^2 u \\ \dot{v} &= k_4 p_{O_2}[s_{O,1x1} w + s_{O,1x2}(1-w)](1-u-v)^2 - k_3 uv \\ \dot{w} &= k_5 \left(\frac{1}{1+\exp(\frac{u_0-u}{\delta u})} - w \right) \end{aligned} \tag{2.45}$$

where variable u denotes the CO coverage, variable v the oxygen coverage, and variable w the fraction of the reconstructed structure. The adsorption processes of CO and oxygen are determined by the respective impingement (impact) rates k_1 and k_4, the sticking coefficients s_{CO} and s_O, and the partial pressures p_{CO} and p_{O_2} of the two components, respectively. k_2 represents the rate constant for the CO desorption, k_3 the rate constant for the surface reaction, and k_5 the rate constant for the surface reconstruction. $s_{O,1x1}$ and $s_{O,1x2}$ denote the initial sticking probabilities of CO and oxygen on the clean surface, respectively. Finally, u_0 determines the threshold above which the surface structure is significantly affected by the CO coverage and δu determines the steepness of this threshold. In these equations only the desorption of CO is taken into account, meanwhile the desorption of oxygen is neglected. Moreover for the temperature used in the model CO is more mobile than oxigen, thus it has bigger probability in finding the site for adsorption. Typical spatiotemporal patterns observed during catalytic CO oxidation on Pt(110) under low pressure conditions are solitary waves and pulses, rotating spiral waves, target patterns, standing waves, and chemical turbulence [58].

2.4 Delayed differential equations

Delay systems (also called systems with after-effects) are infinite-dimensional systems used to describe propagation phenomena or population dynamics. The reaction of "real world" systems to external signals is never "instantaneous" but it needs some time which in mathematical language is described with delay terms. The characteristic of such systems is that their time evolution is described by differential equations which include information on the past history. The presence of delays may induce complex behaviors in the systems, oscillations or instabilities, leading to bad performances in real applications. For example, a chaotic behavior can appear in a system if the delayed state is a nonlinear function, as it for instance happens in the Ikeda equation modelling a nonlinear absorbing medium in lasers [59]:

$$\dot{x}(t) = -\alpha x(t) - \beta \sin x(t-\tau) \tag{2.46}$$

for some particular values of α, β and τ or in the Mackey-Glass equation [60, 61]:

$$\dot{x}(t) = -\alpha x(t) + \beta \frac{a x(t-\tau)}{1 + x^b(t-\tau)} \tag{2.47}$$

for particular values of constant parameters α, β, a, b and τ. Systems with delayed feedback become very complex to study since the effective number of degrees of freedom is infinity. This can be easily understood by noticing that the initial condition of a delayed differential equation has to be given in the whole interval $[x(t_0 - \tau), x(t_0)]$ of function values [62, 63].

The fact that the delay can induce irregular oscillations leads to the development of models for some physiological diseases in which normally periodic behavior changes into irregular one or non-oscillatory behavior changes into the oscillatory. An example is the Cheyne-Stokes respiration which is characterized by an alteration in the regular breathing [64]. The delay in the model is related to the time which needs the information about the level of carbon dioxide (CO_2) to reach the receptors situated in the brainstem. Thus the control system responsible for the ventilation contains a delay line and when such a line is distorted it can induce instabilities.

Other example from physiology is the regulation of hematopoiesis. Hematopoiesis is a process of the formation of blood elements in the body and was modelled by Glass and Mackey (see Eq. 2.47). White and red blood cells, platelets etc. are produced in the bone marrow from where they enter the blood. The decrease of the level of oxygen in the blood causes a release of a substance which in turn causes an increase in a release of the blood elements from the bone marrow. Thus there is a feedback from the blood to the bone marrow. The flux of cells into the blood depends on the cell concentration in the blood at some earlier time $t - \tau$. One manifestation of leukemia is the appearance of

aperiodic oscillations of white cells in blood. In this case the deficiency in bone marrow cell production causes delays and could account for the erratic behaviour in the white cell concentrations.

Delay times accounting for the time needed to reach maturity, the finite gestation period etc. can be also incorporated in the description of the population dynamics. Such models are of the form:

$$\frac{dN(t)}{dt} = f(N(t), N(t-\tau)) \tag{2.48}$$

where $\tau > 0$ is a delay time, $N(t)$ is the population of the species at time t. The conservation equation for the population needed to be satisfied during modelling is the following:

$$\frac{dN}{dt} = \text{births - deaths + migration} \tag{2.49}$$

One of such models describing the population is that proposed by Verhulst [65] (without delays), but modified by a delayed variable:

$$\frac{dN(t)}{dt} = rN(t)\left[1 - \frac{N(t-\tau)}{K}\right] \tag{2.50}$$

where r, K and τ are positive constants. The above equation says that the actual state of the population depends on its state at an earlier time $t - \tau$. Such an equation is one-dimensional, but it can exhibit a rich dynamics depending on the value of τ, including oscillatory or chaotic behaviour.

Further example of delay lines in physiological systems concerns the nervous system which monitors and controls almost every organ system through a series of positive and negative feedback loops. Neurons receive excitatory feedback from local-circuit neurons and stay in a state of persistent activity (”ON” state) after producing their first spike, as suggested by physiological observations [66]. Neurons in the self-sustained ON-state are silenced by inhibitory feedback from their target neurons in the next layer. This feature ensures that neurons fire only during the minimum necessary time and prevents the loss of information from one layer to the next. Similar feedback inhibition schemes are used in models of speech production [67], olfactory recognition [68] and visual search [69]. Inhibitory feedback is usually assumed to be a local process [66], with a delay determined by the local circuitry.

The analytical study of the nonlinear delayed differential equations can be provided through the linear stability analysis. The theory for an autonomous linear delay equations is well-developed and is based on the theory of Laplace transformation. The detailed stability analysis for the linear delayed differential equations is provided in Appendix A.

2.5 Artificial neural networks as a dynamical systems

The development of artificial neural networks has its roots in our attempts to understand the human brain. Thus, the initial concepts were based on to mimic the brains' way of processing information. These studies gave rise to various models of biological neural network structures and learning algorithms. Further studies became directed to the artificial neural networks as a tool for solving different types of problems on the unknown data. In our work we treat with the latter approach to the neural networks.

Having data which come from a known or unknown source, a neural network may be trained to perform classification, estimation, simulation, and prediction of the processes which generate these data and relationships between variables measured. An estimated relationship may be a mapping or a function. There are many types of neural networks. The most popular and most widely used neural networks in practise are the feedforward neural networks or multi-layer perceptrons. Feedforward neural networks are composed of neurons, in which the input layer of neurons are connected through the so-called hidden layers to the output layer of neurons. Every neuron in each layer is connected to every neuron in the adjacent layers. Each interconnection is characterized by a scalar weight which is adjusted during the training process. Each neuron performs a weighted summation of the inputs, which then passes a nonlinear activation function σ, also called the neuron function. The hidden layer nodes typically have sigmoidal transfer functions. The number of input and output nodes is determined by the nature of the modelling problem and its complexity.

The training process of feedforward neural networks is achieved by establishing the weights in the way that a desired input-output relationship is realized. In the values of weights of the hidden units are created internal representations of the input patterns. It has been shown that with a simple feedfoward network with a sufficient number of hidden units it is possible to approximate almost any continuous (one hidden layer) or arbitrary (more than one hidden layer) functions [70]. This result has encouraged people to use neural networks to solve many kinds of problems. Figure 2.17 illustrates a one-hidden-layer feedforward network with three inputs x_1, x_2 and x_3 and three outputs y_1, y_2 and y_3. Each arrow in the figure symbolizes a weight (parameter) in the network. Thus the higher the number of neurons in the network, the more parameter values that have to be established. The problem of determining the network parameters (weights) is essentially a non-linear optimization task. Mathematically the functionality of a hidden neuron is described by:

$$y_i = f\left(\sum_{j=1}^{N} \omega_{ij} x_j\right) \tag{2.51}$$

If f is a sigmoidal function which is a continuous approximation of the unitary jump,

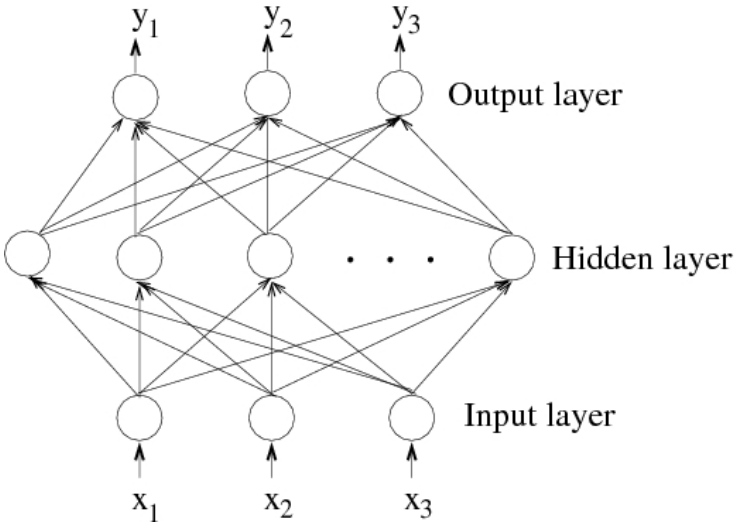

Figure 2.17: *Feed-forward neural network of type 3:a:3.*

then the output signal of a neuron will depend on the sign of the expression $\sum_{j=1}^{N} \omega_{ij} x_j$. Equation 2.51 is linear for the weights ω_{ij}. Let be d_i the values to be learnt by the net. With the use of Euclidean metric we can define the destination function as:

$$E = \frac{1}{2} \sum_{k=1}^{p} ||y^{(k)} - d^{(k)}||^2 = \frac{1}{2} \sum_{k=1}^{p} \sum_{i=1}^{M} (y_i^{(k)} - d_i^{(k)})^2 \tag{2.52}$$

where M is the number of the output neurons and p is the number of teaching vectors $(\mathbf{x}, \mathbf{d})$. Learning of the neural network consists on the minimization of a properly defined destination function as that defined in Eq. 2.52. The minimization is performed in the space $\{\omega_{ij}\}$ of the linear weights.

In recent years new approaches for nonlinear time series modelling have emerged (local and global prediction [71], neural networks [72], delay embedding reconstruction space [34], functional networks [73], etc.), providing more powerful methods and giving new insight into the dynamics of complex systems (see [74, 75] and references therein for an updated survey of this topic). Among these techniques, artificial neural networks have been successfully applied in many practical situations [76, 77]. Moreover, it has been shown that the neural approximate model and the original system exhibit similar dynamical behavior (similar unstable periodic orbits [78], or even similar Lyapunov exponents or fractal dimensions [79]).

Modelling and predicting the dynamics of nonlinear chaotic systems is a challenging problem with important real-world applications (stock market returns [80], weather forecast [81], etc.). It is well known that chaotic behavior implies long-term unpredictability, but the deterministic nature of chaotic systems allows the prediction of their

dynamics to some extent (see Section 2.2). From a theoretical point of view, Lyapunov theory provides a sound framework for this problem, and the inverse of the largest Lyapunov exponent gives a theoretical limit for the prediction horizon attainable for a particular system (see section 2.2.1). However, in practice, the original system is unknown and approximate models fitted to the available data are used to model and forecast its nonlinear dynamics (e.g. neural networks [74]). In this situation, the attainable forecast horizon depends not only on the dynamics of the original system, but also on the error of the approximate model.

The functional structure of the deterministic and low-dimensional chaotic systems can be reconstructed from a time series using appropriate nonlinear techniques. We show it on an example of the Lorenz system defined in Eq. 2.21. Let us assume that we have a time series $\mathbf{u}^n$, obtained from a dynamical system $\dot{\mathbf{u}}(t) = \mathbf{f}(\mathbf{u}(t))$, sampled at equally spaced intervals $\mathbf{u}^n = \mathbf{u}(n\,\Delta t)$, $n = 0, 1, 2, \ldots$. We are interested in approximating the functional model which characterizes the short-term evolution of the time series, $\mathbf{u}^{n+p} = \mathbf{F}(\mathbf{u}^n)$, where $\mathbf{F}$ is given in terms of $\mathbf{f}$, the sampling time Δt, and the prediction step p. To this aim we consider simple feed-forward neural networks with sigmoidal and linear activation functions for hidden and output layers, respectively. The training process is carried out by considering input–output couples of the form $(\mathbf{u}^n, \mathbf{u}^{n+p})$, where p is the prediction step.

We use time series consisting of 2000 sample points obtained from the Lorenz system integrated using a fourth-order Runge-Kutta algorithm with a fixed time step $\Delta t = 10^{-2}$. This set was divided in two parts; the first one (1500 sample points) was used for training purposes whereas the last 500 were reserved for testing the models. We have used the feedforward neural networks of type $3 : a : 3$ (what means 3 inputs, a hidden layers and 3 outputs) since we wanted to train the neural network to be a three dimensional system. We have considered different neural networks with a single hidden layer a with a number of neurons ranging from one to twenty. For each of these network structures, ten simulations were performed with different initial network weights, using the Levenberg-Marquardt method [82, 83] as training algorithm. The best solution in each case was considered as the representative neural approximate model. The root-mean-square (rms) error obtained for predicting the x variable of the Lorenz model with the best neural network with 6 hidden neurons for the training process was 0.13 (less than 0.5% the range of the corresponding variable), and 0.15 for the test data, indicating no over-fitting[5] of the model. However, although the above analysis indicates a good accuracy in one-step ahead prediction using a six neuron network ($3 : 6 : 3$), it does not mean necessarily that the obtained neural model can reproduce the dynamics of the

[5]The term *over-fitting* is used to describe a model which is generally correct in form, but that include extra, unnecessary terms. The extra terms in the model make it more flexible than it should be, allowing it to fit additional data not being included in the data under consideration.

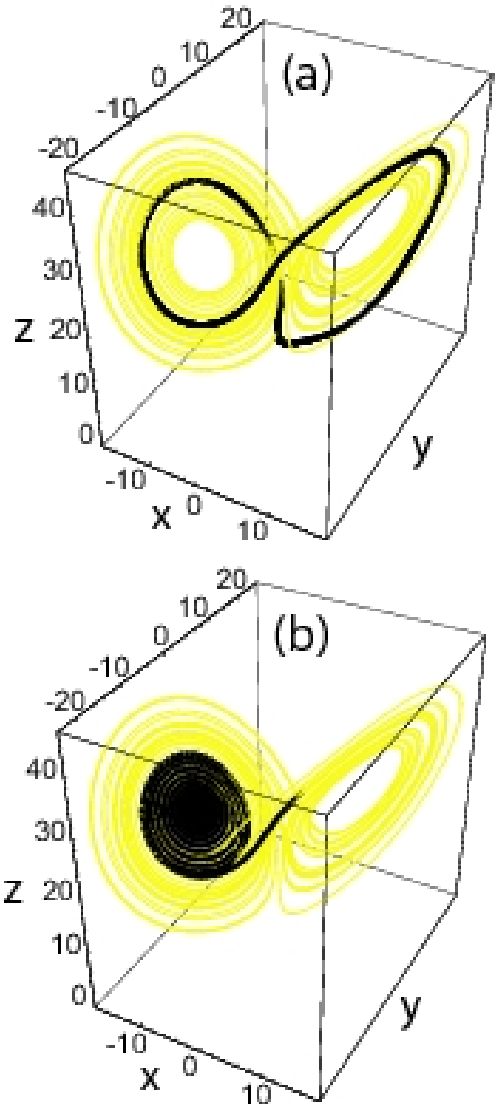

Figure 2.18: *Phase space of two different* $3:6:3$ *neural models trained with the same method, but starting from different initial weight configurations (black colour). The original chaotic orbit of the Lorenz system in the background is shown for illustrative purposes (grey colour).*

Lorenz system when iterated in time [77]. Figure 2.18 shows the evolution of the above network with $a = 6$ hidden neurons iterated from two different initial weight configuration; in the first case, the neural system converges to a periodic trajectory (Fig. 2.18a), whereas in the second case it converges to a fixed point (Fig. 2.18b), neither of them resembling the chaotic behavior of the Lorenz model. When increasing the number of hidden neurons above $a = 10$, the error decreases and the dynamical behaviour of the obtained neural models resembles the original chaotic system. For instance, the training

and test rms errors obtained for $a = 10$ hidden neurons were 2.2×10^{-2} and 2.4×10^{-2}, respectively, indicating that no over-fitting occurs. In this case, the dynamical behavior of the neural model resembles that of the original system. Thus, the neural model can be considered as an approximate replica of the Lorenz model. If we increase the number of hidden neurons above $a = 20$, the training error decreases even further but the neural models start over-fitting the data. We could see that changing the number of hidden neurons is like changing the parameter values of the system.

2.6 Coupled dynamical systems

2.6.1 Synchronization

Under particular conditions coupled systems exhibit coherent behaviour characterized by a situation in which one system follows the dynamics of the other. Such a phenomenon is called synchronization. Typical examples of synchronized behavior in the animal kingdom are the coincident pulses of light produced by male fireflies (see photo in Fig. 2.19) or the synchronized sounds of crickets [84]. In these examples, the interactions between insects are mainly through the mutual perception but they are also determined by environmental external stimuli. There were some experiments which showed that an external periodic stimulus can influence the degree and quality of the synchronization in fireflies [85]. Another biological example is that of cardiac cells whose global synchronized activity results in a regular heart beating. In this case the synchronization is due to entrainment by an external signal which provides a rhythm. It was suggested that the intensive growth of a cancerous tumor is due to synchronous oscillatory processes [2]. The mutual synchronization is also observed in the behavior of human or animal groups. As an example, the applause in an auditorium may change from random to synchronized. Other examples from the animal world include the synchronous motion of the wings in flocks of birds and the synchronous motion of the tails in schools of fish. In fact synchronization phenomena can be encountered almost everywhere where vibrations exist. Apart of living nature there are many correlated motions in the solar

Figure 2.19: Flashing fireflies.

system. For instance the motions of the Earth, Venus and Mercury seem to be correlated. It is based on the Molchanov hypothesis which says that the average motions of the nine planets in the solar system are approximately correlated by nine linear homogeneous expressions with integer coefficients, thus exhibiting a resonance (synchronous) character. It is not an accident that the rotational period of the Moon and the orbital period of the Earth-Moon system are of the same length. Over billions of years the gravitational coupling between the Earth and the Moon has led to such a synchronization. However this synchronization is not yet complete, but billions of years from now the Earth and Moon will have exactly the same rotational period, and these will also exactly equal to the orbital period. Such phase correlations are typical for the synchronization phenomena.

Coupled interacting systems have been the subject of a deep observation since the 17th century. In 1656, Christiaan Huygens (Fig. 2.20) built the world's first pendulum clock to measure the time. He published the classic work *Horologium Oscillatorium*, in which he gave a complete mathematical description of the pendulum and a description of his improved pendulum clock. In early 1665, Huygens discovered "..an odd kind of sympathy perceived by him in these watches [two pendulum clocks] suspended by the side of each other." The pendulum clocks moved with exactly the same frequency and 180 degrees out of phase. When the pendula were disturbed, the anti-phase state was restored within a half-hour and persisted indefinitely. Huygens deduced that the crucial interaction for this effect came from "imperceptible movements" of the common frame supporting the two clocks. Thus if the platform was prevented to move, there was no synchronization at all. Also he noted that the pendula were always attracted to the anti-phase state, never the in-phase state. He thought this synchronization could be used in maritime navigation and spent many years developing and testing designs for pendulum clocks that could work in boats. A version of Huygens original system was provided in a nice demonstration of how systems synchronize [86]. The system in [86] consisted of two pendulum metronomes resting on a light wooden board which sit on two empty soda cans (see photo in Fig. 2.21). However these two pendulum metronomes could be synchronized in-phase which is different from the Huygens experiment and the recent reproduction of Huygens original system reported in [87]. Nevertheless in Ref. [86] it was found that the anti-phase synchronization state could be made stable in the metronome system when the cans were placed on a wet table i.e. enhancing the damping associated with the base motion.

Huygens' synchronization observations have inspired modern studies of "sympathetic" oscillations in many areas of nonlinear science. This interest led to mathematical theories which enable us to understand (at least partially) the behavior of many coupled systems, including very complex ones, in wide areas of natural and technical sciences. Few advances were made in the next two centuries, until the study of syn-

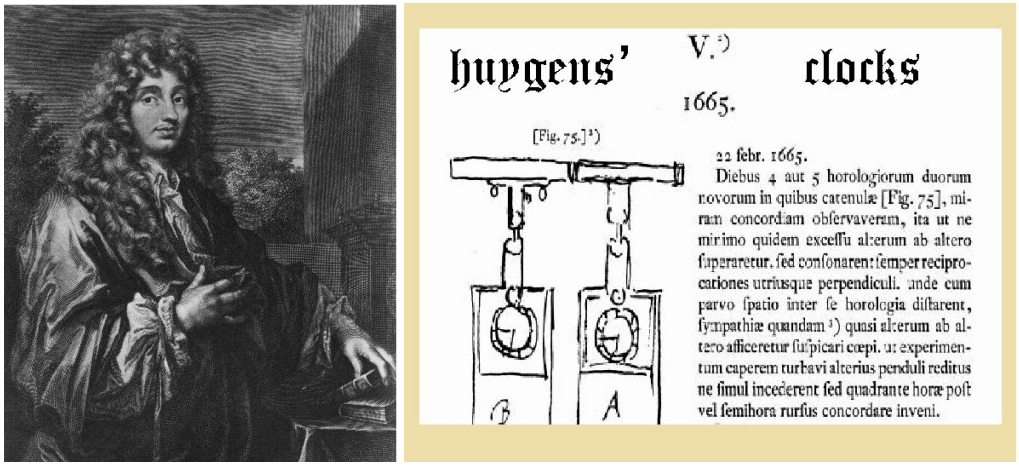

Figure 2.20: Left: Christiaan Huygens. Right: Huygens' clocks.

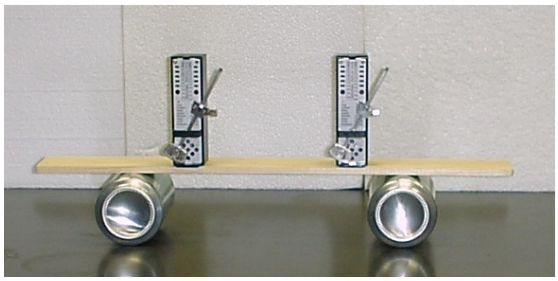

Figure 2.21: Synchronization of metronomes.

chronization was developed by Edward Appleton [88] and Balthasar van der Pol [89]. They demonstrated the existence of synchronization between the frequency of a triode generator and a weak external signal with slightly different frequency (these generators were later used in radio communication devices). Further contributions of other researchers (see review in [90]) concerned synchronization in many nonlinear systems. In the late 1980s researchers turned their attention to the synchronization properties of chaotic systems. The interest was motivated by the potential applications in secure communication systems through the possibility of hiding a message in a chaotic signal during transmission. Pioneering work on synchronous of coupled chaotic systems was made by Yamada and Fujisaka in 1983 [91, 92], Afraimovich, Verichev and Rabinovich in 1986 [93] and by Pecora and Carroll in 1990 [94]. The exhaustive studies on secure communication were initiated in 1992 by Cuomo and Oppenheim [95] who proved experimentally, using electronic circuits that it is possible to mask a message by using a chaotic signal coming from an electronic device. Remarkably, one can then use a copy of the original electronic device to recover the original message. Such subtraction was possible because the two electronic devices were synchronized and hence exhibited the

same dynamics. The advantage of this type of transmission lays in the difficulty of the separation of the message from the chaotic signal. If an observer does not know neither the equations of motion which originated the chaotic signal carrying the message nor the initial conditions, then it will be difficult to extract the hidden message. Thus the interest in synchronizing chaotic systems arises from their complex, unpredictable dynamics (see section 2.2). Nevertheless, it is worth mentioning that there have been some suggestions of methods to decrypt the information and the usefulness of such an encryption method is still under investigation [96].

Interactions between the constituents of physical or biological systems occur due to the existence of different types of connections: global, local, unidirectional or multidirectional. Besides of synchronization due to a direct coupling the systems may be synchronized by interaction via a common medium where the cells interact through the exchange of some substances. Individual cells, cell communities, and also individual organisms could be such objects. One example is the synchronization between the malignant tumor cells immersed in a solution [2].

Different types of coupling are presented on Fig. 2.22. The graphics presented there may be described by the mathematical language. The bidirectionally (symmetrically)

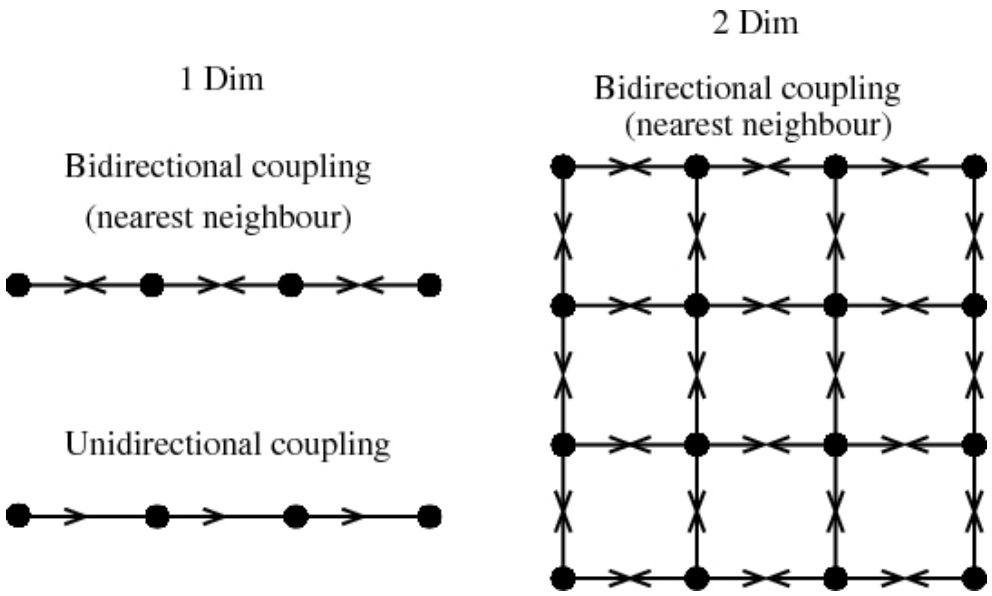

Figure 2.22: Different types of coupling leading to synchronization.

coupled systems in one dimension can be defined as follows:

$$\dot{\mathbf{y}}_i = \mathbf{f}(\mathbf{y}_i) + \mathbf{K}(\mathbf{y}_{i-1} + \mathbf{y}_{i+1} - 2\mathbf{y}_i) \tag{2.53}$$

while the unidirectionally (asymmetrically) coupled systems also in one-dimensional

array can be defined in the following way:

$$\dot{\mathbf{y}}_i = \mathbf{f}(\mathbf{y}_i) + \mathbf{K}(\mathbf{y}_{i-1} - \mathbf{y}_i) \tag{2.54}$$

In both cases described in Eqs. 2.53 and 2.54, the periodic or no-flux (open) boundary conditions can be used.

The synchronization in the systems described in Eqs. 2.53 and 2.54 can occur for particular values of coupling parameters in matrix $\mathbf{K}$ when the difference variables $\mathbf{\Delta}_{ij} = \mathbf{y}_i - \mathbf{y}_j$ vanish. The difference variable multiplied by coefficient matrix $\mathbf{K}$ plays a role of a corrective signal which pushes the systems to the desired state of synchronization. Bidirectionally coupled systems can be also described by means of the spatial derivatives:

$$\dot{\mathbf{y}} = \mathbf{f}(\mathbf{y}) + \mathbf{K}\frac{\partial^2 \mathbf{y}}{\partial x^2} \tag{2.55}$$

where $\frac{\partial^2}{\partial x^2}$ is a second-order spatial derivative. In the case of unidirectionally coupled systems the following description can be used:

$$\dot{\mathbf{y}} = \mathbf{f}(\mathbf{y}) + \mathbf{K}\frac{\partial \mathbf{y}}{\partial x} \tag{2.56}$$

where $\frac{\partial}{\partial x}$ is a first-order spatial derivative.

Apart of the diffusive coupling schemes described before there exists also other schemes leading to synchronization, e.g. the complete replacement, which may be defined as follows:

$$\begin{aligned} \dot{\mathbf{y}_1} &= \mathbf{f}(\mathbf{y}_1, \mathbf{y}_1) \\ \dot{\mathbf{y}_2} &= \mathbf{f}(\mathbf{y}_2, \mathbf{y}_1) \end{aligned} \tag{2.57}$$

where in the response system its variable is replaced by that coming from the driver.

Dissipative forces have a dual influence on the synchronization in many systems. On the one hand, they ensure asymptotic stability along the corresponding coordinates, but on the other hand, they could cause violation of the conditions of existence of synchronous motions, i.e. the suppression of the tendency toward synchronization. At some conditions, the dissipative forces may cause a loss of motion stability.

2.6.2 Anticipated synchronization

This Thesis was developed as a consequence of the publication of H. Voss [97] dealing with a new type of synchronization, namely, the anticipated synchronization occurring in unidirectionally coupled systems. He observed that dissipative chaotic systems with time-delayed feedback can drive near-identical systems in such a way that the driven system **y** anticipates the driver system **x** by synchronizing with future states. The driver system we call a *master* and the driven system we call a *slave*. Voss showed that anticipated synchronization can occur in the following replacement scheme:

$$\dot{x} = -\alpha x + f(x(t-\tau)) \tag{2.58}$$
$$\dot{y} = -\alpha y + f(x) \tag{2.59}$$

where in the function f the delayed variable $y(t-\tau)$ has been replaced by the variable x. The solution of this system is $y(t) = x(t+\tau)$, what means that the slave system at time t will synchronize with the master at time $t+\tau$, thus anticipating the latter ahead in time, by the time interval τ. From the time evolution for the difference variable $\Delta = x(t) - y(t-\tau)$:

$$\dot{\Delta} = -\alpha\Delta \tag{2.60}$$

we obtain that a sufficient condition for synchronization is that $\alpha > 0$. The transient dynamics depends only on the system parameter α and does not include the dependence on the delay time τ. For that reason there is no restriction on the value of the delay time and anticipation may be observed for any τ, but with the limitation that the anticipation time is equal to the delay existing in the master system. Then the synchronization manifold $x = y_\tau$ is globally attracting and asymptotically stable. Thus the slave (response system) at time t synchronizes with the future state of a master (driver) at time $t+\tau$ and anticipates its dynamics. The anticipation does not depend on the form of the function f and can be obtained for arbitrary delay τ, thus indicating that it is valid for high-dimensional systems. This is so because a high-dimensionality is induced by the delay, and is higher as the delay increases.

The other coupling scheme leading to anticipated synchronization proposed by Voss is a dissipative coupling between the master and the slave:

$$\begin{aligned} \dot{\mathbf{x}}(t) &= \mathbf{f}(\mathbf{x}(t)) \\ \dot{\mathbf{y}}(t) &= \mathbf{f}(\mathbf{y}(t)) + \mathcal{K}(\mathbf{x}(t) - \mathbf{y}(t-\tau)) \end{aligned} \tag{2.61}$$

where $\mathbf{x}$ and $\mathbf{y}$ are dynamical variables (three or more dimensional to obtain chaotic dynamics), $\mathbf{f}$ is a vector function, $\mathcal{K}$ is a matrix representing a coupling parameter and τ is a constant delay time. In this case a delayed term appears only in the equation for the

slave system. The above scheme permits to obtain anticipation times equal to the delay time we include in the coupling term. The solution of Eq. 2.61 can be read directly from the form of the dissipative term and is $\mathbf{y}(t) = \mathbf{x}(t+\tau)$, thus leading to the anticipated synchronization. The delay time τ can be manipulated in the response system without influencing the master and may be selected from a range restricted by the stability conditions. The stability conditions are obtained from the delayed differential equations for the difference variable $\mathbf{\Delta} = \mathbf{x}(t) - \mathbf{y}(t-\tau)$:

$$\dot{\mathbf{\Delta}} = \mathbf{A}\mathbf{\Delta} - \mathcal{K}\mathbf{\Delta}_\tau \tag{2.62}$$

where $\mathbf{A}$ is the Jacobian matrix of the linearized system equations in Eq. 2.61. In the case of the delayed coupling between systems without memory, the stability conditions will depend on the value of delay time τ and the coupling constant K. It was shown in Ref. [98] that the systems of Eq. 2.61 coupled in a chain of $N > 1$ slave units can strongly enhance the anticipation time, exceeding typical time scales of the chaotic dynamics.

Since it discovery by Voss, anticipated synchronization was treated as a counterintuitive phenomenon with potential applications. From the practical point of view it could enable simultaneous prediction of the chaotic signal without involving any previous calculation. Moreover, anticipated synchronization has been observed in a wide variety of systems, starting from the simplest linear systems [99] and ending on the complex chaotic ones, suggesting that this synchronization can occur in many classes of systems. Besides the systems described by differential equations, chaotic maps with delayed diffusive coupling have also been studied [100]. The phenomenon has been found in chaotic Rössler and Lorenz systems [98], in chaotic lasers [101] with the diffusive coupling scheme as well as in chaotic Ikeda systems [97] with the complete replacement scheme. Anticipated synchronization has been also demonstrated experimentally in electronic circuits [102] as well an in semiconductor lasers [103].

Chapter 3

Anticipated synchronization: characterization

3.1 Anticipated synchronization in excitable systems driven by noise

In this Section we present numerical and analytical results (published in Refs. [104] and [105]) on anticipated synchronization in excitable systems, in particular in coupled FitzHugh-Nagumo systems driven by different type of noises (section 3.1.1). So far the occurrence of this synchronization was studied in chaotic systems ([97], [100]) in which the unpredictability comes from the intrinsic noise related to existence of unstable periodic orbits. Here we study non-autonomous systems with an external forcing which introduces an element of randomness. In section 3.1.2 we estimate the range of parameters for which the phenomenon can be observed, and we try to provide the analytical description for it. Later in Section 3.1.3 we show that anticipation may be enhanced by arranging coupled systems in a chain (results published in Ref. [106]). We study the influence of noise on the quality of the anticipation in that case and compare it with the anticipated synchronization in non-chaotic autonomous systems. In the last Section 3.1.4 we show through an experiment that this synchronization is robust even when the coupled systems are driven by different realizations of noises (as it is also shown numerically in Section 3.1.1).

3.1.1 Numerical characterization of stability

Let us consider the following coupled system:

$$\begin{aligned} \dot{\mathbf{x}}(t) &= \mathbf{f}(\mathbf{x}(t)) + \mathbf{I}(t) \\ \dot{\mathbf{y}}(t) &= \mathbf{f}(\mathbf{y}(t)) + \mathbf{I}(t) + \mathcal{K}[\mathbf{x}(t) - \mathbf{y}(t-\tau)], \end{aligned} \tag{3.1}$$

where $\mathbf{x}$ and $\mathbf{y}$ are dynamical variables, $\mathcal{K}$ is a positive defined matrix and $\mathbf{I}(t)$ represents a common external forcing. Notice that $\mathbf{y}(t) = \mathbf{x}(t+\tau)$ is not an exact solution of the equations, except in the particular case of $I(t)$ constant or periodic forcing $\mathbf{I}(t+\tau) = \mathbf{I}(t)$. We will show that under appropriate coupling conditions generalized synchronization between $\mathbf{y}(t)$ and $\mathbf{x}(t+\tau)$ occurs and a high correlation between them

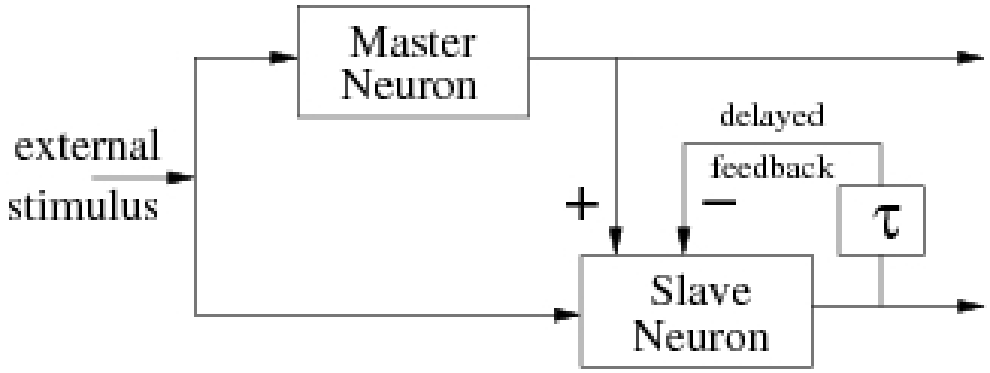

Figure 3.1: *Schematic diagram of two model neurons coupled in a unidirectional configuration, subjected to the same external forcing and with a feedback loop (with a delay time τ) in the slave neuron.*

is observed. This result is even more remarkable when the external forcing is a random signal. Specifically, we have considered models of sensory neurons. In general, sensory

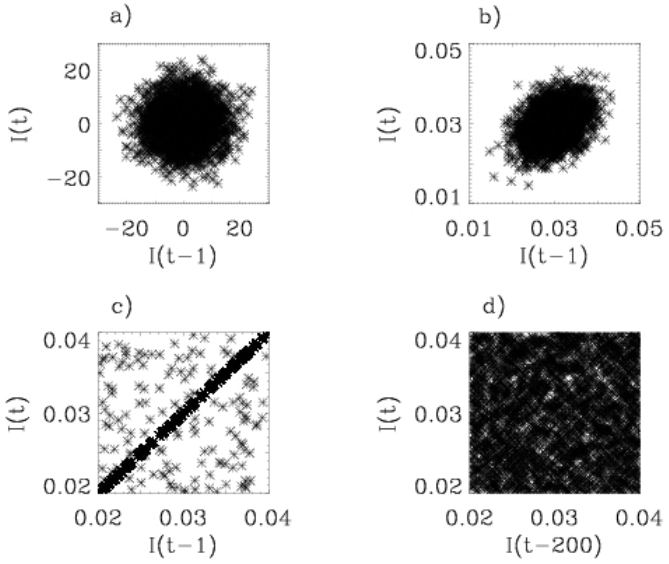

Figure 3.2: *Cobweb diagram for $I(t)$ versus $I(t-1)$ where $I(t)$ is the (a)white (b) colored and (c-d) telegraph-like noise. Diagrams (c-d) for telegraph-like noise show that it remains constant during the particular period, which in our case is $T = 200$.*

neurons work in a noisy environment. As a consequence, the time intervals between spikes contain a significant random component. The topics of synchronous oscillations and noise have received much attention (see, e.g., [107]), since it has been suggested that synchronous firing activity of sensory neurons might be a part of the higher brain func-

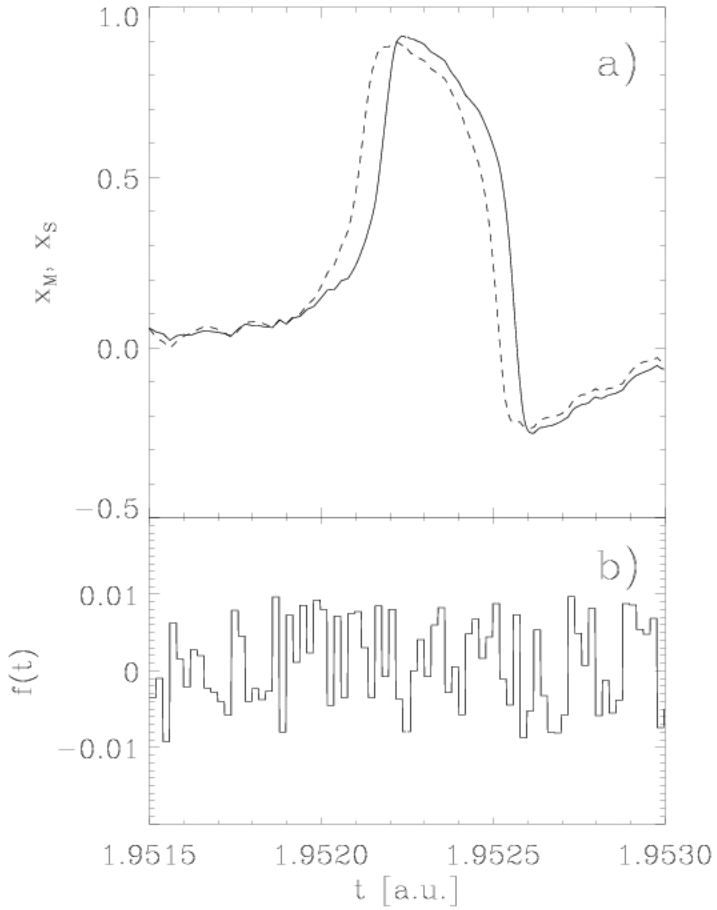

Figure 3.3: *Anticipated synchronization from a numerical integration of the FitzHugh-Nagumo set of Eqs.(3.2-3.3). The parameters are:* $a = 0.139$, $b = 2.54$, $\epsilon = 0.008$, $K = 0.15$. *The external forcing* $I(t)$ *(displayed in the lower panel) is a random amplitude noise of period* $T = 2$, *mean value* $I_0 = 0.03$ *and amplitude* $D = 0.01$. *Notice (upper panel) that the pulse of the slave system* $y_1(t)$ *(dashed line) anticipates the pulse of the master system* $x_1(t)$ *(solid line) by a time approximately equal to the time delay* $\tau = 4$.

tions and a method for integrating distributed information into a global picture [108].

We study anticipated synchronization in the FitzHugh-Nagumo and Hodgkin-Huxley neuron models (see Section 2.1). By coupling two of such systems in an unidirectional configuration as in the scheme shown in Fig. 3.1, we find that when both systems are subjected to the same external random forcing, the slave system fires almost the same train of spikes as the master system does, but at a certain amount of time earlier, i.e., the slave predicts the response of the master.

First we show results based on the FitzHugh-Nagumo model (see Section 2.1). The equations for the master $\mathbf{x} = (x_1, x_2)$ and the slave $\mathbf{y} = (y_1, y_2)$ systems, under unidirectional coupling (see Section 2.6.2) are, respectively:

$$\begin{aligned} \dot{x_1} &= -x_1(x_1 - a)(x_1 - 1) - x_2 + I(t) \\ \dot{x_2} &= \epsilon(x_1 - bx_2) \end{aligned} \tag{3.2}$$

and

$$\begin{aligned} \dot{y_1} &= -y_1(y_1 - a)(y_1 - 1) - y_2 + I(t) + K[x_1(t) - y_1(t - \tau)] \\ \dot{y_2} &= \epsilon(y_1 - by_2) \end{aligned} \tag{3.3}$$

where a, b, and ϵ are constants, K is the positive coupling strength and τ is a delay time (associated to an inhibitory feedback loop in the slave neuron). Note that only the fast variables of the two systems are coupled. When the common external forcing, $I(t)$, is constant in time, the synchronization manifold $x_1(t + \tau) = y_1(t)$, $x_2(t + \tau) = y_2(t)$ is an exact solution of Eqs. 3.2 and 3.3. If the external forcing is above threshold and for appropriate values of K and τ, the master system fires pulses periodically and the coupling induces a constant time shift τ between master and slave spikes.

We consider different types of random external forcing $I(t)$, telegraph-like, coloured and white noise (see Fig. 3.2). The first one "telegraph-like noise" corresponds to a random process whose amplitude remains constant for a time T and then it switches to a new random value chosen uniformly in [$I_0 - D$,$I_0 + D$], where D is the noise intensity and I_0 is a bias. This noise is different than the telegraph (dichotomic) noise, which is defined as a signal of constant amplitude and a period that varies randomly. We chose I_0 very close to (but below) the firing threshold of the excitable system. It would appear at first thought that with this type of external forcing the behaviour of the master system can be easily predicted. However, there are two main factors that make the system response unpredictable: if the effect of the perturbation is not strong enough the system does not fire a pulse; moreover, the system has a refractory time (after firing a pulse) during which, another firing is not possible. Figure 3.3 shows that anticipation occurs with this type of random external forcing for an appropriate value of the coupling strength K: after an initial transient time the two systems synchronize such that the slave system anticipates the fires of the master system by a time interval τ. The firings in the master and the slave systems start at about the same time, and the anticipation phenomenon grows during the rising of the pulse. When the master system noisily evolves near the stable point, the anticipation vanishes. In other words, anticipation is a local process, during firings (this observation will be studied deeper in Section 4.1). The same qualitative results are found with other types of external forcing such as colored or even white noise. Figures 3.4(a-b) display the spikes of the master and slave systems when $I(t)$ is a Gaussian white noise.

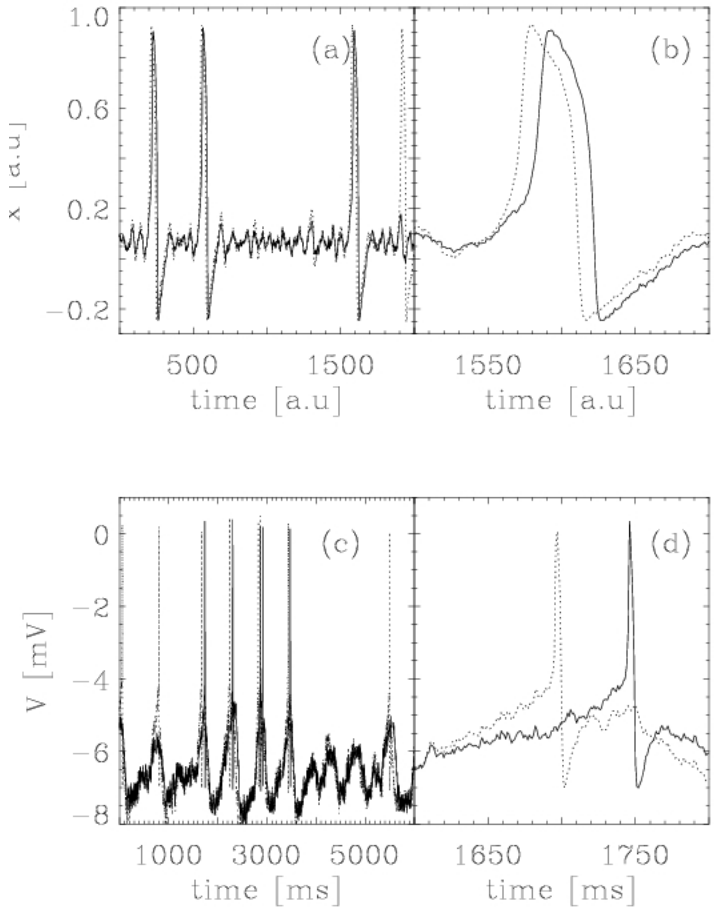

Figure 3.4: *Trains of spikes obtained from numerical simulations of models of unidirectionally coupled neurons subjected to the same external forcing, which is a Gaussian white noise with mean I_0 and correlations $\langle [I(t) - I_0][I(t') - I_0] \rangle = 2D\delta(t - t')$. (a) Simulation of two FitzHugh-Nagumo neurons, Eqs. (3.2-3.3). The parameters are $a = 0.139$, $b = 2.54$, $\epsilon = 0.008$, $I_0 = 0.03$, $K = 0.03$, $\tau = 10$, $D = 2.45 \times 10^{-5}$. (b) Simulation of two Hodgkin-Huxley neurons, Eq. 3.4 with $K = 0.03$ ms^{-1}, τ=50 ms, and D=0.5 mV^2/ms; all other parameters as in [109] ($T = 6$ C, $V_l = -75$ mA in our notation). Left panels show typical spike trains; right panels show with detail a single spike. The solid (dashed) line represents the output of the master (slave) system.*

Sometimes the slave system makes an error in anticipating the master firings. While the slave system always fires a pulse when the master system fires a pulse, it can also fire an "extra" pulse, which has no corresponding pulse in the train of pulses fired by the master. Notice that in Fig. 3.4a an error at about $t = 1900$ occurs. Not surprisingly, we find that the longer the anticipation time τ, the larger the number of errors. However, for a given anticipation time, the number of errors can be reduced considerably if a

chain of an adequate number of slave neurons is considered.

Next we show simulations based on a more realistic neuron's model, namely the model of electro-receptor neurons (for details see Section 2.1). We extend the model to account for two unidirectionally coupled neurons, with a delayed feedback loop in the slave neuron, and subject to a common external forcing $I(t)$, in the same way as in the FitzHugh-Nagumo model. The equations for the master, x, and for the slave, y, neurons are:

$$\begin{aligned} C_M\dot{x} &= -I^x_{Na} - I^x_K - I^x_{sd} - I^x_{sr} - I^x_L + I(t) \\ C_M\dot{y} &= -I^y_{Na} - I^y_K - I^y_{sd} - I^y_{sr} - I^y_L + I(t) + K[x(t) - y(t-\tau)] \end{aligned} \tag{3.4}$$

Figures 3.4(c-d) display the results when the common external forcing $I(t)$ is a Gaussian white noise. We chose parameters such that the systems are excitable. The behaviour observed is qualitatively the same as in the FitzHugh-Nagumo model (the slave neuron anticipates the fires of the master neuron).

We characterize the synchronization in the parameter space (coupling strength, anticipation time) by introducing several quantities to measure the degree of synchronization. To quantify the anticipation time, we compute the mean value $\langle t \rangle$ and the standard deviation σ of the time difference $t = t_i^m - t_i^s$, where t_i^m are the times at which the master neuron fires a pulse, and t_i^s are the times at which the slave neuron fires the corresponding pulse (hence the extra pulses fired by the slave are not taken into account). The variance of the anticipation time for corresponding pulses in the master and slave systems, is defined by:

$$\sigma = \sqrt{\eta - \mu^2}, \qquad \text{where:} \qquad \eta = \frac{1}{N_x}\sum_{n=1}^{N_x}\tau_n^2 \qquad \text{and} \qquad \mu = \frac{1}{N_x}\sum_{n=1}^{N_x}\tau_n. \tag{3.5}$$

where N_x is the number of firings in the master system and τ_n is the time separation between master and slave outputs measured at the threshold value x_{th}. In our simulations we have taken $x_{th} = 0.65$.

Another type of errors occurs when the slave system produces additional firings which are not present in the master system. For these errors we define the relative error parameter:

$$E_r = \frac{N_y - N_x}{N_x} \tag{3.6}$$

where N_x and N_y are the numbers of firings in the master and slave system, respectively. Although the two types of errors, non-constant anticipation time and additional firings in the slave system are closely related, the changes in the anticipation times is significantly more important and appear more often even in the absence of the relative error E_r. Figure 3.5 displays E_r in a gray scale in the parameter space (K, τ). The dark

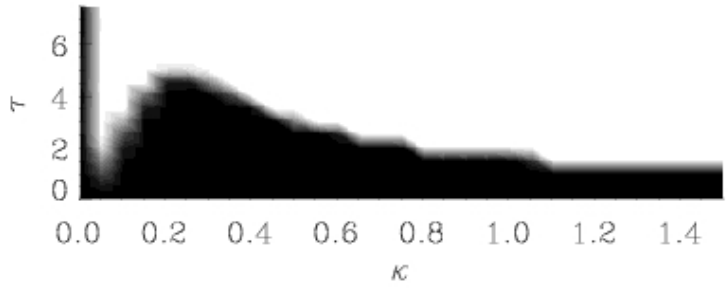

Figure 3.5: *Relative number of errors E_r in the parameter space (K, τ). This has been computed using time series which contain, at least,* 1000 *peaks in the master dynamics. The white region represents a region where the relative number of errors is larger than $E_r = 0.1$.*

(white) region represents a region of high (low) synchronization quality. In order to not to miss too much details, errors larger than $E_r = 0.1$ have been uniformly plotted as white, while black indicates $E_r = 0$, and the gray levels run between these two values. Two different synchronization mechanisms are present in Fig. 3.5. The first one appears

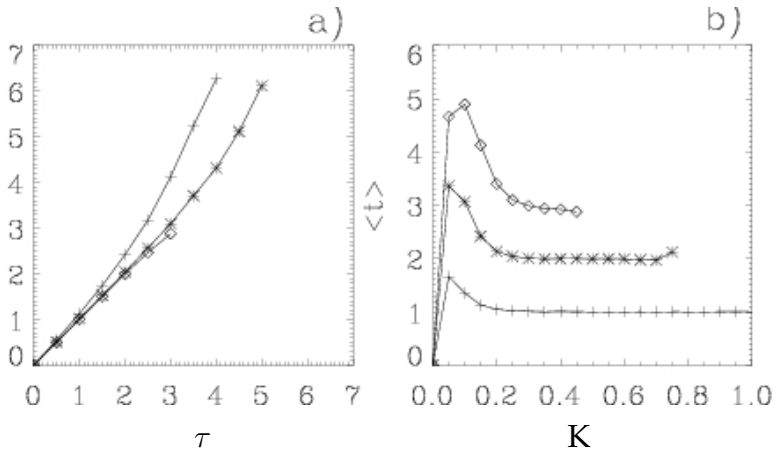

Figure 3.6: *(a) Mean anticipation time as a function of the delay time τ for the following values of the coupling strength: $K = 0.15$ (+), $K = 0.25$ (*) and $K = 0.45$ ($\diamond$). (b) Mean anticipation time as a function of K for $\tau = 1$ (+), $\tau = 2$ (*) and $\tau = 3$ ($\diamond$). The results come from numerical integration of Eqs.(3.30-3.31).*

for very low coupling intensity (the black region near the ordinate axis $K = 0$). This is not a regime of anticipating synchronization, but it corresponds to the synchronization of trajectories by common random forcing [110] which leads simply to $\mathbf{x}(t) = \mathbf{y}(t)$. It is worth to note that the results drawn in Fig. 3.5 resembles the anticipated synchronization regimes obtained for two coupled linear systems, which were studied in detail in Ref. [99].

Beyond this regime of synchronization by common random forcing, a finite value of the coupling K is required to achieve anticipated synchronization. However, a very large value of the coupling worsens the quality of the synchronization. The existence of minimum and maximum values for the coupling in order to exhibit good anticipated synchronization agrees with what was previously found in autonomous chaotic systems [97] and in linear maps [100]. The data shown in the next figures are the result of

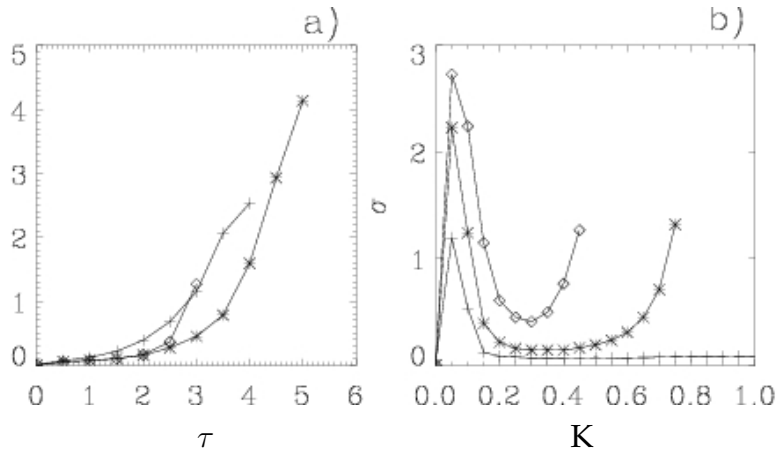

Figure 3.7: *Plot of the standard deviation of the anticipation time, σ, as a function of (a) the delay time τ and (b) the coupling K in the same cases as in Fig. 3.6.*

averaging over a few thousand of spike events. Figure 3.6(a) plots the mean anticipation time $\langle t \rangle$ as a function of τ for different values of the coupling K. The results for large K fall mainly on the line $\langle t \rangle = \tau$ corresponding to the generalized anticipated solution $\mathbf{y}(t) \approx \mathbf{x}(t + \tau)$. Note that if K is small ('+' in Fig. 3.6a) $\langle t \rangle$ could even be larger than τ. However this result does not take into account that the quality of the synchronization is poor in this case (it corresponds to the grey region near the vertical axis in Fig. 3.5) for which the standard deviation σ is large (see Fig. 3.7) indicating a bad synchronization quality. Note, finally, that for each value of K there is a maximum anticipation time, in agreement with the rather sharp transition between synchronized and unsynchronized regimes shown in Fig. 3.5. Figure 3.6(b) plots the mean anticipation time $\langle t \rangle$ as a function of K for different values of τ. The main result is that for each value of τ there is a set of values of K, $K_{min} < K < K_{max}$, such that $\langle t \rangle \sim \tau$ (the plateaus in Fig. 3.6b). For small values of the coupling, $K < K_{min}$ $\langle t \rangle \sim 0$, and this reflects that the two neurons are synchronized (without anticipation) due to the common external forcing (this parameter region corresponds to the dark region close to the vertical axis of Fig. 3.5). If $K > K_{max}$ the anticipation is lost.

More information about the quality of the anticipated synchronization is obtained by looking at the dispersion in the values of $t_i^m - t_i^s$. In Figs. 3.7a and 3.7b we plot the

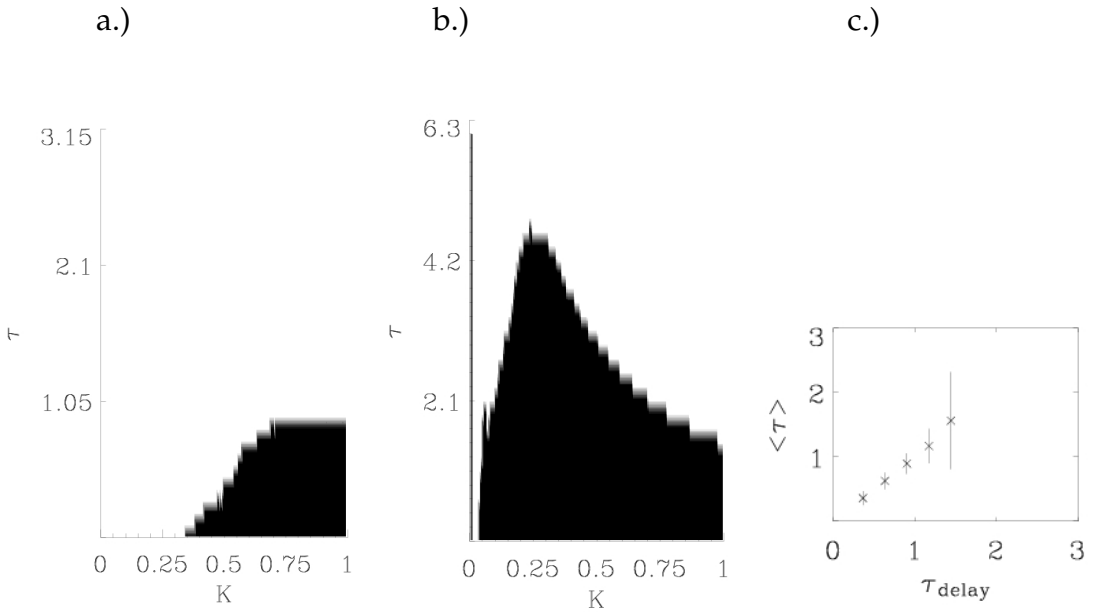

Figure 3.8: *Stability regime for the coupling parameter K and for the delay time τ for one slave where both systems master and slave are driven by different noises. Black colour represents: (a) standard deviation $\sigma < 0.16$ and (b) relative error $E_r < 0.1$. (c) The dependence of the mean anticipation times measured at the threshold value $x_{th} = 0.65$ for coupling value $K = 1$ vs. the delay times used in the equations (cross signs). Vertical lines correspond to standard deviations for which the longest one corresponds to $\sigma = 0.75$.*

standard deviation, σ, in the same cases as in Figs. 3.6a and 3.6b. Certainly, the best synchronization quality can be defined as the one with the small number of errors and the small dispersion in the synchronization time. In this sense, one can see in Fig. 3.7a that σ is an increasing function of τ, indicating that the dispersion (and the quality of the synchronization) worsens for large τ. Note also in Fig. 3.7b that in the interval of coupling strength where good synchronization occurs, $K_{min} < K < K_{max}$, σ decreases significantly.

Numerical results shown in Fig. 3.8 and 3.9 reveal that anticipated synchronization is also possible when both master and slave systems are driven by different white noise sources. We obtain a smaller stability region with the maximum for the anticipation time τ shifted in the direction of larger coupling constant values. This result, showing that the anticipated synchronization can appear even if the different noises are considered, is interesting from the practical point of view. In real systems, biological or man-made ones, component units are usually subject to different noise sources, and the robustness of the synchronization in this case is a useful feature.

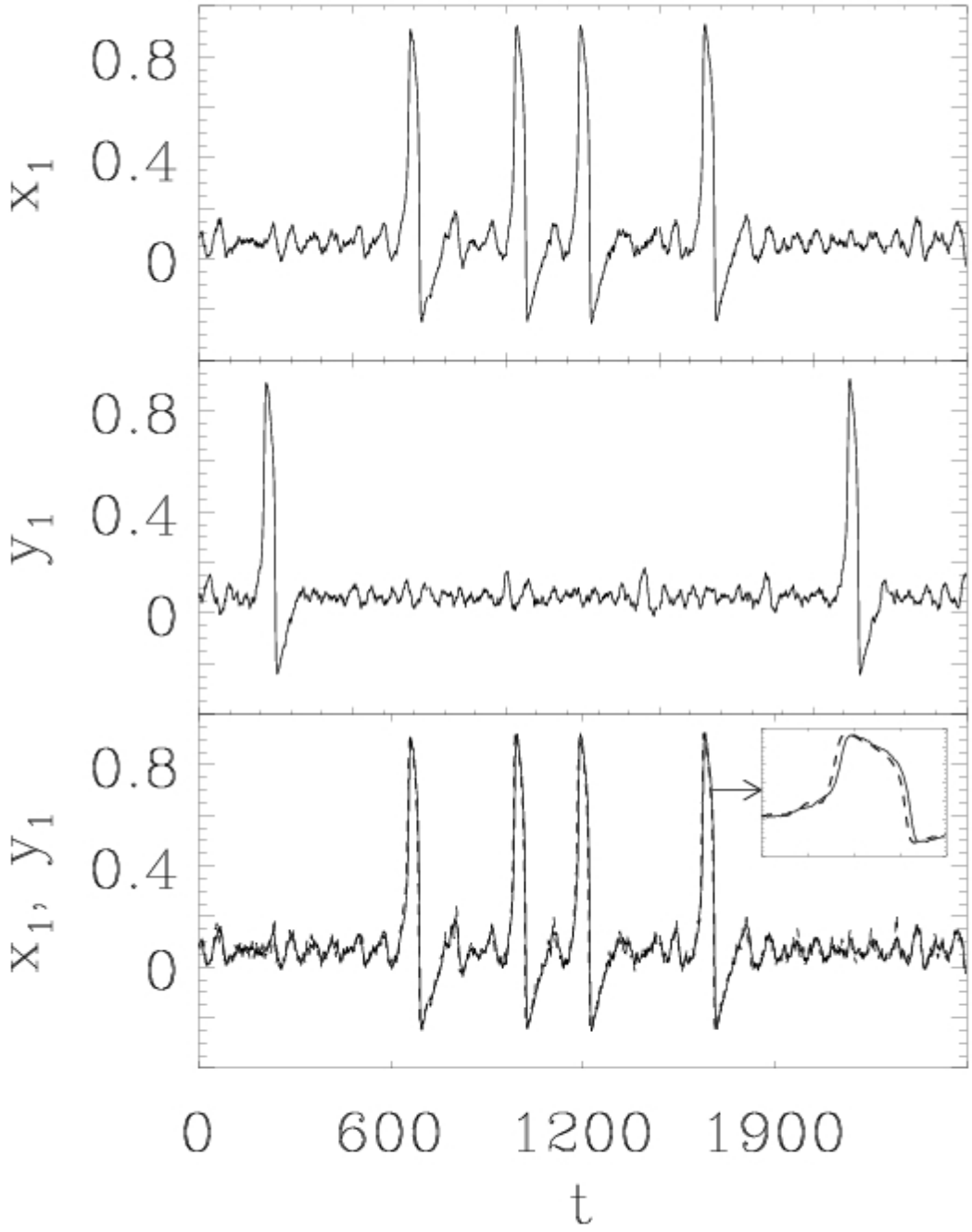

Figure 3.9: *Time series for master (upper panel), uncoupled slave (middle panel) and coupled slave (lower panel) with coupling parameters $K = 0.3$ and $\tau = 3$. Both systems are driven by different realizations of white noise.*

3.1.2 Linear stability analysis

Linearization of the FitzHugh-Nagumo system

In this Section we concentrate on the stability analysis of the anticipated synchronization solution in coupled FitzHugh-Nagumo systems. We recall the anticipated synchronization scheme for the coupled FitzHugh-Nagumo equations with the external forcing:

$$\begin{aligned} \dot{x_1} &= -x_1(x_1-a)(x_1-1)-x_2+I_0 \\ \dot{x_2} &= \epsilon(x_1-bx_2) \qquad (3.7) \\ \dot{y_1} &= -y_1(y_1-a)(y_1-1)-y_2+I_0+K[x_1(t)-y_1(t-\tau)] \\ \dot{y_2} &= \epsilon(y_1-by_2) \qquad (3.8) \end{aligned}$$

where a and b are constants and I_0 is an external forcing assumed constant. We provide the stability analysis for the FitzHugh-Nagumo system by using a piece-wise linear approximation [65] of the cubic function $f(x_1) = -x_1(x_1-a)(x_1-1)+I_0$ in Eq. 3.7. For

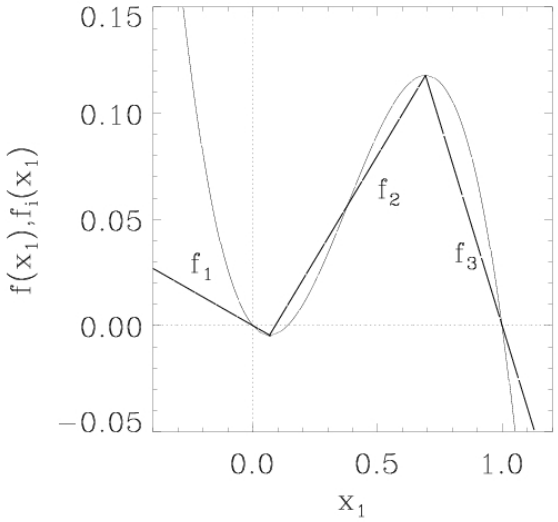

Figure 3.10: *Thin line represents the cubic function in the FitzHugh-Nagumo system, meanwhile the bold lines are the functions obtained after the piece-wise linearization of this cubic function.*

$a = 0.139$ taken in our study we obtain three linear functions representing $f(x_1)$ which have the form: $f_i(x_1) = a_i x_1 + b_i$, where $a_1 = -0.067$, $a_2 = 0.195$, $a_3 = -0.383$, $b_1 = I_0$, $b_2 = -0.0176 + I_0$ and $b_3 = -0.383 + I_0$. We plot these functions in Fig. 3.10.

Considering the solution of the system in Eq. 3.7 which leads to the anticipated synchronization: $y_1(t) = x_1(t+\tau)$, we define the difference variable $\Delta(t) = x_1(t) - y_1(t-\tau)$. We neglect the contribution from the difference $\{x_2(t) - y_2(t-\tau)\}$ by assuming that $\epsilon \approx 0$

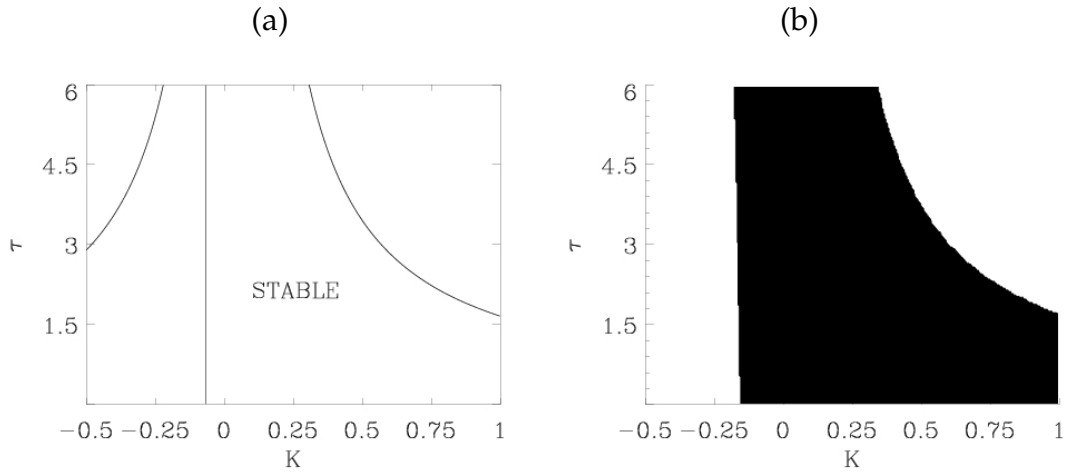

Figure 3.11: *(a) Stability conditions for the master and the slave FitzHugh-Nagumo systems being in the steady (however excitable) state and in the absence of the external forcing. Solid line represents the boarder curve separating the region of the steady and non-steady solutions for the slave. (b) The same as in (a) but obtained through the numerical simulations; black (white) region corresponds to the steady (non-steady) solutions for the slave.*

what means that the action potential x_1 fires almost instantaneously if the perturbation is applied. We write the following differential equation describing the dynamics of $\Delta(t)$:

$$\dot{\Delta}(t) = a_1\Delta(t) - K\Delta(t-\tau) \tag{3.9}$$

where a_1 is the coefficient in the function $f_1(x_1)$ which approximates the cubic function in the FitzHugh-Nagumo equation in the vicinity of the fixed point $(x_1, x_2) = (0, 0)$. If the master and the slave are in an oscillatory or an excitable state and are driven by a constant external forcing, then the following conditions for the anticipated synchronization existence can be derived (detailed calculations are provided in Appendix A):

$$\begin{aligned} K &> a_1 \qquad\qquad\qquad \text{and} \\ \tau &< \frac{\arccos(\frac{a_1}{K})}{\sqrt{K^2 - a_1^2}} \qquad \text{for} \quad K > |a_1| \end{aligned} \tag{3.10}$$

In Fig. 3.11a we draw the curves given by Eq. 3.10. The numerical results for the FitzHugh-Nagumo coupled neurons being in the steady excitable state and in the absence of an external forcing are shown in Fig. 3.11b.

FitzHugh-Nagumo systems driven by a white noise source

In the case of the FitzHugh-Nagumo systems driven by a Gaussian white noise $I(t) = \xi(t)$ with zero mean and auto-correlation $\langle \xi(t)\xi(t') \rangle = 2D\delta(t-t')$, the differential equation for the difference variable $\Delta(t)$ will contain the white noise term of the form $\eta(t) =$

$\xi(t) - \xi(t-\tau)$:

$$\dot{\Delta}(t) = a_1\Delta(t) - K\Delta(t-\tau) + \eta(t) \tag{3.11}$$

with the set of initial conditions $\Delta(t) = \Delta_0(t)$ at $t \in (-\tau, 0)$. It can be easily seen that if the master is driven by the white noise which is retarded by time τ in comparison with the noise injected to the slave then $\eta(t) = \xi(t) - \xi(t+\tau-\tau) = 0$. This corresponds to the case when the constant external forcing is applied to both systems. The cross-correlation diagram for this case obtained through numerical simulations of the systems driven by the noise sources $\xi(t)$ (in the master) and $\xi(t+\tau)$ (in the slave) are shown in Fig. 3.12.

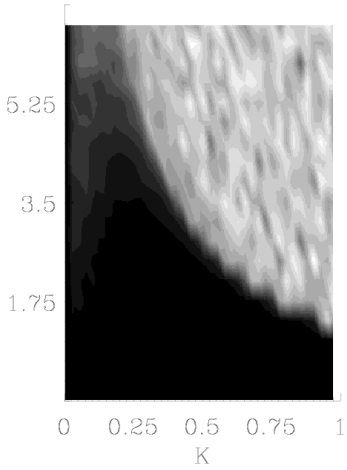

Figure 3.12: *The cross-correlation diagram between the master and the slave outputs ($x_1(t)$ and $y_1(t-\tau)$). Both systems are driven by the white noise sources: $\xi(t)$ in the master and $\xi(t+\tau)$ in the slave.*

To solve Eq. 3.11 we proceed as in the case of the delayed differential equation in the absence of noise (see Appendix A). Stability analysis for delayed differential equations with noise was provided e.g. in Refs. [111, 112]. We define a new variable $h(t) = \Delta(t)e^{-a_1 t}$ and introduce it into the equation 3.11:

$$\dot{h}(t) = -Ke^{-a_1\tau}h(t-\tau) + R(t) \tag{3.12}$$

where $R(t) = e^{-a_1 t}\eta(t)$. Then we apply the Laplace transform getting the following equality:

$$\tilde{h}(z) = \frac{M(z)}{z + Ke^{-a_1\tau}e^{-\tau z}} \tag{3.13}$$

where $\tilde{h}(z) = \mathcal{L}[\Delta(t)]$ and $M(z)$:

$$M(z) = h(0) - Ke^{-a_1\tau}e^{-\tau z}\int_{-\tau}^{0} h(t)e^{-zt}dt + \tilde{R}(z) \tag{3.14}$$

To get the solution for variable $\Delta(t)$ first we need to find the solution for $h(t)$ by applying the inverse Laplace transform to Eq. 3.13:

$$\Delta(t) = h(t)e^{a_1 t} = \sum_{i=1}^{n} \mu_i e^{(a_1+z_i)t} \tag{3.15}$$

where z_i are the zeros of the denominator in Eq. 3.13 and μ_i are the residua at these points, which can be calculated by using the l'Hôpital's rule:

$$\mu_i = \text{Res}_{z=z_i} \frac{M(z)}{z + Ke^{-a_1\tau}e^{-\tau z}} = \frac{M(z_i)}{1 - K\tau e^{-(a_1+z_i)\tau}} \tag{3.16}$$

From Eq. 3.15 we can see that $\Delta(t)$ vanishes for $t \to \infty$ if $a_1 + \mathcal{R}e[z_i] < 0$ and does not depend on the presence of noise; the result is equivalent to the case in which the external forcing is not a noise source.

The previous analysis shows that the stability of the solution of the linear system does not depend on the presence of noise. However, the stability conditions obtained from the numerical simulations of the FitzHugh-Nagumo system in the absence and in the presence of noise are essentially different; in the linear case the stable region is wider. This is due to the fact that the system becomes sensitive to the noise in the presence of nonlinearities in the system. Let us examine qualitatively if the stability condition for the coupling constant can be influenced by noise if the system contains nonlinearities. Let us consider the following equation:

$$\dot{\Delta}(t) = b\Delta(t) + c\Delta^3(t) - K\Delta(t-\tau) + \eta(t) \tag{3.17}$$

where we add the cubic term $c\Delta^3(t)$. Let us assume that $\tau = 0$. The stability of the system requires that the nonlinear term is small with respect to the linear one, thus we get:

$$|(b-K)\Delta| > |c\Delta^3| \to \Delta^2 < \left|\frac{b-K}{c}\right| \tag{3.18}$$

In the linear approximation we get the following solution for Eq. 3.17:

$$\Delta(t) = e^{(b-K)t}\left(\int_0^t \eta(t')e^{-(b-K)t'}dt'\right) \tag{3.19}$$

where we assume that $\Delta(0) = 1$. Equation 3.17 is stochastic and its solution has to be considered in terms of the mean quantities. This yields $\langle\Delta(t)\rangle = 0$ since the mean of the

noise variable is zero. From Eq. 3.19 we calculate the mean value of $\Delta^2(t)$:

$$\begin{aligned}
\langle\Delta^2(t)\rangle &= \left\langle \left(e^{(b-K)t}\int_0^t \eta(t')e^{-(b-K)t'}dt' \right)\left(e^{(b-K)t}\int_0^t \eta(t'')e^{-(b-K)t''}dt'' \right)\right\rangle \\
&= e^{2(b-K)t}\int_0^t\int_0^t \langle\eta(t')\eta(t'')\rangle e^{-(b-K)(t'+t'')}dt'dt'' \\
&= e^{2(b-K)t}\int_0^t\int_0^t 2D\delta(t'-t'')e^{-(b-K)(t'+t'')}dt'dt'' \\
&= 2De^{2(b-K)t}\frac{1-e^{-2(b-K)t}}{2(b-K)} = \frac{D}{b-K}(e^{2(b-K)t}-1)
\end{aligned} \tag{3.20}$$

In the limit $t\to\infty$, assuming that $b-K<0$, we get:

$$\lim_{t\to\infty}\langle\Delta^2(t)\rangle = \frac{D}{K-b} \tag{3.21}$$

Using Eq. 3.18 we obtain the following condition for the stability:

$$\Delta^2 < \left|\frac{b-K}{c}\right| \to \frac{D}{K-b} < \left|\frac{b-K}{c}\right| \to K > \sqrt{D|c|}+b \tag{3.22}$$

The above condition for the coupling parameter K in the coupled systems driven by noise is shifted into the direction of the larger K values and depends on the noise intensity D. It means that the interplay between the nonlinearities and the noise can influence the quality of the anticipated synchronization (as well as the synchronization), making it worse if the intensity of the noise is large and the nonlinearities are strong.

3.1.3 Coupled neurons in a chain

As mentioned in the introductory Section 2.6.2, systems coupled in a chain with many slave units can enhance the anticipation time. In this Section we apply this idea to the coupled FitzHugh-Nagumo systems driven by white noise in order to check whether in this case such an enhancement of anticipation is possible. For this purpose we assume that we have an array of slave systems connected unidirectionally, as shown in Fig. 3.13, which are described by the set of equations:

$$\begin{aligned} \dot{\mathbf{x}} &= \mathbf{f}(\mathbf{x}) + \mathbf{I}(t) \\ \dot{\mathbf{y}}^1 &= \mathbf{f}(\mathbf{y}^1) + \mathbf{I}(t) + K(\mathbf{x}(t) - \mathbf{y}^1(t-\tau_1)) \\ &\vdots \\ \dot{\mathbf{y}}^N &= \mathbf{f}(\mathbf{y}^N) + \mathbf{I}(t) + K(\mathbf{y}^{N-1}(t) - \mathbf{y}^N(t-\tau_N)) \end{aligned} \tag{3.23}$$

where N is the number of slave systems. The desired solution for this system is:

$$y_1^N(t-\tau) = y_1^N(t - \sum_{n=1}^{N} \tau_n) = x_1(t) \tag{3.24}$$

In Fig. 3.14a we show the time series of the master and slave systems coupled by the delayed coupling scheme with a delay time $\tau = 6$. Two errors appear during anticipation: the deformation of the second peak and an extra spike in the slave occurring at the end of the time series. Next step is to take three slaves coupled in a chain with the delay times $\tau_1 = \tau_2 = \tau_3 = 2$, what gives at the third slave the anticipation of master by time $\tau = \sum_{i=1}^{3} \tau_i = 6$. In Fig. 3.14b we show time series for the master and the third slave

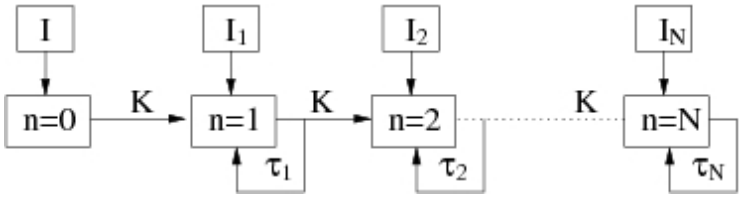

Figure 3.13: *An array consisting of master system ($n = 0$) and N slave systems which are feeded back with a delay time τ and coupled unidirectionally each other with a coupling parameter K.*

systems which anticipates the master by the time $\tau = 6$. The use of a chain enables us to correct the two errors seen in Fig. 3.14a and to achieve an anticipation of order of $\tau = 6$ which in one slave configuration cannot be obtained without errors. In Fig. 3.14c it is shown the successive anticipation of the master by the first slave by time $\tau = 2$, the first slave by the second slave by time $\tau = 2$ and finally the second slave by a third slave, also by time $\tau = 2$. Thus giving in sum a global anticipation time $\tau = 6$.

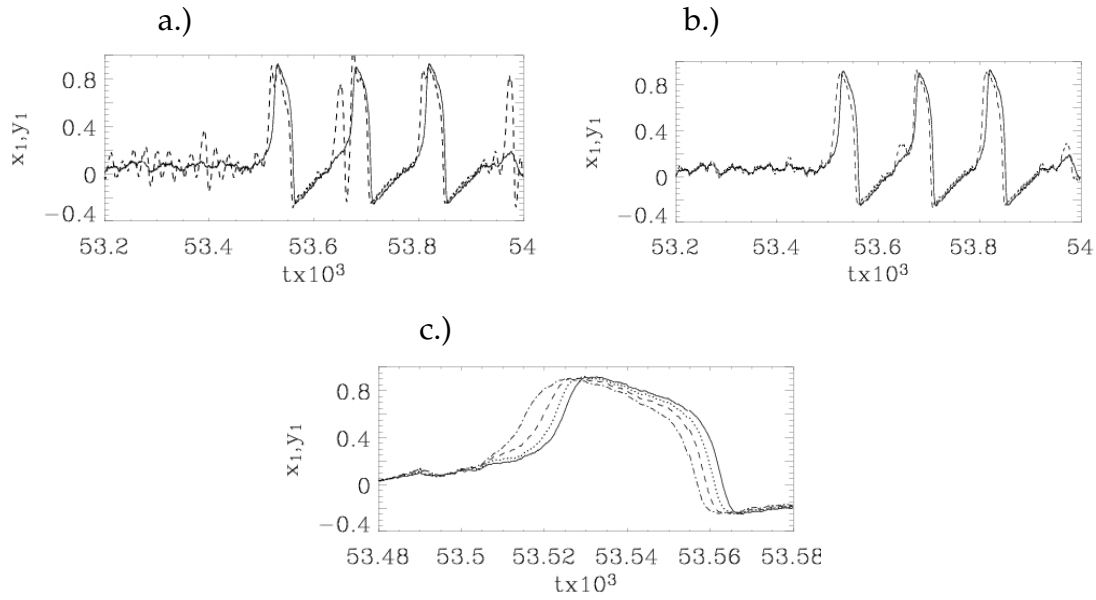

Figure 3.14: *(a) Time series of master (solid line) and slave (dashed line) for* $\tau = 6$ *and* $K = 0.25$. *(b) Time series of master (solid line) and third slave (dashed line) for* $\tau_i = 2$ *(where* $i = 1, 2, 3$*) and* $K = 0.25$. *(c) Time series of one pick for master system (solid line), first slave (dotted line), second slave (dashed line) and third slave (dashed-dotted line).*

The calculation of an average anticipation time with its standard deviation for the long time series and beyond any initial transient revealed that indeed the anticipation is enhanced as the number of slaves increases. The error bars attached to the points in Fig. 3.15 represent the standard deviation values which remain smaller for larger delay times in the case the chain is used. The standard deviation σ of the mean anticipation

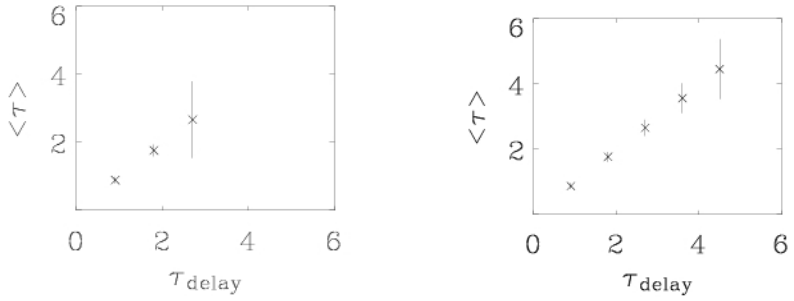

Figure 3.15: *Dependence of the mean anticipation time measured at the threshold value* $x_{th} = 0.65$ *for coupling value* $K = 0.5$ *on delay time used in equations for the case with one slave (left plot) and three slaves with equal delays in each of them (right plot). The standard deviations are plotted in form of vertical lines.*

time for the system composed of the master and three slave FitzHugh-Nagumo systems

driven by noise, with delay times $\tau_1 = \tau_2 = \tau_3 = 2$ has been calculated in the parameters space τ and K and is shown in Fig. 3.16a. We observe changes when delay times in all three slaves differ in such a way that $\tau_1 = 1$, $\tau_2 = 2$ and $\tau_3 = 3$ (see Fig. 3.16b). In this case the black region of high cross-correlations is slightly shifted in the direction of smaller coupling constants K in comparison with the case where $\tau_1 = \tau_2 = \tau_3 = 2$. However for the case in which the delay times are $\tau_1 = 3$, $\tau_2 = 2$ and $\tau_3 = 1$ (see Fig. 3.16c) the maximum τ is shifted in the direction of larger coupling constants K in comparison with the uniform case $\tau_1 = \tau_2 = \tau_3 = 2$. From Figs. 3.16a, b and c it can be seen that the maximum anticipation time obtained with these three type of configurations is approximately the same i.e. cannot be enhanced significantly.

In the case of relative error (the rate of appearance of additional spikes) a larger enhancement is observed (see Fig. 3.17). The best configuration here is the one with equal delays in all slaves $\tau_1 = \tau_2 = \tau_3 = 2$, and it can be seen that other configurations with different delays give smaller regions of stability.

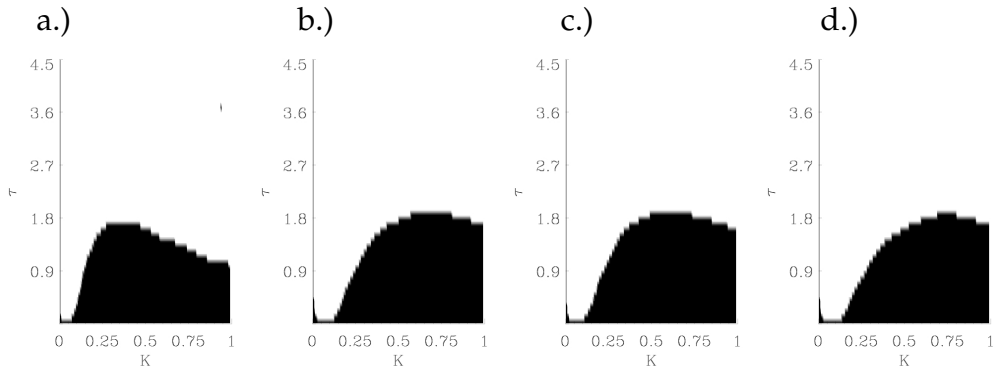

Figure 3.16: *Stability region estimated numerically and determined by dependence of the coupling parameters τ and K for one slave (a) and for three slaves with the following configuration of time delays: (b) $\tau_1 = \tau_2 = \tau_3 = 2$, (c) $\tau_1 = 1$, $\tau_2 = 2$ and $\tau_3 = 3$, (d) $\tau_1 = 3$, $\tau_2 >= 2$ and $\tau_3 = 1$. Dark regions correspond to the standard deviation value $\sigma < 0.15$.*

Considering the anticipated synchronization manifold for FitzHugh-Nagumo coupled neurons (Eq. 3.7) in a chain and assuming that $\tau_n = \tau$ in each subsystem, we can write the following set of N equations:

$$\dot{\mathbf{\Delta}}_n = \beta \mathbf{\Delta}_n - K \mathbf{\Delta}_{n,\tau_n} + K \mathbf{\Delta}_{n-1} \tag{3.25}$$

which in the vector notation take the form:

$$\dot{\mathbf{\Delta}} = \Omega \mathbf{\Delta} - \mathcal{K} \mathbf{\Delta}_\tau \tag{3.26}$$

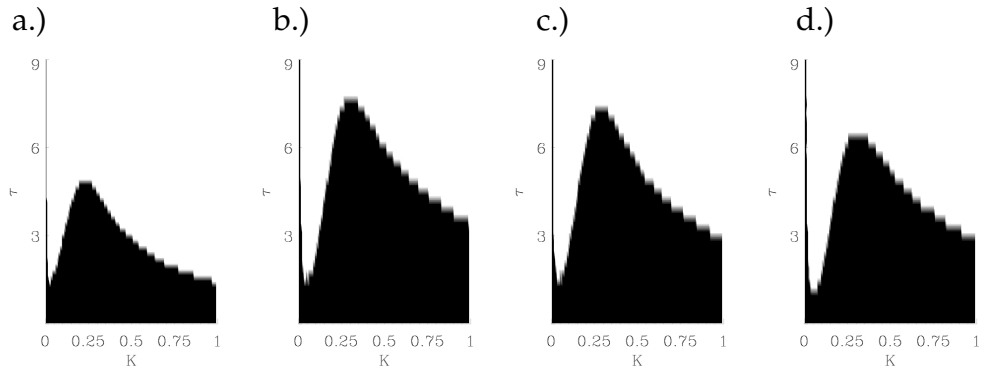

Figure 3.17: *Stability region vs. the relative error E_r for one slave (a) and a cascade of three slaves with $\tau_1 = \tau_2 = \tau_3 = 2$ (b), $\tau_1 = 1$, $\tau_2 = 2$ and $\tau_3 = 3$ (c) and $\tau_1 >= 3$, $\tau_2 = 2$ and $\tau_3 = 1$ (d). Black region corresponds to $E_r < 0.1$.*

where:

$$\mathbf{\Delta} = \begin{bmatrix} \Delta_1 \\ \vdots \\ \Delta_N \end{bmatrix}, \bar{\Omega} = \begin{bmatrix} \beta & 0 & \cdots & \cdots & \cdots & 0 \\ K & \beta & 0 & \cdots & \cdots & 0 \\ 0 & K & \beta & 0 & \cdots & 0 \\ \vdots & & \ddots & \ddots & & \vdots \\ 0 & \cdots & 0 & K & \beta & 0 \\ 0 & \cdots & \cdots & 0 & K & \beta \end{bmatrix}, \mathbf{\Delta}_\tau = \begin{bmatrix} \Delta_{1,\tau} \\ \vdots \\ \Delta_{N,\tau} \end{bmatrix} \tag{3.27}$$

Assuming the solution of this equation as $\mathbf{\Delta} = \mathbf{C}(t)e^{\lambda t}$ for $N = 3$ slaves we get:

$$\begin{bmatrix} \Delta_1 \\ \Delta_2 \\ \Delta_3 \end{bmatrix} = e^{(\beta - Ke^{-\lambda\tau})t} \begin{bmatrix} 1 \\ AKt \\ A^2\left(\frac{(kt)^2}{2} - AKe^{-\lambda\tau}\frac{(K\tau)^2}{2}t\right) \end{bmatrix} \tag{3.28}$$

where $A = (1 - K\tau e^{-\lambda\tau})^{-1}$. The expressions in Eq. 3.28 tend to zero if $Re[\lambda] < 0$ thus we get the following conditions:

$$\tau \;<\; N\frac{1}{K}\frac{\arccos(\frac{-\beta}{K})}{\sqrt{1-\left(\frac{\beta}{K}\right)^2}} \tag{3.29}$$

which is valid for the case in which all slaves in the chain has the same delay time τ in the delayed coupling term.

In the case of the coupled FitzHugh-Nagumo systems operating in the oscillatory regime we also get that the stability region for the standard deviation of the observed anticipation time decreases when the slaves have different delay times (see Fig. 3.18). Note that in this case the relative error (defined in Eq. 3.6) is always zero. The results

obtained for the FitzHugh-Nagumo systems driven by noise as well as operating in the oscillatory state suggest that the phenomenon of the stability breaking when using different delays in each slave appears in forced as well as in unforced systems.

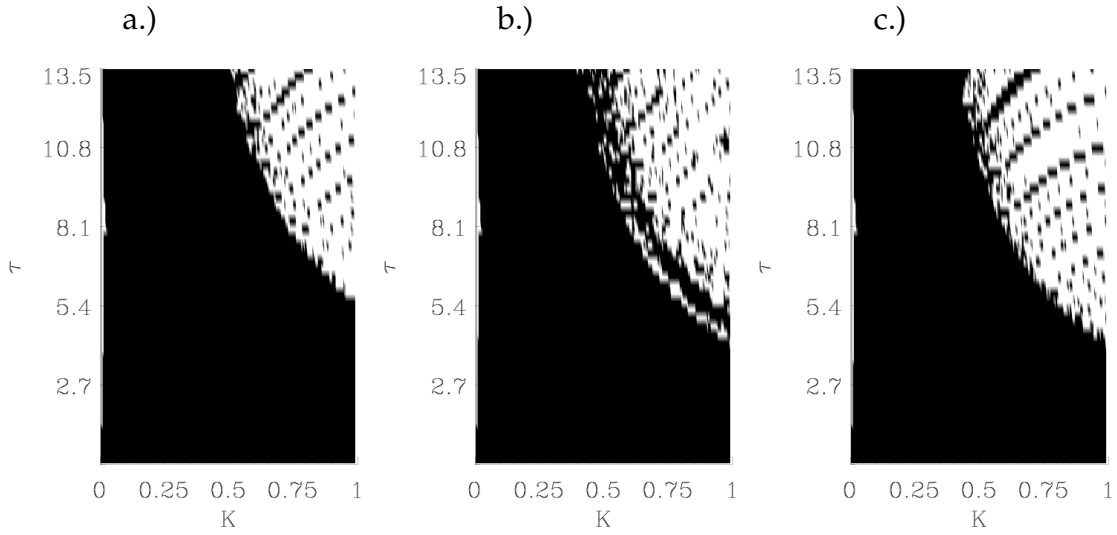

Figure 3.18: *Stability region obtained numerically for three slaves with (a)* $\tau_1 = \tau_2 = \tau_3$*, (b)* $\tau_1 < \tau_2 < \tau_3$ *and (c)* $\tau_1 > \tau_2 > \tau_3$*. Homogenously black region correspond to the standard deviation* $\sigma < 0.1$*.*

3.1.4 Experiments

To assess the robustness of the anticipated synchronization observed in the numerical simulations, we implement the FitzHugh-Nagumo model in analog hardware and construct two coupled electronic neurons (a simplified version of the circuit is shown in Fig. 3.19). The electronic neurons are built using operational amplifiers and the cubic non-linearity described by $x(x-a)(x-1)$ is implemented using analog multipliers (AD633). The resistor R_C controls the strength of the unidirectional coupling between

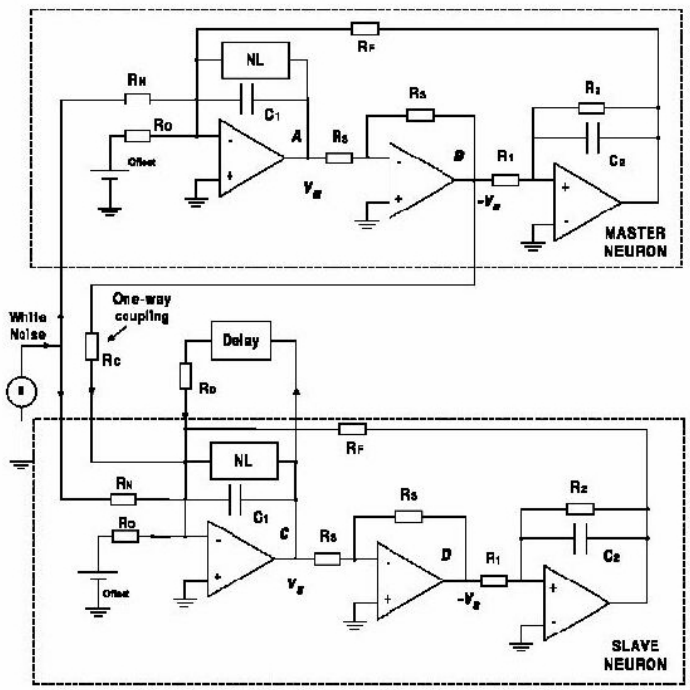

Figure 3.19: *Circuit implementation of two coupled neurons.* R_1 *= 125 k*Ω*,* R_2*=50 k*Ω*,* R_3*=10 k*Ω*,* $R_C = R_D$*=100 k*Ω*,* R_F*=10 k*Ω*,* R_N*=10 k*Ω*,* R_O*= 10 k*Ω*,* C_1*=100 nF,* C_2*=1* μ*F.*

the master and the slave neurons. The resistor R_D ($R_D = R_C$ in our case) controls the strength of the delayed feedback into the slave neuron. The coupling and the delayed feedback have opposite signs: while the master signal is obtained at point B of Fig. 3.19, where the voltage is $-V_m$, the slave signal that goes into the delay line is obtained at point C, where the voltage is $+V_s$. The different signs are due to the inverters that are located in between points A and B and C and D. The threshold on both neurons is controlled by a potentiometer represented by its equivalent circuit: offset and

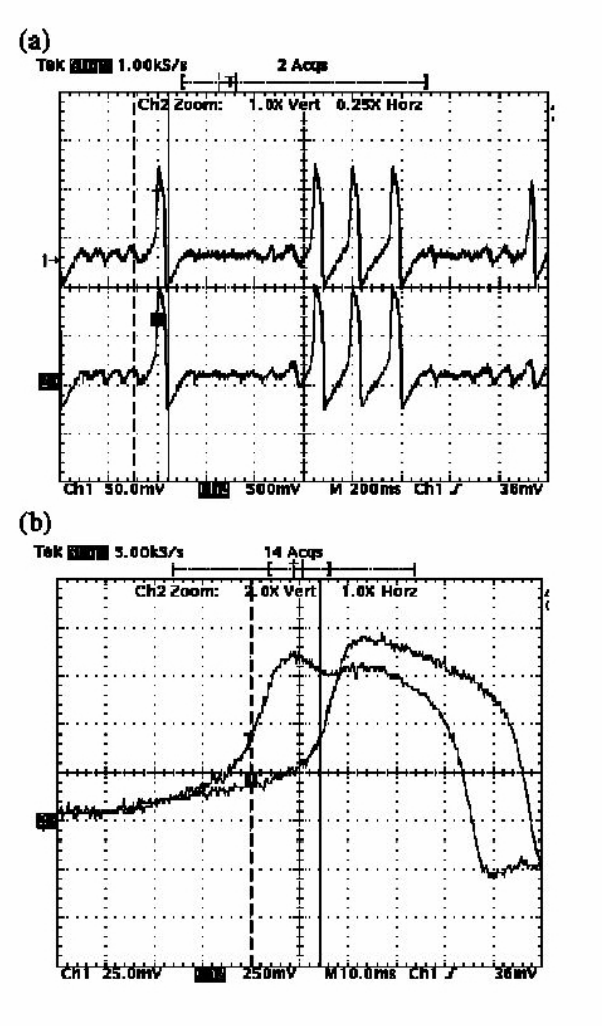

Figure 3.20: *(a) Experimental train of spikes that shows anticipation in the spikes fired by the slave neuron (upper trace) with respect to the spikes fired by the master neuron (lower trace). (b) Detail of a spike fired by the master neuron and anticipated spike fired by the slave neuron. The anticipation time is* 14 *ms approximately.*

R_0. The analog delay line for the delayed feedback in the slave neuron is built using bucket brigade circuits (MN3004). A function generator with white noise output capabilities (HP33120A) is used to excite both electronic neurons. The signals are acquired using LabView and National Instruments DAQ 6025E data acquisition board. Similar electronic neurons have been implemented in [113], where it was shown that their behaviour is very similar to that of biological neurons: when interfaced to biological neurons, hybrid circuits, with the electronic neurons taking the place of missing or damaged biological neurons, could function normally. Our electronic coupled neurons behave very similar as in the numerical simulations. For an appropriate value of the

coupling resistance R_C, we observe that, after a transient, the master and slave electronic neurons synchronize in such a way that the slave neuron anticipates the fires of the master neuron by a time interval approximately equal to the delay time τ of the feedback mechanism. Figure 3.20a shows a typical spike train, and Fig. 3.20b displays in detail a single spike. We observe that, as in the numerical simulations, the firings of

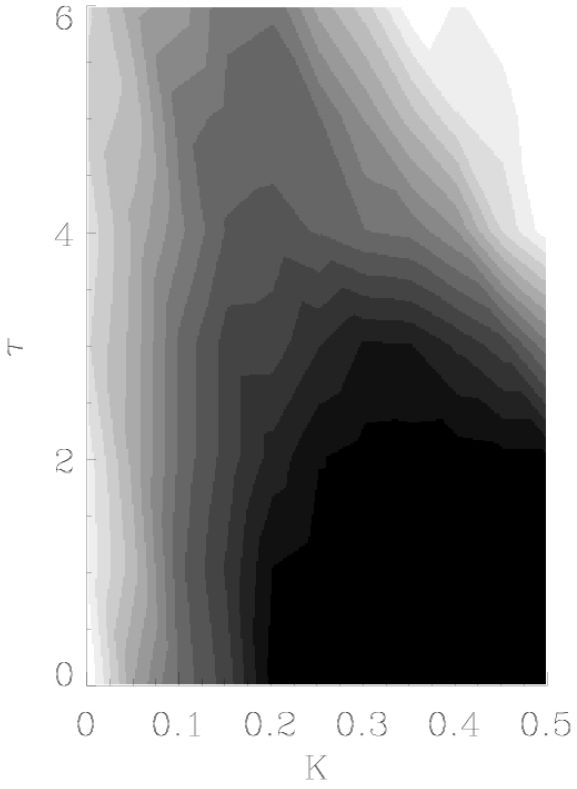

Figure 3.21: *Experimentally obtained cross-correlation diagram between the signal in the parameter space of delay time τ and coupling constant K. Black (white) colour represents high (low) correlations.*

the master and the slave neurons start at about the same time: anticipation begins during the rising of the peak and it vanishes when the neurons are in the unexcited state. Without coupling and feedback ($R_C = R_D = 0$) the neurons fire pulses which are, in general, unsynchronized (due to the small mismatch between the circuits). From the experimental data we construct the cross-correlation diagram between the master and slave time series in the parameter space τ and K (see Fig. 3.21) which is similar to that obtained through the numerical simulations in Section 3.1.

3.2 Anticipated synchronization in spatiotemporal systems

In this Section we turn our attention to the spatiotemporal systems, in particular the complex Ginzburg-Landau equations (section 3.2.1) and the model for chemical reaction of CO oxidation on a platinum surface (section 3.2.2). We characterize numerically and analytically (in the case of complex Ginzburg-Landau equations) the ranges of parameters for which anticipated synchronization can be obtained and study the coupling architecture which could be realized in an experimental setup. In Section 3.2.3 we show that the interplay between the anticipated synchronization and conduction delays can lead to zero-lag synchronization. We show its appearance in coupled spatiotemporal FitzHugh-Nagumo systems and propose the hypothesis on its relevance in real biological systems which process the information through intercellular communication. Finally (section 3.2.4) we analyze the appearance of anticipated synchronization in cellular automata models. The interest in these systems was motivated by their spatial cooperation characteristics leading to self-organization processes. In a particular class of cellular automata we analyze the spatial properties of equations with delayed feedback.

3.2.1 Coupled complex Ginzburg-Landau equations

A well-known model equation which displays a rich variety of spatiotemporal dynamics is the 1-dimensional complex Ginzburg-Landau equation (see Section 2.3):

$$\dot{A} = \epsilon A + (1 + ic_1)A_{xx} - (1 + ic_2)|A|^2 A \tag{3.30}$$

where $A(x,t) \equiv \rho(x,t)e^{i\phi(x,t)}$ is a complex field of amplitude ρ and phase ϕ, the dot denotes a temporal derivative and $A_{xx} = \frac{\partial^2 A}{\partial x^2}$ is the second order derivative with respect to the space variable, $0 \leq x \leq L$, where L is the system length. ϵ is a control parameter inducing instability if it is positive, c_2 is a measure of the nonlinear dispersion and, finally, c_1 is the linear dispersion parameter.

We define master and slave Ginzburg-Landau's systems coupled with delayed coupling in the following way:

$$\dot{A} = \epsilon A + (1 + ic_1)A_{xx} - (1 + ic_2)|A|^2 A \tag{3.31}$$

$$\dot{B} = \epsilon B + (1 + ic_1)B_{xx} - (1 + ic_2)|B|^2 B + \kappa(A - B_\tau) \tag{3.32}$$

with a general complex coupling constant $\kappa = Ke^{i\theta}$. As usual B_τ stands for $B(t-\tau)$ and τ is a constant delay time. The use of a complex coupling is motivated by its relevance in coupled laser systems (see for instance ref. [114]). In numerical simulations we keep $\epsilon = 1$. We integrate numerically Eq. 3.31 and 3.32 by using the two-step method to

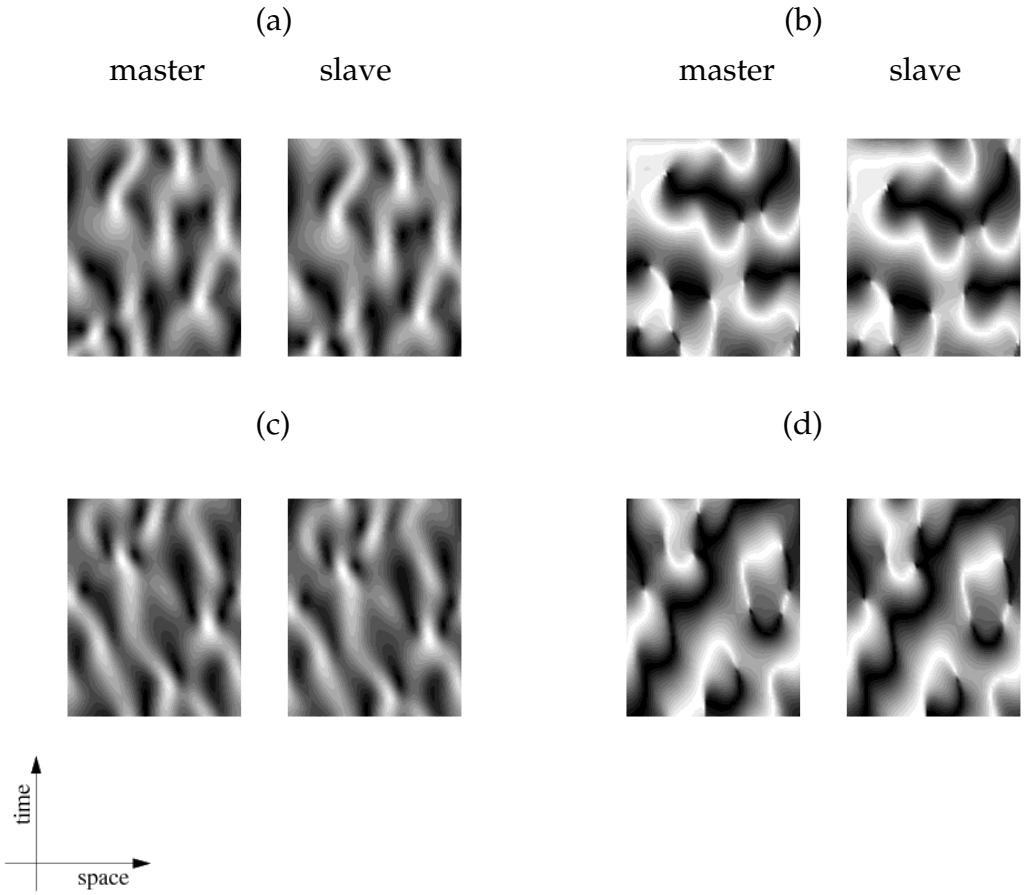

Figure 3.22: *Spatiotemporal dynamics of (a) amplitude and (b) phase. Parameters:* $\tau = 0.6$, $\theta = \frac{\pi}{4}$, $|K| = 0.6$, $N = 64$, $\delta x = 0.2$, $\delta t = 0.002$, $c_1 = 3$, $c_2 = -2.5$ *(in a range of defect turbulence). Spatiotemporal dynamics of (c) amplitude and (d) phase. Parameters:* $\tau = 0.5$, $\theta = 0$, $|K| = 0.75$, $N = 64$, $\delta x = 0.2$, $\delta t = 0.002$, $c_1 = 3$, $c_2 = -2.5$.

integrate the Fourier modes, assuming periodic boundary conditions (for details see Appendix B). We use random initial conditions, different in master and slave, in order to obtain distinct initial dynamics in both systems. We take the parameters for our systems from the previous work [54] where larger system sizes were studied in order to identify regions of the parameter space (for details see Section 2.3). The integration time step is $\delta t = 2 \cdot 10^{-4}$. The size of the system is taken to be $L = N\delta x$ with $N = 64$, and $\delta x = 0.2$ in the defect turbulence regime, $\delta x = 1.6$ in the bichaos regime and $\delta x = 2$ in the phase turbulence regime. We will show that the largest anticipation time is related to the linear autocorrelation time estimated from the long time series. Since all types of dynamics exhibited by the complex Ginzburg-Landau equations have different linear autocorrelation times, we expect that the maximum anticipation time will decrease as we move from the spatiotemporal intermittency into the defect turbulence regime. The

(a)

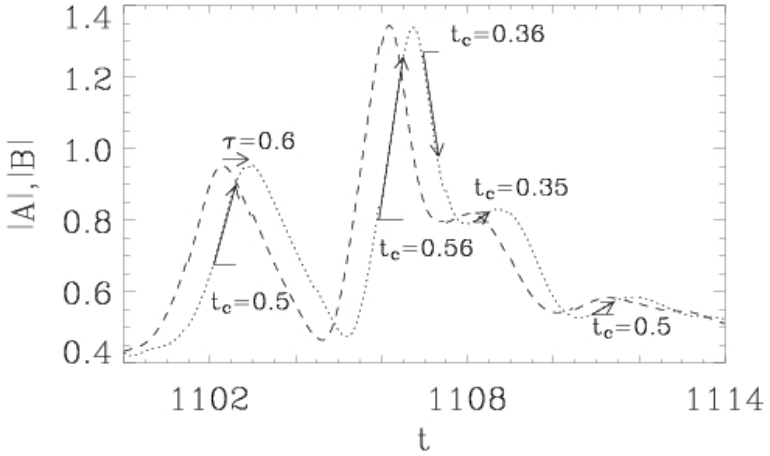

(b)

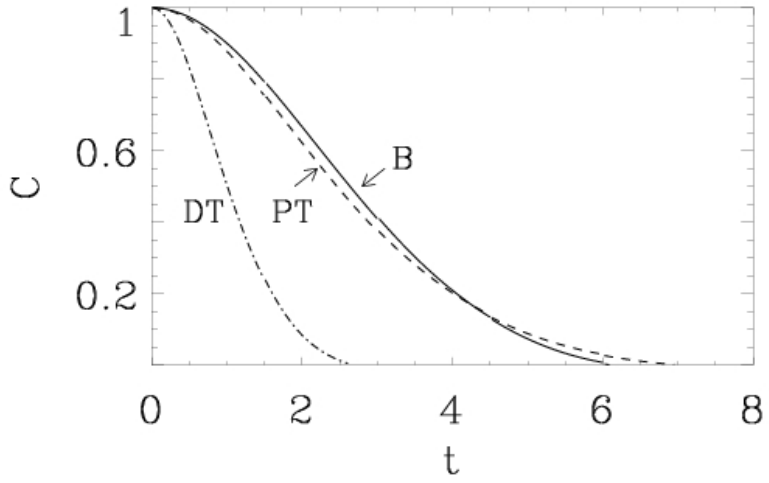

Figure 3.23: *(a) Time series of master (dotted line) and slave (dashed line) complex Ginzburg-Landau equations in the defect turbulence regime. Horizontal arrows mark the anticipation times, no-horizontal arrows mark the parts of the trajectories which are linear and the horizontal solid lines mark the largest linear autocorrelation times distributed along the time series. (b) Autocorrelation function versus time for the three chaotic regimes: defect turbulence, bichaos and phase turbulence.*

spatiotemporal series of amplitude (Fig. 3.22a) and phase (Fig. 3.22b) for the master and slave systems reveal that indeed the slave anticipates the time evolution of the master. Anticipation occurs in the amplitude of the oscillations as well as in the phase. In the case of defect turbulence the maximum anticipation time is $\tau_{max} \approx 0.6$ meanwhile for

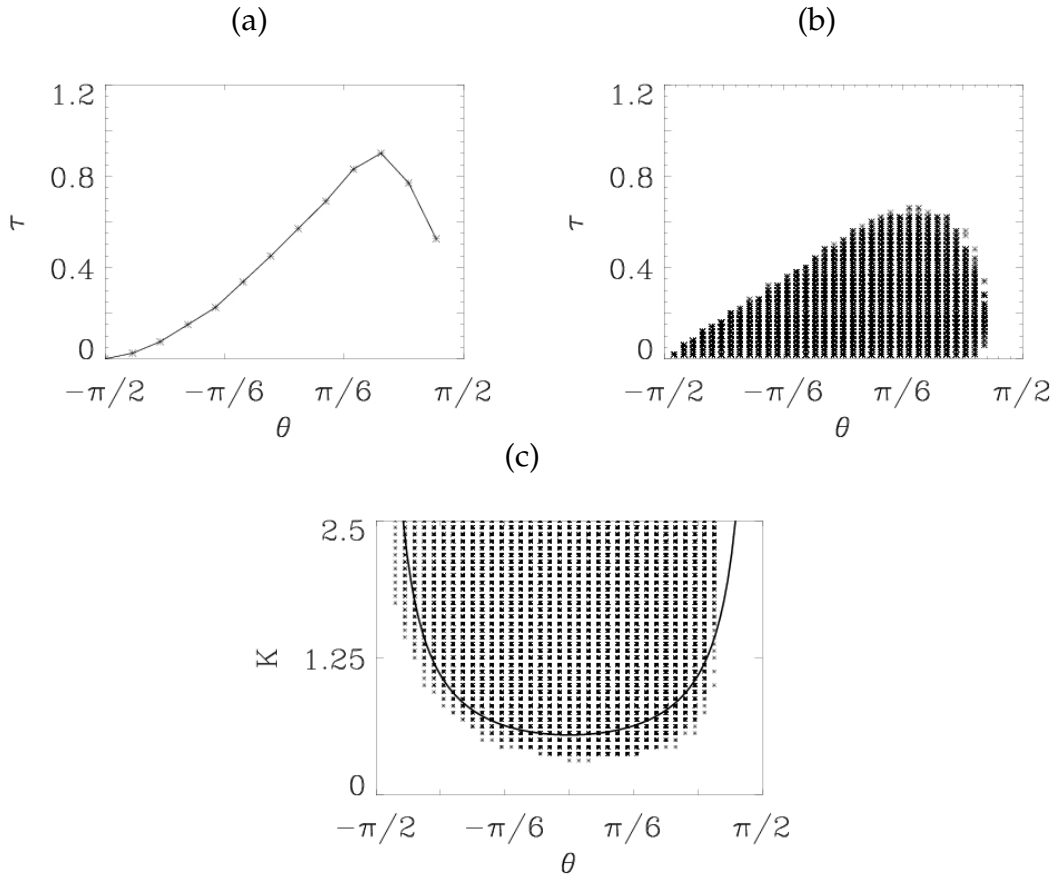

Figure 3.24: *(a) Analytically calculated dependence of maximum anticipation time versus θ representing stable solutions for all possible values of K. We used $c_1 = 3$ and $q^2 = 0.45$. (b) Numerically obtained diagram for the occurrence of anticipated synchronization in the parameter space $\tau - \theta$ representing stable solutions for all possible values of K. Parameters used in numerical simulations: $N = 64$, $\delta x = 0.2$, $\delta t = 0.002$, $c_1 = 3$ and $c_2 = -2.5$. (c) Numerically obtained diagram for the occurrence of anticipated synchronization in the parameter space $K - \theta$. Each plotted point corresponds to several values of τ from the range $[0, 0.6]$. Solid line represents the analytically calculated curve above which anticipation is possible.*

systems in the regime of bichaos this time increases to $\tau_{max} \approx 1.6$, and in the regime of phase turbulence to $\tau_{max} \approx 1.9$. Fig. 3.23a shows time series for the master and slave systems modelled by the complex Ginzburg-Landau equations operating in the defect turbulence regime. In this figure it can be clearly seen that the slave synchronizes and anticipates the output of the master. In the time series we can also notice that the values of the largest anticipation times correspond to the largest linear autocorrelation times.

To prove this we calculate the autocorrelation function:

$$C(t) = \frac{1}{T}\sum_{i=0}^{T} |A(t_i)||A(t+t_i)| \tag{3.33}$$

where T is the time along which we calculate the autocorrelations. Assuming that the correlations decay exponentially $C(t) \sim e^{-\frac{t}{t_c}}$ we get the linear autocorrelation time:

$$t_c \sim -\left[\frac{1}{T}\sum_{i=0}^{T} \frac{\ln\left(C(t_{i+1})/C(t_i)\right)}{t_{i+1}-t_i}\right]^{-1} \tag{3.34}$$

In Fig. 3.23b we plot the autocorrelation functions vs time for the complex Ginzburg-

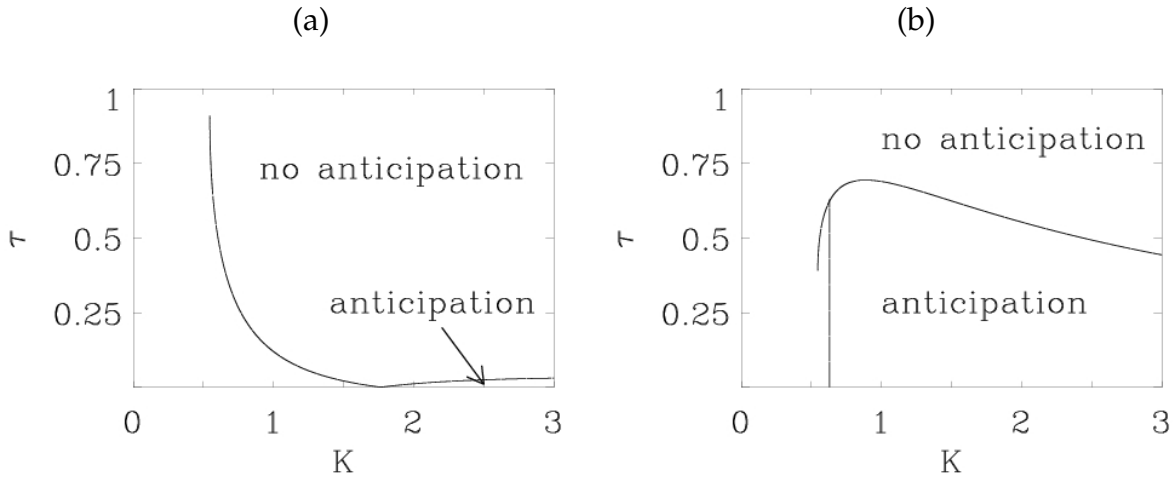

Figure 3.25: *Analytically calculated stability regions in the parameter space τ and K for (a) $\theta = -\frac{2\pi}{5}$ and (b) $\theta = \frac{\pi}{6}$.*

Landau equation in the defect turbulence, bichaos and phase turbulence regimes. Taking the value of T in Eq. 3.34 as the one at which the first zero is reached by $C(t)$, we get the following linear autocorrelation times: $t_c = 0.55$ in defect turbulence regime, $t_c = 1.654$ in bichaos regime and $t_c = 1.76$ in phase turbulence regime; these values correspond approximately to the largest anticipation times obtained numerically.

Interesting feature is that the largest anticipation time occurs for a complex value of the coupling constant, namely for $\theta \approx \frac{\pi}{3}$ (see Fig. 3.24a,b). For this value of θ, the real part of κ is larger than its imaginary part. From the numerical results, and in other regimes as bichaos and phase turbulence, we observed that the stability curve in the parameter space $\tau - \theta$ is always bent over to the direction of positive values of θ with $\theta \approx \frac{\pi}{3}$ at maximum.

In the defect turbulence regime anticipated synchronization occurs for coupling values in a range approximately $K > 0.3$ (see Fig. 3.24c) meanwhile in bichaos and phase

turbulence regimes smaller couplings values are enough. These values can be compared with the magnitudes of the coupling parameter K necessary to observe phase synchronization in unidirectionally coupled complex Ginzburg-Landau equations studied in [115]. In the latter K increases starting from 0.1 and up when going from the phase to strong defect turbulence regimes.

From the linearized Eqs. 3.31 and 3.32, we can rewrite a differential equation in the Fourier space for the difference variable $\Delta_q = A_q - B_{q,\tau}$:

$$\dot{\Delta}_q = [-(1+ic_1)q^2 + \epsilon]\Delta_q - \kappa\Delta_{q,\tau} \tag{3.35}$$

Assuming that the solution is of the form $\Delta_q = e^{\lambda t}$, where $\lambda = \alpha + i\omega$, after introducing it

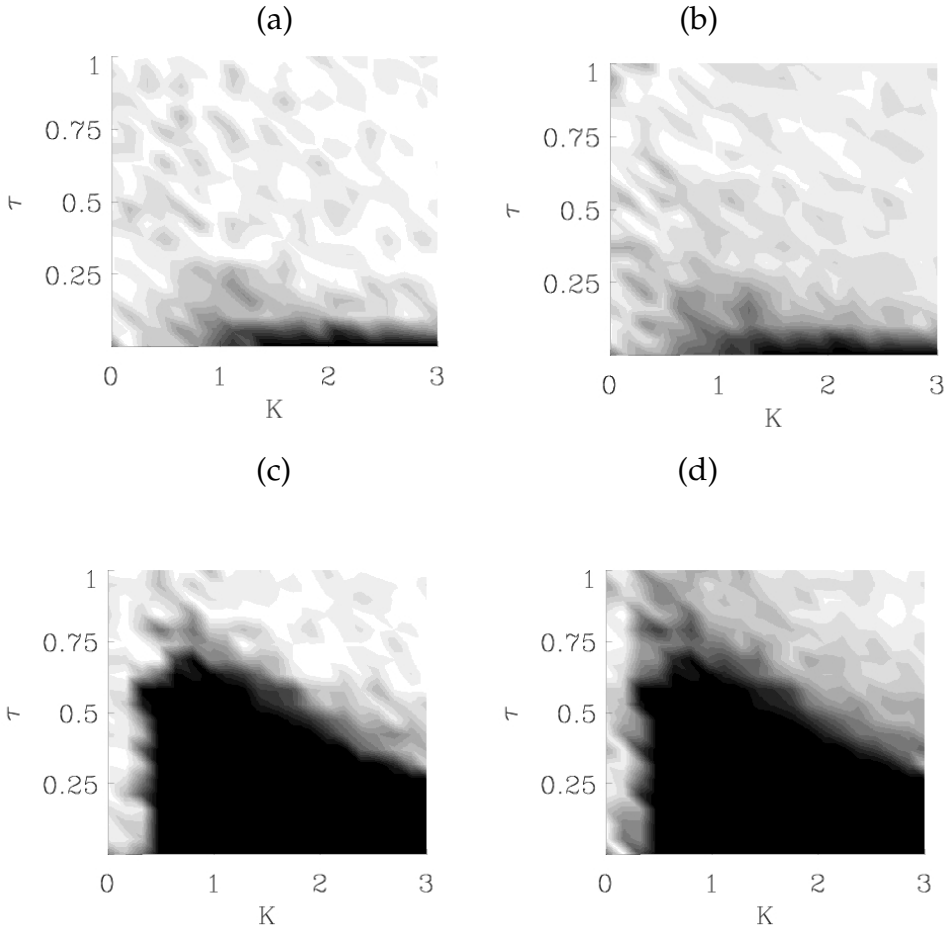

Figure 3.26: *(a) Amplitude and (b) phase correlations between master A and slave B_τ spatiotemporal series for $\theta = -\frac{2\pi}{5}$, $N = 64$, $dx = 0.2$, $dt = 0.002$, $c_1 = 3$, $c_2 = -2.5$. (c) Amplitude and (d) phase correlations between master A and slave B_τ spatiotemporal series for $\theta = \frac{\pi}{6}$, $N = 64$, $dx = 0.2$, $dt = 0.002$, $c_1 = 3$, $c_2 = -2.5$. Black color corresponds to high correlations ($C > 0.99$), meanwhile grey and white correspond to low correlations ($C < 0.99$).*

into Eq. 3.35 and separating into real and imaginary parts we get the following relations:

$$\alpha = -q^2 + \epsilon - e^{-\alpha\tau} K(\cos\theta\cos\omega\tau + \sin\theta\sin\omega\tau) \tag{3.36}$$

$$\omega = -q^2 c_1 + e^{-\alpha\tau} K(\cos\theta\sin\omega\tau - \sin\theta\cos\omega\tau) \tag{3.37}$$

We are interested in the bifurcation points in the parameter space of coupling parameters K, θ and τ. The Hopf bifurcation (i.e. the transition from the steady fixed point state into the oscillatory one) appears at $Re[\lambda] = 0$, when the real part of λ changes its sign from negative to positive. Thus for $\alpha = 0$ we obtain the following relation for the dependence of τ on K and θ as a condition for stability of the anticipated synchronization manifold:

$$\tau(K,\theta) < \Omega^{-1}\arccos[K^{-1}(\Omega'\sin\theta + (\epsilon - q^2)\cos\theta)] \tag{3.38}$$

where $\Omega' = -(K^2 - (\epsilon - q^2)^2)^{\frac{1}{2}}$ and $\Omega = -\Omega' + q^2 c_1$. From Eq. 3.38 we can calculate the condition for coupling constant K:

$$K \geq \frac{|\epsilon - q^2|}{\cos\theta} \tag{3.39}$$

where $\cos\theta \geq 0$ always since $|\theta| \leq \frac{\pi}{2}$. Curves in Eqs. 3.38 and 3.39 separate the stability and instability regions in the coupling parameters space. In Fig. 3.24a,b the stability regions in the parameter space $\tau(\theta)$ obtained analytically and numerically are shown. Both results reveal a bending over in the direction of positive values of θ. In Fig. 3.24c we show the stability regions in the parameter space $K(\theta)$, where the shaded region is obtained though numerical simulations meanwhile the curve is calculated analytically. Finally in Fig. 3.25 we plot the analytical curves $\tau(K)$ for two different θ values: $\theta = -\frac{2\pi}{5}$ in Fig. 3.25a and $\theta = \frac{\pi}{6}$ in Fig. 3.25b. In Fig. 3.26a and b are the diagrams for the amplitude and for the phase, respectively, for $\theta = -\frac{2\pi}{5}$, meanwhile in Fig. 3.26c and d the diagrams are for the amplitude and for the phase, respectively, but for $\theta = \frac{\pi}{6}$.

All analytical curves were calculated for $q = 0.67$, which has been estimated with the use of the results presented in Refs. [116] and [117]. The authors in above mentioned references provide the linear stability analysis for the complex Ginzburg-Landau equation in the presence of the delayed feedback which is used to stabilize the travelling wave solutions of the complex Ginzburg-Landau equation.

Finally in Fig. 3.27 we show the spatiotemporal time series obtained for 2-dimensional locally coupled complex Ginzburg-Landau equations. We observe that the additional dimension makes the system more chaotic and thus, as expected, the maximum anticipation time decreases in comparison with the one-dimensional case. This is due to the fact that the second spatial dimension introduces further instabilities to the systems. Moreover we have also observed that the bending of the $\tau - \theta$ curve changes its direction, in this case it is bent over the negative values of θ.

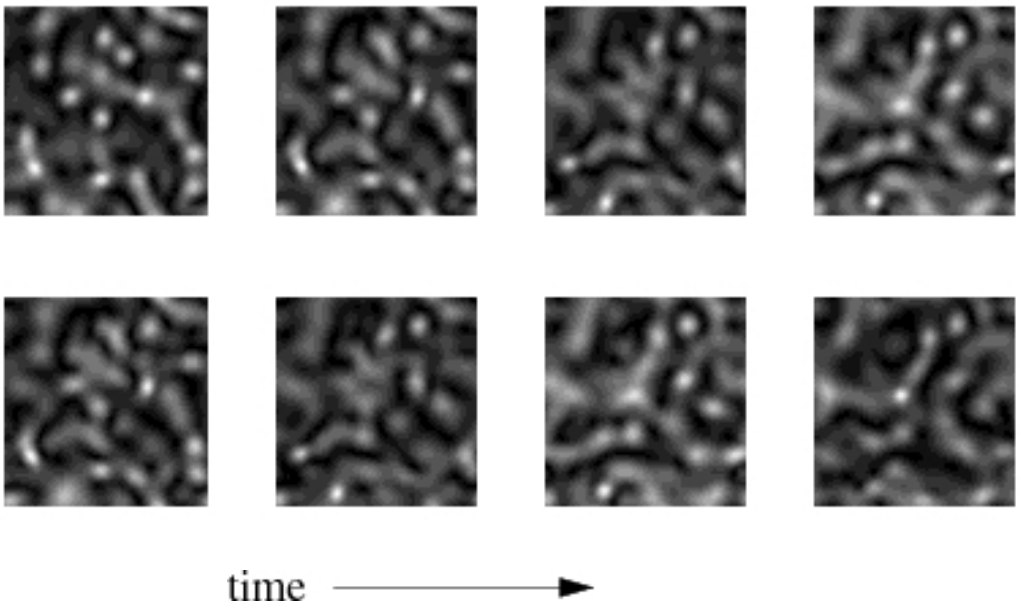

Figure 3.27: *Amplitude evolution of 2-dimensional coupled Ginzburg-Landau equations master (upper row) and slave (lower row) for coupling parameters* $\tau = 0.37$*,* $K = 1.35$ *and* $\theta = -\frac{\pi}{4}$*. Snapshots are shown at times separated by a time unit* τ*. System size is* $N \times N = 64 \times 64$ *with* $dx = 0.3$ *and periodic boundary conditions.*

3.2.2 Modelling prediction of chemical reactions

In this Section we turn our attention to the realistic and specific model for a chemical reaction, namely the catalytic oxidation of the CO on the platinum Pt(110) surface (see Section 2.3 for details). The idea is to find the conditions under which anticipated synchronization in extended systems could be observed in a laboratory experiment. The local coupling considered so far in this thesis is an ideal case, which would be very difficult to attain in a real experiment. Thus we consider the possibility of using global coupling or at least "partially" global, instead of local coupling. An interesting attempt to control and synchronize spatiotemporal chaos in a non local way has already been presented in [118] where the finite number of local controllers were used. It was shown there that a sufficient condition for a robust control is that the number of controllers is equal or even smaller than the number of correlation domains. We expect also in our case that the size of domain which permits anticipated synchronization will be related to spatial autocorrelations, as it was shown for a control method in [118]. We define as the master system for the variables (u_1, v_1, w_1) the model in one spatial dimension described in Section 2.3:

$$\begin{aligned} \dot{u}_1 &= k_1 s_{CO} p_{CO}(1-u_1^3) - k_2 u_1 - k_3 u_1 v_1 + D\nabla^2 u_1 \\ \dot{v}_1 &= k_4 p_{O_2}[s_{O,1x1} w_1 + s_{O,1x2}(1-w_1)](1-u_1-v_1)^2 - k_3 u_1 v_1 \\ \dot{w}_1 &= k_5 \left(\frac{1}{1+\exp(\frac{u_0-u_1}{\delta u_1})} - w_1 \right) \end{aligned} \tag{3.40}$$

We couple a slave system to the master in Eq. 3.40 by using three types of coupling:

1. Diffusive local coupling. In this case we try the simplest diffusive coupling in the equation for variable u_2. Therefore, we consider a slave system defined by the variables (u_2, v_2, w_2) in the following way:

$$\begin{aligned} \dot{u}_2 &= k_1 s_{CO} p_{CO}(1-u_2^3) - k_2 u_2 - k_3 u_2 v_2 + D\nabla^2 u_2 + K(u_1 - u_2(t-\tau)) \\ \dot{v}_2 &= k_4 p_{O_2}[s_{O,1x1} w_2 + s_{O,1x2}(1-w_2)](1-u_2-v_2)^2 - k_3 u_2 v_2 \\ \dot{w}_2 &= k_5 \left(\frac{1}{1+\exp(\frac{u_0-u_2}{\delta u_2})} - w_2 \right) \end{aligned} \tag{3.41}$$

   being K the intensity of the coupling between the two systems.

2. Local coupling in parameter p_{CO}. It seemed that an easy way of coupling the two systems would be by the influence on the p_{CO} parameter. So we take as the equations for the slave system the following ones:

$$\dot{u}_2 = k_1 s_{CO}[p_{CO}^0 - K(u_1 - u_2(t-\tau))](1-u_2^3) - k_2 u_2 - k_3 u_2 v_2 + D\nabla^2 u_2 \tag{3.42}$$

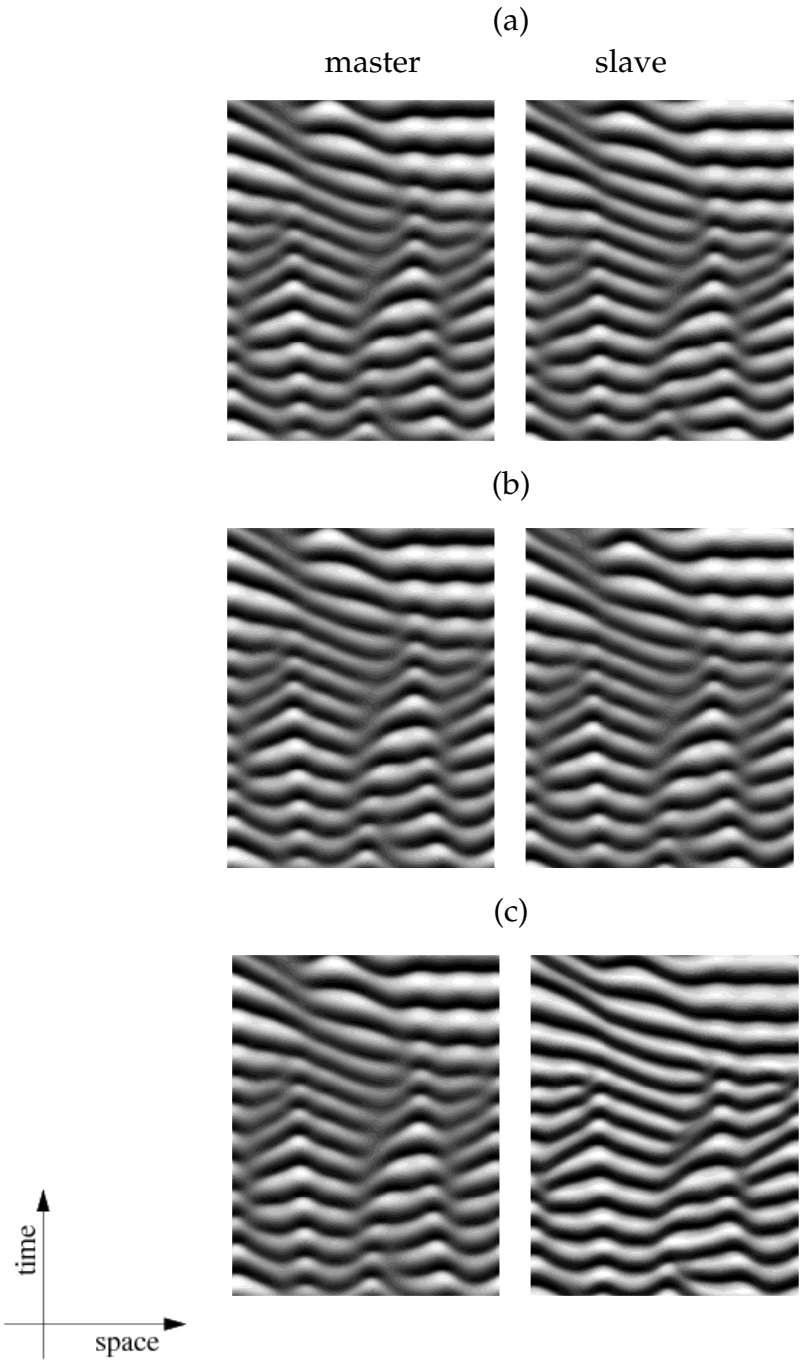

Figure 3.28: *Spatiotemporal dynamics of master (left panels) and slave (right panels) for (a) local diffusive coupling with* $K = -0.45$ *and* $\tau = 1$*, (b) local coupling in parameter* p_{CO} *with* $K = 0.1$ *and* $\tau = 1$*, (c) digital diffusive local coupling with* $K = -0.15$ *and* $\tau = 1$*.*

with equations for variables v_2 and w_2 as in Eq. 3.41. K, again, is the parameter measuring the intensity of the interaction between master and slave systems.

3. Digital diffusive local coupling. This case is included for simplicity, since we think that it might be convenient to consider a scheme in which the coupling depends not on the exact magnitude of the difference between master and slave at each point in time, but just on the difference measured at some particular time step. The digital coupling was used successfully in synchronizing chaotic systems as reported in Ref. [119]. Digital coupling also allows us to observe anticipated synchronization in many systems, not only in the system considered in this Section. The slave system with the digital coupling is defined in the following way:

$$\begin{aligned} \dot{u}_2 &= k_1 s_{CO} p_{CO}(1-u_2^3) - k_2 u_2 - k_3 u_2 v_2 + D\nabla^2 u_2 \\ &+ K(sgn(u_1) - sgn(u_2(t-\tau))) \end{aligned} \tag{3.43}$$

with equations for variables v_2 and w_2 as in Eq. 3.41; $sgn(z)$ is the sign function; if $z > u_{ref}$ then $sgn(z) = 1$, otherwise if $z < u_{ref}$ then $sgn(z) = -1$ where $u_{ref} = 0.3358$.

In each of these three coupling schemes, we obtain a region of parameters (τ, K) in which anticipated synchronization is found. As an example we plot in Fig. 3.28 for each of the three previous schemes a typical result of the numerical simulations. In each figure the time runs vertically from bottom to top and the space is the horizontal direction. The master system is depicted in the left frame, whereas the slave is depicted in the right frame. Note that we have set the simulations such that the master evolution is the same in each of the three cases. It is clearly visual that there is indeed an anticipation of the dynamics of the master by the slave. In Fig. 3.29 we plot in a gray scale the value of the correlation coefficient ρ between the variables $u_1(x,t)$ and $u_2(x,t-\tau)$ (this is further averaged with respect to x and t) as a function of the system parameters (τ, K). Black level indicate a correlation coefficient close to 1 (good correlation and, hence, anticipated synchronization) while the white region is that of poor correlation and a lack of synchronization between the two systems.

The above schemes are for diffusive local coupling. A more realistic approach would require the replacement of the local coupling by the global or partially global one. We consider partially global coupling, being a modification of the schemes introduced in Eqs. 3.42 and 3.43, which we define in the following way:

$$K\left(\frac{1}{\Delta}\sum_{n=1}^{\Delta} u_1(n,t) - \frac{1}{\Delta}\sum_{n=1}^{\Delta} u_2(n,t-\tau)\right) \tag{3.44}$$

where Δ is a region over which the amplitudes u_i for $i = 1, 2$ are averaged. The schematic representation of this coupling is shown in Fig. 3.30. In Fig. 3.31 we show the stability regions in the parameter space $\tau(K)$ for the coupling defined in Eq. 3.44.

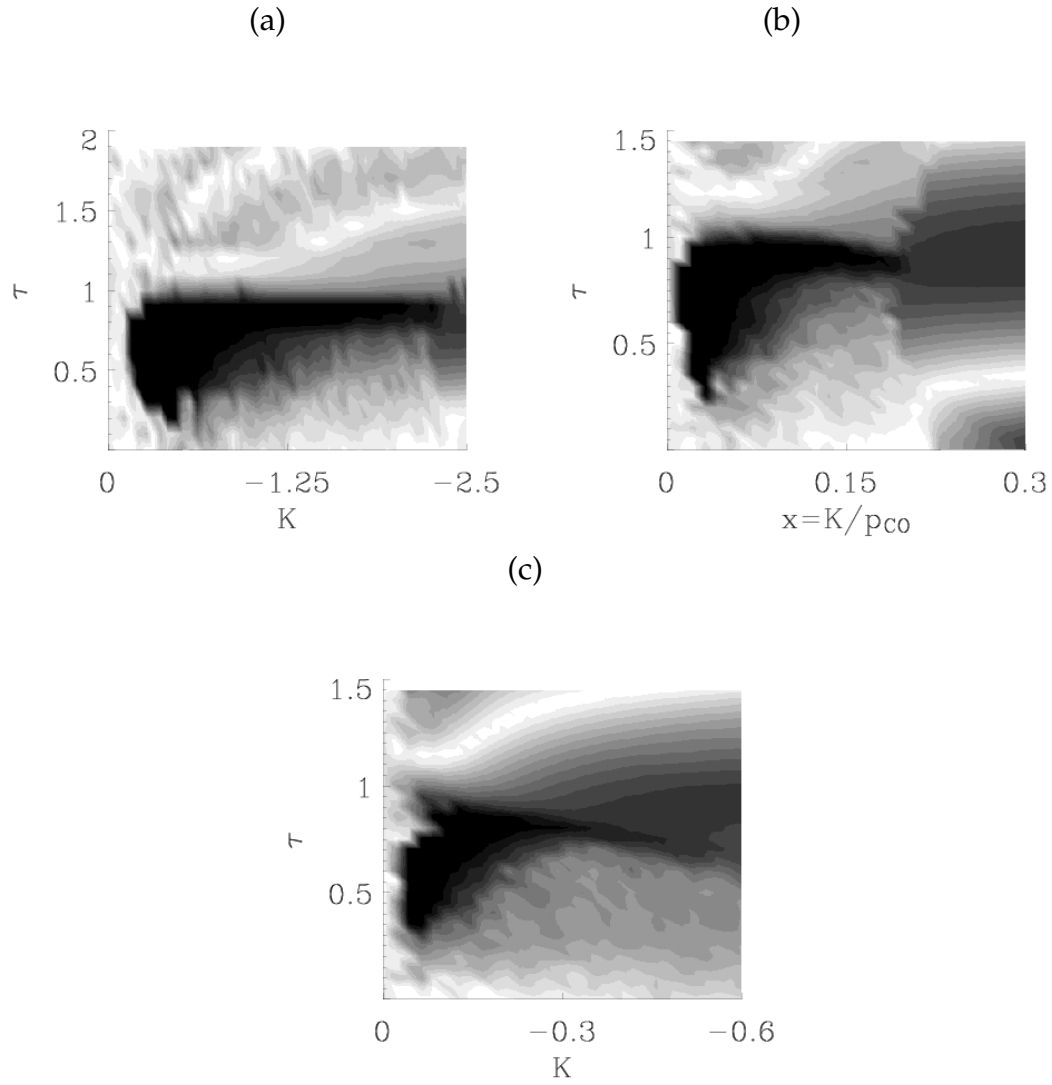

Figure 3.29: *Stability diagram in coupling parameter space K and τ. White regions correspond to the low correlation between signals $u_1(t)$ and $u_2(t-\tau)$, meanwhile black regions to the high correlation (close to 1). Panel (a) corresponds to the simple diffusive coupling, panel (b) is for the coupling in the parameter p_{CO} and panel (c) for the "digital diffusive local coupling".*

The intensity drawn in a grey scale corresponds to the correlations between the signals $u_1(t)$ and $u_2(t-\tau)$ at each point in space. The correlation for the possible maximum anticipation time decreases as the number of averaged grids Δ increases (see Fig. 3.32). For $\Delta = 16$ the anticipated synchronization is still good, but for $\Delta = 20$ becomes destructed (see Fig. 3.33). For larger values of Δ the stability is lost. We have observed that the global coupling does not allow anticipation. However it is possible to implement partially global coupling which we estimated for one-dimensional system to be not larger than 0.016mm.

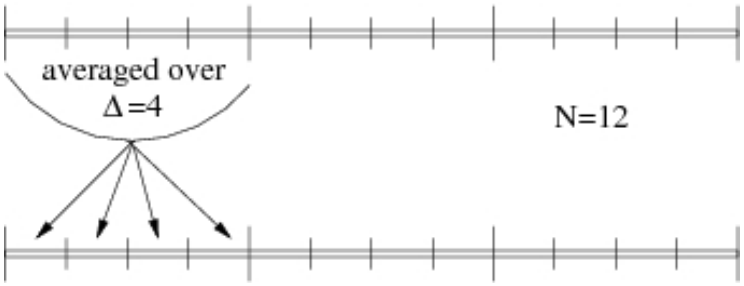

Figure 3.30: Schematic representation of the partially global diffusive coupling.

In the experiment the coupling is partially global with a Gaussian form of the averaged region instead of a uniform one:

$$K\left(\frac{1}{\Delta}\sum_{n=1}^{\Delta}u_1(n,t)f(n,\Delta)-\frac{1}{\Delta}\sum_{n=1}^{\Delta}u_2(n,t-\tau)f(n,\Delta)\right) \tag{3.45}$$

where Δ is a number of grids in which the amplitudes u_i for $i=1,2$ are averaged and the function f is a Gaussian function defined as:

$$f(x,\Delta)=\exp\left(\frac{-(x-\Delta/2)^2}{\Delta^2/(4\ln 2)}\right) \tag{3.46}$$

The function $f(x,\Delta)$ used in the simulations is plotted in Fig. 3.34. Numerical simulations are done for the case $\Delta=16$. In this case we observe that anticipated synchronization is still possible when the Gaussian function is used when averaging (Fig. 3.35 upper panel). The cross-correlation diagrams for the case of $\Delta=16$ with the uniform and the Gaussian forms of the averaged regions are shown in Fig. 3.36.

We have also checked the robustness of the system under parameter mismatches. We observed that the anticipated synchronization is still preserved when the parameter s_{CO} in the slave is larger about 0.3% than that of the master (see Fig. 3.35 lower panel). Further increasing of this parameter prevents anticipated synchronization to occur. It is interesting that if we change the parameter s_{CO} in the slave system to be smaller than in the master, the anticipated synchronization vanishes for smaller mismatches and is acceptably conserved for a mismatch of 0.001%. During the above study we kept the parameter s_{CO} of the master system unchanged.

The global coupling is easier to implement experimentally. Nevertheless, and in order to obtained the best results on anticipation, the experimental setup should be designed for local or partially global coupling, what is more difficult in practise, but not impossible[1]. The other fact which we find interesting is the different shape of the

[1]The realization of the local coupling can be done by using a laser light.

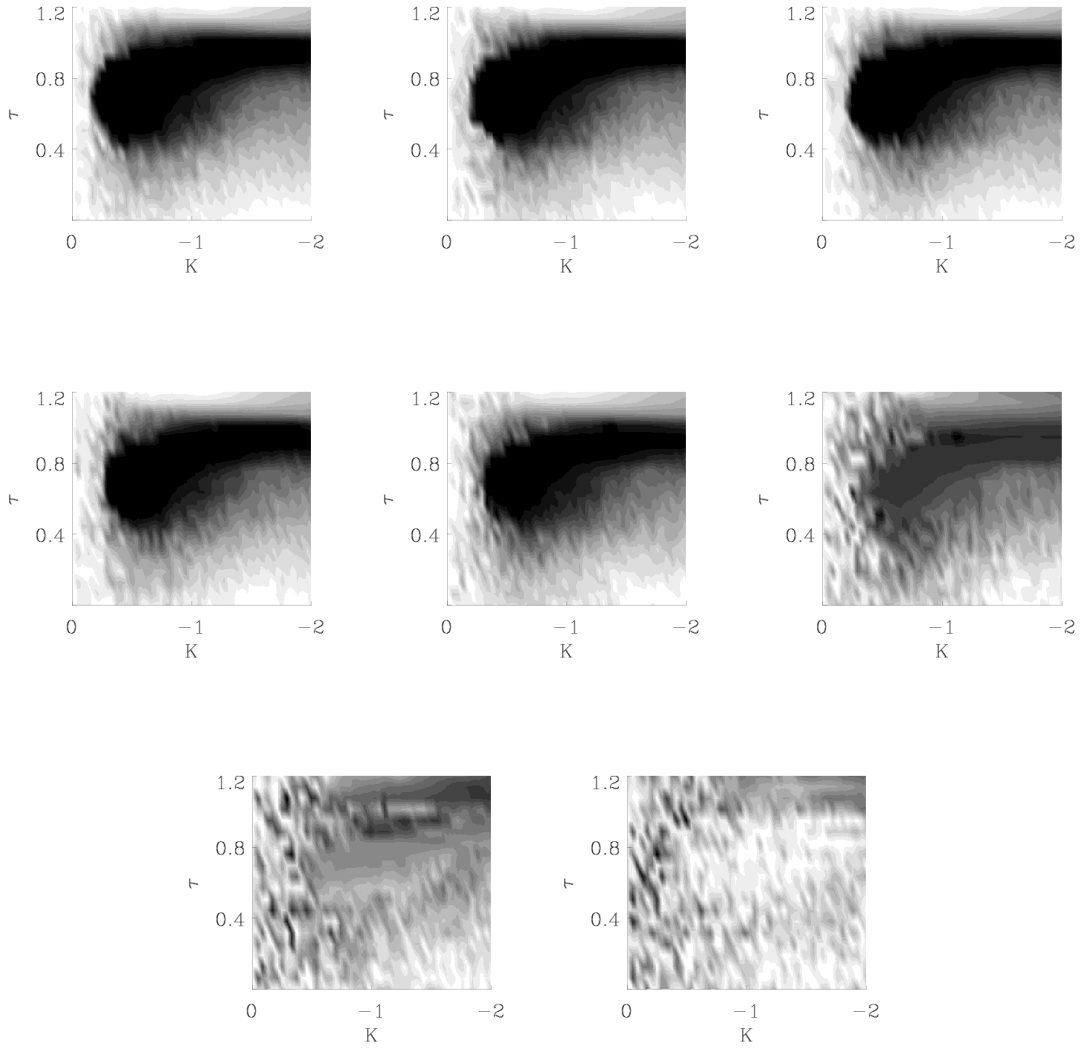

Figure 3.31: *From left to right in down direction – number of averaged grids: 2, 4, 5, 8, 10, 16, 20, 25. Size of the system is* 0.4*mm with* $N = 400$ *and step* $\delta x = 0.001$*mm. Black colour correspond to the maximum correlation between* $u_1(t)$ *and* $u_2(t - \tau)$.

cross-correlation diagrams in the coupling parameter space τ and K, which have always qualitatively similar shapes for all the studied systems, being bounded up by the curve $\tau < \frac{1}{K}$, for positive values of K. In the system considered in this Section, the cross-correlation diagram has a different shape and appears for negative coupling values thus being some kind of exception from the observations made so far.

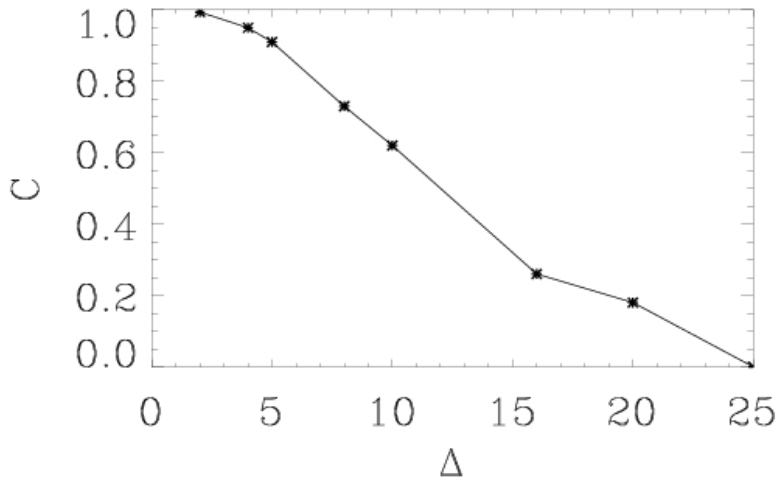

Figure 3.32: *Correlation value of the maximum possible anticipation time* $\tau \approx 1$ *as a function of the number of averaged grids* Δ*. The size of the studied system is* 0.4mm *with* $N = 400$ *and* $\delta x = 0.001$mm*.*

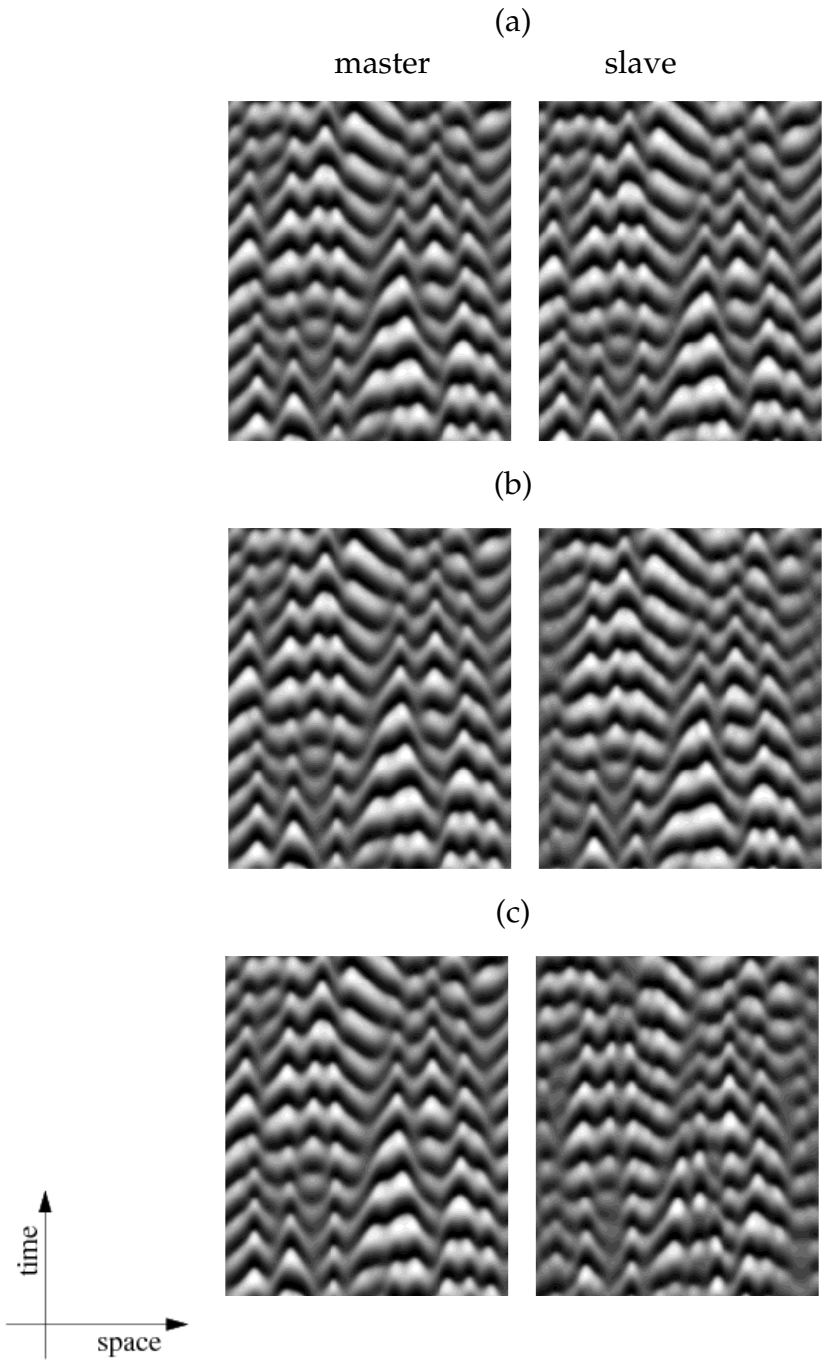

Figure 3.33: *Time series for delay time* $\tau = 0.96$ *and: (a)* $K = -1.6$ *and* $\Delta = 10$*, (b)* $K = -1.08$ *and* $\Delta = 16$*, (c)* $K = -1.24$ *and* $\Delta = 20$*. The horizontal axis represents space and the vertical one time, which goes forward in the up direction.*

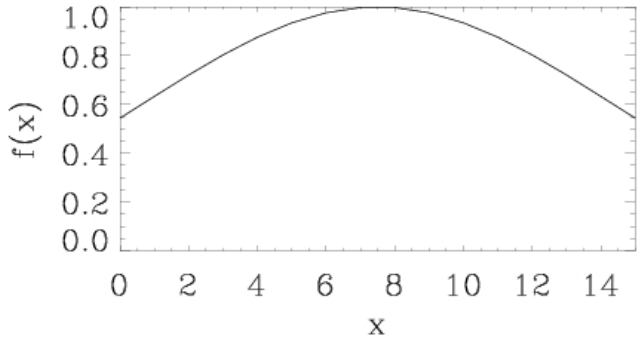

Figure 3.34: *Gaussian form used in numerical simulations for the averaged region* $\Delta = 16$.

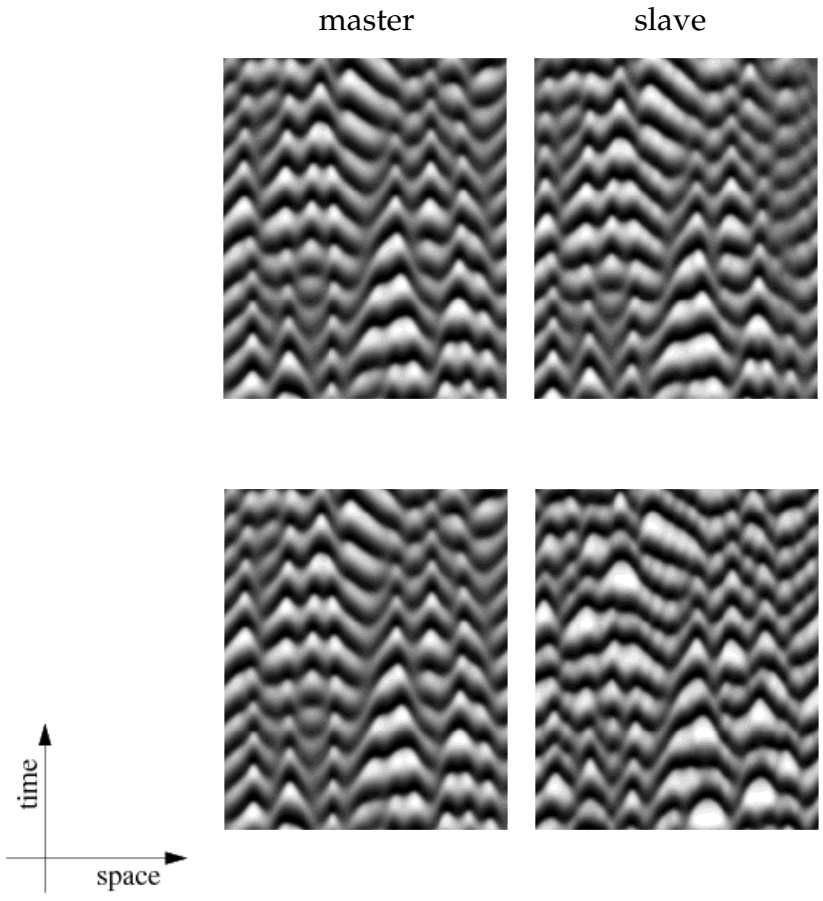

Figure 3.35: *Time series for delay time* $\tau = 0.96$, $K = -1.24$ *and* $\Delta = 16$. *Upper panel for* $s_{CO}^{master} = s_{CO}^{slave}$, *and lower one for* $s_{CO}^{slave} = 1.003 s_{CO}^{master}$ – 0.3% *difference in parameters.*

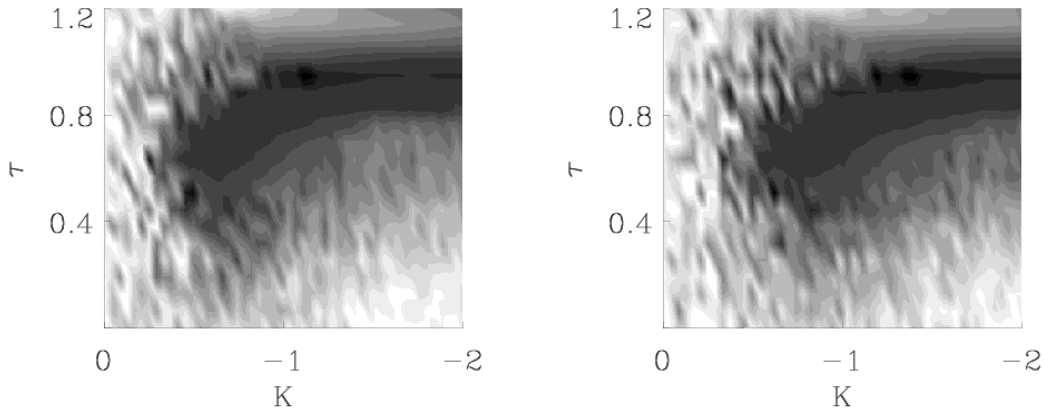

Figure 3.36: *Number of averaged grids: 16. Size of the system is* 0.4mm *with* $N = 400$ *and step* $\delta x = 0.001$mm*. Black colour corresponds to the maximum correlation between* $u_1(t)$ *and* $u_2(t - \tau)$*. Averaging with step function (left panel) and Gaussian function (right panel).*

3.2.3 Zero-lag synchronization in excitable systems

Experiments on the brain activity revealed the existence of simultaneous oscillations in the activity of cortical areas separated by millimeter distances [120], despite of the axonal transmission times that are expected to cause phase shifts between these oscillations. Several authors have pointed out that the simultaneous firing of selective neurons in the brain, the so-called feature binding, plays a crucial role in visual processing [121] as well as in conscious experience [122]. Experimental observations of synchronized signal firings at zero lag brought us to the speculation that in real biological systems synchronization between neurons with different excitability thresholds may appear. The

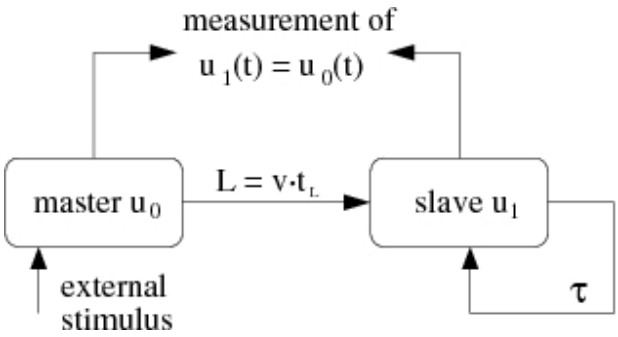

Figure 3.37: *Schematic presentation of the interaction between the external perturbation, master and slave. Delayed feedback in the slave can enable the detection of zero-lag synchronization in spite of the spatial distance L which exists between two areas in the brain.*

synchronization in the brain appears in response to the external stimuli detected by the sensory receptors. We consider the master as a sensory receptor which is fed with an external stimulus (see Fig. 3.37). As shown in section 5.1.1 anticipation of the master's pulse by the slave may be observed even if the perturbation is applied only to the master. Thus, if both systems are spatially separated by distance L, the compensation of the time t_L needed for an electric pulse to travel through the axon from the master to the slave neuron could be achieved if the anticipation mechanism is present with a delay term $\tau = t_L$.

We demonstrate the occurrence of the zero-lag synchronization in the simple example of two Adler equations coupled unidirectionally in the following way. Let us consider the equations:

$$\begin{aligned} \dot{x} &= \mu - \cos x + I(t) \\ \dot{y} &= \mu - \cos y + K(x(t - t_L) - y(t - \tau)) \end{aligned} \tag{3.47}$$

where the eternal singular perturbation $I(t)$ is applied only to the master. In Fig. 3.38 we see that the zero-lag synchronization between the master and the slave can occur

when the delay time τ is equal to the conduction delay t_L and for a particular coupling strength value.

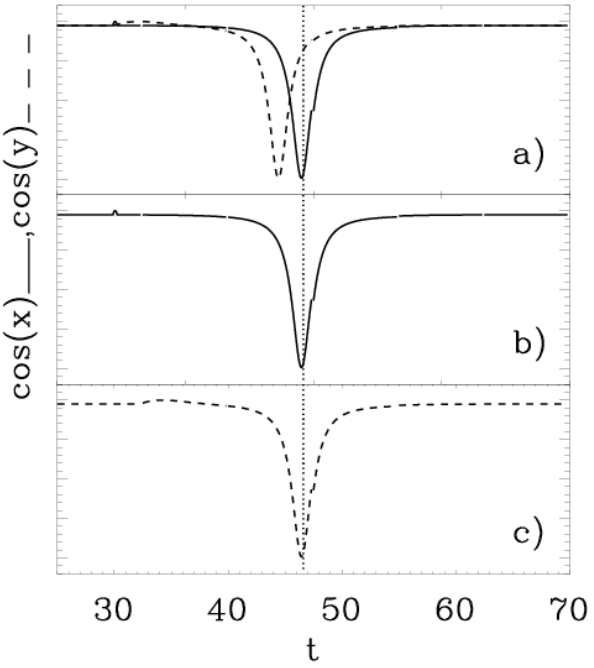

Figure 3.38: *Zero-lag synchronization between Adler systems. Master (solid line) and slave (dashed line) are coupled with the delayed coupling scheme. The anticipation is seen in (a). In (c) is shown the slave, which gets the delayed in time by $t_L = \tau$ due to conduction delays signal from the master.*

However, in order to simulate the connection between two distinct areas in the brain it is convenient to consider spatially extended systems exhibiting the prototype model for neuron dynamics. To assess this problem we use the following set of spatially extended FitzHugh-Nagumo equations for the master:

$$\begin{aligned} \dot{u}_0 &= u_0 + v_0 - \frac{u_0^3}{3} + D\nabla^2 u_0 \\ \dot{v}_0 &= \epsilon(-u_0 + a) + D\nabla^2 v_0 + I(t) \end{aligned} \tag{3.48}$$

and for the slaves:

$$\begin{aligned} \dot{u}_i &= u_i + v_i - \frac{(u_i)^3}{3} + D\nabla^2 u_i + K(u_{i-1}(t - t_L) - u_i(t - \tau_i)) \\ \dot{v}_i &= \epsilon(-u_i + a) + D\nabla^2 v_i \end{aligned} \tag{3.49}$$

where index i for $i = 1, ..., N$ stands for the i-th slave in a cascade, $\nabla^2 = \frac{\partial^2}{\partial z^2}$ is a spatial derivative operator, D is a diffusion constant, ϵ and a are constant parameters, t_L

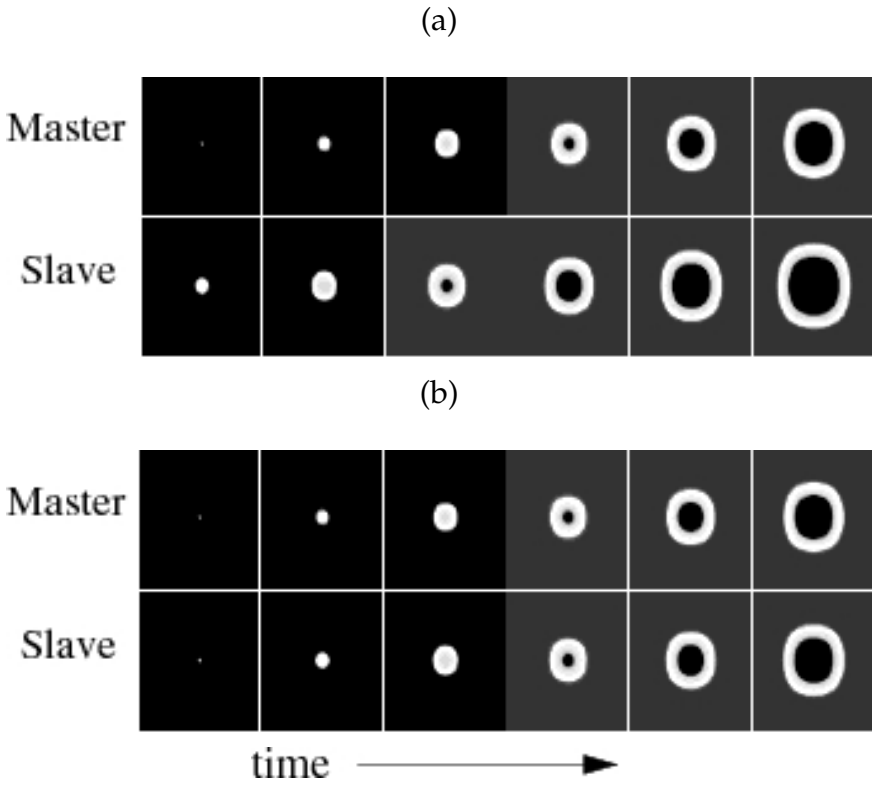

Figure 3.39: *The travelling waves of two coupled FitzHugh-Nagumo spatially extended systems (master and one slave) of size* 80×80 *with* $dx = 1$ *for parameters* $\tau = 15$, $K = 0.25$, $a = -1.08$, $D = 0.1$, $\epsilon = 0.02$, $p = 0.2948$ *and* $\Delta t = 1$. *Two cases are considered: (a)* $t_L = 0$ *and (b)* $t_L = 15$.

is the time it takes the signal to travel from the master to the slave and $I(t)$ is an external stimulus of amplitude p and duration Δt applied to the master. Here the coupling parameter K is considered as crucial in the communication between master and slave, since it transmits to the slave the information about the external perturbation. In simulations of Eqs. 3.48 and 3.49 we could observe synchronization i.e. $u_1(t) = u_0(t)$ for $t_L \neq 0$ if the anticipation time τ corresponded exactly to the time t_L. Then the time it takes the pulse to travel through the axon could be compensated, giving rise to the simultaneous firing of neurons.

In Fig. 3.39 we show results of the numerical simulations of two coupled FitzHugh-Nagumo systems given by Eqs. 3.48 and 3.49. In Fig. 3.39a we present the situation in which the slave emits the travelling wave faster then the master does even if the local perturbation $I(t)$ is applied only to the master. We consider $t_L = 0$ (no spatial distance between two brain areas) and we observe the anticipation. On the other hand if we take $t_L = \tau$ then, for particular value of the coupling strength, we observe that the master and slave emit travelling waves simultaneously in time as it is seen in Fig. 3.39b.

The interaction of many distant cortical areas could be modelled by considering ad-

ditional slave units (slave areas). It was shown that cascade of slave units enables the anticipated synchronization between the unit i and $i+1$ in the way that the total anticipation time between the master and the last slave is the sum of all anticipation times existing in the cascade $\tau_N = \sum_{i=1}^{N} \tau_i$ [97]. The interesting feature of the coupled arrays of excitable systems is that the perturbation applied in one place is able to propagate through the cascade (this phenomenon was already studied in bidirectionally coupled oscillators undergoing a homoclinic chaotic dynamics [123]). The anticipation phenomenon moreover permits such a propagation without time loses due to conduction delays.

3.2.4 Cellular automata

Cellular automata were introduced by mathematician J. von Neumann [124] who tried to develop an abstract model of self-reproduction in biology. The theory of cellular automata was completed after suggestions of S. Ułam [125]. Cellular automaton is a set of self-operating machines with a available set of logical operations which are performed in discrete space and discrete time. Many cellular automata models are examples of simple dynamical systems which produce ordered patterns such as those observed in nature. A cellular automaton consists of an array of N nodes characterized by one of two possible binary states 0 or 1. Each node performs locally logical operations by means of Boolean functions which are known as rules (for details see [126] and [127]). The 1-dimensional cellular automaton has $2^8 = 256$ possible rules, which have been cataloged by S. Wolfram [128]. The value of each node is updated due to a particular rule in discrete time steps and all nodes are updated simultaneously at the same time step. We consider the rule "90" in the Wolfram notation which consists on updating each node by performing XOR operation of only two neighbouring nodes. Let consider $M+1$ – unidirectionally coupled cellular automata:

$$\begin{aligned} x_0^{(n+1)}(i) &= x_0^{(n)}(i-1) \oplus x_0^{(n)}(i+1) \\ x_1^{(n+1)}(i) &= x_1^{(n)}(i-1) \oplus x_1^{(n)}(i+1) \oplus x_0^{(n)}(i) \oplus x_1^{(n)}(i-d) \\ &\vdots \\ x_M^{(n+1)}(i) &= x_M^{(n)}(i-1) \oplus x_M^{(n)}(i+1) \oplus x_{M-1}^{(n)}(i) \oplus x_M^{(n)}(i-d) \end{aligned} \tag{3.50}$$

where coupling is based on the information flow from one cellular automaton to the other at time n. The first cellular automaton is a master, meanwhile the others are slaves. Variable $x_m^{(n)}(i)$ for $i = 1, \ldots, N$ represents the state of the ith node in the N-length array at time n. For particular values of the initial conditions, taken here as all 0's with the only 1 at the middle of the array (see Fig. 3.40a), the state of N nodes of each cellular automaton after iteration in time becomes the well-known Sierpiński triangle [129]. We consider the master and $M = 5$ slave systems defined in Eq. 3.50 (graphical representation of equations for master and slaves is shown in Figs. 3.40a,b). Spatiotemporal series in Figs. 3.41a,b show that the same pattern shifted in time can be produced by slaves for $d = 1$. The 5th slave cellular automaton is shifted in time by $M \cdot d = 5$ steps in comparison with the master. Above results show that anticipated synchronization in cellular automata may be obtained when the feedback variable in the coupling term is delayed in space and not in time. This similarity between both delayed coupling schemes; time delay and space delay, suggests the space-like properties of the systems with time-delayed feedback. It was already reported in [130] that the system with time-delayed feedback may be represented by N-dimensional spatially extended

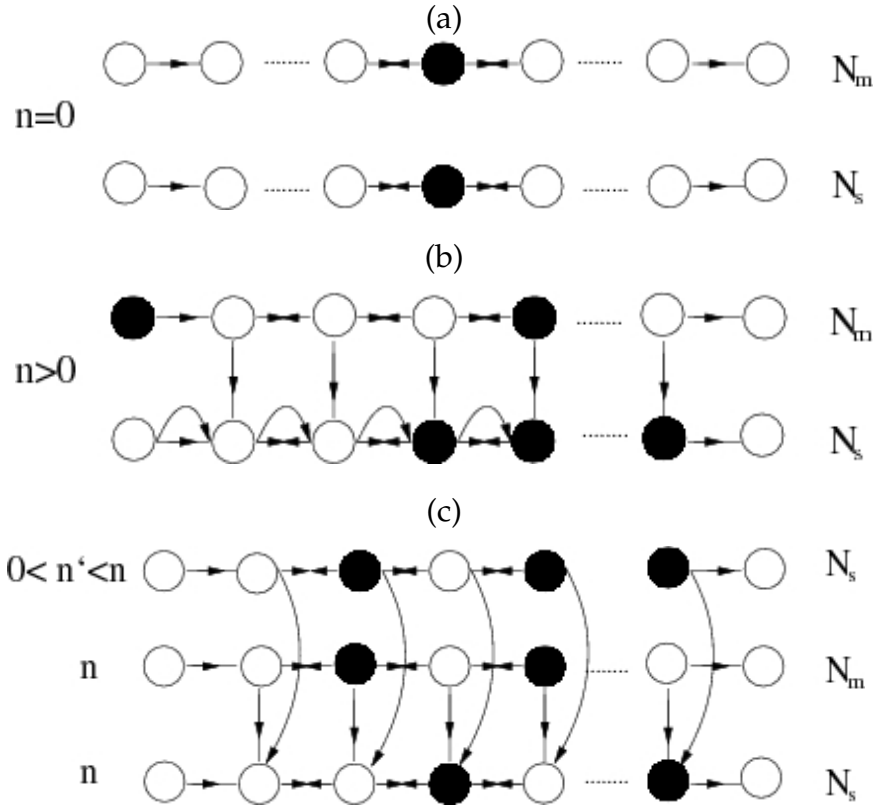

Figure 3.40: *(a) Initial state of master and slave cellular automata with number of nodes $N_m = N_s$. The state of both systems consist of one state '1' and $N_m - 1$ states '0'. (b) Schematic nodes of master and slave cellular automata for $n \neq 0$. The arrows show the spatial couplings of nodes. (c) Schematic nodes of slave cellular automaton for $n' \neq 0$ and master and slave cellular automata for $n \neq 0$ where $n > n'$. The arrows show the couplings with time-delayed feedbacks.*

system because it has the similar spatial properties (for instance defects). The same considerations may be applied to the slave system which contains in the coupling term the time-delayed variable.

The standard delayed coupling scheme leading to anticipated synchronization contains the delayed in time variable and for M+1 – unidirectionally coupled cellular automata is the following:

$$\begin{aligned} x_0^{(n+1)}(i) &= x_0^{(n)}(i-1) \oplus x_0^{(n)}(i+1) \\ x_1^{(n+1)}(i) &= x_1^{(n)}(i-1) \oplus x_1^{(n)}(i+1) \oplus x_0^{(n)}(i) \oplus x_1^{(n-\tau_1)}(i) \\ &\vdots \\ x_M^{(n+1)}(i) &= x_M^{(n)}(i-1) \oplus x_M^{(n)}(i+1) \oplus x_{M-1}^{(n)}(i) \oplus x_M^{(n-\tau_M)}(i) \end{aligned} \tag{3.51}$$

where τ_m for $m = 1, \ldots, M$ are delay times of the slave systems. The chain of cellular automata with time delayed feedback in the coupling term is presented graphically

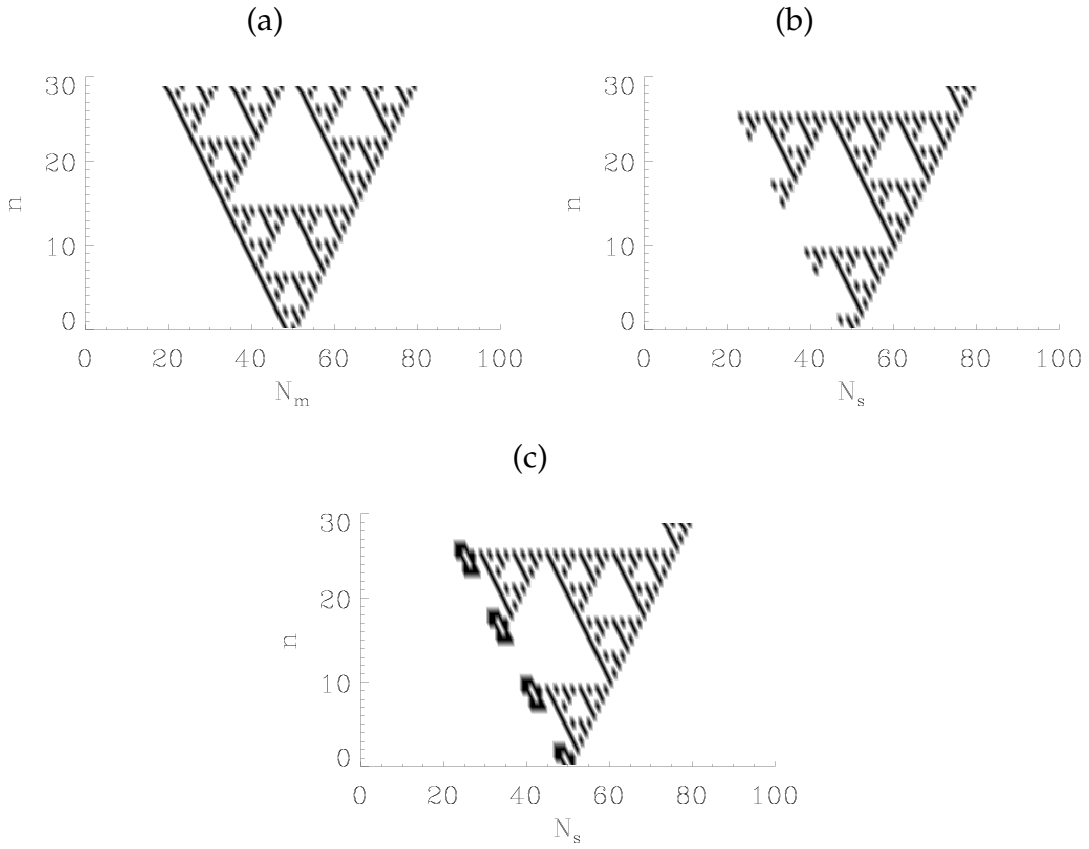

Figure 3.41: *(a) Output of the master cellular automaton. (b) Output of the 5th slave cellular automaton x_5 with spatial coupling, which anticipates the master's sequence in time by $\tau' = 5$. (c) Output of the 5th slave cellular automaton x_5 with time delayed feedback, which anticipates the master's sequence in time by $\tau' = 5$.*

in Figs. 3.40a,c. Numerical results shown in Figs. 3.41a,c reveal that the same pattern shifted in time can be produced by slaves with delays of magnitude $\tau_m = 1$. Then the 5th slave cellular automaton is shifted in time by $\tau' = M \cdot \tau_m = 5$ following the summing rule for which the variable $x_M^{(n)}(i)$ anticipates $x_0^{(n)}(i)$ by a time $\tau' = \sum_{m=1}^{M} \tau_m$. Anticipation of the future patterns of the master cellular automaton could enable synchronous behaviour of a set of real-working units (for instance cellular automata implemented electronically) which are coupled and separated by distance s from each other. When the anticipation time corresponds to the time needed by a signal to go from one unit to the other through the distance s, then such cellule would be able to perform parallel operations, for instance during image processing [131].

An interesting phenomenon appears in the slave outputs for the delay times $\tau > \tau_c$ where τ_c is a critical delay time. For such delay times the patterns remain stable for any τ and have a form different than Sierpiński triangle. In Fig. 3.42 the pattern produced

by the $i = 4$ slave cellular automaton zooms in the pattern produced by the $i = 2$ slave cellular automaton. On the other hand, the pattern produced by the $i = 3$ and $i = 5$ slave cellular automata have different form than that produced by the $i = 2$ and $i = 4$ slave cellular automata. Nevertheless, the same occurs, the $i = 5$ slave cellular automata zooms in the pattern produced by the $i = 3$ slave cellular automata. The only difference between the patterns of $i = 2$ and 4 as well as between $i = 3$ and $i = 5$ slave cellular automata consists in the scales of the patterns. These two different types of triangles appear in an oscillatory way during the time evolution of the cellular automata with the scale increasing.

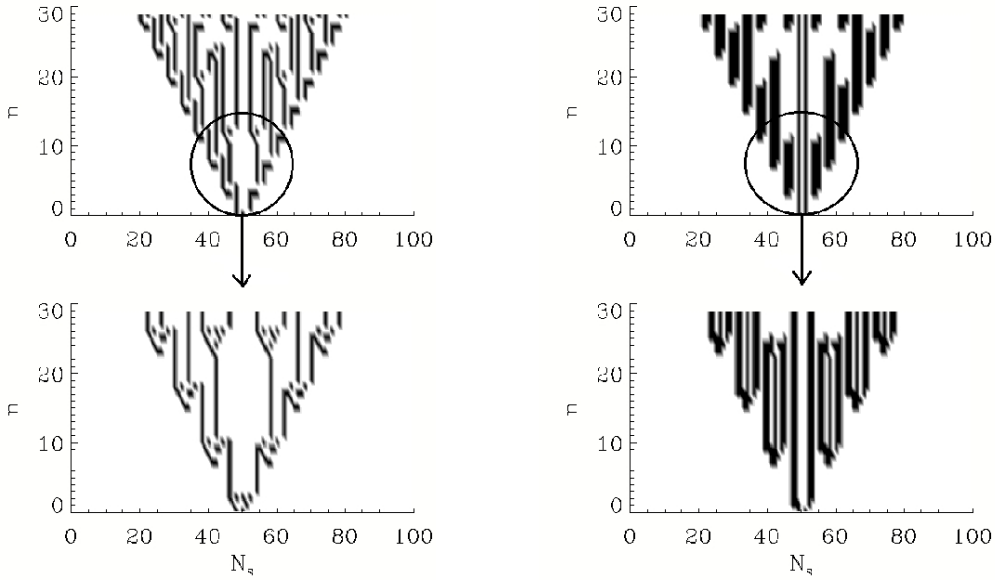

Figure 3.42: *From the upper left to the lower right: the spatiotemporal pattern produced by the second, third, fourth and fifth slave cellular automata.*

3.3 Conclusions

In this Chapter we presented analytical and numerical stability analysis for the anticipated synchronization in FitzHugh-Nagumo neurons driven by noise. Analytical stability analysis revealed that the typical shape of the cross-correlation diagram in the parameter space K and τ in chaotic systems as well as in the case of FitzHugh-Nagumo systems driven by noise may be related, and be due to internal or external noise sources. In numerical simulations, the lack of synchronization was characterized by two types of errors, additional firings in the slave system and the standard deviation of anticipation times between master and slave. Numerical simulations, as well as an experimental implementation of FitzHugh-Nagumo equations, showed that anticipated synchronization is robust even when different realization of noises are injected into the master and the slave. Finally, coupling of many systems in a chain enabled us to obtained larger anticipation times and allowed to eliminate errors occurring during synchronization.

Further we studied the occurrence of anticipated synchronization in spatiotemporal systems, in particular in complex Ginzburg-Landau equations and in the model for chemical reaction of CO oxidation on the platinum surface. The ranges of parameters obtained through numerical simulations, as well as those calculated analytically, revealed a new features. It appeared that the best coupling in the coupled complex Ginzburg-Landau equations for obtaining the largest anticipation times is a complex one, maintaining however the positive real part of the coupling constant K with the standard shape of cross-correlation diagram in the parameter space τ and K observed so far in many systems. We introduced the phase factor to the coupling constant and showed that it causes an increase in the largest anticipation time in comparison with commonly used real coupling constant. However, in the case of the model for chemical reaction of CO oxidation on the platinum surface the coupling constant had to be taken negative in order to obtain anticipated synchronization. Moreover the shape in the parameter space τ and negative K appeared to be different than it is usually observed in other systems. On the example of Ginzburg-Landau system we showed that the magnitude of the largest anticipation time is related to the linear autocorrelation time of the system. As a consequence, the largest anticipation time varies when system parameters are varied. Thus the maximum anticipation time in the defect turbulence regime was the smallest one in comparison with the one achieved in the bichaos and the phase turbulence regimes. Finally, the decreasing of linear autocorrelation times induced by adding of new spatial dimensions leads to a decrease of the maximum anticipation time, as was shown in the two dimensional case.

Since experimental requirement are rather for non local coupling, we searched for other possibilities for coupling the systems. Numerical simulations revealed that in the realistic model for chemical reaction of CO oxidation on the platinum surface the antic-

ipated synchronization is possible for partially global coupling, through averaging the domains (however of limited sizes) of the master and couple them with the corresponding domains in the slave.

Finally, we demonstrated that the delayed feedback enables zero-lag synchronization between spatially separated neural tissues. We considered the master system as the sensory receptor which receive the stimulus and send the information to the distant areas of the brain which we considered as a slave. Since the experimental observation show that some cortical areas in the brain synchronizes without time lags, we think that our hypothesis may be relevant to this problem.

In the last part of the Chapter we have discussed unidirectionally coupled cellular automata and also in this case, we have showed that the slave cellular automaton may anticipate the future pattern of the master cellular automaton. The fact that the cascade of slave systems enables larger anticipation times could be useful in performing fast data processing or other tasks with use of cellular automata. An array of real-working cellular automata with particular couplings (with spatial or time delay), could perform calculations in parallel and synchronously with zero time lag between their output signals. Finally, the possibility of obtaining the anticipated synchronization with the delayed coupling term containing the delayed in space variable instead of delayed in time, is the proof that the slave system with the delayed coupling may be considered as a spatially extended N dimensional system.

Chapter 4

Dynamical mechanisms of anticipated synchronization

Anticipated synchronization has been often described as a rather counterintuitive phenomenon due to the possibility of the slave system to anticipate the unpredictable evolution of the master [97, 99, 102]. In Section 4.1 we provide a simple explanation for the physical mechanism behind the anticipated synchronization using delayed coupled excitable systems subject to a common forcing (published in Ref. [134]). In Section 4.2 we study in detail the anticipated synchronization in chaotic systems. The use of the modified system approach allows us to understand many features of the phenomenon. Finally in section 4.3 we compare the anticipated synchronization method with the delayed feedback control method.

4.1 Mechanism of anticipated synchronization in excitable systems

4.1.1 Characterization of the response time

In order to deepen into the actual mechanism responsible for the anticipated synchronization, we consider two unidirectionally-coupled identical Adler's systems (see Section 2.1 and Ref. [135]) with delayed coupling subject to a common external perturbation $I(t)$,

$$\dot{x} = \mu - \cos(x) + I(t) \tag{4.1}$$

$$\dot{y} = \mu - \cos(y) + K(x - y_\tau) + I(t) \tag{4.2}$$

When $I(t) = \xi(t)$ is a zero-mean Gaussian noise, anticipated synchronization occurs as shown in Fig. 4.1, where we plot the master and slave outputs for a particular value of $K > 0$ and τ. Note that the slave system anticipates the firing of a pulse in the master by a time interval approximately equal to τ. If we increase the coupling constant K or the delay time τ beyond some values, anticipated synchronization is degraded, i.e., the

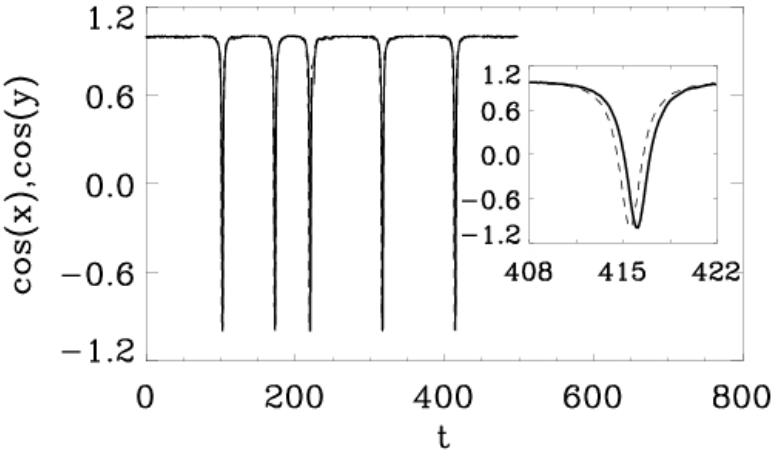

Figure 4.1: *Time series of the master system x (solid line) and slave system y (dashed line) subjected to white Gaussian noise of zero mean and correlations $\langle \xi(t)\xi(t')\rangle = D\delta(t-t')$, obtained by numerical simulation of Eqs. 4.1 and 4.2. Other parameters are: $\mu = 0.95$, $K = 0.01$ $\tau = 1$. The noise intensity is $D = 0.017$.*

slave system can emit pulses which do not have a corresponding pulse in the master's output, although the reverse case never occurs. Upon further increasing K or τ, the anticipation phenomenon disappears. The results are analogous to those obtained for the FitzHugh-Nagumo model (see Section 3.1).

In order to understand the mechanism of the observed phenomenon, we first analyze the behavior of the master system alone under the effect of a single perturbation $I(t) = p_0\delta(t - t_0)$ acting at a certain time t_0. The effect of this perturbation appears only as a discontinuity of the $x(t)$ variable at time t_0 as $x(t_0^+) = x(t_0^-) + p_0$. The condition for the perturbation to be larger than the excitability threshold, is that $x(t_0^+) > x_+$, where x_+ is the unstable fixed point of Eq. 4.1. From now on, we set the initial condition to be in the rest state, $x(t_0^-) = x_-$, where x_- is the stable fixed point of Eq. 4.1, such that the minimum value for the amplitude in order to excite a pulse is $p_0 > 2\arccos\mu$ and the system develops a pulse after a certain response time t_r. This time can be precisely defined as the time it takes $x(t)$ to reach a given reference value, e.g. $x_r = \pi/2$. From Eq. 4.1 we have $t_r = \int_{x(t_0^+)}^{\pi/2} \frac{dx}{\mu - \cos x}$ which yields

$$t_r = \frac{1}{\sqrt{1-\mu^2}} \ln\left[\frac{(1-b)(b^{-1}\tan\frac{x(t_0^+)}{2}+1)}{(1+b)(b^{-1}\tan\frac{x(t_0^+)}{2}-1)}\right] \tag{4.3}$$

where $b = \sqrt{\frac{1-\mu}{1+\mu}}$. In Fig. 4.2 (upper panel) we plot the response time as a function of the parameter μ for a given value of the perturbation amplitude p_0. Note that below the excitability threshold, $p_0 < 2\arccos(\mu)$ (equivalently $\mu < \cos(p_0/2)$), t_r does

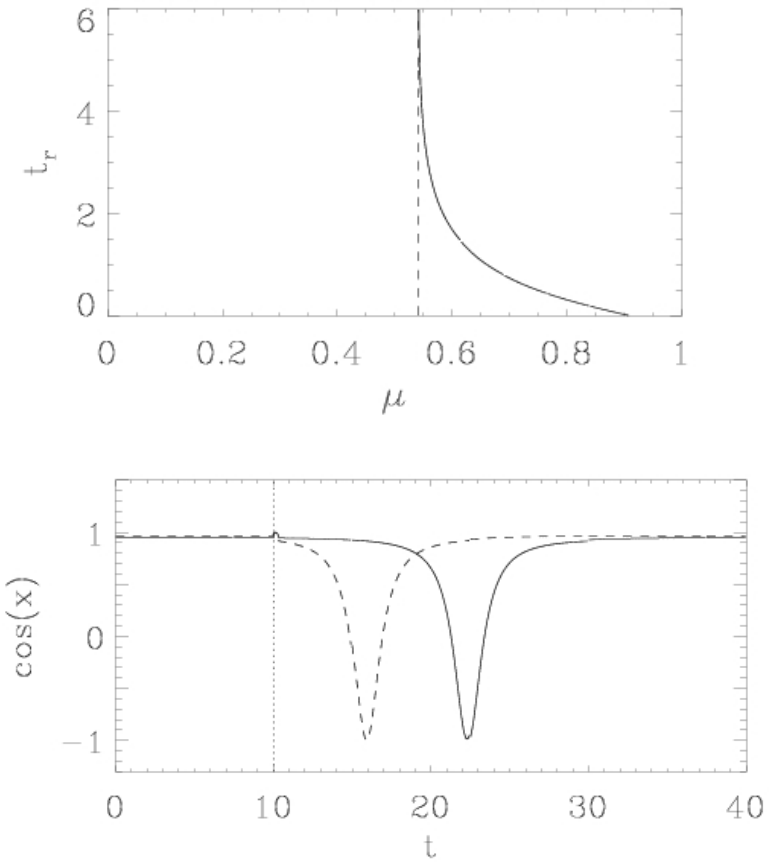

Figure 4.2: *Upper panel: Response time t_r versus μ for the Adler system x perturbed by $p_0\delta(t)$ with $p_0 = 2$ from Eq. 4.3. Lower panel: time series for $x(t)$ for $\mu = 0.95$ (solid line) and $\mu = 0.97$ (dashed line). Both systems have been perturbed at $t_0 = 10$ by a pulse of constant amplitude $p = 1.7$ and duration $\Delta t = 0.4$. Note that, in agreement with the left panel, the system with the larger value of μ pulses before the one with the smaller value.*

not exist. For $\mu > \cos(p_0/2)$ the response time t_r is a decreasing function of μ which approaches zero as $\mu \to 1$. This shows that the response time to an above-threshold external perturbation progressively decreases as the Andronov bifurcation point ($|\mu| = 1$) is approached, in agreement with the numerical result shown in Fig. 4.2 (lower panel). The fact that the response time decreases with lower excitability threshold, and that in the coupled system the slave can emit pulses that are not followed by a pulse in the master, suggests that the mechanism for anticipation in the master-slave configuration is that the slave has a lower excitability threshold than the master. This is supported by the following qualitative argument: Let us assume that at $t = t_0$ both systems, master and slave, are in the rest state $x(t_0^-) = y(t_0^-) = x_-$. The effect of the perturbation changes both values to $x(t_0^+) = x(t_0^-) + p_0$, $y(t_0^+) = y(t_0^-) + p_0$. Due to the cou-

pling, the slave can be considered to have, at this time, an effective system parameter $\mu_{\text{eff}}(t_0) = \mu + K[x(t_0^+) - y(t_0^+ - \tau)] = \mu + Kp_0$. Since $\mu_{\text{eff}}(t) > \mu$ also for all times t such that $t_0 \leq t < t_0 + \tau$, the excitability threshold of the slave has been reduced and the response time decreases.

4.1.2 Effect of the delayed coupling term on the excitable system

To give a more rigorous evidence for this explanation, we consider now two coupled systems, Eqs. (4.1-4.2), in the presence of a single perturbation which we choose to be a pulse of constant amplitude p and duration Δt acting at time t_0 in which both systems are in the rest state $x(t_0^-) = y(t_0^-) = x_-$. The results are reported in Fig. 4.3. For a sufficiently large perturbation, the master and the slave respond with an excitable spike and the slave pulse anticipates the master pulse (Fig. 4.3a). For small perturbation amplitude no pulses are generated and both systems respond proportionally to the applied stimulus (Fig. 4.3c). However, an intermediate amplitude of the perturbation triggers the emission of an excitable pulse by the slave system while the master responds linearly (Fig. 4.3b). This confirms a lowering of the excitability threshold of the slave as compared to the master (see Fig. 4.4), which is systematically found for all coupling parameters that yield anticipated synchronization. The process of decreasing of the excitability threshold of the slave stops for the coupling value $K \approx 0.1$ and it is because for larger coupling values the slave system starts to oscillate with an amplitude that goes to infinity. This is due to the presence of a time delay which makes the system infinite dimensional and thus may induce periodic oscillations and even chaos (see Section 2.4). Therefore the effect of this particular coupling scheme on the slave system is to lower its excitability threshold in such way that the difference between the response time of the master and the slave to an external perturbation equals approximately the delay in the coupling term, τ. It is worth noting that when K or τ tend to zero, not surprisingly the thresholds for the slave and the master tend to be equal, while for large values of τ the difference between the two thresholds is very large.

The same reasoning followed during the explanation of the anticipated synchronization in excitable systems can be used if the perturbation applied to both systems is a white noise source. This allows us to explain why the erroneous synchronization events correspond to the slave system firing a pulse that is not followed by a pulse in the master: for a particular noise level the master response is proportional to the perturbation while the slave emits an excitable pulse. By increasing the noise level both master and slave emit excitable pulses, each pulse of the slave being anticipated respect to that of the master.

Since, as we have already shown, master and slave systems respond to external perturbations with different response times, a question which arises is whether it is possible

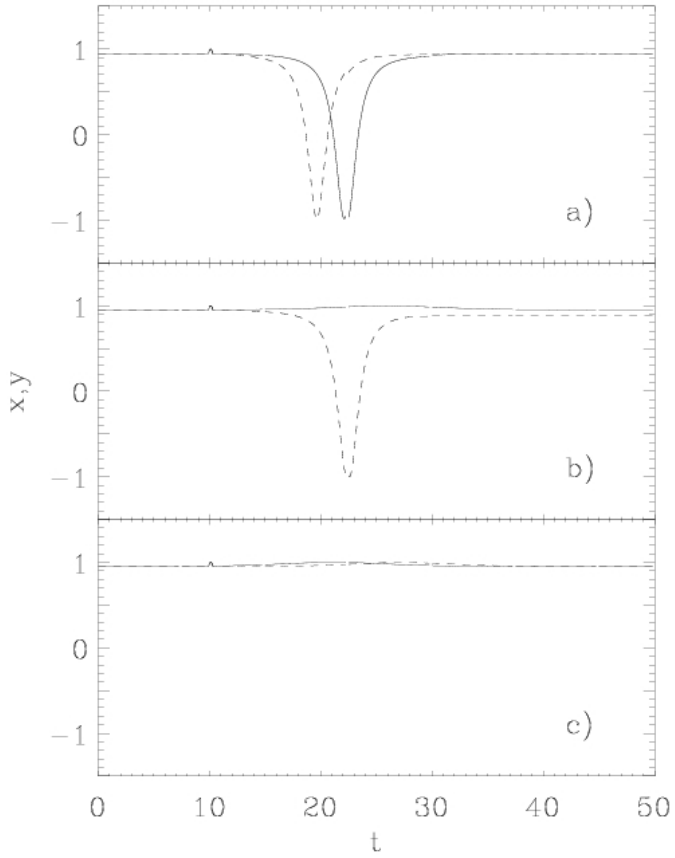

Figure 4.3: *Response of the master (solid line) and slave (dashed line) for three different amplitudes of the singular perturbation of duration* $\Delta t = 0.4$ *at time* $t_0 = 10$*: (a)* $p = 1.7$*, (b)* $p = 1.65$ *and (c)* $p = 1.61$*. Other parameters are* $\mu = 0.95$*,* $\tau = 5$ *and* $K = 0.01$*.*

to chose the parameters such that the anticipation time is arbitrarily large or not. In particular, if the anticipation time can be larger than the master response time, $\tau > t_r$, a result that would violate the causality principle. In order to answer this question, we plot in Fig. 4.5 the results of integrating Eqs. 4.1 and 4.2 under the effects of a single perturbation for three different values of the parameter τ. When $\tau < t_r$ (Fig. 4.5a) the anticipation time is approximately equal to τ. However, when $\tau \gg t_r$, the anticipation time strongly differs from the delay time, such that the slave anticipates the master by a time interval always lower than t_r (Fig. 4.5b,c). This is a reasonable limit for the anticipation time: the pulse cannot anticipate the perturbation which created it. In other words, master and slave are both "slaves" of the external perturbation.

In order to assess the generality of our hypothesis, we have also considered two

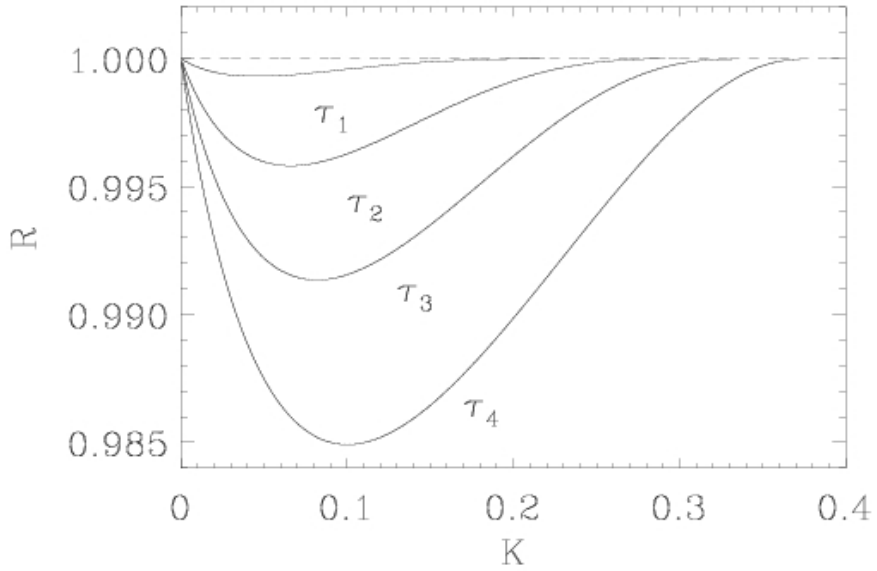

Figure 4.4: *The ratio for Adler's system between the slave and the master excitability threshold as a function of K for $\tau_1 = 0.05$, $\tau_2 = 0.2$, $\tau_3 = 0.35$ and $\tau_4 = 0.5$. Considered system have parameter $\mu = 0.95$. Perturbation is applied at time $t_0 = 10$ with magnitude $p = 1.635$ and duration $\Delta t = 0.4$. The dashed line corresponds to the constant excitability threshold of the master.*

delayed coupled FitzHugh-Nagumo systems:

$$\begin{aligned} \dot{x_1} &= x_2 + x_1 - \frac{x_1^3}{3} \\ \dot{x_2} &= \epsilon(a - x_1) \qquad (4.4) \\ \dot{y_1} &= y_2 + y_1 - \frac{y_1^3}{3} + K(x_1 - y_{1,\tau}) \\ \dot{y_2} &= \epsilon(a - y_1) \qquad (4.5) \end{aligned}$$

In the excitable regime, which occurs when $|a| > 1$, the system possesses a single steady state. As the critical value $|a_c| = 1$ is approached, the excitability threshold is lowered [136]. In this sense, the control parameter a plays the same role as the parameter μ in Adler's equation. In fact, we have checked that also in this case the response time of the system to an external perturbation decreases as the critical value a_c is approached (see Fig. 4.6). The response time in FitzHugh-Nagumo system in Eq. 4.4 may be calculated by integrating the following equation: $dt = \frac{x_1^2-1}{\epsilon(a-x_1)}dx_1$. Then, we define the response time as the time needed for the system to go from $x_1^0 = a+\eta$ (where $-|a| < \eta < 0$ if $a > 0$ or $|a| > \eta > 0$ if $a < 0$) to the reference point which we take as $x_1^1 = 0$. Then the

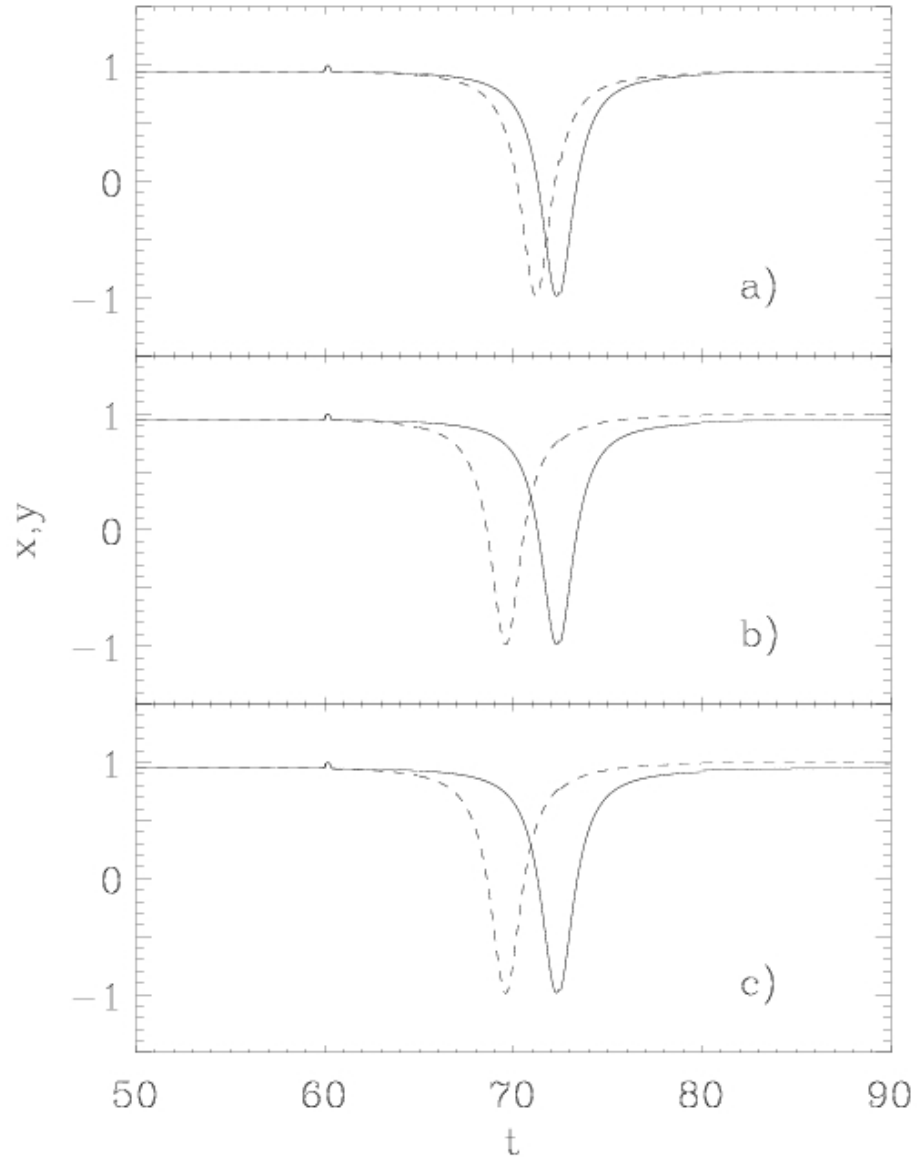

Figure 4.5: *Two coupled Adler systems (master and slave) with a coupling parameter* $K = 0.01$ *and delay time (a)* $\tau = 1$*, (b)* $\tau = 5$ *and (c)* $\tau = 50$*. Both systems have* $\mu = 0.95$ *and are perturbed at time* $t_0 = 60$ *with a pulse of magnitude* $p = 1.7$ *and duration* $\Delta t = 0.4$*.*

equation for the response time $t_r = \Delta t = t_1 - t_0$ is the following:

$$t_r = \frac{1}{\epsilon}\left[(1-a^2)\ln\left(\frac{a}{\eta}\right) + (a+\eta)^2\right] \tag{4.6}$$

where the dependence on parameters ϵ and a is evident. As ϵ increases the response time decreases and as $\epsilon \to 0$ the response time becomes very fast, almost instantaneous. This

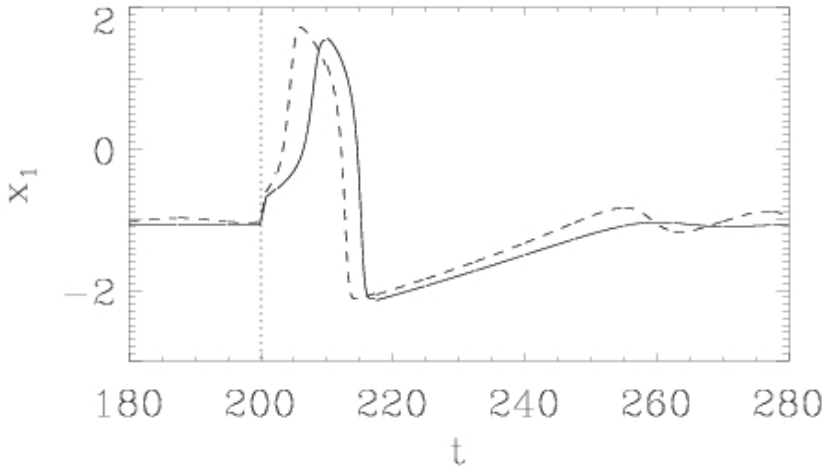

Figure 4.6: *Time series of the variable x_1 of the FitzHugh-Nagumo system for $a = -1.01$ (dashed line) and $a = -1.08$ (solid line). In both cases it is $\epsilon = 0.09$. As indicated by the vertical dotted line, the system is perturbed at a time $t_0 = 200$ by a pulse of amplitude $p = 0.4$ and duration $\Delta t = 1$. Note that the response time decreases with increasing a.*

analytical result is in agreement with the well known characteristics of the parameter ϵ. On the other hand as the absolute value of the parameter a increases, the distance from the steady fixed point, to the reference point $x_1^1 = 0$ increases and is equal to $|a|$, thus making a contribution to longer response times. For the unidirectionally delayed coupled system we find, as before, that the excitability threshold for the slave is lower than that of the master (see Fig. 4.7) and that the maximum anticipation time is limited by the response time of the master. We have also calculated numerically the ratio between the slave and the master excitability thresholds as a function of K for different values of delay time τ (see Fig. 4.8), which exhibits the same behaviour as the Adler's system: for a particular range of coupling parameter K the excitability threshold of the slave decreases, and this process becomes stronger as the delay time τ increases. However, the process of decreasing of the excitability threshold stops at some particular delay time values, as in the previously discussed case of the Adler's system, because the difference variable $\Delta = x - y_\tau$ becomes non-zero for $\tau > t_r$.

Finally, it is worth mentioning that we have also found the same phenomenology for two delayed coupled Hodgkin-Huxley systems. The ubiquity of this effect is an indication that the lowering of the excitability threshold of the slave in a delayed coupling scheme is a general mechanism for the anticipated synchronization in excitable systems.

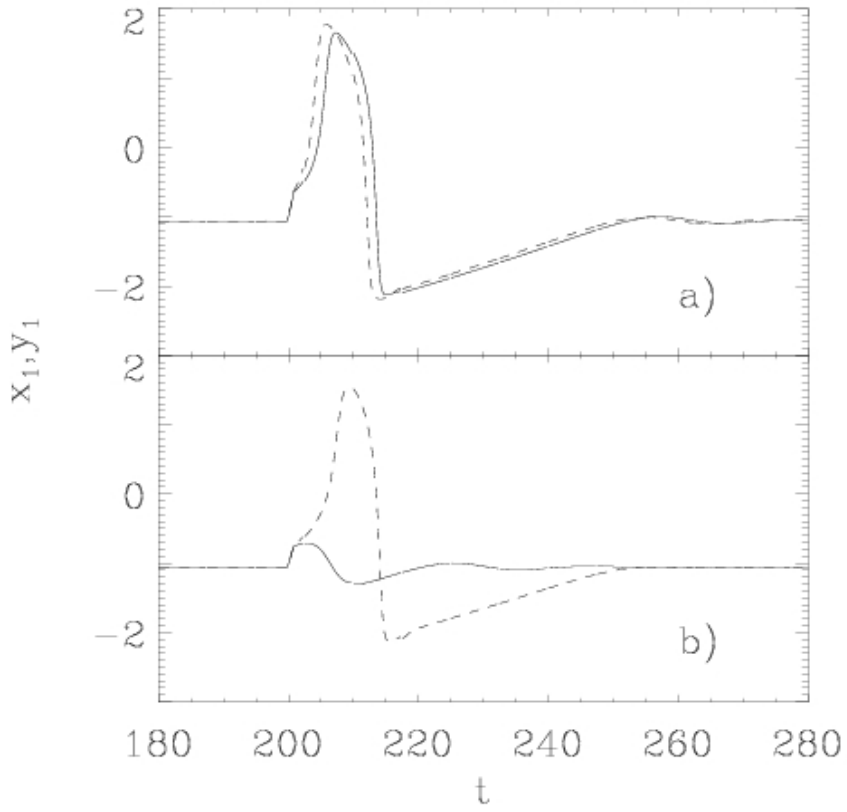

Figure 4.7: *Response of the master (x_1, solid line) and slave (y_1, dashed line) for two coupled FitzHugh-Nagumo systems with $a = 1.01$, $\epsilon = 0.09$, $\tau = 4$, $K = 0.1$, after perturbation at $t_0 = 200$ by a pulse of amplitude p and duration $\Delta t = 1$. For large amplitude, $p = 0.4$, case (a), both systems pulse whereas for the smaller amplitude, $p = 0.3$, case (b), there is only a pulse in the slave variable.*

4.1.3 Analysis of the delayed coupling term

Let us look at the delayed coupling term $K(x - y_\tau)$ as a particular case of the more general form: $\alpha(x - y) - \beta(y_\tau - y)$. For $\alpha = \beta = K$ the general form reduces to the form of the delayed coupling scheme. The first term $\alpha(x - y)$ is a synchronization term which for particular values of the coupling constant α pushes systems to synchronize. The term $\beta(y_\tau - y)$ is the one used in the delayed feedback control method proposed by Pyragas [45] to control the dynamics of the system, i.e. to induce a transition from chaos to the stable periodic orbits or stable fixed points, or vice versa. In other words, the delayed feedback control term changes the parameters of the system, what can be easily seen when looking at the bifurcation diagrams of the master and the slave. In figure 4.9 we see that the Hopf bifurcation in the master and the slave occurs at different values of the parameter a. This difference is determined by parameters K and τ.

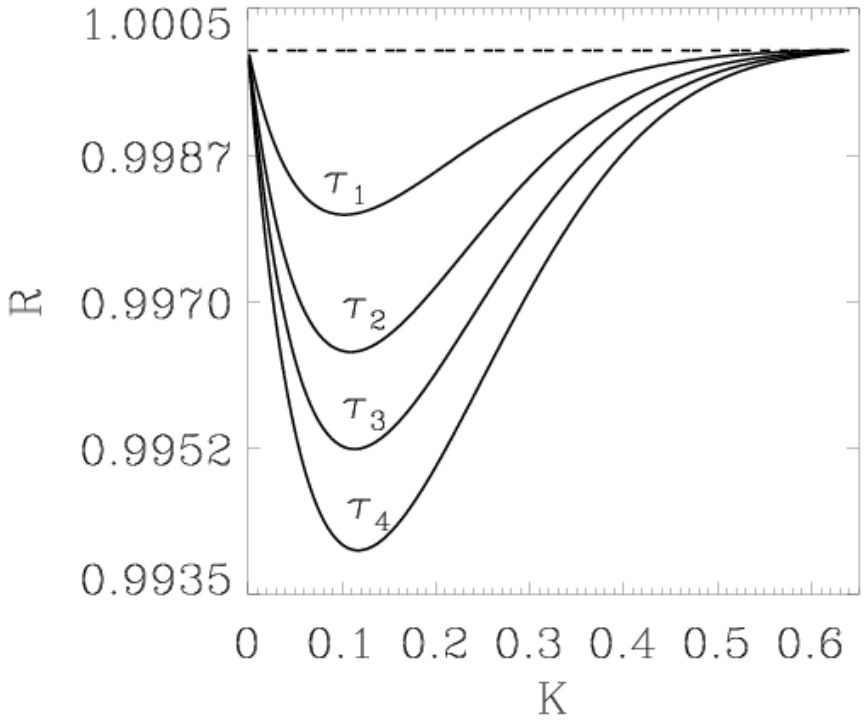

Figure 4.8: *The ratio for FitzHugh-Nagumo system between the slave and the master excitability threshold as a function of K for $\tau_1 = 0.05$, $\tau_2 = 0.08$, $\tau_3 = 0.1$ and $\tau_4 = 0.12$. The dashed line corresponds to the constant excitability threshold of the master.*

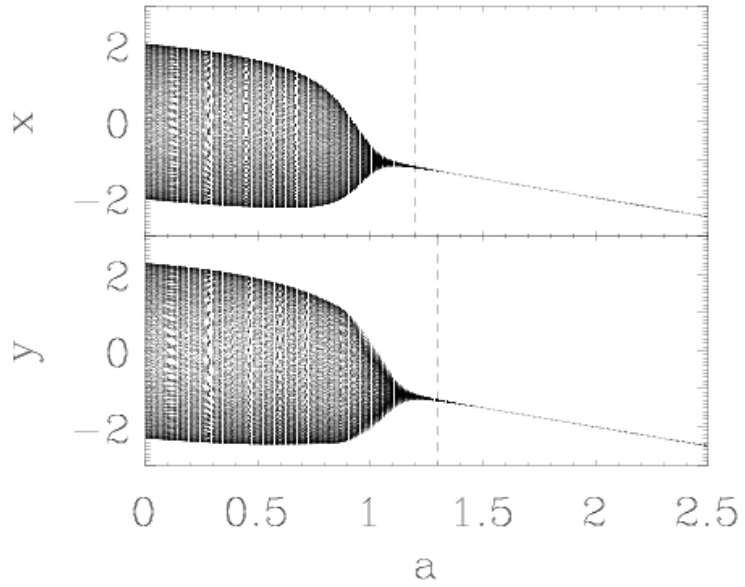

Figure 4.9: *Bifurcation diagrams for two coupled FitzHugh-Nagumo systems master* **x** *and slave* **y**. *Delayed coupling term has the following parameter values: $K = 0.15$ and $\tau = 3$.*

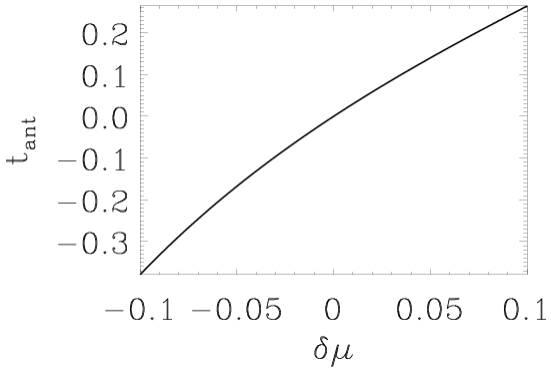

Figure 4.10: *An anticipation time t_{ant} observed between a master and a slave responses depending on the difference $\delta\mu$ of the parameters μ_{slave} of master and μ_{master} of slave. Both systems are coupled unidirectionally with a constant parameter K and fixed zero delay time $\tau = 0$. The control parameter in this case is μ_{slave} of the slave system, meanwhile μ_{master} of master is left constant.*

A further confirmation of this mechanism is that, for $\tau = 0$, the slave can still anticipate the master, whenever the parameters in both systems are different. We study in details the relation between t_{ant} and $\delta\mu$, where t_{ant} is the difference time between masters' and slaves' responses and $\delta\mu = \mu_{slave} - \mu_{master}$. Numerical results for Adlers' system (see Fig. 4.10) show that the anticipated synchronization appears when $\mu_{slave} > \mu_{master}$. When $\mu_{slave} < \mu_{master}$ the synchronization also occurs but is retarded (then $t_{ant} < 0$).

In the case of the FitzHugh-Nagumo systems driven by noise we observe the same phenomenology. First we couple with the synchronization scheme $K(x - y)$, the master being in the excitable regime with the slave being in the oscillatory regime. The effect of this way of coupling (see Fig. 4.11) is that for the particular value of the coupling strength K, the slave synchronizes to the master with retardation. On the other hand, when we reverse the configuration and consider the master in the oscillatory regime and the slave in the excitable regime, we observe that the slave synchronizes and anticipates with the master (see Fig. 4.12).

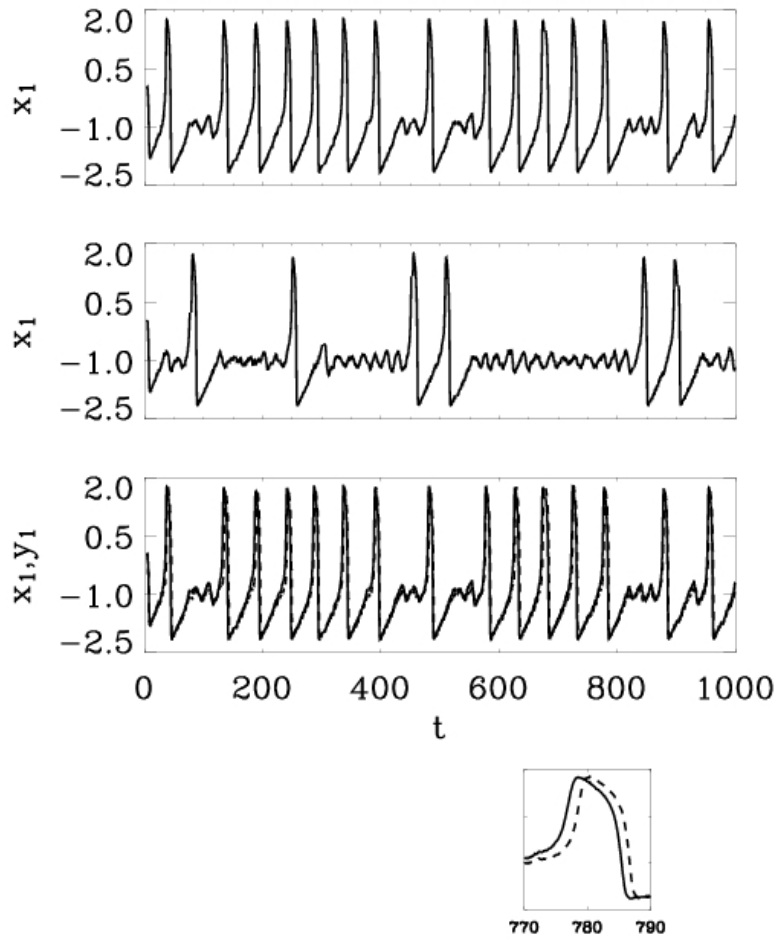

Figure 4.11: *Upper and middle panels: uncoupled master and slave FitzHugh-Nagumo systems with parameters, respectively,* $a = 0.97$ *and* $a = 1.01$. *Lower panel: coupled master (solid line) and slave (dashed line) with the synchronization scheme* $K(x - y)$ *for* $K = 0.1$.

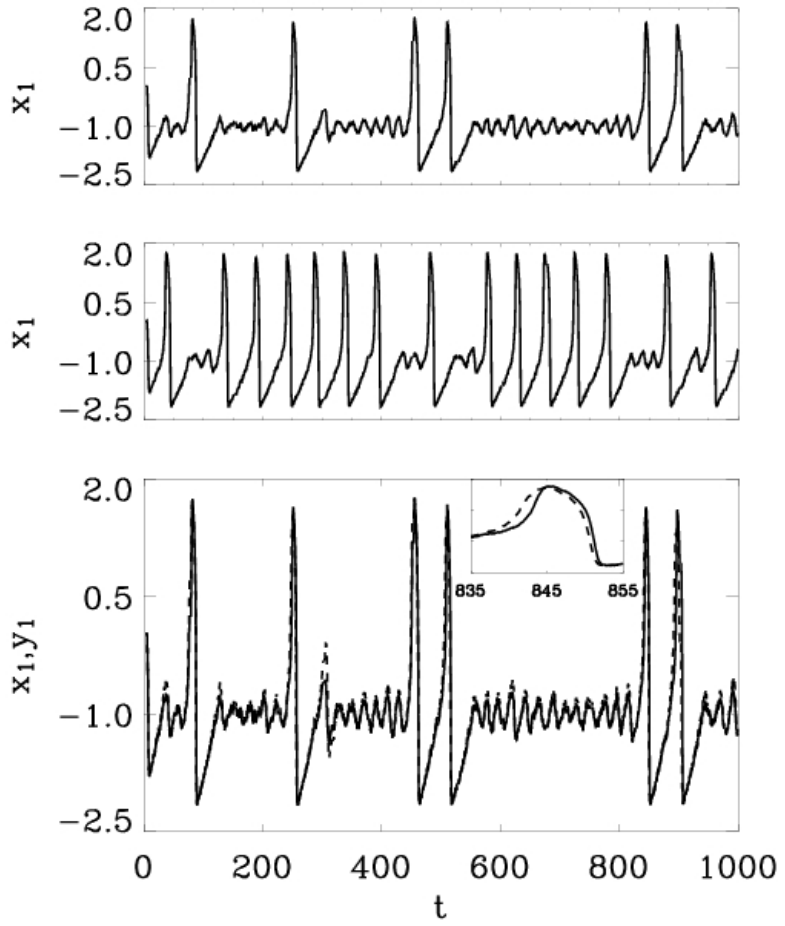

Figure 4.12: *Upper and middle panels: uncoupled master and slave FitzHugh-Nagumo systems with parameters, respectively,* $a = 1.01$ *and* $a = 0.97$*. Lower panel: coupled master (solid line) and slave (dashed line) with the synchronization scheme* $K(x - y)$ *for* $K = 0.35$*.*

4.2 Modified-system approach to chaotic systems

Recently a new modified-system approach has been proposed in order to understand the reasons for the occurrence of synchronization [137]. The authors in [137] show that synchronization of the slave $\dot{\mathbf{y}} = \mathbf{f(y)} + \mathbf{K(x\text{-}y)}$ with the output of the master $\dot{\mathbf{x}} = \mathbf{f(x)}$ is possible for such parameters at which the uncoupled slave $dot\mathbf{y} = \mathbf{f(y)} - \mathbf{Ky}$ is in the period-one oscillatory or in the steady-state regimes.

The system of differential equations for $\mathbf{y}$ with $\mathbf{K}$ can be considered as the result of two processes taking place simultaneously. The first term, $\mathbf{Ky}$, is proportional to the slaves' variable and the second one, $\mathbf{Kx}$, is the amplitude of the external signal. Both processes are correlated with each other by means of the parameter value $\mathbf{K}$, nevertheless can be considered separately in order to understand better the mechanisms of synchronization.

In this Section we apply this modified system approach to clarify the occurrence of anticipated synchronization in chaotic systems.

4.2.1 Diffusive delayed coupling scheme

We consider two unidirectionally coupled systems in the master-slave configuration:

$$\begin{aligned} \dot{\mathbf{x}} &= \mathbf{f}(\mathbf{x}) \\ \dot{\mathbf{y}} &= \mathbf{f}(\mathbf{y}) + K(\mathbf{x} - \mathbf{y}_\tau) \end{aligned} \tag{4.7}$$

where the slave is coupled to the master only through one variable. We treat separately the effects of the coupling term $K(\mathbf{x}-\mathbf{y}_\tau) \rightarrow K_1\mathbf{x} - K_2\mathbf{y}_\tau$, one part of which is an external forcing of magnitude K_1, coming from the master system, while the second part is the delayed feedback term of magnitude K_2. Let us first look at the behavior of the modified slave system:

$$\dot{\mathbf{y}} = \mathbf{f}(\mathbf{y}) - K_2\mathbf{y}_\tau \tag{4.8}$$

which is free from any influence of the master.

In particular, we consider two Rössler systems (see Section 2.2), the master:

$$\begin{aligned} \dot{x_1} &= -x_2 - x_3 \\ \dot{x_2} &= x_1 + a\,x_2 \\ \dot{x_3} &= b + x_3(x_1 - c) \end{aligned} \tag{4.9}$$

and the modified slave:

$$\begin{aligned} \dot{y_1} &= -y_2 - y_3 - K_2 y_{1,\tau} \\ \dot{y_2} &= y_1 + a\,y_2 \\ \dot{y_3} &= b + y_3(y_1 - c) \end{aligned} \tag{4.10}$$

where K_2 is the coupling constant which will serve us as the control parameter. The regime where anticipated synchronization occurs between these systems, in the case when $K = K_1 = K_2$ is plotted in Fig. 4.13.

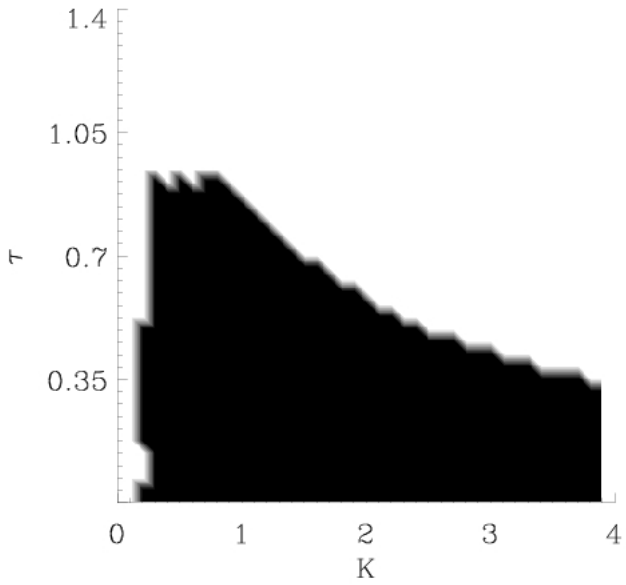

Figure 4.13: *The cross-correlation diagram between signals of the master $x_1(t)$ and the slave $y_1(t-\tau)$ Rössler coupled system in the parameter space $K-\tau$. Black (white) color means high (low) correlations.*

The effect of delayed feedback on the chaotic system is well known and exhaustively studied since the publication of Pyragas in 1992 [45]. A delayed feedback loop adequately applied to a system leads to the stabilization of the chaotic trajectories of the system, changing them to periodic oscillations or even fixed points solutions. We are interested however, in how the delay time and the coupling constant are related during the delayed feedback control process. To assess this problem we consider the coupling constant as the control parameter and look at the bifurcation diagrams for different values of the delay time.

In Fig. 4.14 we plot the bifurcation diagrams of the master Rössler system (Eq. 4.9) and the modified slave Rössler system (Eq. 4.10). We can see that while the master undergoes the route to chaos, the modified slave with non-zero delay time τ and coupling constant K_2 is in the fixed point state for a wide range of parameter c. In view of this observation, anticipated synchronization is induced by the external forcing $K_1 x_1$ in the slave being in the fixed point state. To clarify this observation we analyze in more detail the effects of the delay feedback on the slave system.

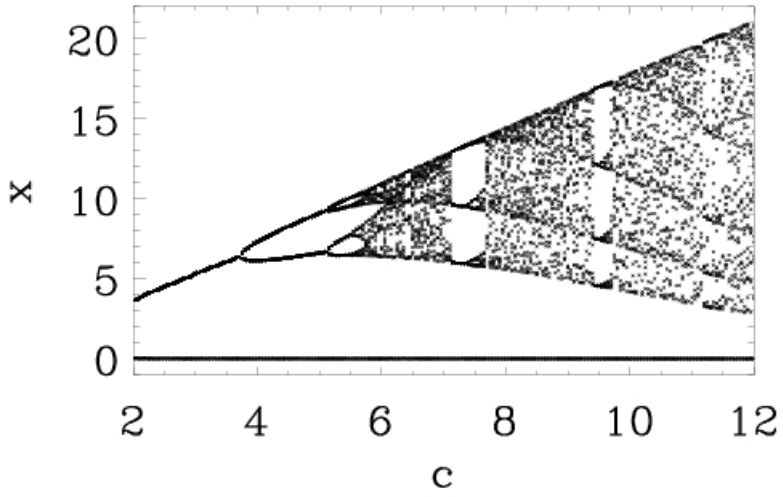

Figure 4.14: *Bifurcation diagram for the master Rössler system with the change of the control parameter c. The line below the bifurcation diagram shows that the slave, with $K_1 = 0$ (uncoupled from the master), $K_2 = 2$ (with delayed feedback term) and $\tau = 0.1$, remains in the steady fixed point state whenever c is changed. Maxima of the time series are plotted.*

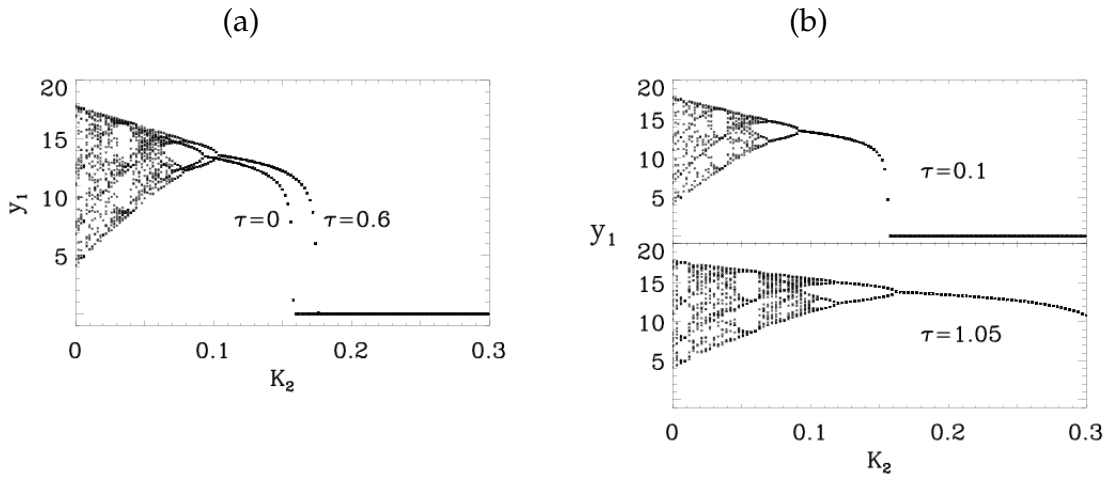

Figure 4.15: *Bifurcation diagrams for the uncoupled slave system $K_1 = 0$ driven by the delayed feedback term $K_2 y(t - \tau)$. Bifurcation diagrams are provided for the delay times: (a) $\tau = 0$ and $\tau = 0.6$, (b) $\tau = 0.1$ and $\tau = 1.05$. Maxima of the time series are plotted.*

In Fig. 4.15a we plot the bifurcation diagrams for the modified slave, Eq. 4.10, for two delay values $\tau = 0$ and $\tau = 0.6$ vs. K_2. The slave system undergoes a transition from chaotic to periodic oscillations and finally to the fix point state through an inverse cascade of period doubling. This transition depends on the value of delay time τ. For

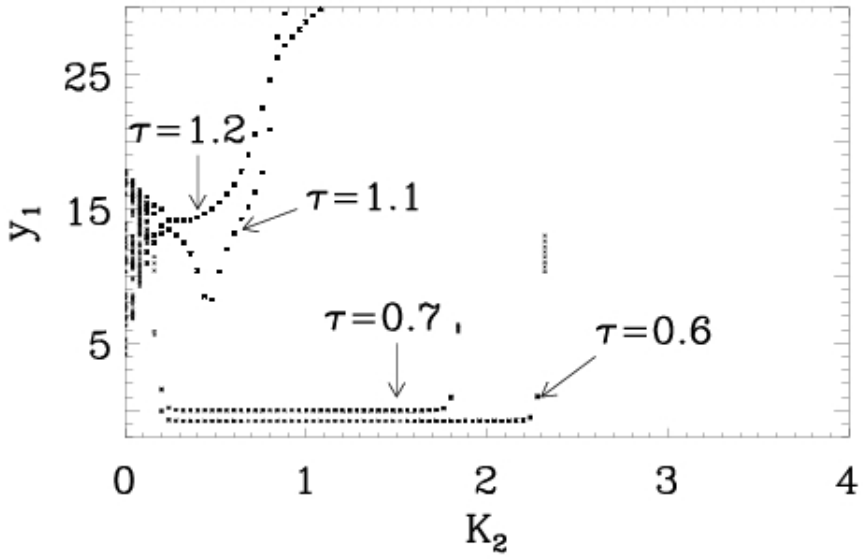

Figure 4.16: *Bifurcation diagrams for the uncoupled slave system $K_1 = 0$ driven by the delayed feedback term $K_2 y(t-\tau)$. Bifurcation diagrams are provided for different delay times $\tau = 0.6$, $\tau = 0.7$, $\tau = 1.1$ and $\tau = 1.2$. Maxima of the time series are plotted.*

small delays the system reaches the fix point state at smaller coupling values, while for larger delays it requires larger values of the coupling constant. The bifurcation diagram for $\tau = 0.6$ is shifted to the right (in the direction of larger values of K_2) in comparison with the diagram for $\tau = 0$. This shift is responsible for the synchronization being anticipated. Large delays in the slave yields chaotic state for particular values of K_2 whereas small delays yields steady or oscillatory regular states for the same coupling strength K_2. It seems that the bifurcation diagram for the larger delay shown in the lower panel of Fig. 4.15b, has the same form but it is somehow stretched horizontally in comparison with the bifurcation diagram for the smaller delay presented in the upper panel of Fig. 4.15b. If the coupling constant K_2 in the lower panel is rescaled by multiplying it, approximately, by a factor 2 we observe in both panels exactly the same bifurcation diagrams.

Furthermore, when comparing the bifurcation diagrams of Fig. 4.16 with the cross-correlation diagram in Fig. 4.13 it is seen that the stability of the anticipated synchronization manifold depends on the stability of the modified system: if the modified system is in its steady state, then anticipated synchronization is possible. Otherwise, if the modified slave is oscillatory or chaotic, anticipated synchronization cannot occur. Thus the form of the cross-correlation diagram is strictly determined by the form of the inverse bifurcation diagrams for the modified slave system. The white region represent-

ing small cross-correlations for small couplings at any time delay, is caused by the fact that the modified slave has still some internal oscillatory, regular or irregular, dynamics for such couplings. As the system goes into the steady state at some critical coupling value, the anticipated synchronization can be observed, otherwise if the system never reaches the steady state, anticipation is never observed (it occurs for large delays). It is worth noting that with increasing coupling the instability of the modified slave (see bifurcation diagrams in Fig. 4.16) is due to the appearance of oscillations whose amplitude grows to infinity.

Now, let us look at the effect of the external forcing coming from the master. An external signal can excite chaotic dynamics in a system initially being in the steady state. It shifts again the system back through the inverse cascade of the period doubling. Since the inverse bifurcation diagrams for different delays differ in form, the external forcing, which for all delays is the same $K_1 x_1$, will induce different changes in the slave system. The external force eliminates the distance between the fixed point and the region where the unstable orbits exist. Since the dynamics of a chaotic system consists, in principle, of an infinite number of unstable periodic orbits then the slave may be pushed to visit the unstable periodic orbits of the master. The term $K_1 x_1$ can be considered in fact as a force, since when it is switched off the slave returns to its steady fixed point.

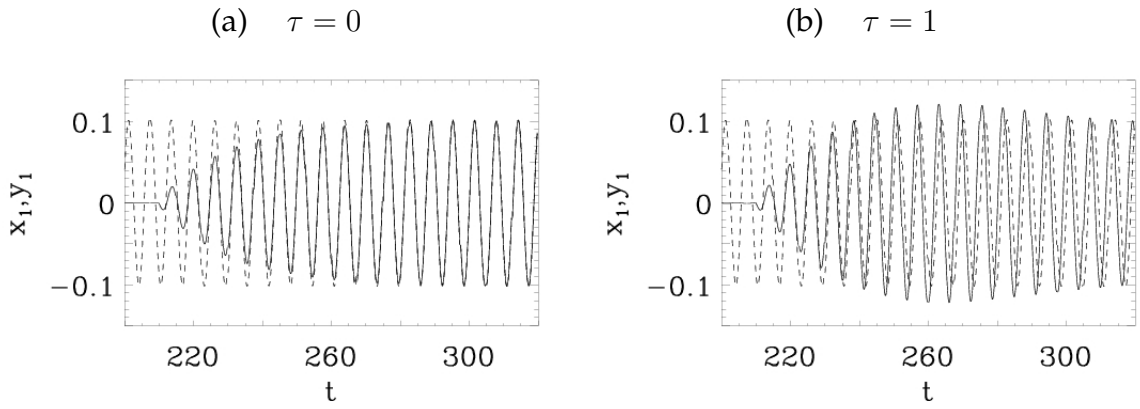

Figure 4.17: *Time series for coupled master (dashed line) and slave (solid line) harmonic oscillators with the coupling strength $K = 0.1$ and delay times (a) $\tau = 0$ and (b) $\tau = 1$. The slave first is stabilized by delayed feedback signal into the steady fixed point and then at time $t = 210$ the external forcing from the master is applied.*

The above considerations show that the anticipation phenomenon is related only to the form of the modified system and thus depends only on the delayed feedback term. As the delayed feedback term $K_2 y_{1,\tau}$ is responsible for the frequency and the phase shifts of the oscillations, the external force $K_1 x_1$ is responsible for the amplitude of oscillations of the slave. In fact, when changing the value of the constant coupling to $K_1 = 0.5 K_2$,

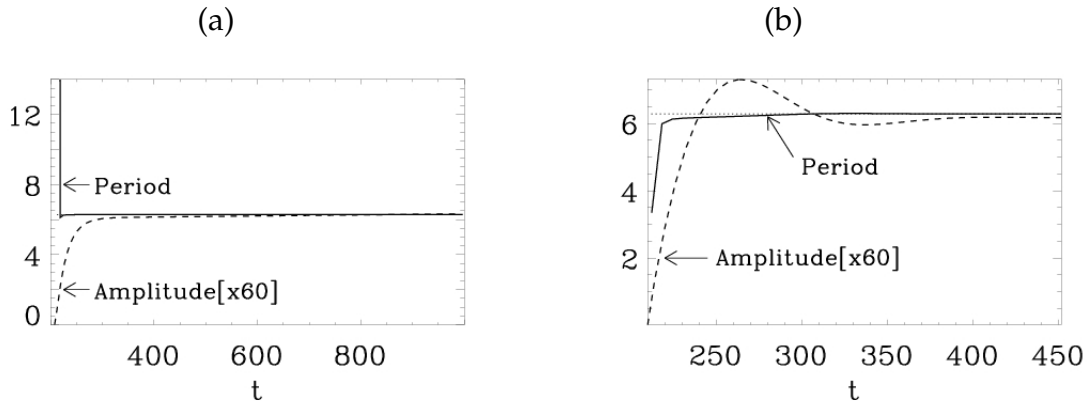

Figure 4.18: *Amplitude and period of oscillations of the slave system during the transient time for coupling strength $K = 0.1$ and delay time (a) $\tau = 0$ and (b) $\tau = 1$.*

we observed that the slave synchronizes with the master with the anticipation but with a half amplitude than that in the master. The anticipation is observed unchanged since during the transient time the delayed variable induces the changes in frequencies in the slave what leads to the anticipation phenomenon. We prove this statement by showing that an "extra" time, giving the contribution to anticipation, accumulates during the transient, and is due to the squeezing in frequency of oscillations in the slave. This squeezing is accompanied by an increase of amplitude. We show it on the example of two coupled harmonic oscillators:

$$\text{Master: } \begin{cases} \dot{x}_1 &= -\frac{k}{m}x_2 \\ \dot{x}_2 &= x_1 \end{cases} \qquad \text{Slave: } \begin{cases} \dot{y}_1 &= -\frac{k}{m}y_2 + K_1x_1 - K_2y_{1,\tau} \\ \dot{y}_2 &= y_1 \end{cases}$$

with the frequency $\omega_0 = \sqrt{\frac{k}{m}}$. In Fig. 4.17a and 4.17b the transitions to synchronization are shown, for the slave with the following coupling terms: $K_1x_1 - K_2y_1$ and $K_1x_1 - K_2y_{1,\tau}$. When the external force K_1x_1 is switched-on (at time $t_0 = 200$) we observe the response of the slaves during the transient time, i.e., the time which is needed to establish the synchronization. For the case where the synchronization with no anticipation establishes, the slave starts to oscillate with the constant frequency equal to that of the master (Fig. 4.17a). However in the case of anticipated synchronization, during the transient, the slave oscillates with different frequencies than that in the master until the anticipated synchronization establishes (Fig. 4.17b), i.e. the frequency of the slave adjusts to the frequency of the master. These changes in frequencies contribute to the occurrence of anticipation and are strictly related to the existence of delay in the equations. The effects of two terms K_1x_1 and $K_2y_{1,\tau}$ may be estimated analytically through the linear stability analysis, where only the term $K_2y_{1,\tau}$ contributes to the change of frequency of the harmonic oscillator, taking the form $\omega = \sqrt{\frac{k}{m(1-K_2\tau)}}$. It is seen that this

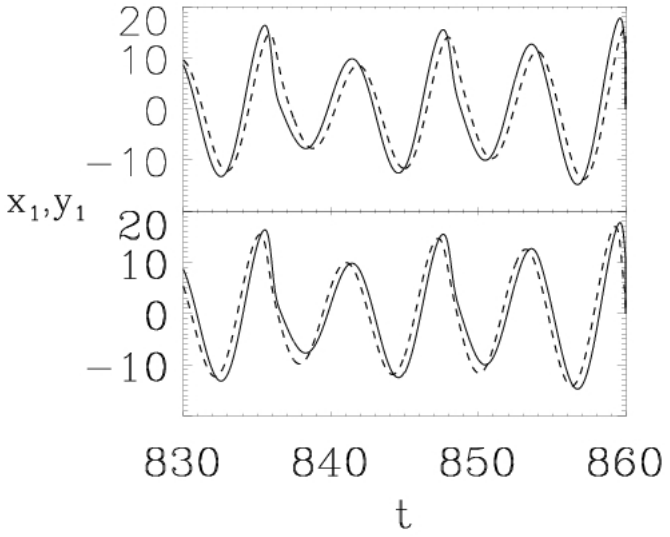

Figure 4.19: *Two coupled Rössler systems with parameter mismatches and coupling scheme $K(x-y)$. Parameter values are: $d = 0.55$ and $K_2 = 1.35$ (upper panel); $d = 1.35$ and $K_2 = 0.9$ (lower panel).*

frequency is larger than ω_0 ($\omega > \omega_0$), where ω_0 is a frequency of the master and for $\tau = 0$ reduces to $\omega = \omega_0$.

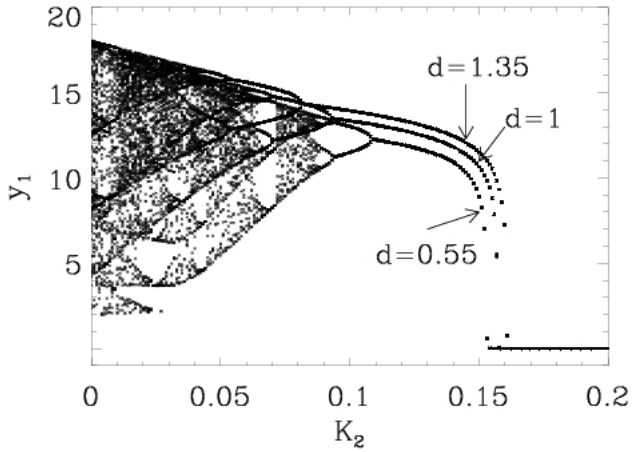

Figure 4.20: *Bifurcation diagrams for Rössler slave systems with feedback $K_2 y_2$ of intensity K_2 being the control parameter. The following values of parameter d are considered: $d = 0.55$, $d = 1$ and $d = 1.35$. Maxima of the time series are plotted.*

The delayed feedback in the anticipated synchronization scheme changes the system dynamics, i.e. changes the parameters of the slave system. Thus, in principle, the anticipated synchronization could appear between two chaotic systems coupled with the diffusive scheme without delay, but with some parameter mismatches. This problem has been already studied in [138], where it is shown that indeed coupling of chaotic systems with parameter mismatches can give anticipated or retarded synchronization. We have demonstrated in Section 4.1, in an example of non-chaotic excitable systems, that anticipated or retarded synchronization can be induced by coupling two systems with different excitability thresholds (which are determined by the system parameters). Let us now consider as a master the system $\{x_1, y_1, z_1\}$ described by Eq. 4.9 and as a modified slave the following one:

$$\begin{aligned} \dot{x_2} &= -dy_2 - z_2 - K_2 x_2 \\ \dot{y_2} &= x_2 + a\, y_2 \\ \dot{z_2} &= b + z_2(x_2 - c) \end{aligned} \tag{4.11}$$

where we introduced a new parameter d; $d = 1$ when the two coupled systems are identical. In Fig. 4.19 we show the time series for the systems of Eqs. 4.9 and 4.11 for different values of the parameter d. In Fig. 4.19 (upper panel) the retarded synchronization, meanwhile in Fig. 4.19 (lower panel) the anticipated synchronization are observed.

The bifurcation diagrams presented in Fig. 4.20 show that for the slave, which anticipates the master (for $d = 1.35$), the first bifurcation leading to the disappearance of the period-1 oscillations occurs faster for larger coupling strength than in the case of zero-lag synchronization (for $d = 1$). Also for the zero-lag synchronization, the same bifurcation appears faster than in the case of retarded synchronization ($d = 0.55$). According to the presented analysis of the bifurcation diagrams, we conclude that the mechanism of the appearance of anticipated synchronization in the above case is similar to the case where delayed feedback is included in the coupling term. However, the quality of the anticipated synchronization obtained by coupling the systems with parameter mismatches is worst than in the case for delayed coupling scheme. We suspect that it is due to the differences in the bifurcation diagrams shown for different values of parameter d in Fig. 4.20. In this case we cannot make any rescaling in order to obtain exactly the same diagrams as it could be done in the case with the delayed coupling scheme (see Fig. 4.15b).

4.2.2 Complete replacement scheme

So far we have considered systems without memory coupled by diffusive coupling. However, anticipated synchronization can also be observed between systems containing internal delays and coupled through replacement scheme, for example in the Ikeda

equations (studied in [97]):

$$\dot{x} = -\alpha x - \beta \sin x_\tau \tag{4.12}$$

$$\dot{y} = -\alpha y - \beta \sin x \tag{4.13}$$

where $\alpha, \beta > 0$. In Eq. 4.13 the delayed variable y_τ of slave is replaced by variable x coming from the master. Time series for the above set of equations in the chaotic regime are presented in Fig. 4.21. The bifurcation diagrams in Fig. 4.22 show that Eq. 4.12 exhibits chaos for particular ranges of parameter values. Starting from $\beta = 0$ (Fig. 4.22a) or from $\tau = 0$ (Fig. 4.22b) and increasing them, one can observe the period doubling transition into chaos.

In the previous Section, we considered the delayed coupling scheme as a separate actions of the two terms $K_1 x$ and $K_2 y_\tau$, where the first one was the external forcing

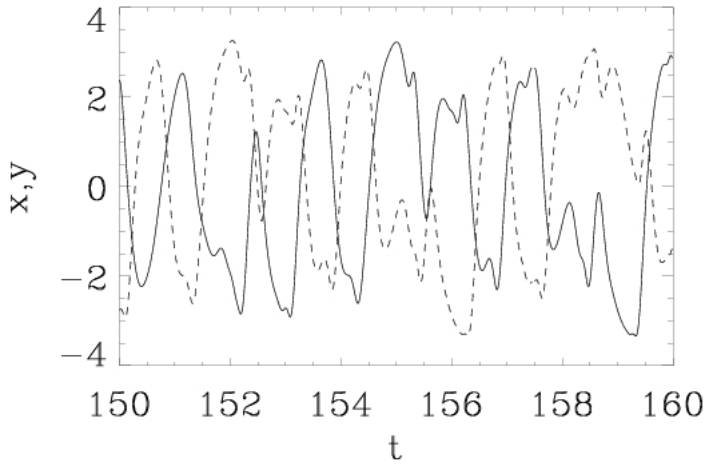

Figure 4.21: *Time series for master (solid line) and slave (dashed line) Ikeda equations. Parameters are:* $\alpha = 5$, $\beta = 18$ *and* $\tau = 3$.

coming from the master meanwhile the latter was a delayed variable of the slave. In the case of the replacement scheme of Eqs. 4.12 and 4.13, the two actions reduce to one, namely to switch on the external forcing coming from the master. This is because the slave system before switching-on the external forcing is already in the steady state. The same result of anticipated synchronization would be obtained if we first consider the slave as $\dot{y} = -\alpha y$ to which we add the external force of the form of $-\beta \sin x$. We prove this hypothesis by showing that the anticipated synchronization is still possible in the system equations 4.12 and 4.13 when the slave system contains the term $\beta_1 \sin y_\tau$, with the constant β_1 such that the slave remains in the stable fixed point state. We use the master from Eq. 4.12 and the following equation for the slave:

$$\dot{y} = -\alpha y - \beta_1 \sin y_{\tau_1} - K \sin x \tag{4.14}$$

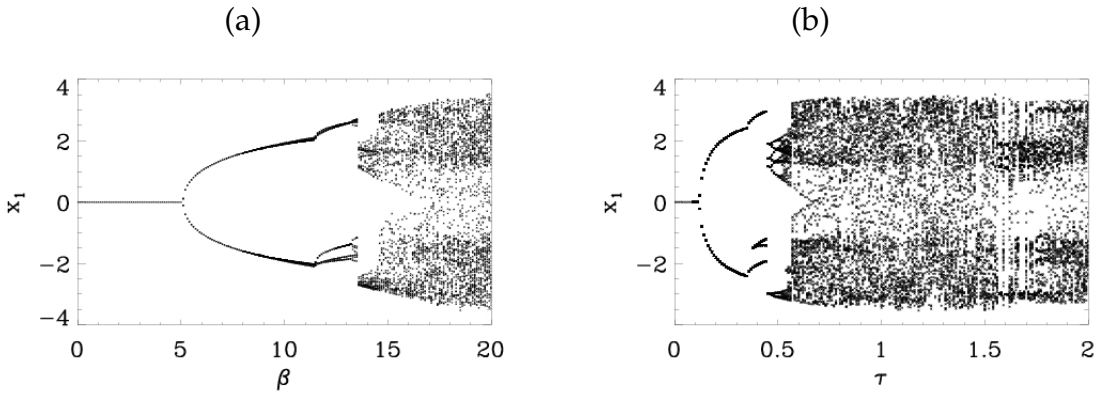

Figure 4.22: *(a) Bifurcation diagram for Ikeda equation in function of β as a control parameter. The parameters of the system are: $\alpha = 5$ and $\tau = 300$. (b) Bifurcation diagram for Ikeda equation in function of delay time τ as a control parameter. The parameters of the system are: $\alpha = 5$ and $\beta = 18$. Maxima of the time series are plotted.*

with the condition obtained through linear stability analysis: $\beta = \beta_1 + K$. Numerical simulations revealed that the condition for the occurrence of anticipated synchronization is that the slave system at $K = 0$ has to be in a stable fixed point or in oscillatory (period one) state. We suspect that during the successful anticipated synchronization the slave at $K = 0$ can be in an oscillatory period one state, because the external forcing from the master enters to the slave in the function $\sin x$. Nevertheless, if the slave exceeds the period one oscillation, anticipated synchronization cannot occur. This result is similar to that for the occurrence of generalized synchronization published in [137].

Following the previous analysis and according to the bifurcation diagram shown in Fig. 4.22a we see that anticipation should occur for parameter β_1 in the range $\beta_1 \in \langle 0, 11 \rangle$. Indeed, we observed through numerical simulations of Eqs. 4.12 and 4.14 that the anticipated synchronization can be obtained only when parameter β_1 is in the range mentioned above and for particular values of constant $K = \beta - \beta_1$. The anticipation time is always equal to the delay τ existing in the master system and there is no restriction for its magnitude. Moreover, the cross-correlation diagram in Fig. 4.23 shows that high correlations between $x(t)$ and $y(t - \tau)$ correspond exactly to the steady fixed point and oscillatory, period one states. Thus, in order to obtain anticipated synchronization in the considered systems it is necessary to have the master and the slave with equal internal delays or very small delay in the slave.

Finally, the above analysis is also valid for the anticipated synchronization mechanism in systems with many delay lines, studied for instance in [139]. Considering the

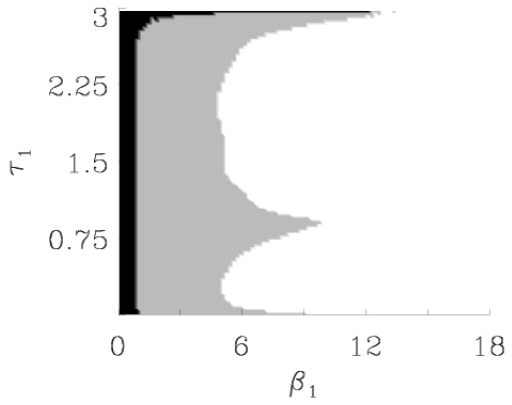

Figure 4.23: *Cross correlation diagram between master and slave outputs for Ikeda equations in the parameters space of the slave β_1 and τ_1. Other parameters are $\alpha = 5$, $\beta = 18$ and $\tau = 3$ and $K = \beta - \beta_1$. Magnitude of correlations are described by colors: $C < 0.9$ (white), $0.9 < C < 0.999$ (grey) and $C > 0.999$ (black).*

system:

$$\dot{x} = -\alpha x - \beta_1 \sin x_{\tau_1} - \beta_2 \sin x_{\tau_2} \tag{4.15}$$

$$\dot{y} = -\alpha y - \beta_3 \sin y_{\tau_1} - \beta_4 \sin y_{\tau_2} - K \sin x_{\tau_3} \tag{4.16}$$

the synchronization occurs in coupled systems only when delays τ_1 and τ_2 are equal in both systems. Delay τ_3 in a slave is in fact the conduction delay, which gives a trivial solution for anticipation, zero-lag or retardation times equal to $\bar{\tau} = \tau_1 - \tau_3$ or to $\bar{\tau} = \tau_2 - \tau_3$, depending on the choice of parameters β_i for $i = 1, ..., 4$ and K. If $K = \beta_1 - \beta_3$ and $\beta_2 = \beta_4$ then we get the lag time $\bar{\tau} = \tau_1 - \tau_3$, otherwise if $K = \beta_2 - \beta_4$ and $\beta_1 = \beta_3$ then we get $\bar{\tau} = \tau_2 - \tau_3$. The choice between conditions: $K = \beta_1 - \beta_3$ and $K = \beta_2 - \beta_4$ determines the control parameters, in the first case it will be β_3 and in the latter β_4. In order to observe anticipated synchronization in this case, the slave system (with $K = 0$) has to be in a stable fixed point or oscillatory (period one) state as well.

4.3 Anticipated synchronization as a delayed feedback control

In Section 2.2.3 we described the methods which enable us to control unstable orbits in chaotic flows. One of such method is a delayed feedback control (DFC) which is achieved via the modification of some system parameter p in the following way:

$$p(t) = K(y(t-\tau) - y(t)) \tag{4.17}$$

where τ is a positive constant time delay, being the period of the oscillations we want to stabilize. The delayed feedback control in Eq. 4.17 may be interpreted in terms of the coupled systems theory as the self synchronization since the current state $y(t)$ of the system tends to synchronize with its past state $y(t-\tau)$. It occurs when the control is efficient leading to $p(t) \to 0$, for some particular values of the parameter K and τ. On the other hand, the anticipated synchronization operates with the following term:

$$q(t) = -K(y(t-\tau) - x(t)) \tag{4.18}$$

where in place of the current state of the system being controlled ($y(t)$), the variable at current state of the other system (master $x(t)$) is injected. Thus the anticipated synchronization may be interpreted as a process in which the slave system is controlled to obtain the set of unstable periodic orbits which visits the master (if it is chaotic). A delayed feedback control in this case consists on pushing the slave to have the output of the master shifted ahead in time by τ, instead of the one periodic orbit usually desired to obtain through delayed feedback control. In fact, in the delayed feedback control the stabilization of the periodic orbit is obtained but without any reference periodic orbit. The description of the delayed feedback control as self-synchronization is here an adequate proof for the lack of the reference orbit: the system synchronizes with itself. In the case of anticipated synchronization we know exactly the time series of the master and thus we can estimate the phase shifts between the controlled slave system and the master. The slave can be controlled because its equations have the same form of the master and thus the attractors of both systems are the same. The slave has the same infinite set of unstable periodic orbits, and for that reason it is possible to generate the unstable periodic orbits of master in the slave.

The above fact indicates that in principle it might be possible to synchronize any two systems such that the slave system contains all unstable (or stable) periodic orbits of the master. This is the reason for which the chaotic system may be synchronized to the simple oscillator frequency [140] or to the other chaotic system but with lower dimension [141, 142] and not vice versa. The slave should have dimension equal or higher than that of the master. To show this we provide numerical simulations of two coupled sys-

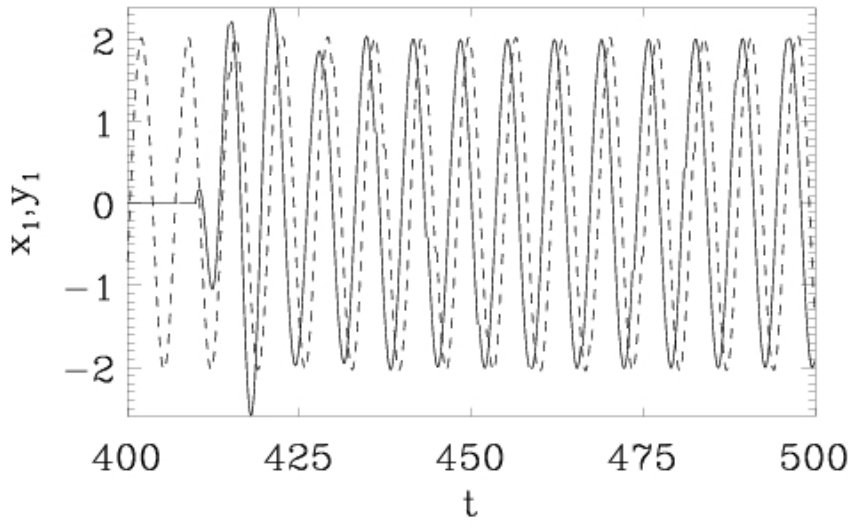

Figure 4.24: *Anticipated synchronization between the harmonic oscillator of frequency* $\omega_0 = 0.85$*, period* $T \approx 6.8$ *and amplitude* $A_0 = 2$ *being the master (dashed line) and the Rössler system being a slave (solid line) with chaotic period* $T \approx 6$*. Delay time is* $\tau = 0.8$ *and the coupling parameter* $K = 0.55$*.*

tems by a delayed coupling scheme: the harmonic oscillator (Eq. 4.11) and the Rössler system (Eq. 2.20). The result is presented in Fig. 4.24, where the anticipated synchronization is observed for particular coupling parameter K and delay time τ. The Rössler system is forced by the delayed term Ky_τ and after reaching the steady fixed point (see Section 4.2), at time $t = 410$, the external forcing coming from the harmonic oscillator is switched on. After the transient, the slave starts to synchronize with the master and anticipates it by time τ. We checked that there exists a wide range of parameters for which instead of the complete anticipated synchronization, the phase anticipated synchronization occurs i.e. the slave has the frequency (with phase shift τ) as that of the master but the amplitude of these oscillations is different. The additional condition for the successful entrainment of the slave is that the harmonic oscillator should have the frequency near the frequency of the Rössler system. This is because the Rössler system has the fixed chaotic period (for our set of parameters $T = 6$) i.e. the period is constant but the amplitude changes chaotically. Then in order to control the Rössler system one needs to choose the external forcing of the period $T_{ext} \approx 6$. This can be clearly seen from the cross-correlation diagrams in the parameter space τ and K obtained from numerical simulations for different frequencies of external forcing (see Fig. 4.25).

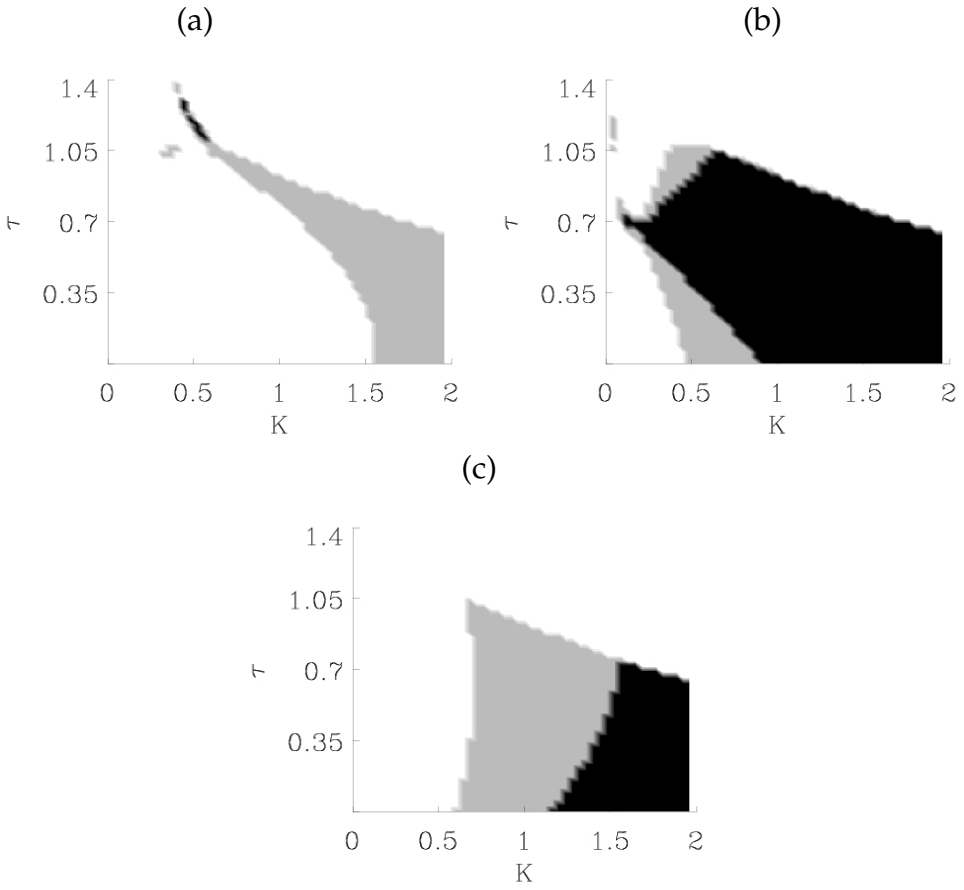

Figure 4.25: *Diagrams with cross-correlations between the outputs of the master harmonic oscillator and the slave Rössler system in the coupling parameters space τ and K for different periods of the harmonic oscillator: (a) $T = 5$, (b) $T = 6$ and (c) T=6.8. Black colour corresponds to correlations $C > 0.99$, grey to $0.9 < C < 0.99$ and white to $C < 0.9$. The chaotic period of the Rössler system in all cases was $T = 6$.*

4.4 Conclusions

In this Chapter we have provided a simple explanation of the physical mechanism behind the anticipated synchronization in coupled excitable systems. Our conclusion is that the anticipation in the slave is due to a reduction of its excitability threshold induced by the delayed coupling term. As a consequence, the master and the slave respond to the common external forcing with different response times. The proposed dynamical picture allows us to explain all the general features of the phenomenon as well as to determine in a natural way the maximum permitted anticipation time. This mechanism allows to explain all the observations in the regime of anticipated synchronization in such dynamical systems, in particular the erroneous firing of pulses in the slave observed in FitzHugh-Nagumo systems driven by noise. In addition, it evidences the causality of this phenomenon: the master and slave systems follow the applied external perturbations, although the response time of the slave system is shorter due to the effects of the coupling.

Once the mechanism of anticipated synchronization in excitable systems is understood, we turned our attention to chaotic systems. In particular, we studied in detail anticipated synchronization using a modified system approach. The modified system approach uses the uncoupled slave system but driven partially by the anticipated synchronization scheme, namely, by the delayed feedback term. We observed that the delayed term in the coupling scheme pushes the slave system into the stable fixed point state. Consequently, the external force coming from the master is injected into the system being in the stable state. The external forcing pushes the stable slave into the chaotic orbit regime, giving rise to the anticipated synchronization. Moreover, we noticed that the cross correlation diagram which characterizes the stability of the anticipated synchronization between the master and the slave in the parameter space $K - \tau$, is fully determined by the form of the bifurcation diagrams of the modified slave system. Anticipated synchronization regimes correspond to the fixed point states on these bifurcation diagrams. Lag synchronization and the same qualitative characteristics of bifurcation diagrams are observed when coupled systems with parameter mismatches are studied. This result suggests that the delayed feedback in the anticipated synchronization scheme acts on the system parameters, changing them in such a way that lag synchronization can also be obtained.

Finally, we have revealed the similarity between the anticipated synchronization phenomenon and the delayed feedback control. In view of the control theory, we interpret the anticipated synchronization as a control of the slave which gives the set of unstable periodic orbits occurring in the master, but shifted ahead in time. This similarity is due to the resemblance of the coupling term used in delayed feedback control as well as in the anticipated synchronization. The only difference between the delayed

feedback control and the anticipated synchronization scheme is that in the former the reference orbit does not exist (since the self-synchronization takes place), while in the latter the master system serves as the reference and permits to estimate the phase shifts of the slave induced by the delay time.

Chapter 5

Practical approach to predictability with anticipated synchronization

In Section 5.1 we present a new control method for perturbed excitable systems based on two steps: prediction and prevention. The method is applied to the Adler system. For prediction we use the anticipated synchronization scheme, considering two unidirectionally coupled excitable systems in a master-slave configuration. The master is forced externally and its dynamics will be controlled, while the slave is an auxiliary system which is used to predict the master's behaviour. We demonstrate that efficient control may be achieved for particular regimes of coupling parameters.

Predictability of chaotic systems is limited, besides the precision of the knowledge of the initial conditions, by the error of the models used to extract the nonlinear dynamics from the time series. In Section 5.2 we analyze the predictions obtained from the anticipated synchronization scheme using a chain of slave neural network approximate replicas of the master system. We compare the maximum prediction horizons obtained with those attainable using standard prediction techniques with neural networks.

5.1 Predict-prevent control method for excitable systems

In this Section we propose a novel control method for perturbed excitable systems which we call "predict-prevent". We consider two unidirectionally coupled systems in the master-slave configuration, where only the master is subject to the external perturbation. The unperturbed slave is used to predict the response of the master system to this perturbation. The slave is driven by a coupling with the master within the anticipated synchronization scheme. We consider two steps in the method, first the prediction of the master's response and then the prevention of the response by the master to that perturbation.

5.1.1 Prediction of the master response

To illustrate the method we consider two unidirectionally coupled Adler systems in a configuration which allows to predict the response of the master:

$$\dot{x} = \mu - \cos x + p\delta(t - t_p) \tag{5.1}$$
$$\dot{y} = \mu - \cos y + K(x - y(t - \tau)) \tag{5.2}$$

where μ is the constant parameter. If $|\mu| < 1$ the system is excitable and otherwise it is oscillatory (modulus 2π). At the critical point $|\mu| = 1$ a saddle-node bifurcation on invariant circle occurs. Other parameters are: K is the constant coupling parameter, τ is the constant positive delay time and p is the magnitude of the perturbation applied at time $t = t_p$. Note that the perturbation is applied only to the master. For particular coupling parameters τ and K the anticipation of the master by slave is possible (see Fig. 5.1a,c).

The master will fire a spike when the external stimulus exceeds the value $2|\arccos\mu|$. We linearize Eq. 5.2 for the slave around $\tau \approx 0$ getting the following equation: $\dot{y} = \mu/(1 - K\tau) - \cos y/(1 - K\tau) + K(x - y)/(1 - K\tau)$. In order to excite the spike in the slave, the following condition should be satisfied: $K(x-y)/(1-K\tau) > 2|\arccos\mu|$, since the slave needs the same magnitude of perturbation as the master does in order to give the non-linear response. Assuming that at the time t_0 when the perturbation is applied to the master, it has not given any pulse yet, thus we have $x(t_0) = -\arccos\mu + p$. On the other hand the slave is in its steady state $y(t_0) = -\arccos\mu$. After introducing these expressions to the above mentioned condition and rearranging terms, we are left with the following conditions for the slave to anticipate the master:

$$\tau < \frac{1}{K} \qquad \text{and} \qquad \tau > \frac{1}{K} - \frac{p}{2|\arccos\mu|} \tag{5.3}$$

These conditions are plotted in Fig. 5.1b and reproduce qualitatively the numerically obtained regions of anticipation presented in Fig. 5.1a.

5.1.2 Suppression of the master response

So far we have shown that we can predict the response of the master when it is subjected to the external perturbation. Now we use this prediction to suppress the spike in the master. We can suppress it by applying an the additional perturbation:

$$\dot{x} = \mu - \cos x + p\delta(t - t_p) + \epsilon\delta(t - t_\epsilon) \tag{5.4}$$
$$\dot{y} = \mu - \cos y + K(x - y_\tau) \tag{5.5}$$

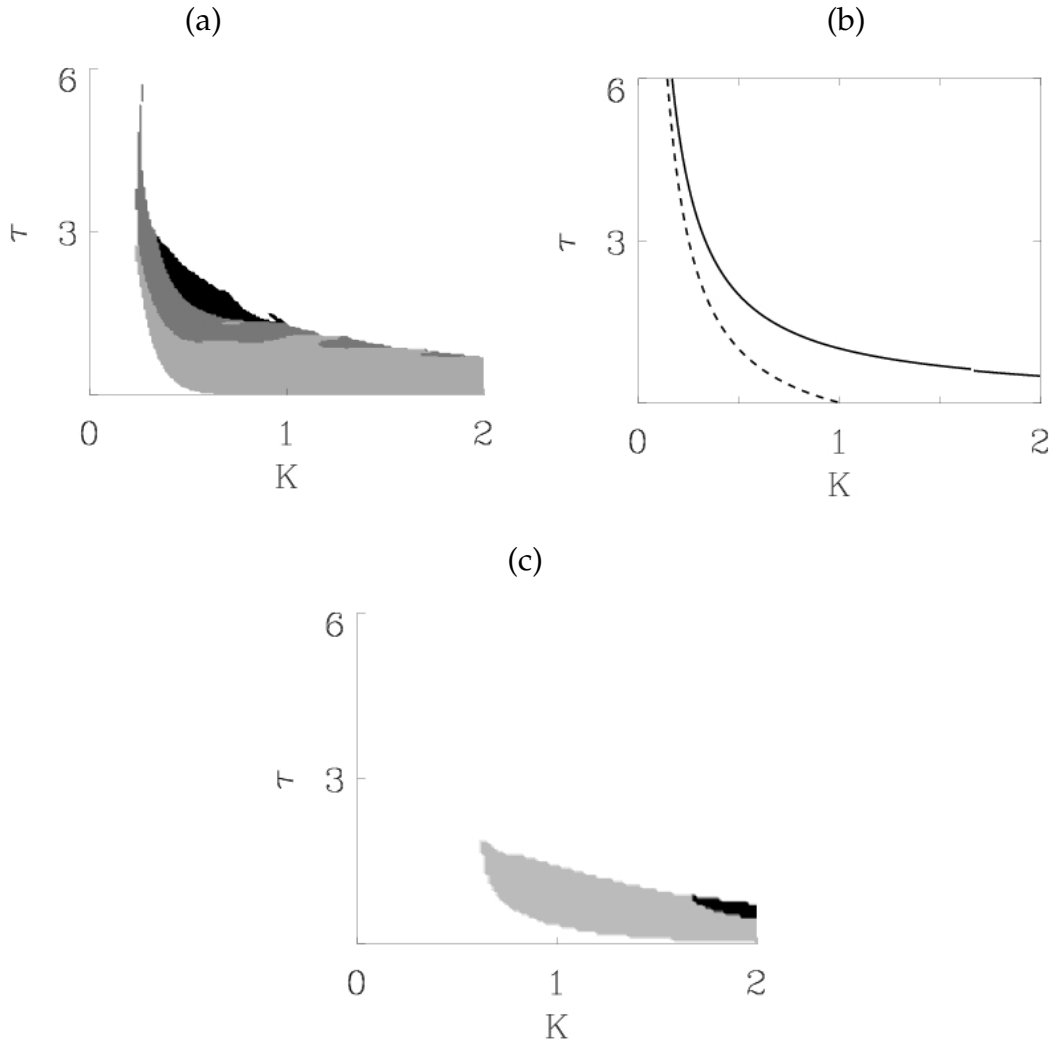

Figure 5.1: *The difference between the response times of the master and slave with delayed coupling term in the parameter space* (τ, K)*. White region corresponds to the unstable or retarded slave, other colors to the anticipation times* $0 < t_{ant} < 1$ *(light grey),* $1 < t_{ant} < 6$ *(dark grey) and* $t_{ant} > 6$ *(black). The perturbation magnitudes are (a) p=1.635 and (c) p=2.8. (b) Analytically obtain region for anticipation in* (K, τ) *space bounded by the solid and dashed curves (see Eq. 5.3).*

where p is the magnitude of the perturbation applied at time t_p with duration Δt, ϵ is the magnitude of the corrective perturbation which suppresses the response of master and is taken to be $\epsilon = -p$. Time t_ϵ is the time at which the corrective perturbation is applied ($t_\epsilon > t_p$) such that it satisfies the condition $cos(y(t_\epsilon)) < cos(y_{th})$ for the threshold value y_{th} taken as the steady state of the slave $y_- = -\arccos \mu$. In this case t_ϵ is estimated at the time at which the slave starts to escape from its steady state. The threshold value may be

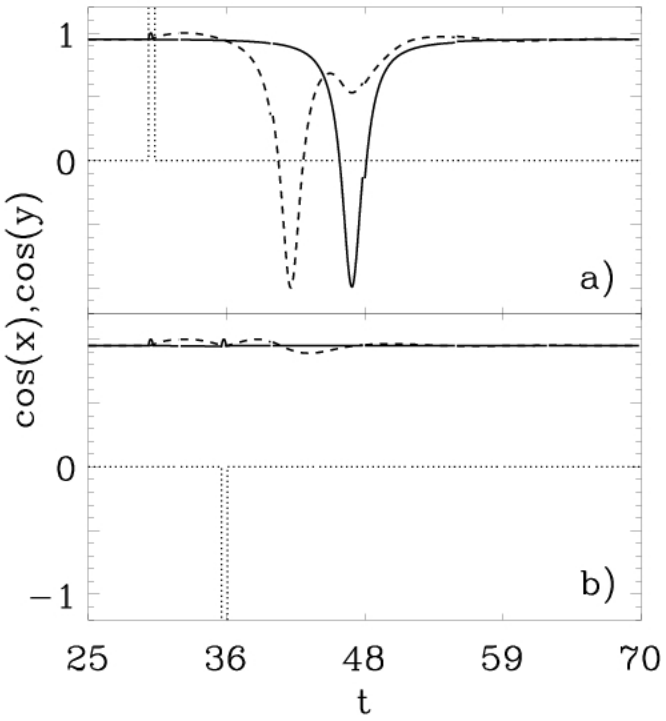

Figure 5.2: *(a) Prediction of the response of the master system by the slave with the parameters* $\tau = 3.84$ *and* $K = 0.24$*. (b) Suppression of one spike. Dashed line represents the slave and solid line the master. The dotted line represents the perturbation in (a) and the corrective pulse in (b).*

also taken as $cos(y(t_\epsilon)) < cos(y_+)$ (where $y_+ = \arccos \mu$ is an unstable fixed point) what would be the case in the practical implementation where the difficulty in distinguishing between the escape from the steady state and fluctuations caused by noise could appear. In Fig. 5.2 we demonstrate that the control is efficient and it enables the suppression of the spike in the master. In other studies we have also applied our control method to suppress two consecutive spikes appearing in the master (see Fig. 5.3). In this case if the second perturbation appears when the master is still in the refractory time, then it can occur that the slave responds to it meanwhile the master remains quite. Thus we face with false alarms given by the slave.

False alarms appear for some range of coupling parameters τ and K which we have estimated numerically. In Fig. 5.4 we present the results for the case for which the perturbation is too weak to excite a pulse in the master. The black region corresponds to the situation in which the slave correctly predict the pulse of the master, meanwhile white region corresponds to the situation in which the slave fires a spike. In the latter case the delay time is too long and the lowering of the excitability threshold of the slave is too strong. It is worth noting that the curve which separates the black and white regions is the stability curve for the appearance of stable anticipated synchronization between two

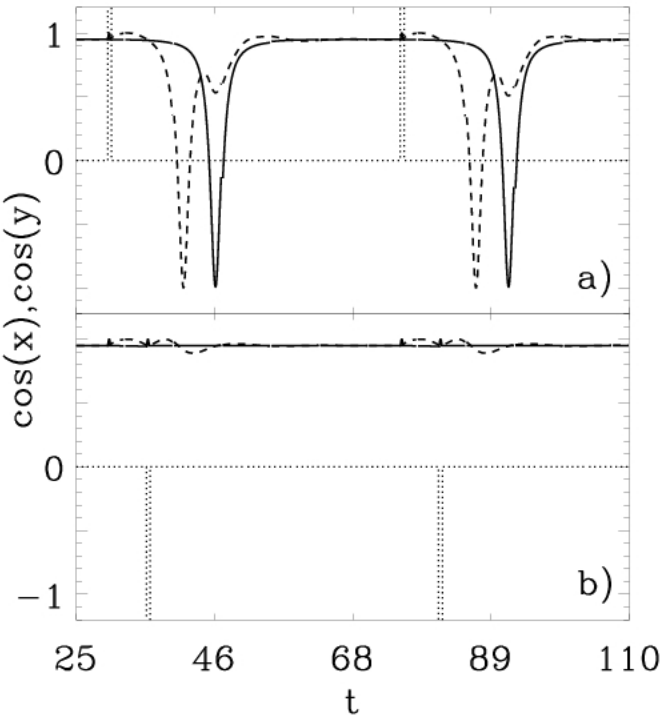

Figure 5.3: *(a) Prediction of the responses of the master system by the slave with the parameters* $\tau = 3.84$ *and* $K = 0.24$. *(b) Suppression of two spikes. Dashed line represents the slave and solid line the master. The dotted line represents the perturbation in (a) and the corrective pulse in (b).*

identical systems and is similar to the curves obtained in other systems. Our prediction scheme considers the anticipated synchronization between two non-identical systems because the perturbation is applied only to the master. However, if the master does not fire and it responds to the perturbation linearly, then, in the approximation, we can neglect the perturbation. This situation corresponds to the anticipated synchronization scheme between two identical systems and hence we obtain the well-known stability region.

The largest anticipation times can be achieved when the magnitude of the applied perturbation is only slightly larger then the value of an excitability threshold of the master (the excitability threshold is defined by the distance between the stable and unstable fixed points of the system). It is a consequence of the fact that the maximum anticipation time that is possible to achieve is equal to the response time of the master. Since the considered perturbation will only push the master slightly above the threshold, it will start to follow the homoclinic connection exactly from the unstable fixed point and will have a longer path to reach the stable fixed point. In the case in which the perturbation is larger than the threshold value, the master starta its excursion much further from its

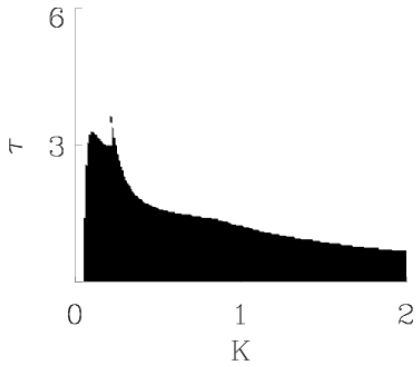

Figure 5.4: *The case when the perturbation is too weak to excite a pulse in the master. The black region corresponds to the situation in which the slave correctly predict that the master will not give a pulse, meanwhile white region corresponds to the situation in which the slave gives a pulse (false alarm).*

unstable fixed point, and will reach the steady state faster (see Fig. 5.5).

To get rid with the case when the perturbation exceeds significantly the threshold value it is necessary to use stronger coupling values as it is seen on Fig. 5.1b. Thus, to be sure that we can control all types of perturbations we need to choose quite strong coupling K and not too large delay times τ. If we are able to estimate the range of magnitudes of perturbations which disturb the master, then we can manipulate the coupling parameters and choose the coupling K and delay time τ from the range which permits larger anticipation times.

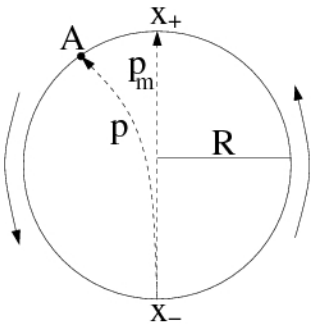

Figure 5.5: *Schematic explanation of the excitation of the Adler system in polar coordinates. The minimal perturbation p_m needed to excite a pulse is defined as the distance between the stable x_- and unstable x_+ fixed points which is $p_m = 2R = 2|\arccos\mu|$. Such perturbation permits the slowest response time of the master (from x_+ to x_-) and thus the largest anticipation time for the slave. If the applied perturbation is $p > p_m$ then the response time of the master is faster (from A to x_-) and the maximum anticipation time decreases.*

5.1.3 Synchronization of systems with parameter mismatches

Anticipated synchronization can be also observed in the case in which the delayed coupling term $K(x - y_\tau)$ is replaced by the synchronization coupling term $K(x - y)$. However, in this case we need to introduce a mismatch between the parameters of the master and the slave, which we define as $\delta\mu = \mu' - \mu > 0$, where μ is the parameter of the master and μ' is the parameter of the slave. We have observed that for particular values of K and $\delta\mu$, and when the perturbation is applied only to the master, anticipation between the master and the slave can occur. Numerical results for this case are presented in Fig. 5.6.

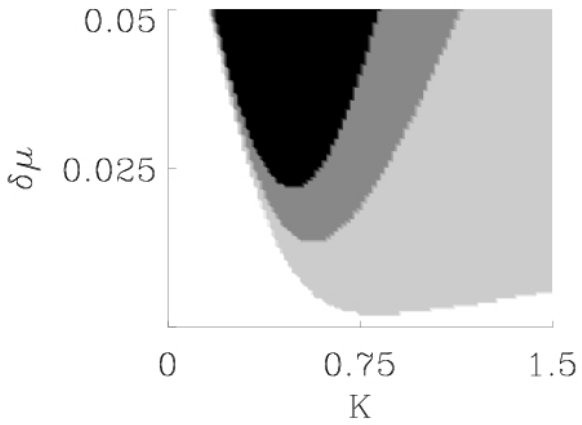

Figure 5.6: *Two Adler systems coupled with the synchronization scheme and with the parameter mismatch $\delta\mu$. The perturbation magnitude is p=1.635. White region corresponds to the retarded slave, other colors to the anticipation times $0 < t_{ant} < 0.1$ (light grey), $0.1 < t_{ant} < 0.25$ (dark grey) and $t_{ant} > 0.25$ (black).*

5.2 Neural networks and anticipated synchronization: a comparison

Theoretically, an arbitrary large forecast horizon can be obtained using a chain of anticipated synchronized exact replicas (slaves) of the original system [143] (see Fig. 5.7a). However, it has been recently shown that this scheme is unstable to propagating perturbations (the spatiotemporal character of the coupled chain introduces a convective-like instability into the synchronization manifold [144]). Therefore, in a practical problem where the slave systems are approximate replicas, there is no information about the maximum attainable anticipation time.

In this Section, we analyze this problem using neural networks, one of the most popular non-parametric statistical learning techniques, for approximating the nonlinear dynamics from the available data (time series) [75]. The obtained neural models are used as slaves in the anticipated synchronization scheme (see Fig. 5.7b) and the results are compared with the exact-replicas case. Moreover, the practical forecast horizon obtained is compared with an alternative standard forecasting method (forward iteration of the neural model from the initial state, Fig. 5.7c). The results presented in this Section were published in Ref. [145].

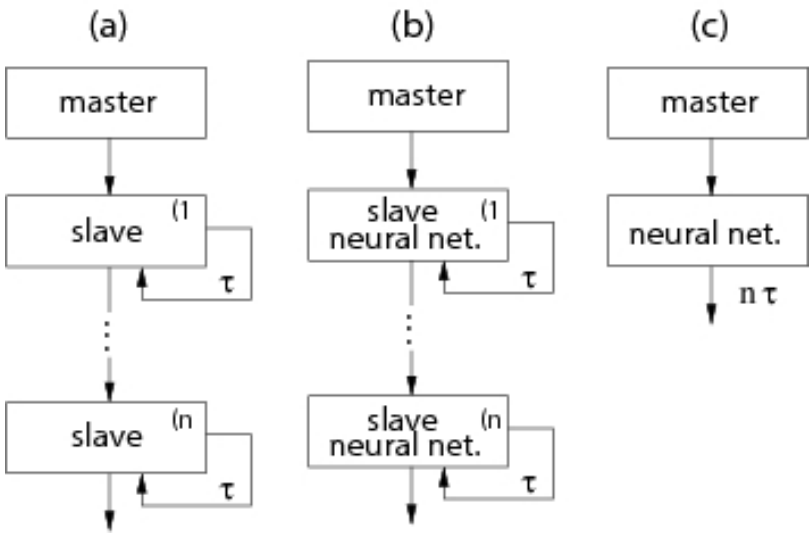

Figure 5.7: *Scheme of the three different approaches to prediction studied. (a) anticipated synchronization chain with identical slave copies, (b) anticipated synchronization chain with slave neural networks, and (c) neural network forward iteration prediction.*

5.2.1 Theoretical limits for anticipation times in chaotic systems

We illustrate the delayed coupling scheme with two benchmark chaotic systems, the Lorenz and Rössler models, with different strong and weak chaotic behaviors, respectively. The Lorenz model is defined by the set of differential equations in Eq. 2.21 (see Section 2.2), which we study for the parameter values $\sigma = 10$, $b = 8/3$, and $r = 28$, with a corresponding largest Lyapunov exponent $\lambda = 0.9$ [132]. This gives a bound for the prediction horizon $t = 1/\lambda = 1.11$. The Rössler model in Eq. 2.20 with $a = 0.15$, $b = 0.2$ and $c = 10$ has a largest Lyapunov exponent $\lambda = 0.09$, giving a prediction horizon $t = 1/\lambda = 11.1$. Note that the theoretical prediction horizons of both systems differ by one order of magnitude.

We take two identical Lorenz and two identical Rössler systems, $\mathbf{u}_0$ for masters and $\mathbf{u}_1$ for slaves, and couple them by using the scheme of Eq. 2.61 with coupling only in the x variable, i.e. $\mathbf{K}\left(\mathbf{u}_0(t) - \mathbf{u}_1(t-\tau)\right) = (K(x_0(t) - x_1(t-\tau)), 0, 0)$. Fig. 5.8a shows the stability region of the anticipated manifold $\mathbf{u}_1(t) = \mathbf{u}_0(t+\tau)$ for the Lorenz systems by plotting in a grade scale the cross-correlation function between $x_1(t)$ and $x_0(t+\tau)$. From this figure, we estimate that the maximum anticipation time, $\tau = 0.13$, is reached for $K = 19$. In the case of coupled Rössler systems the maximum anticipation time is $\tau = 0.91$ for $K = 0.5$ (see Fig. 5.8c). In both cases, these maximum anticipation times are shorter that the inverse of the largest Lyapunov exponents and, in fact, they are similar to the linear prediction times of the original systems: 0.16 (Lorenz) and 0.95 (Rössler). These values are obtained as the horizon where the error of a linear prediction is larger than 5% of the system's range, and agree with those values obtained from the autocorrelation function. This suggests that the anticipated synchronization mechanisms is limited to a neighborhood of t where $\mathbf{u}_1(t-\tau)$ can be linearly approximated in terms of $\mathbf{u}_1(t)$. We proof it analytically as follows: in order to eliminate the delay term $\mathbf{u}_1(t-\tau)$ in Eq. 2.61 we consider the linear expansion, $\mathbf{u}_1(t-\tau) = \mathbf{u}_1(t) - \tau\dot{\mathbf{u}}_1(t)$. Substituting in Eq. 2.61, we get the following equation:

$$\dot{\mathbf{u}}_1(t) = \mathbf{f}(\mathbf{u}_1(t)) + \mathcal{K}\left(\mathbf{u}_0(t) - \mathbf{u}_1(t) + \tau\dot{\mathbf{u}}_1(t)\right) \tag{5.6}$$

rearranging terms in the derivative, we get:

$$\dot{\mathbf{u}}_1(t) = \frac{\mathcal{I}}{\mathcal{I} - \mathcal{K}\tau}\mathbf{f}(\mathbf{u}_1(t)) + \frac{\mathcal{K}}{\mathcal{I} - \mathcal{K}\tau}\left(\mathbf{u}_0(t) - \mathbf{u}_1(t)\right). \tag{5.7}$$

where $\mathcal{K}$ is a matrix composed on diagonal of the coupling constants K. Thus, using a first-order approximation, the anticipated synchronization scheme reduces to a non-anticipated one but with different drive and response systems. Then the synchronization manifold is not $\mathbf{u}_1(t) = \mathbf{u}_0(t)$, but $\mathbf{u}_1(t) = \mathbf{u}_0(t) + \tau\mathbf{f}(\mathbf{u}_0(t))$ in the first-order approximation. This approach has been used to obtain anticipated synchronization in an

array of chaotic RF (radio frequency) circuits [133]. The time evolution for the response system given by Eq. 5.7 corresponds to that of the drive system but with a different time scale $t' = t/(1 - K\,\tau)$. Anticipation requires $t' > t$ or, (at first order) $0 < 1 - K\,\tau < 1$, giving the following two constraints for anticipated synchronization: $K\,\tau > 0$ and $K\,\tau < 1$.

This simple prediction has been compared with the numerical synchronization diagrams of the Lorenz and Rössler systems in the case when all variables are coupled using a diagonal coupling matrix $\mathcal{K}$, (this has been chosen in order to improve the quality of the approximation in Eq. 5.6). Figure 5.8a shows the stability region for the Lorenz system together with the simple prediction curve $K\,\tau = 1$. For comparison, we have included in figure 5.8b the synchronization diagram coming directly from the approximation scheme in Eq. 5.7. Note the similarity between the two figures so confirming the validity of our simple approximation. The smaller correlation values for the case with linear approximation (being $C > 0.95$ in Figs. 5.8b,d instead of $C > 0.999$ as in Figs. 5.8a,c) are related to the fact that phase rather than complete synchronization is achieved. The amplitude of oscillations in the slave is smaller in comparison to that in the master.

The bound $K > 0$ is only a necessary condition for the anticipated synchronization, but it turns out that a minimum coupling value is required in order to achieve synchronization. Figures 5.8c and 5.8d show the equivalent results for the Rössler system. The results shown in figure 5.8 show that in these chaotic systems anticipated synchronization can be effectively considered as the standard synchronization scheme between two non-identical systems, in which the slave runs at a different time scale than the master.

It might look deceiving that the anticipated synchronization scheme discussed here can not forecast longer than the linear prediction time and much less than the inverse of the largest Lyapunov exponent. We will show in the next Section that the situation improves dramatically when we consider a chain of coupled chaotic slave systems. In this case, the anticipation time can be made larger than any of those characteristic times mentioned above.

5.2.2 Coupled systems in a chain

We illustrate the delayed coupling scheme with two benchmark chaotic systems, the Rössler (Eq. 2.20) and Lorenz (Eq. 2.21) models, with different strong and weak chaotic behaviors, respectively, indicating short and long theoretical forecast horizons (see section 5.2.1).

To make anticipated synchronization longer it is necessary to consider a chain of slave systems. Voss [143] already considered a chain of coupled systems and showed that the stability of the system can be enhanced and larger anticipation times can be obtained. The behavior of a chain of connected systems has been also studied for

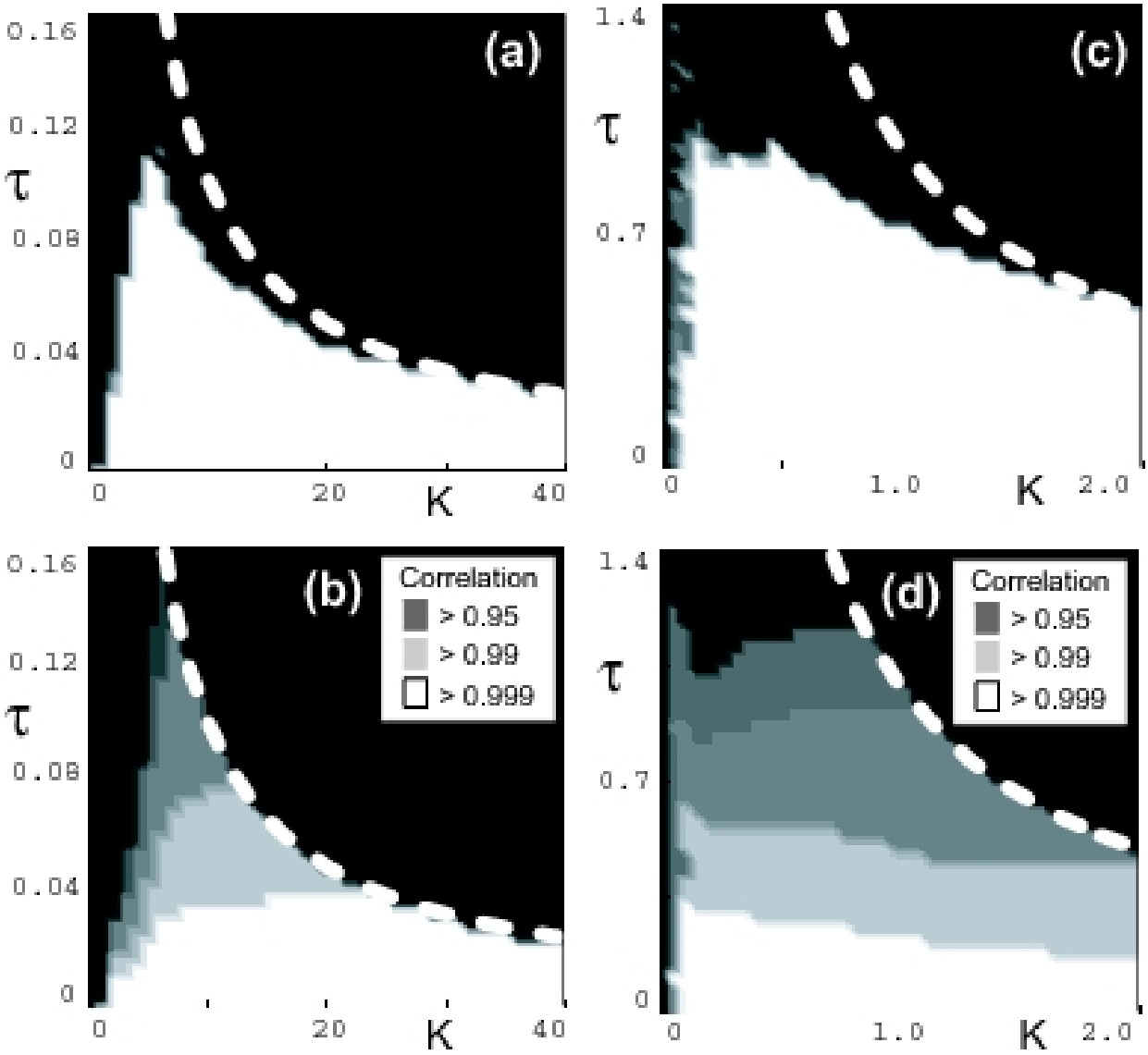

Figure 5.8: *Cross-correlation intensity in the parameter space K and τ for anticipated synchronization scheme with an identical copy of a Lorenz slave for (a) anticipated synchronization scheme (Eq. 2.61) and (b) the first-order approximation scheme (Eq. 5.7). Panels (c-d) as in (a-b) but for the Rössler system. The dashed lines in the top-right corners corresponds to the curves $K\tau = 1$. White(black) color corresponds to high(low) correlation.*

FitzHugh-Nagumo neuron model subjected to noise (see Section 3.1.3), where it has been shown that coupling of above systems in a chain decreases the number of errors in the response neurons and makes anticipated synchronization more stable.

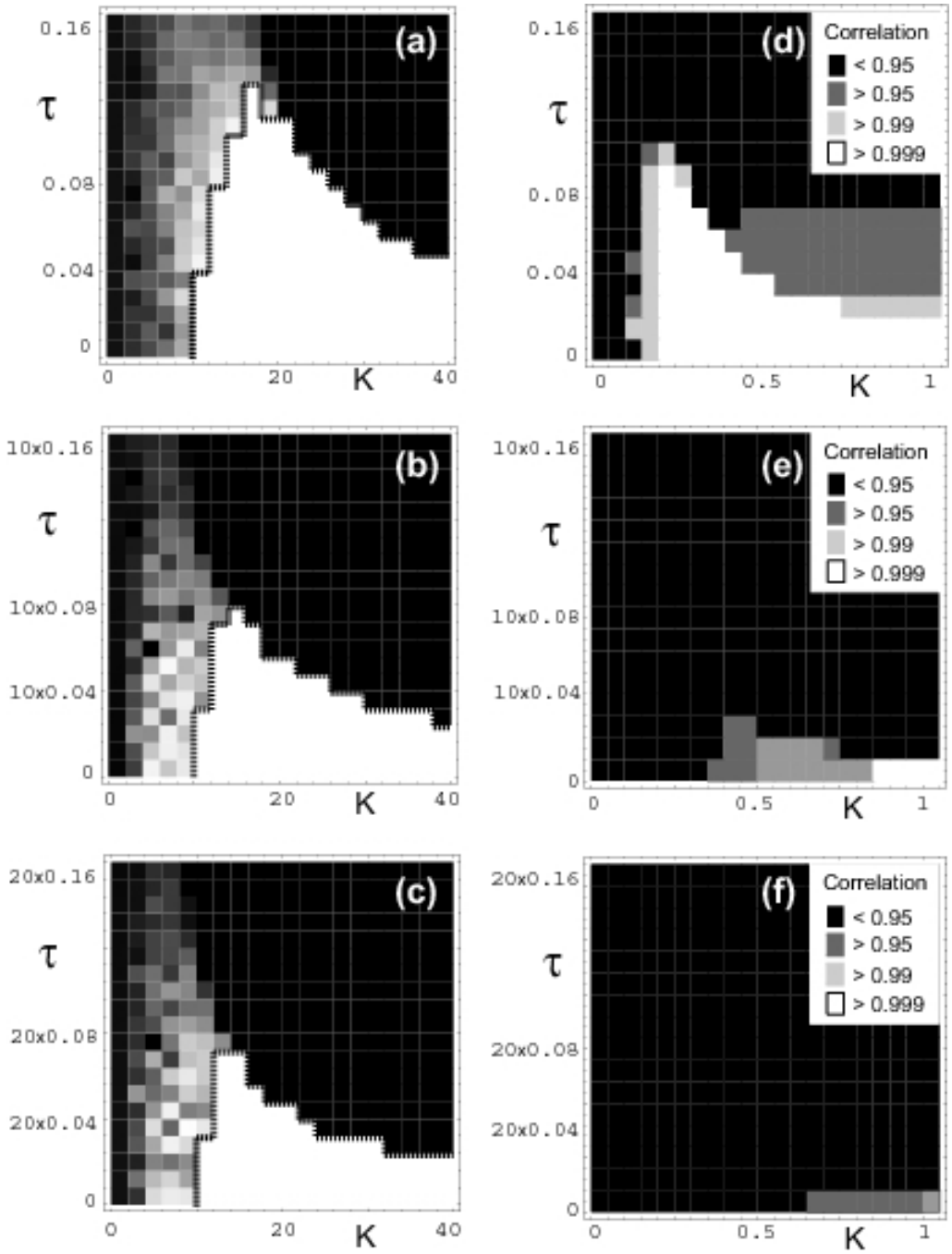

Figure 5.9: *Cross-correlation intensity in the parameter space K and τ for anticipated synchronization scheme with identical copies of (a) one Lorenz slave, (b) ten slaves, (c) twenty slaves. Panels (d-f) as in (a-c) but for the case of slave neural networks. Black(white) color corresponds to high(low) correlations.*

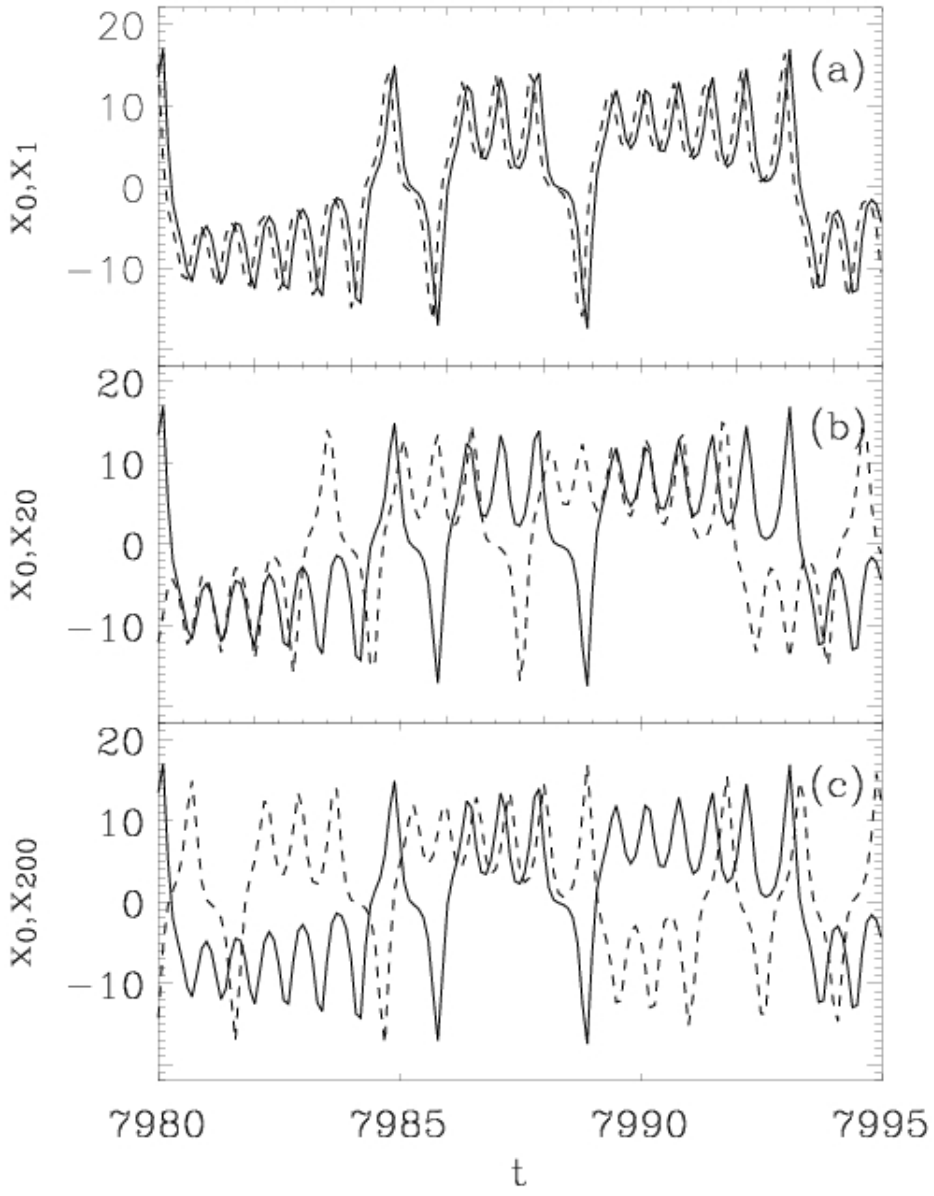

Figure 5.10: *Time series of the master Lorenz system (solid line) and (a) the first slave, (b) the twentieth slave and (c) two hundredth slave. Time series for slave are drawn with dashed line.*

A chain of identical $N+1$ unidirectionally coupled systems is defined in the follow-

ing way:

$$\begin{aligned}
\dot{\mathbf{u}}_\mathbf{0}(t) &= \mathbf{f}(\mathbf{u}_0(t)) \\
\dot{\mathbf{u}}_\mathbf{1}(t) &= \mathbf{f}(\mathbf{u}_1(t)) + \mathbf{K}\left(\mathbf{u}_0(t) - \mathbf{u}_1(t-\tau)\right) \\
&\cdots \\
\dot{\mathbf{u}}_\mathbf{N}(t) &= \mathbf{f}(\mathbf{u}_N(t)) + \mathbf{K}\left(\mathbf{u}_{N-1}(t) - \mathbf{u}_N(t-\tau)\right)
\end{aligned} \tag{5.8}$$

where subsystem $\mathbf{u}_0$ is the master and subsystems $\mathbf{u}_i$, $i = 1, ..., N$ are slaves. In this scheme, convective-like instabilities introduced by the spatiotemporal character of the chain reduces the maximum delay time τ as compared to the case of a single slave [144]. However, since the anticipation time of the N-th slave as compared to the master is $N\,\tau$, the total prediction time can be much larger than that of the single slave scheme. Figures 5.9b and c show the stability regions K vs τ for a chain of $N = 10$ and $N = 20$ coupled Lorenz systems, respectively. These figures illustrate how, although the delay time τ decreases with N, the total anticipation time $N\tau$ increases significantly with N. The set of figures 5.10a-c show a typical time series obtained by coupling a single, twenty, and two hundred slave systems. For the latter we have reached an anticipation time of 4 time unit, much larger than the characteristic times of the Lorenz system for which the inverse largest Lyapunov exponent is 1.1. Similar results were obtained for the Rössler system. A word of caution is necessary here. The above results consider that the slaves are perfect copies of the master. In other words, that we know exactly the master's equations of motion and parameters. In most practical situations it might not be possible to know the functional form of the chaotic dynamics and only a time series of the system dynamics is available. Then approximate models can be obtained and used as slave systems [146]. Neural networks is one of the most popular learning methods for this task.

5.2.3 Anticipated synchronization with neural network replicas

Once we have established that the neural network is a good copy of the dynamical system (see Section 2.5), we use this copy as the slave in a synchronization scheme. For instance, let us consider the synchronization scheme (Eq. 2.54) for two diffusively coupled systems, where the master is the Lorenz system $\mathbf{u}_0$ and the slave is its neural network copy $\mathbf{u}_1$ with $a = 10$ hidden neurons. Figure 5.11c shows the evolution of the synchronization error, measured as the difference $x_1^n - x_0^n$ between the x variables of the master and the slave. Notice that after $n = 500$ steps, the two systems synchronize rather well although there is a residual error. In the case that the slave is a *perfect* copy the error vanishes after the transient time, as shown in figure 5.11a. The residual error observed in the synchronization of the neural network copy can be assimilated to the

slave being an *imperfect* copy of the master. To quantify this imperfection, we have used as a slave a Lorenz system with mismatch parameters $\sigma = 10.1$, $r = 27.5$ and $b = 8/3$, i.e. assuming a certain mismatch in two of the parameters. As shown in figure 5.11b the resulting synchronization errors are similar to that of the neural network. From these figures, we could state that the dynamical accuracy of the neural approximate model is roughly equivalent to a 2% mismatch in the system's parameters. In the case of

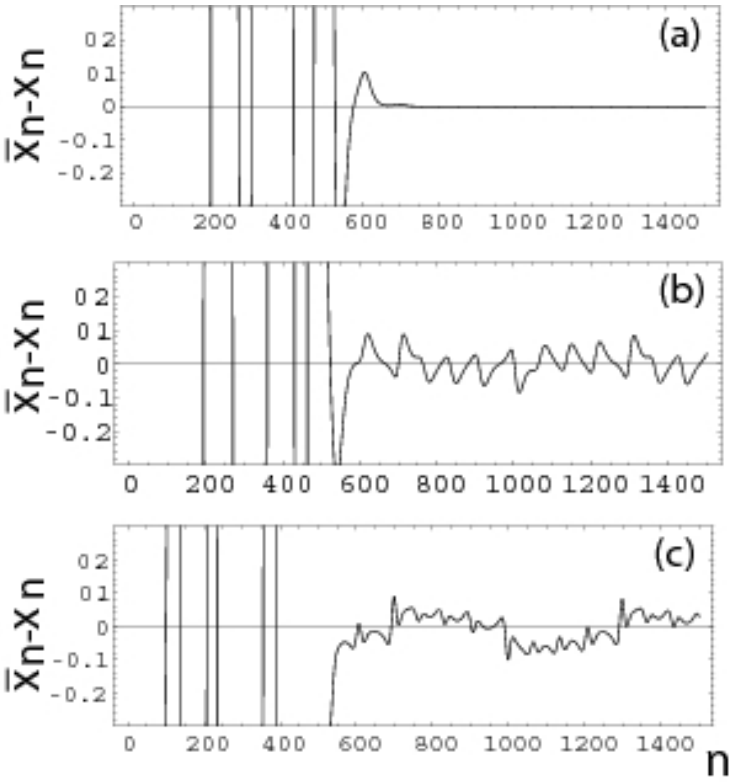

Figure 5.11: *(a) Synchronization error with two identical systems; (b) synchronization error with a slave system with mismatch parameters ($\sigma = 10.1, r = 27.5, b = 8/3$); and (c) synchronization error with a neural approximate slave model.*

the Rössler model we performed the same simulations obtaining a similar behavior. A neural network with 12 hidden neurons was found to be appropriate for approximating the system dynamics. In this case, the obtained rms errors were 2.4×10^{-4} and 3.2×10^{-4} for the training and test data.

Now we consider the general anticipated synchronization scheme in Eq. 5.8 using as master the Lorenz system $\mathbf{u}_0$, and as a chain of slaves N identical neural network models $\mathbf{u}_1, \ldots, \mathbf{u}_N$, as discussed previously. In our work we have used the package Neural Networks of *Mathematica* which supports many techniques for function estimation. Figure 5.9d shows the stability regions K vs τ obtained when coupling the

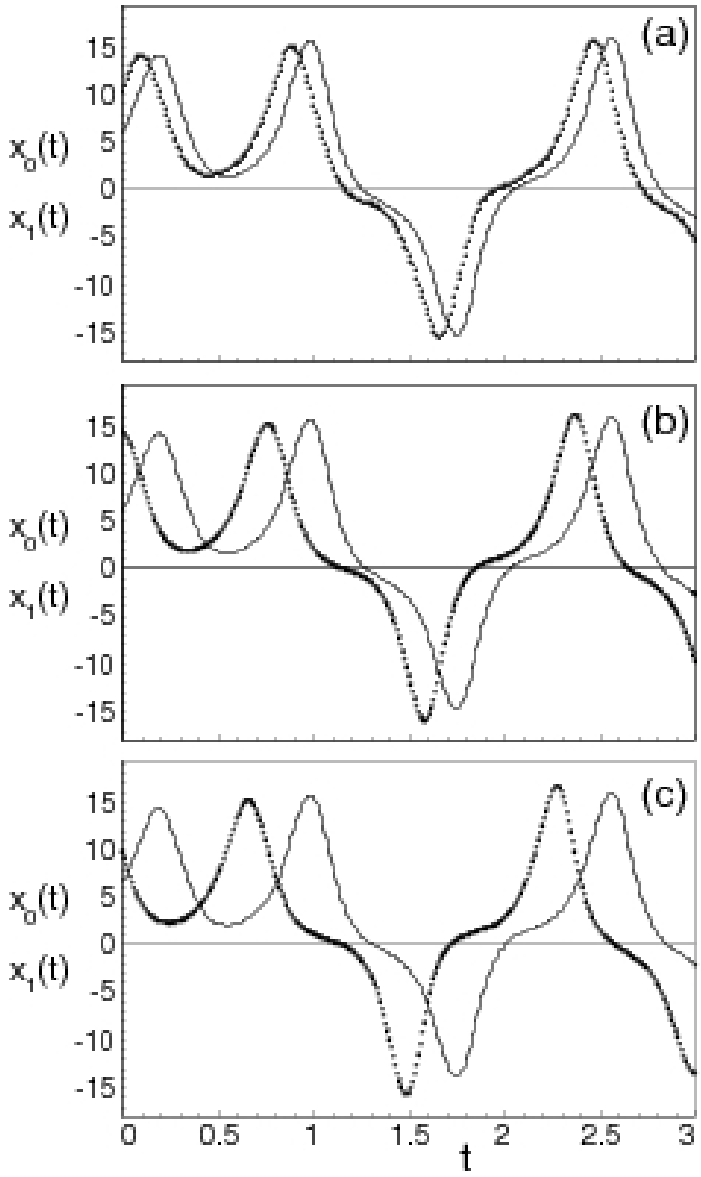

Figure 5.12: *Time series of variable $x(t)$ of master Lorenz system and (a) first slave neural network with $\tau_i = 0.08$, $K = 0.2$ (b) tenth slave neural network with $\tau_i = 0.03$, $K = 0.4$ and (c) twentieth slave neural network with $\tau_i = 0.01$, $K = 0.7$ for $i = 1, ..., N$, where N is a number of slave neural networks in a chain (slaves are drawn with dotted line and master with solid line).*

Lorenz system to $N = 1$ neural network with two hidden layers each containing four neurons. Comparing figures (a) and (d) we observe the reduction of the stability region when the slave is a neural network with respect to the identical slaves case. In fact, the performance of the chain of neural network slaves worsens as the number N increases, see Figs. 5.9e-f. Therefore, we get a maximum anticipation time of 0.33 for

$N = 20$, which has to be considered as the maximum prediction horizon for the Lorenz system using the anticipated synchronization scheme with neural network slaves (see Fig. 5.12). A similar analysis in the Rössler model using this technique yields a maximum anticipation time of 4.1 for $N = 20$. These prediction horizons are much shorter than those obtained with anticipated synchronization when the slaves are perfect copies of the master, as discussed in the previously.

5.2.4 Standard prediction with neural networks

We now compare the use of the anticipated synchronization scheme with neural networks as slave systems with the standard prediction technique consisting on iterating forward in time the neural approximate model from an initial condition. Whereas in the former method the maximum anticipation time does not depend on the initial point, it turns out that in the latter case, the attainable forecast horizon depends on the precise location of the initial condition within the attractor. The forecast horizon T is defined as the time it takes for the absolute value of the difference between the neural network reconstructed orbit and the actual orbit to be larger than 2%. As shown in figures 5.13a-b, lower horizon values correspond to initial conditions in the unstable regions of the attractor where transitions are more likely to occur. More detailed information is obtained from the histogram of horizon times, as shown in Figs. 5.14a for the Lorenz and 5.14b for the Rössler systems. The distributions are quite broad and the mean values are $\langle T \rangle = 1.12$, and $\langle T \rangle = 11.8$, respectively. These values are close to the inverse of the largest Lyapunov exponent. In the same figures we have indicated the location of the maximum prediction times using anticipated synchronization combined with neural networks. It is worth mentioning that the anticipation times using perfect replicas of the master system are beyond the shown scale for the x-axis. Note that the anticipating horizon obtained using standard prediction with neural networks is larger (in average) than the values obtained with anticipated synchronization (dashed lines in Fig. 5.14). In the latter, the horizon is constant over the attractor whereas the standard prediction approach only provides an average forecast value. Thus, depending on the type of application, one method would be better than the other.

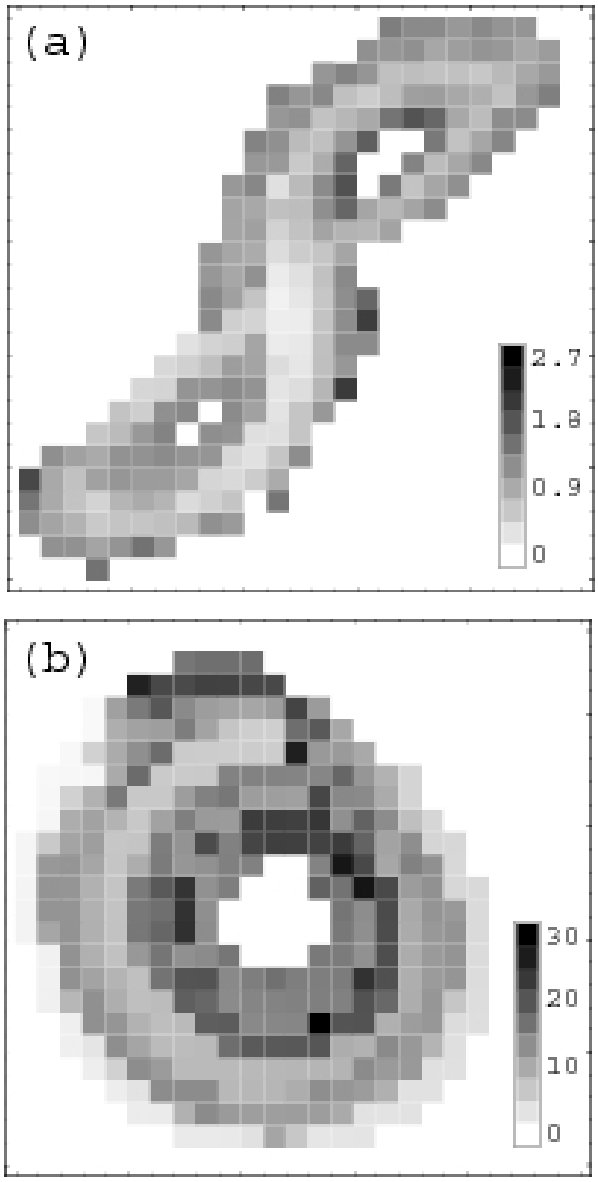

Figure 5.13: *Residuals $x_n - \hat{x}_n$ for two neural models with (a) Histogram produced by 10000 points on the attractor; (b) histogram of the averaged prediction horizon obtained with a neural network.*

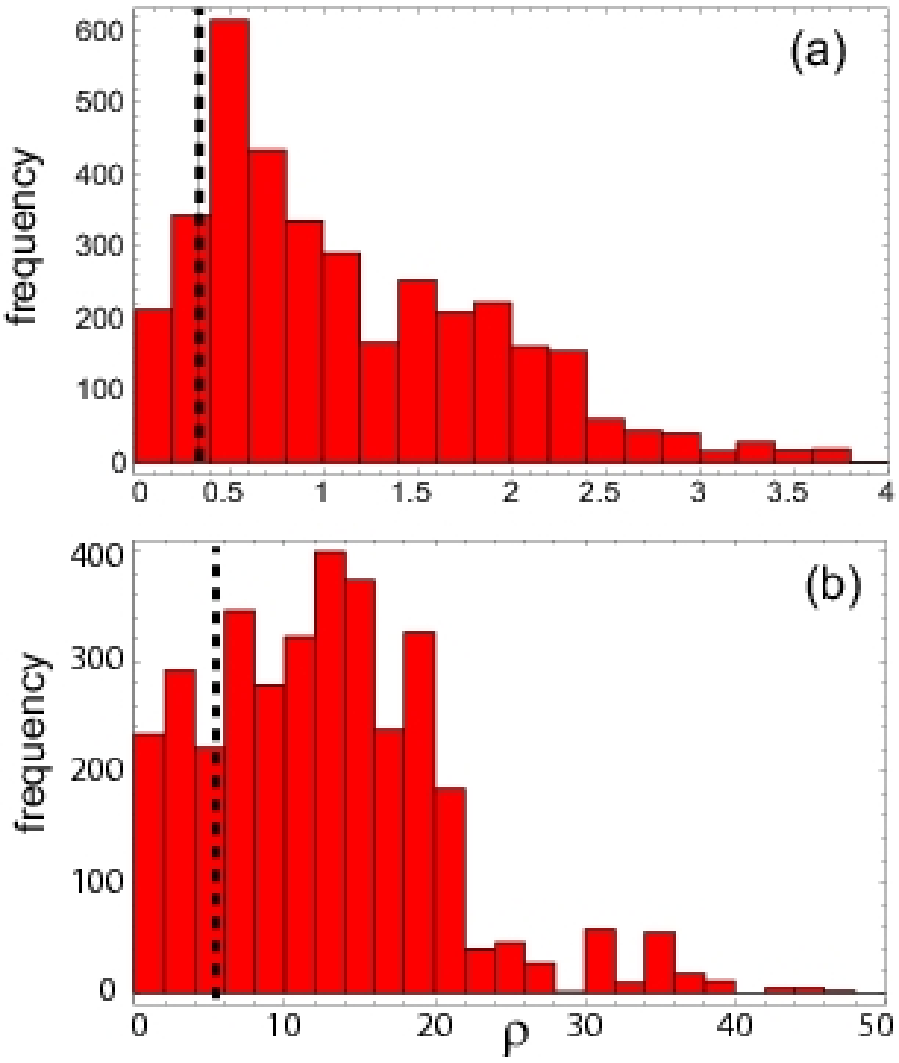

Figure 5.14: *Histogram of the prediction horizon obtained from a sample of size 3000 for (a) the Lorenz model (the horizon values range from 0 to 4, with a mean $T = 1.12$) and (b) the Rössler system with the horizon values range from 0 to 50, with a mean $T = 11.8$. The vertical dashed lines corresponds to the fixed forecast horizon obtained with neural networks connected with anticipated synchronization scheme. The numerical results obtained with identical copies of the systems coupled with the anticipated synchronization scheme show that the fixed forecast horizon is very large in this case and is located outside of the range of this histogram.*

5.3 Conclusions

We have proposed a new predict-prevent control method for perturbed excitable systems, consisting in two steps: prediction made by slave with the use of the anticipated synchronization scheme and correction applied to the master in order to suppress its response. We have shown that a delayed coupling term which lowers the excitability threshold of the slave, allows the slave to react faster to the perturbation than the master does. The causality principle is not violated, since the response of the slave never occurs before the perturbation to the master is applied; the slave responds before the master does but after the perturbation appears. The information about the perturbation is transmitted through the coupling with the master even though the master has not fired a spike yet. Such anticipation is possible whenever the slave has the excitability threshold sufficiently lower than that of the master and thus its response time to the perturbation is faster in comparison with that of the master. The proposed method is only valid for excitable systems, and it could be interesting to implement this method to other systems, specially chaotic ones. Since many biological systems, as heart tissue or neurons in the brain, exhibit excitable dynamics, we are convinced that the application of this method could open new possibilities for controlling of arrhythmias or brain diseases. The way to realize this would be to program the controller which neglects the regular heart beating but predict and correct the unwanted ones.

We considered two alternative practical techniques to anticipate the dynamics of chaotic systems. On the one hand, a neural network trained to the available data which can be iterated forward in time reproducing the same orbit of the chaotic system up to a given horizon. One shortcoming of this method is that the prediction horizon, close to the inverse of the largest Lyapunov exponent, can be only given in probabilistic terms. The second technique which we have considered is a chain of neural networks replicas of the master system combined with the anticipated synchronization scheme. In this case the horizon anticipation time adopts a fixed value. However, the numerical simulations have shown that the maximum horizon is shorter than the one obtained by iterating the neural network. These results are closely related to the differences between the perfect knowledge of the chaotic system and its neural network reconstruction. The mismatch is produced during the, necessarily imperfect, training of the neural network. Thus the success of the technique combining anticipated synchronization and neural networks depends on the successful training of the neural network itself.

The forecast horizon in the anticipated synchronization scheme with a single slave is of the order of the linear correlation time of the system. A chain of slaves allows to overcome this limitation and, when the slaves are perfect copies, we obtained anticipation times which are much longer than the prediction horizon obtained by iterating the neural network. Thus for effective implementation of the combined scheme of neural

networks with anticipated synchronization it is essential to have a more accurate reproduction of the dynamics of the master system. It would be interesting to continue the study with such a network and we are convinced that it could exploit the predictive power of the anticipated synchronization scheme applied to a chain of coupled systems.

Chapter 6

Summary and open problems

Anticipated synchronization is an intriguing phenomenon which so far has not been observed in any biological or natural system. However, all the ingredients necessary for the anticipated synchronization to occur, i.e. the interaction between two or more dynamical systems and the existence of delay lines, can be easily found in biological systems and they are in fact very common in Nature. Less common are the unidirectional interactions, an example being the communication between the cells constituents of the nervous system, where apart from the bidirectional coupling, the unidirectional coupling was found. Could anticipated synchronization be a useful tool in the communication between neurons? Or maybe could it play a role in some prediction processes taking place in the brain? By contributing to the understanding of this phenomenon from the dynamical point of view, by revealing its limitations and its potential utility, we have attempted to answer some of the questions.

In this thesis we have presented the results of some studies of anticipated synchronization in different dynamical systems, demonstrating the general aspects of the phenomenon. Anticipated synchronization was considered as counterintuitive effect due to the possibility of anticipating the unpredictable dynamics of chaotic systems and even stochastic ones. In the case of the delayed coupling scheme of the form $K(x - y_\tau)$ we have shown that the anticipation cannot exceed the time corresponding to the linear autocorrelation time of the system, thus being in agreement with our intuition. The same concerns excitable systems for which we have shown that the anticipation time is limited by the response time of the master system to the external stimulus and cannot exceed it, thus preserving the causality principle.

We summarize all the results presented in this thesis as follows:

Summary of the results

- Characterization of the anticipated synchronization in dynamical systems.

    1. We have studied the occurrence of anticipated synchronization in many systems, with the particular attention to the excitable ones driven by an external random forcing. The detailed study, including an experimental approach

to the problem, was motivated by the existence of an excitable dynamics in neurons. Since neurons in the brain are known to cooperate in a noisy environment, we considered the noisy activation of the spikes in the excitable systems and we estimated the quality of the anticipated synchronization in that cases.

We characterized the stability of the FitzHugh-Nagumo systems coupled with the delayed coupling scheme. Numerical simulations of the equations for the master and the slave systems revealed that the quality of the anticipation in the presence of noise depends highly on the existence of the nonlinear terms in the systems. We showed that the stronger the nonlinearities in the system and the higher the intensity of the noise, the worst the quality of the anticipated synchronization. We found that coupling the systems in a chain enables us to achieve larger anticipation times and improves the quality of the anticipated synchronization.

In order to estimate the robustness of this phenomenon, we designed electronic circuits exhibiting the dynamics of the FitzHgh-Nagumo equations. Although noise sources were applied to the master and the slave, nevertheless anticipated synchronization was observed. The numerical simulations and the linear stability analysis also revealed that the injection of different realization of noises in the master and the slave does not limit the occurrence of this phenomenon.

2. The next stage of our studies was to account for the spatiotemporal dynamics. The prototype model for the spatiotemporal systems is the complex Ginzburg-Landau equation. The coupling of two complex Ginzburg-Landau equations has been achieved by using a complex coupling parameter. The largest anticipation times were obtained for the non-zero imaginary part of the complex coupling parameter. We found that the stability conditions obtained from the linear stability analysis were in good agreement with the numerical simulations.

   The study of the anticipated synchronization in spatiotemporal systems has been motivated by its potential use in the prediction of chemical reactions. In particular we considered the model of CO oxidation on a platinum surface. The study of the two coupled surfaces revealed that the coupling strength has to be negative in order to observe anticipated synchronization. Moreover, we have provided the study of different types of coupling configurations leading to the anticipated synchronization, in particular the local, partially global and global coupling. The local coupling revealed to be the best configuration yielding the highest quality of the anticipation. The partially global coupling

consisted on the coupling between point-to-point sub-surfaces of the master and sub-surfaces of the slave. Using partially global coupling we could observe the anticipation, but its quality was worse than in the case of the local coupling. We found that there exists a limit for the size of the sub-surfaces for which, when exceeded, the anticipated synchronization cannot be observed. The maximum anticipation time τ_{max} in the local and the partially global coupling remains the same. What changes is the quality of the anticipation which becomes worse for delay times starting from $\tau = 0$ and ending at $\tau = \tau_{max}$. Finally, the global coupling did not enable us to observe the anticipated synchronization.

Due to spatial separation the transmission of signals between neurons is not instantaneous and needs some time to be accomplished. These transmission times are called conduction delays. In order to model such a situation we considered the spatially separated FitzHugh-Nagumo equations. Furthermore we connected two spatial areas of the FitzHugh-Nagumo cells in the master-slave configuration using the delayed coupling scheme. The conduction delays together with the internal delays of the delayed coupling scheme gave rise to the zero-lag synchronization. Such a synchronization can occur even if the external stimulus is applied only to the master system. The possibility of the occurrence of zero-lag synchronization could be of importance in the feature binding processes which, according to the newest theories for the brain functioning, allow to perceive the objects. The feature binding manifests itself in the synchronous firing of groups of neurons situated in different regions of the brain in response to some external stimulus. Such a synchronous firing occurs simultaneously despite the fact that the cooperating neurons are spatially separated from each other.

Spatiotemporal systems can be represented by a discrete map as well. One example of bidirectionally coupled discrete maps are cellular automata models. A cellular automata work in binary units and carry out logical operations. They can exhibit a complex dynamics and produce different types of patterns, including fractal ones. We coupled two arrays of cellular automata by using a local delayed coupling scheme. As a result we observed anticipated synchronization between the master and the slave cellular automata. The limitation for the anticipation time was one time step ($\tau = \Delta t \rightarrow 1$), but larger anticipation times could be achieved by using a chain of slave cellular automata. Then the total anticipation time between the master and the last slave in the chain was equal to the number of the slaves multiplied by the time step ($\tau = N\Delta t \rightarrow N$). We found that when the delayed coupling

scheme is applied, but with spatial delay instead of a time delay, anticipated synchronization in time can also be observed. This result shows that systems with delay contain many characteristics of the spatially extended systems.

- Dynamical mechanism of the anticipated synchronization

  1. The study of anticipated synchronization in excitable systems driven by noise revealed that it cannot occur for arbitrary coupling strength and delay time values. If the parameters were not appropriately chosen, the quality of the synchronization is low. Two types of errors were found to occur in the slave system: one corresponds to the dispersion of the anticipation time and the other corresponds to additional spikes which appear only in the slave system. The occurrence of additional spikes in the slave gave us the idea that it could be related to the Delayed Feedback Control method of Pyragas. Firing more often in response to the same external stimulus (the same noise was applied in the master as well as in the slave) would mean that the slave is more excitable or, in other words, that its excitability threshold is lower. We numerically proved this hypothesis in many examples showing that indeed the anticipated synchronization appears due to the lowering of the excitability threshold in the slave reduced by the delayed coupling term. As a consequence its response time to an external stimulus is shorter than that of the master. The calculated analytical expressions for the response times in the Adler and FitzHugh-Nagumo systems turned out to strongly depend on the system parameters. As a result anticipated or retarded synchronization can occur in the two systems if the parameter mismatches are carefully chosen and the systems are coupled with a synchronization scheme which does not contain delay. Control of the excitability threshold by the delayed feedback could be used in neural systems to control the responses to external stimuli.

  2. Once the anticipated synchronization in excitable systems was understood, we turned our attention to the study of this phenomenon in chaotic systems. The modified system approach revealed that the occurrence of anticipated synchronization is determined by the dynamical state of the slave system under the effect of the delayed feedback term Ky_τ. Only if the slave system is in the steady state the external forcing Kx can induce synchronization and anticipation. The differences between the bifurcation diagrams for different values of delay times determine the magnitude of the phase shifts between the master and the slave.

     Similar mechanisms for the anticipated synchronization that occurs in excitable systems, were found in chaotic systems. We found that anticipated or

retarded synchronization can be achieved between coupled chaotic systems when carefully choosing parameter mismatches.

3. The resemblance of the anticipated synchronization scheme and the delayed feedback control method was analyzed in details. We found the same mechanisms underlying both schemes. The anticipation in the anticipated synchronization scheme can be observed because we preserve the reference system (the master) and the comparison between time series of the master and the slave systems can be done. In the case of the delayed feedback control method, referred to as the self synchronization, the reference system is perturbed since the system synchronizes with itself. This considerations led us to the question why chaotic systems can be synchronized to simple oscillator frequencies and not vice versa. The reason is that the synchronization between two any systems to occur requires that the attractor of the slave system contains the periodic orbit(s) existing in the master (in the case of the coupled chaotic systems, the slave should have a similar attractor structure to that of the master). We proved this in the example of the harmonic oscillator taken as the master and the Rössler system taken as the slave, showing that indeed anticipated synchronization between these two systems can be achieved.

- Practical approach to predictability via anticipated synchronization

1. The understanding of the dynamical mechanism underlying the anticipated synchronization in excitable systems led us, in a natural way, to the development of a control method for perturbed excitable systems. The method consists in two steps, the prediction and the prevention. First, by using of the slave system coupled to the master with the anticipated synchronization scheme, we predict the response of the master system. We design the system in such a way that the external stimulus is applied only to the master, and the information about its existence propagates to the slave through the coupling. The firing of the slave provides us with the information that the perturbation has been applied to the master (even though it is still quiescent). Then we apply the corrective pulse to the master system in order to prevent its response. Such a control method has two significant advantages; it does not require any previous calculations and the corrective pulse is applied to the master only if it is necessary, i.e. if an undesired behaviour starts to develop.

2. The prediction of the dynamics of chaotic systems by using neural networks is a strongly developing branch of applied science. We were interested in comparing the predictive capacities of two approaches, one which uses the standard neural networks and the other which uses the anticipated synchro-

nization scheme. By coupling the slave systems in a chain, with the delayed coupling scheme. However, the latter approach, although it can lead to very large anticipation times, holds only for an ideal case, when all the slave systems in the chain are identical copies. In the case of parameter mismatches, the quality of the anticipated synchronization degrades. In order to follow the practical requirements for the data analysis, we considered as the master the data obtained from the embedding procedure, and as the slave, the entrained neural network. The crucial differences between the considered approaches were that in the case of the standard neural networks, the prediction horizon (anticipation) was attained in a probabilistic way, i.e. depending on the initial conditions of the system. In the case of the anticipated synchronization the prediction horizon was fixed and depended only on the successful training of the slave to the data from which we wanted to make a forecast.

Open problems

There are many open problems which require further study. One of such a problem is to provide a mathematical description of the anticipated synchronization in chaotic systems as it was done for excitable systems. A definition of the maximum anticipation time in terms of the response time of the master system is required. In this thesis only intuitive and qualitative descriptions have been provided, based on some numerical examples.

Another problem which needs additional study is the control and prediction using the anticipated synchronization scheme. So far only theoretical studies have been provided and it would be interesting to check its functionality in real systems through experiments. Also it would be interesting to test chemical synapse coupling in neuron's models in order to check the validity of our results. In our work we paid particular attention to the prediction and control of excitable systems, referring to the dynamics of the heart or the brain, as well as to chaotic systems, referring to the dynamics of chemical reactions. In both cases we considered the diffusive delayed coupling scheme, which gave relatively small anticipation time, limited by the linear autocorrelation functions of the system. This limitation can be overcame when considering a chain of coupled systems. However, the dynamics of a chain is very sensitive to the parameter mismatches between the coupled systems, thus being a disadvantage in real applications.

On the other hand, the complete replacement scheme allows us to overcome this limitation in a very significant way. Thus we think that it would be interesting to study the replacement scheme in real world systems containing internal delays. In fact, there are many of such systems in Nature. As an example, we mention models for weather dynamics, which are much more complex than, e.g. the Lorenz model. Apart of being

multi-variable, the additional complexity comes from the delay effects related to the spatial distribution of elements such as air, humidity, temperature, pressure, etc. Thus the interaction between the above mentioned elements can be modified by the delays, and in consequence can contribute to the chaotic behaviour of the system. If the estimation of the existing delays would be possible, then a particular coupling scheme could be used, and an approximate anticipation of the chaotic dynamics of the weather could be achieved.

Appendix A

Stability analysis for linear differential equations with delay

In this Section we consider simple coupled linear systems and estimate analytically the stability regimes for the occurrence of anticipated synchronization. Let us first consider the following coupled systems:

$$\begin{aligned} \dot{x}(t) &= a \\ \dot{y}(t) &= a + K(x(t) - y(t-\tau)) \end{aligned} \tag{A.1}$$

where $\tau \in \mathcal{R}^+$. In order to study the stability of the anticipated synchronization manifold we define the new variable $\Delta(t) = x(t) - y(t-\tau)$ being the difference between the variables of the master $x(t)$ and the slave $y(t-\tau)$, where the latter is delayed in time by τ. Since the anticipated synchronization solution is $y(t) = x(t+\tau)$, we want to know for which coupling strength K and delay time τ the difference variable $\Delta(t)$ vanishes. The anticipated synchronization manifold for the coupled systems in A.1 is described by the following differential equation:

$$\dot{\Delta}(t) = -K\Delta(t-\tau) \tag{A.2}$$

where $\Delta(t) = \Delta_0(t)$ for $t \in (-\tau, 0)$ (the initial conditions). This equation can be solved with the use of the Laplace transform,

$$\mathcal{L}[f(t)] = \tilde{f}(z) = \int_0^\infty e^{-zt} f(t) dt \tag{A.3}$$

We apply this transform to the differential equation for $\Delta(t)$ in Eq A.2 getting:

$$\mathcal{L}[\dot{\Delta}(t)] = -K\mathcal{L}[\Delta(t-\tau)] \tag{A.4}$$

The Laplace transform of $\Delta(t-\tau)$ is calculated in the following way:

$$\begin{aligned} \mathcal{L}[\Delta(t-\tau)] &= \int_0^\infty e^{-zt}\Delta(t-\tau)dt = \int_{-\tau}^\infty e^{-z(t'+\tau)}\Delta(t')dt' \\ &= e^{-z\tau}\left[\int_{-\tau}^0 e^{-zt'}\Delta(t')dt' + \int_0^\infty e^{-zt'}\Delta(t')dt'\right] \\ &= e^{-z\tau}\int_{-\tau}^0 e^{-zt'}\Delta_0(t')dt' + e^{-z\tau}\tilde{\Delta}(t) \end{aligned} \tag{A.5}$$

where $\tilde{\Delta}(z) = \mathcal{L}[\Delta(t)]$ and $t' = t - \tau$. After introducing the expression from Eq. A.5 into Eq. A.4 we get:

$$z\tilde{\Delta}(z) - \Delta(0) = -K\left[e^{-z\tau}\int_{-\tau}^{0} e^{-zt'}\Delta_0(t')dt' + e^{-\tau z}\tilde{\Delta}(z)\right] \tag{A.6}$$

After rearrangement of the terms in Eq. A.6 we obtain the following solution:

$$\tilde{\Delta}(z) = \frac{M(z)}{z + Ke^{-\tau z}} \tag{A.7}$$

where $M(z) = \Delta(0) - Ke^{-\tau z}\int_{-\tau}^{0} e^{-zt'}\Delta_0(t')dt'$. In order to obtain the solution for $\Delta(t)$, the inverse Laplace transform should be applied to Eq. A.7. As long as the poles of $\tilde{\Delta}(z)$ are simple[1] we get the following solution for $\Delta(t)$:

$$\begin{aligned}
\Delta(t) = \mathcal{L}^{-1}[\tilde{\Delta}(z)] &= \frac{1}{2\pi i}\oint_C e^{zt}\tilde{\Delta}(z)dz = \sum_{i=1}^{n}\text{Res}_{z=z_i}e^{zt}\tilde{\Delta}(z) \\
&= \sum_{i=1}^{n}\lim_{z\to z_i}(z - z_i)e^{zt}\tilde{\Delta}(z) \\
&= \sum_{i=1}^{n} e^{z_i t}\lim_{z\to z_i}(z - z_i)\tilde{\Delta}(z) \\
&= \sum_{i=1}^{n}\mu_i e^{z_i t}
\end{aligned} \tag{A.8}$$

where z_i are the zeros of the denominator in Eq. A.7 and μ_i are the residua[2] of Eq. A.7 at these points:

$$\mu_i = \text{Res}_{z=z_i}\frac{M(z)}{z + Ke^{-\tau z}} = \frac{M(z_i)}{1 - K\tau e^{-z_i\tau}} \tag{A.9}$$

From Eq. A.8 is seen that the vanishing of $\Delta(t)$ is determined by the sign of the real parts of z_i. Hence to estimate the stability conditions we need to find the roots of the transcendental equation:

$$z_i = -Ke^{-\tau z_i} \tag{A.10}$$

[1] A pole of a function $f(z) = \frac{g(z)}{(z-a)^n}$ is a value of z at which the function has a singularity, i.e. at $z = a$. If n is chosen as small as possible (of order 1), then it is called a simple pole.

[2] At a simple pole the residue is given by: $\text{Res}_{z=a}f(z) = \lim_{z\to a}(z - a)f(z)$. In the case of the function $f(z) = \frac{g(z)}{h(z)}$ where $g(z)$ and $h(z)$ are analytic and $g(a) \neq 0$, $h(a) = 0$, $h'(a) \neq 0$, the l'Hôpital's rule can be used to calculate the residua: $\text{Res}_{z=a}\frac{g(z)}{h(z)} = \frac{g(a)}{h'(a)}$.

where $z_i = \alpha + i\omega$. Separation of the real and imaginary parts in Eq. A.10 yields:

$$\alpha = -Ke^{-\alpha\tau}\cos\omega\tau \tag{A.11}$$

$$\omega = Ke^{-\alpha\tau}\sin\omega\tau \tag{A.12}$$

At $\alpha = 0$, what corresponds to the point at which Hopf bifurcation occurs, Eq. A.11 is satisfied when:

$$\omega = \pm\left(n + \frac{1}{2}\right)\frac{\pi}{\tau} \tag{A.13}$$

where $n \in \mathbf{Z}$. The roots of Eq. A.10 can be also found by plotting the left and right hand

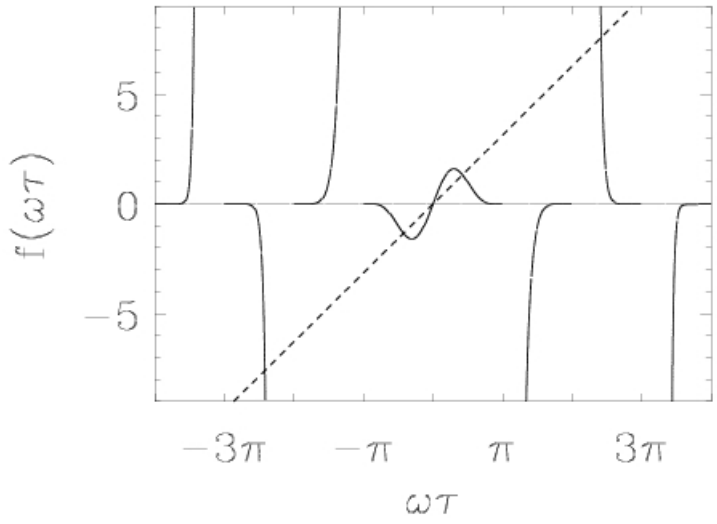

Figure A.1: *The geometric conditions for possible solutions of the equation A.14 - roots of the transcendental equation A.10 are located at the points where the plotted functions crosses. Dashed line represents $f(\omega\tau) = \omega\tau$ and the solid one $f(\omega\tau) = K\tau e^{\frac{\omega\tau}{\tan\omega\tau}}\sin\omega\tau$.*

sides of the following equality (see Fig. A.1):

$$x = K\tau e^{\frac{x}{\tan x}}\sin x \tag{A.14}$$

where $x = \omega\tau$. From Eq. A.14 we can see that at $x = \left(n + \frac{1}{2}\right)\pi$, $\tan x \to \infty$, thus giving $e^{\frac{x}{\tan x}} \to 1$ what finally leads to the relation:

$$\tau = \pm\left(n + \frac{1}{2}\right)\frac{\pi}{K} \tag{A.15}$$

In figure A.2 we plot the curves $\tau(K)$ from Eq. A.15 for different values of n. We can notice that the stable region is bounded only by the curve calculated for $n = 0$, that is

$\tau = \pm\frac{\pi}{2K}$. Moreover, from Eq. A.11 we can read that $\cos\omega\tau \geq 0$ in the range $\langle -\frac{\pi}{2}, \frac{\pi}{2}\rangle$ and $e^{-\alpha\tau} \geq 0$ always. Thus, since we are looking for the solutions when α is negative, we need to consider only the positive part of the condition in Eq. A.15 (for $n = 0$), that is $\tau = +\frac{\pi}{2K}$. Then we are left with the following relation:

$$0 < K\tau < \frac{\pi}{2} \tag{A.16}$$

Since we assume that $\tau \in \mathcal{R}^+$, thus the anticipated synchronization can not occur at negative coupling strengths in the case of Eq. A.1.

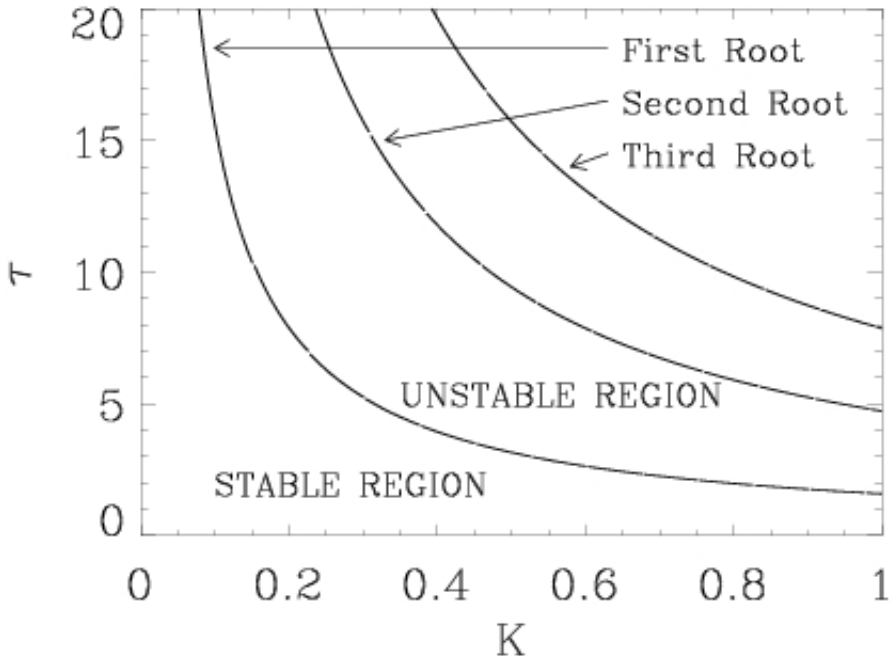

Figure A.2: *Curves obtained from Eq. A.15 for $n = 0$ (first root), $n = 1$ (second root) and $n = 2$ (third root). Stable region is located below the curve calculated for $n = 0$.*

Now we consider the other coupled systems of the form:

$$\begin{aligned} \dot{x} &= a + bx \\ \dot{y} &= a + by + K(x - y_\tau) \end{aligned} \tag{A.17}$$

where the dynamics of the difference variable $\Delta(t) = x(t) - y(t - \tau)$ is described by the following differential equation:

$$\dot{\Delta}(t) = b\Delta(t) - K\Delta(t - \tau) \tag{A.18}$$

Let us introduce the new variable $h(t) = \Delta(t)e^{-bt}$. Then Eq. A.18 becomes:

$$\dot{h}(t) = -Ke^{-b\tau}h(t-\tau) \tag{A.19}$$

having the form of Eq. A.2 where the following replacement has been done $K \to Ke^{-b\tau}$. We can proceed in the same way as before, getting the following solution for $h(t)$:

$$h(t) = \sum_{i=1}^{n} \mu_i e^{z_i t} \tag{A.20}$$

where z_i are the zeros of the characteristic equation

$$z_i = -Ke^{-b\tau}e^{-\tau z_i} \tag{A.21}$$

Taking the first root $z_0 = \alpha + i\omega$ we get the following relations:

$$\alpha = -Ke^{-b\tau}e^{-\alpha\tau}\cos\omega\tau \tag{A.22}$$
$$\omega = Ke^{-b\tau}e^{-\alpha\tau}\sin\omega\tau \tag{A.23}$$

Using the solution for $h(t)$ in Eq. A.20 we get the solution for the difference variable $\Delta(t)$:

$$\Delta(t) = h(t)e^{bt} = \sum_{i=1}^{n} \mu_i e^{(b+z_i)t} \tag{A.24}$$

from which we can read that $\Delta(t)$ vanishes if $b + \mathcal{R}e[z_i] < 0$. In order to estimate the conditions at which Eq. A.24 vanishes as $t \to \infty$, we assume that at the critical point $\mathcal{R}e[z_0] = \alpha = -b$. Then Eqs. A.22 and A.23 yield

$$-b = -K\cos\omega\tau \tag{A.25}$$
$$\omega = K\sin\omega\tau \tag{A.26}$$

From Eq. A.25 we calculate $\omega = \frac{1}{\tau}\arccos(\frac{b}{K})$ and introduce it into the equation A.26:

$$\tau = \frac{\arccos(\frac{b}{K})}{\sqrt{K^2 - b^2}} \tag{A.27}$$

where $|K| > |b|$. It can be easily seen that the above relation at $b = 0$ reduces to that obtained in Eq. A.16. Equation A.27 gives us the stability condition in the region $K > |b|$. However, additional conditions can be read from Eq. A.25 giving us the following relations, for $b > 0$:

$$-K\cos\omega\tau < -|b| \to K > |b| \tag{A.28}$$

b	K	Condition for stability
$b = 0$	$K < 0$	DOES NOT EXIST
	$K > 0$	$0 < K\tau < \frac{\pi}{2}$
$b > 0$	$K < 0$	DOES NOT EXIST
	$K > 0$	$K > b$ and $\tau < \frac{\arccos(\frac{b}{K})}{\sqrt{K^2-b^2}}$
$b < 0$	$K < 0$	$K > b$
	$K > 0$	$K > 0$ and $\tau < \frac{\arccos(\frac{b}{K})}{\sqrt{K^2-b^2}}$ for $K > \|b\|$

Table A.1: *Stability conditions for the anticipated synchronization in coupled linear systems given as the dependence on the coupling strength K, delay time τ and parameter of the system b.*

and for $b < 0$:

$$-K\cos\omega\tau < |b| \rightarrow K > -|b| \tag{A.29}$$

Finally, the stability conditions are:

$$\begin{aligned} \tau &< \frac{\arccos(\frac{b}{K})}{\sqrt{K^2-b^2}} \quad \text{for } K > |b| \text{ and:} \\ K &> b \end{aligned} \tag{A.30}$$

To check the validity of the analytically obtained conditions, we provide numerical simulations of the linear systems in Eq. A.17. The numerical results are presented in Fig. A.3, where the parameter b was taken to be zero, positive or negative.

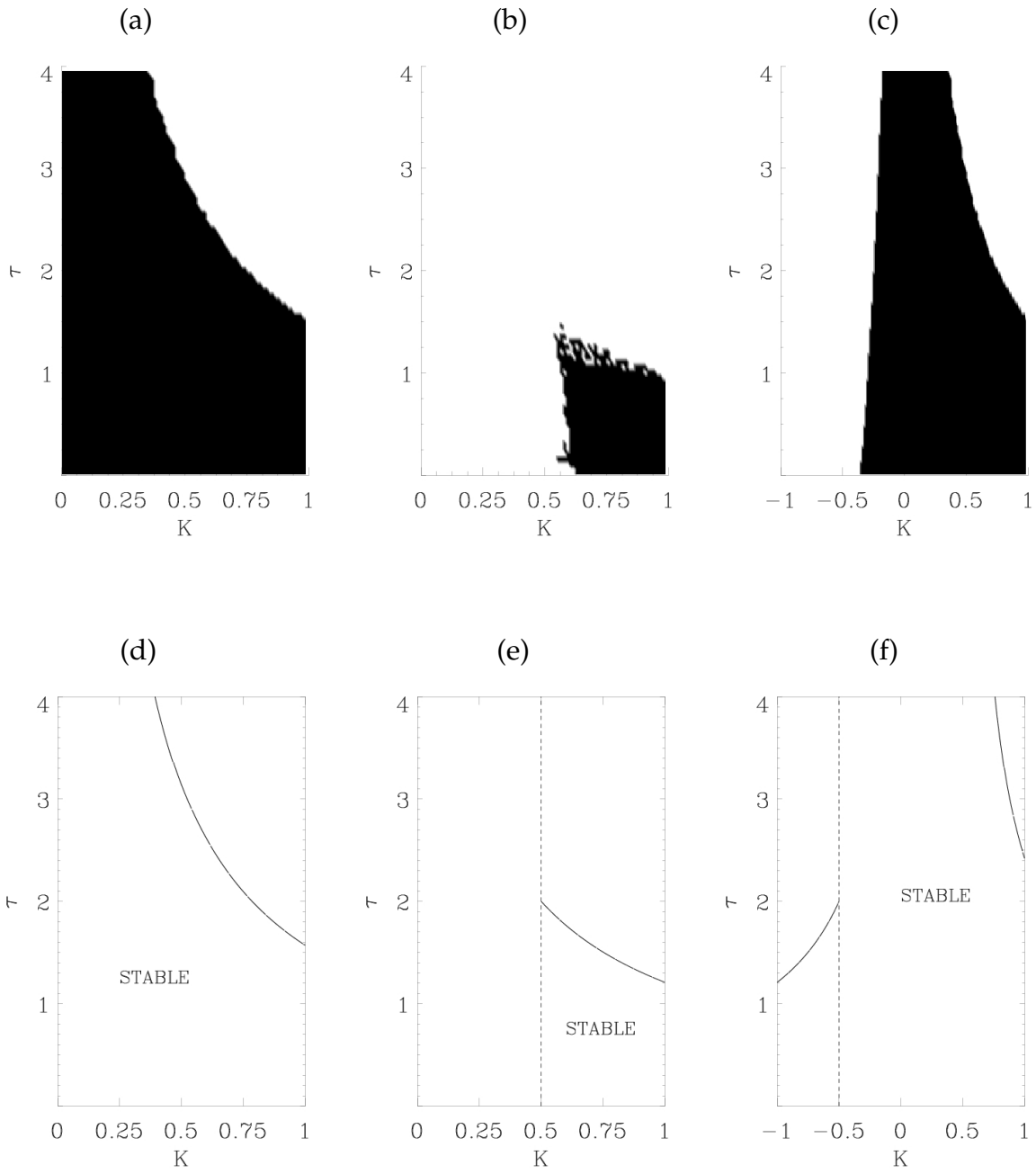

Figure A.3: *Upper panel: cross-correlation diagrams for the anticipated synchronization manifold* $\Delta(t) = x(t) - y(t-\tau)$ *for the coupled systems described by Eq. A.17. Black (white) colour represents the regimes of parameters at which the difference* $\Delta(t)$ *exponentially vanishes (grows) as* $t \to \infty$*. Lower panel: analytically obtained conditions for stability. The parameter* b *was: (a,d)* $b = 0$*, (b,e)* $b = 0.5$ *and (c,f)* $b = -0.5$*.*

Appendix B

Numerical integration

Differential equations with delay

In simulations of the delayed differential equations we use the Euler integration method or the predictor-corrector method called Adams-Bashforth-Moulton, which is known to have good stability properties [147]. The first one is well known and for the differential equation of the form $\dot{x} = f(x)$ follows the iteration formula:

$$x_1 = x_0 + \delta t \cdot f(x_0) \tag{B.1}$$

where $x_k = x(t + k\delta t)$ for $k = 0, 1$ and δt is an integration time step. The fourth order Adams-Bashforth-Moulton method consists of the Adams-Bashforth part being a predictor:

$$x_1 = x_0 + \frac{\delta t}{24}(55f(x_0) - 59f(x_{-1}) + 37f(x_{-2}) - 9f(x_{-3}) + \mathcal{O}[(\delta t)^5] \tag{B.2}$$

where $x_k = x(t + k\delta t)$ for $k = -3, -2, -1, 0, 1$. In this algorithm the current point t, together with the three previous points $t - \delta t$, $t - 2\delta t$ and $t - 3\delta t$ is used to predict the value x at the next point $t + \delta t$. The Adams-Moulton part is a corrector:

$$x_1 = x_0 + \frac{\delta t}{24}(9f(x_1) + 19f(x_0) - 5f(x_{-1}) + f(x_{-2}) + \mathcal{O}[(\delta t)^5] \tag{B.3}$$

If the function f consists of the additive white noise term $\xi(t)$, i.e. $f(x) \to f(x,t) = h(x) + \xi(t)$ then the Euler method for the equation $\dot{x} = f(x,t)$ becomes:

$$x_1 = x_0 + \delta t \cdot h(x_0) + \sqrt{\delta t} g(t) \tag{B.4}$$

where $g(t)$ is a Gaussian random number.

Partial differential equations

Complex Ginzburg-Landau equation (CGLE) is integrated in the Fourier space. The forward Fourier transform is defined as:

$$F(k) = \int_{-\infty}^{\infty} f(x) e^{-ikx} dx \tag{B.5}$$

and the inverse Fourier transform is:

$$f(x) = \int_{-\infty}^{\infty} F(k) e^{ikx} dk \tag{B.6}$$

After applying a forward Fourier transform to the CGLE, each Fourier mode A_q evolves according to:

$$\partial_t A_q(t) = -\alpha_q A_q(t) + \Phi_q(t) \tag{B.7}$$

where $\alpha_q = (1 + ic_1)q^2 - 1$ and Φ_q contains a non-linear term of the CGLE. At any time, Φ_q is calculated in the real space, after taking the inverse Fourier transform of A_q and then is Fourier transformed again. Equation B.7 is integrated by the method similar to the two-step method [148, 149]. From Eq. B.7 we get:

$$\frac{A_q(t)}{e^{-\alpha_q t}} = A_q(t_0) + \int_{t_0}^{t} \Phi_q(s) e^{\alpha_q s} ds \tag{B.8}$$

Writing Eq. B.7 at times $t \to t + \delta t$ and $t \to t - \delta t$ we get two expressions:

$$\frac{A_q(t+\delta t)}{e^{-\alpha_q (t+\delta t)}} = A_q(t_0) + \int_{t_0}^{t+\delta t} \Phi_q(s) e^{\alpha_q s} ds \tag{B.9}$$

$$\frac{A_q(t-\delta t)}{e^{-\alpha_q (t-\delta t)}} = A_q(t_0) + \int_{t_0}^{t-\delta t} \Phi_q(s) e^{\alpha_q s} ds \tag{B.10}$$

After substraction of Eq. B.10 from Eq. B.9 we get:

$$\frac{1}{e^{-\alpha_q t}} \left(\frac{A_q(t+\delta t)}{e^{-\alpha_q \delta t}} - \frac{A_q(t-\delta t)}{e^{\alpha_q \delta t}} \right) = \int_{t_0}^{t+\delta t} \Phi_q(s) e^{\alpha_q s} ds - \int_{t_0}^{t-\delta t} \Phi_q(s) e^{\alpha_q s} ds \tag{B.11}$$

where the right hand side may be rearranged into one integral $\int_{t-\delta t}^{t+\delta t} \Phi_q(s) e^{\alpha_q s} ds$. Assuming that δt is small we make Taylor expansion of $\Phi(s)$ getting $\Phi(s) = \Phi(t + \delta t) \cong \Phi(t)$, so the integral in Eq. B.11 reduces to the calculation of the integral of an exponential function: $\int_{t-\delta t}^{t+\delta t} e^{\alpha_q s} ds = \frac{e^{\alpha_q (t+\delta t)} - e^{\alpha_q (t-\delta t)}}{\alpha_q}$. Introducing it to the Eq. B.11 we get the following expression:

$$A_q(t+\delta t) = e^{-2\alpha_q \delta t} A_q(t-\delta t) + \frac{1 - e^{-2\alpha_q \delta t}}{\alpha_q} \Phi_q(t) + \mathcal{O}((\delta t)^3) \tag{B.12}$$

which is called slaved leap frog [150]. To calculate $\Phi_q(t)$ in Eq. B.12 we use $A_q(t)$ calculated from the expression:

$$A_q(t) = e^{-\alpha_q \delta t} A_q(t-\delta t) + \frac{1 - e^{-\alpha_q \delta t}}{\alpha_q} \Phi_q(t-\delta t) + \mathcal{O}((\delta t)^2) \tag{B.13}$$

which was derived in the similar way as was done for $A_q(t + \delta t)$ in Eq. B.12, but considering the difference between the amplitudes $A_q(t + \delta t)$ and $A_q(t)$. Having defined all integration steps, below is listed the order of actions which need to be performed:

1. Calculation of $\Phi_q(t-\delta t)$ from $A_q(t-\delta t)$ by going into the real space.
2. Calculation of $A_q(t)$ from Eq. B.13.
3. Calculation of $\Phi_q(t)$ from $A_q(t)$ by going into the real space.
4. Calculation of $A_q(t+\delta t)$ from Eq. B.12 by using $A_q(t-\delta t)$ and $\Phi_q(t)$.

At each iteration we calculate $A_q(t+\delta t)$ from $A_q(t-\delta t)$, thus the integration time step is $2\delta t$.

Integration of the model of CO oxidation on a Pt(110) surface [57] was performed by using a finite difference scheme for partial differential equations. For one spatial dimension the integrating algorithm is the following:

$$\nabla_x^2 f(t,x) \approx \frac{1}{\Delta^2}[f(t,x+\Delta) - 2f(t,x) + f(t,x-\Delta)] \tag{B.14}$$

where $\nabla_x^2 = \frac{\partial^2}{\partial x^2}$ is a Laplacian operator and Δ denotes the spatial sampling interval. For two spatial dimensions it takes the form:

$$\begin{aligned} \nabla_{xy}^2 f(t,x,y) &\approx \frac{1}{\Delta^2}[f(t,x+\Delta,y) + f(t,x-\Delta) + f(t,x,y+\Delta) + f(t,x,y-\Delta) \\ &- 4f(t,x,y)] \end{aligned} \tag{B.15}$$

where $\nabla_{xy}^2 = \frac{\partial^2}{\partial x^2} + \frac{\partial^2}{\partial y^2}$. We have used periodic or open (no-flux) boundary conditions.

Bibliography

[1] N. Wiener, Cybernetics, 2nd edition, Cambridge Massachusetts: MIT Press (1961).

[2] I. I. Blekhman, Synchronization in Science and Technology, Asme Press New York (1988).

[3] E. M. Izhikevich, Int. J. of Bifurc. and Chaos **10**, 1171 (2000).

[4] A. L. Hodgkin, A. F. Huxley, J. Physiol. (London) **117**, 500 (1952).

[5] R. FitzHugh, Biophys. J. **1**, 445 (1961).

[6] J. S. Nagumo, S. Arimoto, S. Yoshizawa, Proc. IRE. **50**, 2061 (1962).

[7] P. Philipson, P. Schuster, Inter. Journ. of Bifurc. and Chaos **14**, 1539-1548 (2004).

[8] A. A. Andronov, E. A. Leontovich, J. J. Gordon, A. G. Maier, Wiley New York (1973).

[9] P. Coullet, T. Frisch, J. M. Gilli, S. Rica, Chaos **4**, 485 (1994).

[10] E. A. Jackson, Perspectives of Nonlinear Dynamics vol. 1, Cambridge University Press (1989).

[11] J. E. Marsden, M. MacCracken, Applied Math. Sci.**19** Springer-Verlag (1976).

[12] A. L. Hodgkin, J. Physiol. **107**, 165 (1948).

[13] G. B. Ermentrout, Neural Comput. **8**, 979 (1996).

[14] F. C. Hoppensteadt, E. M. Izhikevich, Weakly Connected Neural Networks, Springer-Verlag, New York (1997).

[15] D. Hansel, G. Mato, C. Meunier, Neural Comput. **7**, 307 (1995).

[16] A. T. Winfree, Sci. Amer. **248**, 144 (1983).

[17] M. Shibata, J. Bureš, J. Neurobiol. **5**, 107 (1974).

[18] B. P. Belousov, Wiley, New York (1985, original work: 1951)

[19] A. M. Zhabotinskii, Biofizika **9**, 306 (1964).

[20] E. R. Hunt, Phys. Rev. Lett. **67**, 1953 (1991).

[21] R. Shaw, The dripping Faucet as a Model Chaotic System, Aerial Press, Santa Cruz (1984).

[22] H. G. Solari, M. A. Natiello, G. B. Mindlin, Nonlinear Dynamics. A Two-way Trip from Physics to Math, Institute of Physics Publishing (1996)

[23] O. E. Rössler, Phys. Lett. A **57**, 397 (1976).

[24] S. Smale, Differentiable dynamical systems, Bulletin of the American Mathematical Society **73**, 747-817 (1967).

[25] E. N. Lorenz, Journal of Atmospheric Sciences **20**, 130 (1963).

[26] Meeting of the American Association for the Advancement of Science, December 1972, Washington.

[27] B. Mandelbrot, The Fractal Geometry of Nature, New York, NY: W. H. Freeman and Company (1982).

[28] W. T. Coffey, Yu P. Kalmykov, J. T. Waldron, The Langevin Equation. With Applications in Physics, Chemistry and Electrical Engineeing, World Scientific (1996).

[29] F. Verhulst, Nonlinear Differential Equations and Dynamical Systems, Springer-Verlag (1990).

[30] R. Ritz, T. J. Sejnowski, Curr. Opin. Neurobiol. **7**, 536 (1997).

[31] B. Schäfer, M. G. Rosenblum, J. Kurths, Nature (London) **392**, 239 (1998).

[32] B. Blasius, A. Huppert, L. Stone, Nature (London) **399**, 354 (1999).

[33] J. A. Freund, L. Schimansky-Geier, P. H anggi, Chaos **13**, 225 (2003).

[34] N. H. Packard, J. P. Crutchfield, J. D. Farmer, R. S. Shaw, Phys. Rev. Lett. **45**, 712-16 (1980).

[35] F. Takens, Lecture Notes in Mathematics (red. D. A. Rand, L. S. Young) **898**, Springer-Verlag, Berlin, 366-81 (1981).

[36] R. Mané, Lecture Notes in Mathematics (red. D.A. Rand,L.S. Young) **898**, Springer-Verlag, Berlin, 230-42 (1981).

[37] A. M. Fraser, H. Swinney, Phys. Rev. A **33**, 1134-40 (1986).

[38] H. D. I. Abarbanel, R. Brown, J. J. Sidorowich, L. S. Tsimring, Rev. Mod. Phys. **65**, 1331-92 (1993).

[39] E. Ott, C. Grebogi, J. A. Yorke, Phys. Rev. Lett. **64**, 1196 (1990).

[40] J. I. Casaubon, Complexity **9**, 1-3 (2002).

[41] T. Kapitaniak, Controlling Chaos, Academic Press, London (1996).

[42] W. L. Ditto, S. N. Rauseo, M. L. Spano, Phys. Rev. Lett. **65**, 3211 (1990).

[43] C-C. Chen, Physics Letters A **213**, 148-154 (1996).

[44] S. J. Schiff, K. Jerger, D. H. Duong, T. Chang, M. L. Spano, W. L. Ditto, Nature **370**, 615-620 (1994).

[45] K. Pyragas, Phys. Lett. A **170**, 421 (1992).

[46] T. Ushio, IEEE TRans. Circuits Syst. I **43**, 815 (1996).

[47] W. Just, T. Bernard, M. Ostheimer, E. Reibold, H. Benner, Phys. Rev. Lett. **78**, 203 (1997).

[48] H. Nakajima, Phys. Rev. A **232**, 207 (1997).

[49] H. Nakajima, Y. Ueda, Physica D **111**, 143 (1998).

[50] K. Pyragas, Synchronization: Theory and Applications, Ed. A. Pikovsky and Y. Maistrenko, NATO Sciene Series II, Physics and Chemistry vol. 109, p. 221 (2002).

[51] K. Pyragas, Phys. Rev. Lett. **86**, 2265 (2001).

[52] K. Pyragas, V. Pyragas, I. Z. Kiss, J. L. Hudson, Phys. Rev. Lett. **89**, 244103 (2002).

[53] A. M. Turing: The chemical basis of morphogenesis, Phil. Trans. Roy. Soc. Lond. **B237**, 37-72 (1952).

[54] B. Shraiman, A. Pumir, W. Van Saarloos, P. Hohenberg, H. Chaté, M. Holen, Physica D **5**7, 241 (1992).

[55] M. I. Rabinovich, A. B. Ezersky, P. D. Weidman, *The Dynamics Of Patterns*, pp. 48, World Scientific (2000).

[56] K. Krisher, M. Eiswirth, G. Ertl, J. Chem. Phys. **96**, 9161 (1992).

[57] M. Bertram and A. S. Mikhailov, Phys. Rev. E **63**, 066102 (2001).

[58] S. Jakubith, H. H. Rotermund, W. Engel, A. v. Oertzen, G. Ertl, Phys. Rev. Lett. **65**, 3013 (1990).

[59] K. Ikeda, Opt. Comm. **30**, 257 (1979).

[60] L. Glass, M. C. Mackey, Ann. Science **197**, 287-289 (1977).

[61] L. Glass, M. C. Mackey, Ann. N. Y. Acad. Sci. **316**, 214-235 (1977).

[62] F. C. Hoppensteadt, Analysis and Simulation of Chaotic Systems, Series: Applied mathematical sciences, Springer-Verlag (1993).

[63] D. Zwillinger, Handbook of Differential Equations, Academic Press (1992).

[64] G. Benchetrit, P. Baconnier, J. Damongeot, Concepts and Formalizations in the Control of Breathing. Manchester University Press (1987).

[65] J. D. Murray, Mathematical Biology, Springer-Verlag (1993).

[66] R. J. Douglas, K. A. C. Martin, J. Physiol. **440**, 735 (1991).

[67] G. Houghton, in Dale R., Mellish C. and Zock M. (eds.) Current research in natural language generation, Academic Press, London, 287-319, (1990).

[68] R. Granger, J. Ambros-Ingerson, U. Staubli, G. Lynch, in Gluck M. A. and Rumelhart D. (eds) Neuroscience and Connectionist Theory, Lawrence Erlenbaum Associates, London, 95-129, (1990).

[69] G. W. Humphrey, H. J. Muller, Cognitive Psychology **25**, 43-110 (1993).

[70] G. Cybenko, Mathematics of Control, Signals, and Systems, **2**, 303 (1989).

[71] J. D. Farmer and J. J. Sidorowich, Phys. Rev. Lett. **59**, 845 (1987).

[72] H. S. Stern, Technometrics, **38(3)**, 205 (1996).

[73] E. Castillo and J. M. Gutiérrez, Physics Letters A, **244**, 71 (1998).

[74] H. Kantz and T. Schreiber, Nonlinear Time Series Analysis, 2nd edition. Cambridge University Press (2003).

[75] E. Castillo, A. Cobo, J. M. Gutiérrez, and M. E. Pruneda, *An Introduction to Functional Networks with Applications*. Kluwer Academic Publishers (1999)

[76] G. W. Greenwood, IEEE Transactions on Evolutionary Computation, **1**, 244 (1997).

[77] J. C. Principe, A. Rathie J. M. Kuo, International Journal of Bifurcation and Chaos, **2**, 989 (1992).

[78] J. A. K. Suykens and J. Vandewalle, IEEE Transactions on Circuits and Systems I, **42**, 499 (1995).

[79] G. Cheng, Y. Cheng, and H. Ogmen, IEEE Control Systems, October, 29 (1997).

[80] M. Frank and T. Stengos, Journal of Economic Surveys, vol.**2**, pp. 103-133 (1988).

[81] T. N. Palmer, Journal of Climate, **12**, 575 (1999)..

[82] K. Levenberg, Quart. Appl. Math. **2**, 164-168 (1944).

[83] D. Marquardt, SIAM J. Appl. Math. **11**, 431-441 (1963).

[84] S. T. Strogatz, Nonlinear Dynamics and Chaos: with applications to physics, biology, chemistry, and engineering, Addison-Wesley (1997).

[85] J. Copeland, A. Moiseff, Integr. Comp. Biol. **44**, 259-263 (2004).

[86] J. Pantaleone, A. J. Phys. **70**, 992 (2002).

[87] M. Bennett, M. F. Schatz, H. Rockwood, K. Wiesenfeld, Proceedings (A) of the Royal Society **458**, no 2019, pp 563 (2002).

[88] E. V. Appleton, Proc. Cambridge Phil. Soc. (Math. and Phys. Sci.) **21**, 231 (1922).

[89] B. van der Pol, Phil. Mag. **3**, 64 (1927).

[90] A. Pikovsky, M. Rosenblum, J. Kurths, Intern. J. of Bifurc. and Chaos **10** 2291 (2000).

[91] T. Yamada, H. Fujisaka, Prog. Theor. Phys. **70**, 1240 (1983).

[92] T. Yamada, H. Fujisaka, Prog. Theor. Phys. **72**, 885(1984).

[93] V. S. Afraimovich, N. N. Verichev, M. I. Rabinovich, Inv. VUZ Rasiofiz. RPQAEC **29**, 795 (1986).

[94] L. M. Pecora, T. L. Carroll, Phys. Rev. Lett. **64**, 821 (1990).

[95] K. M. Cuomo, A. V. Oppenheim, Phys. Rev. Lett. **71**, 65 (1993).

[96] M. J. Ogorzałek, H. Dedieu, Proc. IEEE Int. Symposium Circuits and Systems 98, vol. 4, 522525 (1998).

[97] H. U. Voss, Phys. Rev. E **61**, 5115 (2000).

[98] H. U. Voss, Phys. Rev. Lett. **87**, 014102 (2001).

[99] O. Calvo, D. R. Chialvo, V. M. Eguiluz, C. Mirasso, R. Toral, Chaos **14**, 1 (2004).

[100] C. Mirasso, E. Hernandez-Garcia, C. Masoller, Phys. Lett. A **295**, 39 (2002).

[101] C. Masoller, Phys. Rev. Lett. **86**, 2782 (2001).

[102] H. Voss, Int. J. of Bifurcation and Chaos **12**, 1619 (2002).

[103] P. Davis, T. Aida, S. Saito, Y. Liu, Y. Takiguchi and J. M. Liu, Applied Physics Letters **80**, 4306 (2002).

[104] M. Ciszak, O. Calvo, C. Masoller, C. Mirasso, R. Toral, Phys. Rev. Lett. **90**, 204102 (2003).

[105] R. Toral, C. Masoller, C. Mirasso, M. Ciszak, O. Calvo, Physica A **325**, 192 (2003).

[106] M. Ciszak, R. Toral, C. Mirasso, (short review), Modern Physics Letters B **18**, 1135-1155 (2004).

[107] A. Longtin, A. Bulsara, F. Moss, Phys. Rev. Lett. **67** (1991), 656 ; J. J. Collins, Carson C. Chow, Thomas T. Imhoff, Phys. Rev. E **52**, R3321 (1995); Nature **376**, 236 (1995); D. R. Chialvo, A. Longtin, J. Muller-Gerking, Phys. Rev. E **55**, 1798 (1997).

[108] L. Glass, M. C. Mackey, From clocks to chaos: the rhythms of life, Princeton University Press, Princeton, NJ, (1988).

[109] H. A. Braun, M. Huber, M. Dewald, K. Schäfer, K. Voigt, Int. J. of Bifurcation Chaos Appl. Sci. Eng. **8**, 881 (1998); U. Feudel, A. Neuman, X. Pei, W. Wojtenek, H. Braun, M. Huber, F. Moss, Chaos **10**, 231 (2000); W. Braun, B. Eckhardt, H. A. Braun, M. Huber, Phys. Rev. E **62**, 6352 (2000).

[110] R. Toral, C. R. Mirasso, E. Hernández-García, O. Piro., Chaos **11**, 665 (2001).

[111] E. Hernández-García, N. B. Abraham, M. San Miguel, F. De Pasquale, J. Appt. Phys. **72**, No. 4, 1226 (1992).

[112] E. Hernández-García, C. R. Mirasso, K. A. Shore, M. San Miguel, IEEE Journal of Quantum Electronics **30**, no. 2, 241 (1994).

[113] R. C. Elson, A. I. Silverston, R. Huerta, N. F. Rulkov, M. I. Rabinovich, H. D. I. Abarbanel, Phys. Rev. Lett. **8**1, 5692 (1998).

[114] J. Garcia-Ojalvo, J. Casademont, C. R. Mirasso, M. C. Torrent, J. M. Sancho, Int. J. of Bifurcation and Chaos **9**, 2225-2230 (1999).

[115] L. Junge, U. Parlitz, Phys. Rev. E **6**2, 438 (2000).

[116] K. A. Montgomery, M. Silber, Nonlinearity **1**7, 2225-2248 (2004).

[117] C. Beta, A. S. Mikhailov, Physica D **1**99, 173-184 (2004).

[118] S. Boccaletti, J. Bragard, F. T. Arecchi, Phys. Rev. E **5**9, 6574 (1999).

[119] U. Parlitz and I. Wedekind, Inter. J. of Bifurc. and Chaos **10**, 2527 (2000).

[120] P. König, W. Singer, P. R. Roelfsema, A. K. Engel, Nature **385**, 157 (1997).

[121] P. König, W. Singer, A. K. Engel, A. K. Kreiter, Proceedings of National Academy of Sciences **88**, 6048 (1991).

[122] Ch. Koch, F. Crick, Scientific American **10** (2002).

[123] F. T. Arecchi, E. Allaria, I. Leyva, Phys. Rev. Lett. **91**, 234101 (2003).

[124] J. von Neumann, "The General and Logical Theory of Automata", in: Collected Works, Vol. 5, Macmillan New York, pp. 288-328 (1963); John von Neumann, Theory of Self-Reproducing Automata, University of Illinois Press Urbana, (1966).

[125] S. Ułam, "Random Processes and Transformations", in: S. Ulam, Sets, Numbers and Unverses, MIT Press Cambridge, pp. 326-337 (1974).

[126] R. Serra, G. Zanarini, Complex systems and cognitive processes, Springer-Verlag Berlin Heidelberg (1990).

[127] S. Wolfram, New kind of science, Champaign, Wolfram Media (2002).

[128] S. Wolfram, ed., Theory and Applications of Cellular Automata, World Scientific Singapore, (1986).

[129] W. Sierpiński, Compt. Rendus Acad. Sci. Paris **160**, 302-305 (1915).

[130] G. Giacomelli, R. Meucci, A. Politi, F. T. Arecchi, Phys. Rev. Lett. **73**, 10991102 (1994).

[131] A. Rosenfeld, Computer **16**, 14 (1983).

[132] A. Wolf, J. B. Swift, H. L. Swinney, J. A. Vastano, Physica D **16**, 285 (1985).

[133] D. J. Corron, J. N. Blakely, S. D. Pethel, 8th. Experimental Chaos Conference, AIP Conference Proceedings 742, Eds. S. Boccaletti, B. J. Gluckman, J. Kurths, L.M. Pecora, R. Meucci, and O. Yordanov.

[134] M. Ciszak, F. Marino, R. Toral, S. Balle, Phys. Rev. Lett. **93**, 114102 (2004).

[135] M. Eguia, G. Mindlin, Phys. Rev. E **61**, 6490 (2000).

[136] S. Barland, O. Piro, M. Giudici, J. Tredicce, S. Balle, Phys. Rev. E, **68**, 036209 (2003).

[137] A. E. Hramov, A. A. Koronovskii, Phys. Rev. E **71**, 067201 (2005).

[138] M. G. Rosenblum, A. S. Pikovsky, J. Kurths, Phys. Rev. Lett. **78**, 4193 (1997).

[139] E. M. Shahverdiev, Phys. Rev. E **70**, 067202 (2004).

[140] A. S. Pikovsky, M. G. Rosenblum, G. V. Osipov, J. Kurths, Physica D **104**, 219-238 (1997).

[141] K. Pyragas, Phys. Rev. E **56**, 5183 (1997).

[142] S. Guan, C. H. Lai, G. W. Wei, Phys. Rev. E **72**, 016205 (2005).

[143] H. U. Voss, Phys. Rev. Lett. **87**, 014102 (2001).

[144] C. Mendoza, S. Boccaletti, A. Politi, Phys. Rev. E **69**, 047202 (2004).

[145] M. Ciszak, J.M. Gutiérrez, A Cofiño, C. Mirasso, R. Toral, L. Pesquera, S. Ortín, Phys. Rev. E **72**, 046218 (2005).

[146] H. U. Voss, Chaos **13**, 327 (2003).

[147] W.H. Press, B. P. Flannery, S. A. Teukolsky, W. T. Vetterling, Numerical Recipes in C, The Art of Scientific Computing, Cambridge University Press (1988).

[148] R. Montagne, PhD Thesis (1996).

[149] R. Montagne, E. Hernández-García, A. Amengual, M. San Miguel, Phys. Rev. E **5**6, 151 (1997).

[150] U. Frisch, Z. S. She, O. Thual, J. Fluid Mech. **1**68, 221 (1986).